DISSERTATION

TRACKING THE IMPACT OF WILDFIRE ON THE SOIL MICROBIOME ACROSS TEMPORAL SCALES

Submitted by

Amelia Rose Nelson

Department of Soil and Crop Sciences

In partial fulfillment of the requirements

For the Degree of Doctor of Philosophy

Colorado State University

Fort Collins, Colorado

Spring 2024

Doctoral Committee:

Advisor: Michael Wilkins

Thomas Borch
Ed Hall
Charles Rhoades
Kelly Wrighton

ABSTRACT

TRACKING THE IMPACT OF WILDFIRE ON THE SOIL MICROBIOME ACROSS TEMPORAL SCALES

As climate change progresses, the western United States is experiencing shifting wildfire behavior to more frequent and severe wildfires. Wildfires reduce soil microbial biomass and alter the soil microbiome community composition, selecting for “pyrophilous” microbial taxa with encoded traits that enable them to persist during wildfire or thrive in the soil thereafter. The soil microbiome is a key player in ecosystem carbon (C) cycling through the mediation of soil organic matter decomposition and stabilization. In addition to post-fire shifts in the soil microbiome, wildfire decreases soil C pools through combustion and alters C quality via fire-induced transformations to aromatic pyrogenic C (PyC). The intricate interplay between wildfire-induced alterations to soil microbiome composition and function, and subsequent ecosystem C cycling, remains poorly understood across different temporal and spatial scales. Leveraging multi-omics data alongside soil chemistry information (e.g., mass spectrometry) can offer insights into how shifting wildfire behavior may influence microbially mediated C cycling in forest ecosystems across the western US. To address this knowledge gap, I developed an extensive multi-omic dataset from burned Colorado subalpine coniferous forest soils collected over time (spanning 1 to 60 years following burning) and disturbance severity (low and high fire severity). This dataset includes 108 metagenomes and 12 metatranscriptomes, resulting in 1651 metagenome-assembled genomes (MAGs) that

represent many of the dominant putative pyrophilous taxa previously identified in compositional studies. This dissertation presents the key findings derived from this comprehensive dataset, with the primary goal of addressing how wildfire impacts the soil microbiome with a focus on microbial interactions with soil C.

Chapter 1 serves as a comprehensive literature review, providing an overview of prior research relevant to the research presented thereafter. It underscores the timely relevance of this dissertation research by examining how wildfire behavior is shifting globally with climate change and anthropogenic forcing. Given the critical role of forest ecosystems as significant global C sinks, understanding the repercussions of wildfires on ecosystem biogeochemistry is imperative. I broadly summarize previous research regarding severe wildfire impacts to soils and the soil microbiome and focus on existing knowledge gaps regarding the function of the post-wildfire soil microbiome across differing burn severities and time since fire.

In **Chapter 2**, I characterize how burn severity impacts the soil microbiome one year post-fire in Colorado (CO) subalpine coniferous forests using soil samples collected in July 2019 from within the 2018 Ryan and Badger Creek fire burn scars that represent a burn severity gradient (control, low, moderate, and high severity burned soils). I used a suite of tools to understand both the impacts to soil chemistry and the soil microbiome, including Fourier-transform ion cyclotron resonance mass spectrometry (FTICR-MS) to characterize dissolved soil organic matter, 16S rRNA gene and ITS amplicon sequencing for soil microbiome composition, and coupled metagenomics and metatranscriptomics to identify shifts in soil microbial functional potential. The combination of these tools allowed me to characterize the entire soil microbiome, including bacteria, fungi, and viruses. From

metagenomic sequencing, I recovered 637 MAGs, 1982 unique DNA and RNA viral populations, and 2 fungal genomes from low and high severity burned soil samples. I broadly found that Actinobacteria dominated the fraction of enriched and active bacterial taxa within high severity surficial soils and exhibited traits (e.g., heat resistance, fast growth, expression of genes for degrading aromatic PyC) that enabled them to survive the soil heating and thrive after the disturbance. Ectomycorrhizal fungi (EMF), key symbionts of coniferous trees and other plant taxa, were depleted in severely burned soils. Lastly, there were abundant viruses targeting dominant Actinobacteria MAGs that likely played important roles in assembly of the post-wildfire soil microbiome and serve as top-down controls of C cycling within the system. Overall, this study served as a holistic and comprehensive snapshot of the post-wildfire soil microbiome at one point in time and laid the foundation for forming hypotheses and guiding the subsequent studies.

Building upon the groundwork laid in Chapter 2, **Chapter 3** broadly evaluates the relative importance of putative pyrophilous traits identified between one year and 11 years following wildfire. Additionally, I explored the applicability of other proposed conceptual life history strategy frameworks (e.g., Y-A-S framework) in defining post-wildfire soil microbial dynamics. I utilized a series of soil samples collected from a chronosequence of CO wildfire burn scars representing 1, 3, 5, and 11 years following low- and high-severity wildfire. Using genome-resolved metagenomic approaches and combining this newly generated MAG catalog with the MAGs reconstructed from sequencing in Chapter 1 resulted in a total of 825 bacterial MAGs. Again, this dataset was coupled to various soil chemistry datasets, microbial biomass measurements (via PLFA), and marker gene sequencing data. I found that the potential for fast growth was an important bacterial trait

driving dominance in the post-wildfire soil microbiome for up to approximately 11 years post-fire. Moreover, I observed that MAGs investing in traits aimed at acquiring diverse resources from the external environment often dominated severely burned soils, aligning with the 'A' strategy outlined in the Y-A-S framework. These insights suggest that microbial trait profiles play a pivotal role in shaping post-wildfire soil microbial successional dynamics. Furthermore, the study marks a significant step towards unraveling how trait-based frameworks can offer valuable insights into post-disturbance microbial ecology.

In **Chapter 4**, the focus shifts to investigating one of the most extreme scenarios that can occur in a terrestrial ecosystem with severe wildfire: a burning-induced aboveground vegetation shift. Pile burning is a common fuel reduction or site preparation practice wherein logging residue is burned on the forest floor and, because of the high soil temperatures often reached during pile burning, can serve as a surrogate for studying impacts to soil caused by severe wildfire. Following clear-cut harvesting, pile burning can lead to the creation of persistence openings dominated by herbaceous plants within successfully regenerating conifer forest. In this study, a paired 60-year chronosequence of burn scar openings and surrounding forests that regenerated after clear-cut harvesting provided a unique opportunity to study soil microbiome changes associated with two distinct ecosystem development trajectories (i.e., burning-induced aboveground vegetation shift, regenerating coniferous forest). The primary objective was to identify whether the belowground soil microbiome exhibited resilience to a disturbance-induced aboveground vegetation shift. I collected soils from the aforementioned chronosequence and interrogated soil microbiome composition (via marker gene sequencing), functional

potential (via metagenomics), and function (via laboratory incubations). There were compositional shifts in the soil microbiome that mirrored the ongoing aboveground vegetation shifts, with short-term changes to microbial community composition and C cycling functionality closely resembling a post-wildfire soil microbiome (e.g., PyC degradation). However, over the six-decade chronosequence the soil microbiome composition and function both displayed resilience, converging with that of the surrounding regenerating forest. This final research chapter extended the findings from the previous studies by exploring the longevity of wildfire impact to the soil microbiome in the extreme case of a burning-induced aboveground vegetation shift.

The final chapter (**Chapter 5**) summarizes the key findings of this doctoral research and discusses potential research implications and applications along with future research directions and remaining knowledge gaps. In summary, the aims of this dissertation research were to identify how burn severity influences the soil microbiome composition and function one year post-fire (**Chapter 2**), assess the longevity of these impacts and the applicability of conceptual traits-based frameworks to the post-fire soil microbiome (**Chapter 3**), and evaluate the resilience of the belowground soil microbiome to a burning-induced multidecadal aboveground vegetation shift (**Chapter 4**). This research significantly advances our understanding of the impacts of wildfires on crucial forest ecosystems, with a specific emphasis on ecosystem C cycling.

ACKNOWLEDGEMENTS

Earning this degree has been a group effort spanning the past five years, and I am incredibly thankful for the community - in and out of science - who have provided support. First and foremost, thank you to my advisor, and now friend, **Dr. Mike Wilkins**. Our paths first crossed in 2017 when I was an undergraduate student unsure of my career and science path and, unbeknownst to me, it turned out to be microbiology. You saw potential in me that I could not and took a chance on a young scientist with no formal microbiology background and, *ahem*, a C- in her only official college biology course. I thoroughly enjoyed every afternoon beer, field day (whether the cowpea field or burnt forest), and science meeting together, and you've taught me that you can be both a supportive and, perhaps more importantly, kind mentor. To the rest of my committee, **Dr. Kelly Wrighton**, **Dr. Ed Hall**, **Dr. Chuck Rhoades**, and **Dr. Thomas Borch**, thank you for providing new perspectives to my research and challenging me to grow as a scientist.

I am immensely grateful to the science community and the **Wilkins-Wrighton lab** for their support and guidance during my time at CSU. **Dr. Kaela Amundson**, thank you for answering my constant questions, sharing Bob's afternoon beers, and for helping me retain my sanity with friend WFH workdays during COVID. So much of this degree has been made lighter because of your friendship. **Reb Daly**, thank you for helping with constant sample and lab coordination, along with lab training, during my first few years here. To **Dr. Adrienne Narrowe**, your dedicated mentorship and patience in guiding me through the intricacies of processing sequencing data has been invaluable. I am deeply grateful for the countless hours you spent with me during my early years, which laid the

foundation for all I was able to learn and accomplish during my time at CSU. Thank you. To **Tim Fegel**, thank you for processing *so many* of my soil samples and coordinating field campaigns and another thank you to **Dr. Chuck Rhoades** for spending hours with me in the Ryan fire when I started so I could understand how to be a proficient field soil scientist. To **Dr. Holly Roth**, it was a joy to do much of my PhD alongside you and be the first graduate students in the wildfire group. Field work was infinitely more fun with you there – and a special shoutout to comet NEOWISE. Lastly, I'm incredibly fortunate to have developed an amazing science community outside of CSU. **Dr. Devin Smith**, you helped me get through the first few tumultuous years of graduate school when uncertainty and confusion seemed to be the norm. Our biweekly phone calls throughout my PhD have been a constant source of support and I love having you as a science best friend. **Dr. Grace (Grack) Carlson**, you were my first science friend back in freshman year at IU and I have loved going on this journey with you, from kids in Introductory Geology to braving the academic job market together.

Beyond my scientific community, I am eternally grateful to the family with whom I've shared the past 29 years. To my dad, **Rick Nelson**, you encouraged me at the age of 16 to pursue geology and embark on a career path where others did not look like me. From kindergarten, reading every afternoon in the guest room together, to high school travelling the east coast with you on college visits, you are the reason I am here. I will always hear your loud cheers from bike races ("Go Meels!") in my head during big life moments. I love you. To my mom, **Deana Nelson**, you have encouraged me to be brave and independent, and I will always admire your strength. Thank you both for your consistent support and love – your influence has shaped me in ways I can never fully

express. To my big brothers, **Brad** and **Max Nelson**, you have always been my role models and I continue to admire and look up to you both. To my Papaw (**Phil Myers**), who has not only been a grandfather but also a close friend, and my Mamaw (**Cheril Myers**), who left us far too soon. To **Maggie Terriquez (Bender)** and **Madison Sucese (Viering)**, the childhood friends who have evolved into my family, thank you both for being unfailingly supportive best friends throughout every stage of life.

Thank you to my furry best friend, **Leo Indy Nelson-Kuhn**, for being a constant source of joy and reminding me to find happiness in the simple things each day. Your enthusiasm for life has been a grounding force during my last year of graduate school. The playful *insistence* on taking breaks for fun activities, even amidst deadlines, has been a much-needed reminder to embrace the present moment. Lastly, the most profound thank you to my life partner, fiancé, and best friend, **Spencer Kuhn**. You've been with me from the beginning of this journey and have celebrated every moment – whether it's finishing a rough draft of an abstract or my first paper getting the journal cover. You are the reason I can, and am, following this dream of mine. Thank you.

AUTOBIOGRAPHY

Education

2019-2024 Ph.D., Soil and Crop Sciences, Colorado State University (CO, USA)
2017-2019 Master of Science, Earth Science, The Ohio State University (OH, USA)
2013-2017 Bachelor of Science, Geological Sciences, Indiana University (IN, USA)

Publications

Fowler, J.A., **Nelson, A.R.**, Bechtold, E.K., Paul, R., Wettengel, A.M., McNorvell, M.A., Stevens-Rumann, C.S., Fegel, T.S., Anderson, E., Rhoades, C.C., Wilkins, M.J. (2024). "Pile burns as a proxy for high severity wildfire impacts on soil microbiomes" In review at Geoderma.

Nelson, A.R., Fegel, T.S., Danczak, R.E., Roth, H.K., Dunn, O.I., Turvold, C.A., Borch, T., Barnes, R.A., Wilkins, M.J. (2024). "Soil microbiome feedbacks during disturbance-driven forest ecosystem conversion" In press at ISME J.

Roth, H.K., Simpson, M.J., McKenna, A.M., Chen, H., Srikanthan, N., Fegel, T.S., **Nelson, A.R.**, Rhoades, C.C., Wilkins, M.J., Borch, T. (2023) "Fire severity controls on transformation of organic nitrogen and carbon in high-elevation forest soils" Soil & Environmental Health, doi: 10.1016/j.seh.2023.100023.

Caiafa, M.V., **Nelson, A.R.**, Borch, T., Roth, H.K., Fegel, T.S., Rhoades, C.C., Wilkins, M.J., Glassman, S.I. (2023). "Distinct fungal and bacterial responses to fire severity and soil depth across a ten-year wildfire chronosequence in beetle-killed lodgepole pine forests" Forest Ecology and Management, doi: 10.1016/j.foreco.2023.121160.

Nelson, A.R., Narrowe, A. B., Rhoades, C. C., Fegel, T. S., Daly, R. A., Roth, H. K., ... & Wilkins, M. J. (2022). "Wildfire-dependent changes in soil microbiome diversity and function" Nature Microbiology, doi: 10.1038/s41564-022-01203-y. Cover article for September 2022 issue.

Roth, H.K., McKenna, A.M., **Nelson, A.R.**, Rhoades, C.M, Fegel, T.S., Young, R.B., Wilkins, M.J., Borch, T. (2022) "Impacts of beaver ponds on biogeochemical cycling of organic nitrogen within a fire-impacted watershed." Environmental Science: Processes & Impacts, doi: 10.1039/D2EM00184E.

Nelson, A.R., Toyoda, J., Chu, R.K., Tolic, N., Garayburu-Caruso, V., Saup, C.M., Renteria, L., Wells, J.R., Stegen, J., Wilkins, M.J., Danczak, R.E. (2022). "Implications of sample treatment on characterization of the riverine dissolved organic matter." Environmental Science: Processes & Impacts. doi: 10.1039/D2EM00044J.

Roth, H.K., Borch, T., Young, R.B., Bahureksa, W., Blakney, G.T., **Nelson, A.R.**, Wilkins, M.J., McKenna, A.M. (2022). "Enhanced Speciation of Fire-Derived Dissolved Organic Matter Enabled by 21 T FT-ICR Mass Spectrometry" Analytical Chemistry, doi: 10.1021/acs.analchem.1c05018.

Bryant, S. R., Sawyer, A.H., Briggs, M.A., Saup, C.M., **Nelson, A.R.**, Wilkins, M.J., Christensen, J., Williams, K.H. (2020) "Seasonal manganese transport in the hyporheic zone of a snowmelt-

dominated river (East River, Colorado).” Hydrogeology Journal. doi: 10.1007/s10040-020-02146-6.

Nelson, A.R., Sawyer, A.H., Gabor, R.S., Saup, C.M., Bryant, S.R., Harris, K.D., Briggs, M.A., Williams, K.H., Wilkins, M.J. (2019). “Heterogeneity in hyporheic flow, pore water chemistry, and microbial community composition in an alpine streambed.” JGR: Biogeosciences, doi: 10.1029/2019JG005226.

Saup, C.M., Bryant, S.R., **Nelson, A.R.**, Harris, K.D., Sawyer, A.H., Christensen, J., Tfaily, M., Williams, K.H., Wilkins, M.J. (2019). “Hyporheic zone microbiome assembly is linked to dynamic water mixing patterns in snowmelt-dominated headwater catchments.” JGR: Biogeosciences, doi: 10.1029/ 2019JG005189.

Yanites, B.J., Mitchell, N.A., Bregy, J.C., Carlson, G.A., Cataldo, K., Holahan, M., Johnston, G.H., **Nelson, A.R**., Valenza, J., Wanker, M. (2017), “Landslides control the spatial and temporal variation of channel width in southern Taiwan: implications for landscape evolution and cascading hazards in steep, tectonically active landscapes.” Earth Surface Processes and Landforms, doi: 10.1002/esp.4353.

DEDICATION

This dissertation is dedicated

To dad, who instilled in me a curiosity in the world and a love of learning.
I am proud to be your daughter.

TABLE OF CONTENTS

Chapter 1: Introduction

1.1 Wildfires in the Anthropocene

Wildfire behavior is shifting in response to climate change and human intervention (e.g., fire suppression). Climate change is causing increased average air temperature, the breaching of historically extreme temperature thresholds, and increases in the frequency, duration, and intensity of drought – all of which can influence wildfire ignition probability and ensuing wildfire extent and severity. This is happening globally – the Brazilian Amazon experienced a 36% increase in fire frequency during the extreme drought year of 2015[1], southern Europe and the Mediterranean have seen a surge in wildfires during the 21st century[2,3] with a predicted increase in future high fire danger days[4], and, between 2010 and 2015, Australia witnessed a 40% increase in bushfire frequency[5] with a heightened likelihood of larger wildfires in the future attributed to drought and climate[6]. Besides factors linked to climate change, human activities have significantly impacted global wildfire behavior. These include heightened ignitions due to human activities such as fireworks, powerline mishaps, and campfires[7,8]; changes in fuel loads stemming from fire suppression policies, resulting in ecosystems more susceptible to severe crown fires[9,10]; and shifts in land use, with more individuals residing at the wildland-urban interface[8,11]. Combined, both climatic variables and anthropogenic activities have resulted in altered wildfire regimes across the planet, with wildfires increasing in severity, frequency, and extent[12].

The western United States is susceptible to these changes in wildfire behavior driven by both climate and human impacts. Though wildfire has long been a dominant

driver of ecosystem patterns across the Rocky Mountains – with the subalpine pine forests of the Rockies historically shaped by infrequent stand-replacing wildfires[13] – these ecosystems have been especially vulnerable to anthropogenically-driven changes in wildfire behavior during the 21st century. Western US forests had burned area over ten times greater in 2003-2012 as compared to 1973-1982[14] and an extreme record-setting fire season in 2020 that was largely enabled by climactic variables (e.g., atmospheric aridity)[15]. The increasingly severe and frequent wildfire in the western US impacts society through various avenues. These include significant financial burdens stemming from wildfire mitigation, response, and property damage costs (estimated at $16.5 billion in the US in 2020 alone)[16], adverse effects on human health due to diminished air quality, ramifications for the agricultural sector[17], and enduring consequences for ecosystem services provided by the affected landscapes, such as provisioning of freshwater resources.

1.2 The effects of severe wildfire on soils

Wildfires serve as a natural and beneficial disturbance in many ecosystems. One example is the subalpine pine forests of the Colorado Rockies (CO, USA), where wildfires have historically generated open habitats for understory species, increasing the number of ecological niches and biodiversity and reducing fuel for future severe wildfires[18]. However, altered wildfire regimes to behavior outside of what the ecosystem normally experiences can have deleterious impacts on ecosystem biogeochemistry.

Severe wildfire influences both the physical and chemical properties of soils, with impact increasing with burn severity (i.e., temperature and duration of burning)[19]. Most

intuitively, wildfire initially increases surface soil temperatures to approximately 90-400°C during burning[19], a phenomenon that can persist after the fire due to loss of aboveground vegetation[20]. Burning also raises soil hydrophobicity[21], resulting in heightened overland flow[21] following precipitation events, and contributes to the loss of soil structural stability and aggregation[22]. Collectively, these changes render burned watersheds more susceptible to erosion and result in an amplified influx of nutrient-rich ash and sediments into surface waterways[23,24].

Wildfire causes reductions to soil carbon (C) pools that can last a decade post-fire, with more severe wildfire resulting in greater losses[25,26], and chemically alters remaining soil C through the formation of pyrogenic C (PyC) that is formed via the combustion of biomass. PyC is composed of myriad compounds ranging from dehydrated sugars to condensed polyaromatic hydrocarbons[27], with increased burn severity and burn temperature resulting in more aromatic PyC[28]. In addition to affecting soil C pools, wildfires also impact both the quantity and speciation of soil nitrogen (N). This is particularly significant because N often serves as a limiting factor for primary productivity in forest ecosystems. Combustion and volatilization during wildfire decreases total soil N[29] and combustion transforms soil organic N, with the formation of N-dense heterocycles (e.g., carbazole) in severely burned surface soils[30]. Inorganic N pools also shift; the pyrolysis of organic matter results in increased surface soil concentrations of ammonium (NH_4^+) and nitrate (NO_3^-), much of which can be leached into nearby streams[31]. Lastly, the denaturation of organic acids induced by wildfire can increase surface soil pH[32,33]. Notably, all the aforementioned soil properties that shift due to wildfire (e.g., soil pH, soil

C quality and quantity, N availability, soil structure, temperature, aboveground vegetation) are key factors influencing the assembly of the belowground soil microbiome[34].

1.3 Wildfire impact on the soil microbiome

The microorganisms that inhabit soil are an often overlooked, but key player, in terrestrial ecosystems; the soil microbiome mediates nutrient and C cycling processes[35], regulates soil C decomposition and stabilization[35–37], and facilitates the acquisition of nutrients by plants via symbiotic relationships[38,39]. Wildfire leads to a prolonged (~10 year) decline in soil microbial biomass with impacts that lessen with soil depth, as deeper soils are insulated from the heat generated by wildfires[40,41]. Fungi exhibit greater sensitivity to wildfire compared to bacteria[40] primarily due to differences in thermal tolerance and death of plant hosts during fire[42]. There is a concurrent wildfire-induced loss of microbial diversity[43–45], with general decreases in the relative abundances of species within bacterial phyla Verrucomicrobia and Acidobacteria[43,45,46] and fungal phyla Basidiomycota[47,48], along with subsequent increases in the relative abundance of the bacterial phyla Actinobacteria and Firmicutes[45,49]. Arguably one of the most crucial microbial groups adversely affected by wildfire is the ectomycorrhizal fungi (EMF), essential symbionts for aboveground vegetation. Severe wildfires can devastate EMF populations for more than a decade in pine forests[47]. Given their intimate and critical relationship with aboveground vegetation, this impact could significantly influence vegetation reestablishment following the fire. The impacts of wildfire on soil microbiome biomass and composition increase with wildfire burn severity, with greater impacts to the soil microbiome following high severity burning[45,50,51] and lesser impacts by prescribed

burning than a wildfire as prescribed burning is often of a lower intensity[40,52]. Recovery of soil microbiome composition and biomass following wildfire can occur on a range of months to decades[53–55] and is mediated by dispersal from surrounding unburned sites[56].

Certain bacterial taxa, like the Actinobacteria *Blastococcus* and *Arthrobacter* and Proteobacteria *Massilia*, have been identified in post-wildfire soils across various ecosystems (e.g., California chaparral[49], Mediterranean holm oak forests[57,58], CO coniferous forests[45], boreal forests[50]). These taxa have been proposed to be "pyrophilous", or fire-loving, taxa that possess specific traits that enable them to persist during wildfire or thrive in their aftermath. The hypothesized pyrophilous traits encompass characteristics that facilitate microbial survival amidst the heightened temperatures induced by wildfires, like dormancy, sporulation, or heat resistance genes (e.g., heat shock proteins)[59,60], akin to the concept of plant seed banks as plant adaptations to wildfire. Another purported pyrophilous trait is copiotrophy, or fast growth, to quickly grow and occupy newly open niche space in the soil[49,60,61]. Post-fire, with the long-term shifts in soil chemistry, traits enabling the cell to persist in the altered soil conditions (e.g., increased pH, altered soil C chemistry) like the ability to utilize and degrade aromatic PyC are also hypothesized to be important in determining the structure of the post-wildfire soil microbiome[60]. The ability to degrade PyC has been experimentally tested – the fungus *Pyronema domesticum*, commonly found in burned soils[62], demonstrated the ability to degrade ^{3}C-labeled PyC in the laboratory[63] and *Arthrobacter* can degrade diverse aromatic compounds related to toxins and fuel-contaminated soils[64–66]. Further, *Arthrobacter* are often found to persist in environmentally harsh soils and encode stress resistance genes that allow them to do so (e.g., desiccation stress, low resources), all of

which likely lend to their persistence in post-wildfire soils[67,68]. Collectively, these traits, recently termed the traits-based fire ecology framework[60], likely define soil microbial community successional changes following wildfire across ecosystems and might influence microbially-mediated biogeochemical cycling. Notably, much of the previous post-wildfire soil microbiome research consists of field studies identifying microbial community compositional shifts[49–51] or testing metabolisms in the lab[63] but few are able to bridge this gap to assess the relevance of these metabolisms or traits in real post-wildfire soil environments.

1.4 Terrestrial carbon cycling following severe wildfire

The alterations in soil microbial community composition and function due to wildfires are likely to have a profound impact on broader ecosystem biogeochemical cycling, given that the soil microbiome plays a pivotal role in many biogeochemical processes[35]. Globally, forests are an important C sink that store ~45% of terrestrial ecosystem C and capture 7.6Gt of CO_2 each year[69]. Shifting wildfire behavior to more frequent and/or severe wildfire in forest ecosystems may result in shifts from globally important C rich ecosystems to those with a lower C-carrying capacity (e.g., grasslands)[70]. Therefore, it is imperative to understand the feedbacks between wildfire behavior, the soil microbiome, and ecosystem C cycling.

It has been long considered that, though a wildfire disturbance releases C from a forest ecosystem in the form of CO_2 from biomass combustion, it also contributes to soil C storage through the formation of recalcitrant PyC that is largely unavailable to microbial degradation and can persist for hundreds to thousands of years[71]. Indeed, low severity

wildfire increases the stability of soil C and inhibits microbial respiration, therefore adding C storage to an ecosystem[72,73]. In contrast, C alterations induced by high severity wildfire or high intensity soil heating can decrease soil C sink strength by resulting in lower soil microbiome carbon use efficiency (CUE) and subsequent increases in C respiration and efflux from the soil[73], along with increased soil C loss due to erosion. Laboratory studies have also shown that PyC is chemically complex and has components that can be readily biomineralized by microbes[63,74]. Moreover, the prevalence of microbial copiotrophic traits following severe wildfire could exacerbate the loss of soil C as copiotrophs are believed to grow less efficiently than oligotrophs[61,75] and evidence indicating microbial degradation of PyC[63] challenges the long-standing notion that it is largely resistant to microbial degradation. Consequently, it is still poorly understood how shifting wildfire behavior influences soil microbiome function as related to C cycling and the emergent ecosystem C budget – this is an especially important knowledge gap to address for the important C-rich forest ecosystems of the globe.

1.5 Metagenomics advances our understanding of the post-wildfire soil microbiome

Previous research on the post-wildfire soil microbiome (discussed in ***Section 1.3***) has primarily relied on marker gene sequencing to identify post-wildfire community compositional shifts. However, this approach fails to establish a link between these composition shifts and any impacts to critical emergent ecosystem functions. This work has been complemented by experimental laboratory research with pure cultures of putative pyrophilous taxa that demonstrate their ability to persist in harsh conditions[68] or

degrade PyC[63]. Metagenomic approaches have the potential to bridge the gap between field-based compositional analyses and laboratory studies but, to date, only two studies have applied metagenomic sequencing to soils collected from post-wildfire ecosystems[59,76] to identify functional potential shifts. Neither used genome-resolved metagenomic approaches, or processing metagenomic sequencing to individual metagenome-assembled genomes (MAGs) that represent a group of sequences with similar characteristics (e.g., bacterial taxa within the Actinobacteria), which can link potential pyrophilous traits to taxonomy to support previous laboratory observations. Furthermore, this approach provides insight into the many non-culturable microbes present in soils, facilitating a more comprehensive understanding of soil microbiome function. The coupling of metatranscriptomics with genome-resolved metagenomcs, which has not previously been conducted in post-wildfire soils, holds additional promise for inferring functional shifts associated with changes in gene expression profiles linked to MAGs. Despite notable caveats and critiques[77], these tools offer valuable information on microbial community properties (e.g., encoded genes, transcripts) as well as microbial community membership (i.e., taxonomy) which helps lead to the ultimate goal of predicting impact to microbial processes[78].

1.6 Filling in the post-wildfire soil microbiome timeline of the Colorado Rockies

There remain significant knowledge gaps surrounding the impact of wildfire on the soil microbiomes. As previously mentioned, prior research has failed to establish a direct link between microbial composition and function in real-world field settings. Additionally, studies often lack a comprehensive investigation across various factors such as time,

burn severities, or fail to encompass the entire soil microbiome, including bacteria, fungi, and viruses. My doctoral research aims to address these knowledge gaps by employing a diverse array of tools (e.g., marker gene sequencing, metagenomics, metatranscriptomics, FTICR-MS, soil chemistry) to characterize the post-wildfire soil microbiome in the ecologically significant subalpine forest ecosystems of the Colorado Rocky Mountains (USA; **Figure 1.1**) across time and fire severity. This research effort has spanned 5 years and 640 soil samples from fire-impacted CO coniferous forests, not counting countless others from collaborative side projects near Yellowstone National Park (MT, USA) and in burned beaver wetlands. From these soil samples, I have compiled an extensive multi-omic dataset including 108 metagenomes and 12 metatranscriptomes representing different burn severities (low and high severity) and across time (1-year post-fire to a 60-year chronosequence). These sequencing efforts, totaling nearly 9 Tb of data, have resulted in 1651 metagenome-assembled genomes that span the Actinobacteria (n = 861 MAGs), Proteobacteria (n = 315), Acidobacteria (n = 115), along with 17 other bacterial phyla (**Figure 1.1**). Further, putative pyrophilous taxa from previous studies are represented, including the Actinobacteria Arthrobacter (n = 14) and Blastococcus (n = 11), and Proteobacteria Massilia (n = 9). With this comprehensive dataset, my dissertation research had three key objectives, each detailed in the following three primary research chapters (overviewed in **Figure 1.2**):

1. In **Chapter 2**, published in *Nature Microbiology* in the fall of 2022[79], my objective was to investigate the influence of burn severity on the soil microbiome one year post-fire. This study represents one of the most comprehensive overviews of the post-wildfire soil microbiome to date,

characterizing bacteria, fungi, and viruses using 16S rRNA gene and ITS amplicon sequencing, coupled metagenomics and metatranscriptomics, FTICR-MS, and other soil chemistry analyses.

2. In **Chapter 3**, I utilize soil samples from a chronosequence of wildfire burn scars spanning 1, 3, 5, and 11 years post-fire. Employing genome-resolved metagenomic approaches, my aim was to identify whether pyrophilous traits identified in **Chapter 1** remain relevant a decade after the disturbance. Additionally, I assess whether other microbial ecology trait-based conceptual frameworks apply to the post-wildfire soil microbiome.
3. In my final research chapter, **Chapter 4**, I shift focus to examine whether the soil microbiome is resilient in the face of burning-induced aboveground vegetation shifts over multidecadal timescales. This investigation utilizes a unique set of soil samples representing a chronosequence of burn pile scars ranging from 2 to 6 decades post-burning.

Furthermore, this doctoral research greatly enhances our understanding of the post-wildfire soil microbiome in forest ecosystems and the implications for ecosystem C budgets amid shifting wildfire behavior with climate change.

Chapter 1 Figures

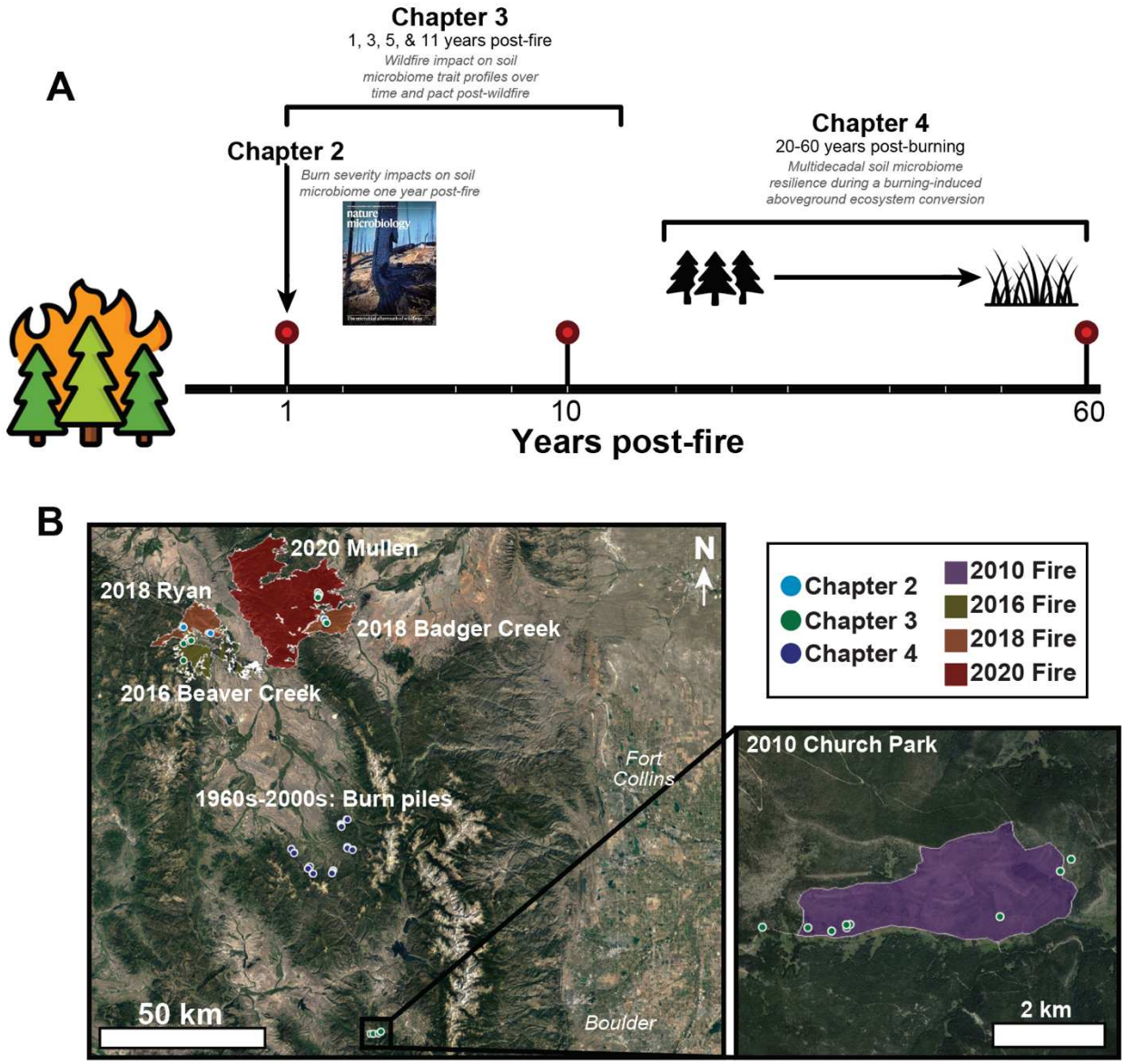

Figure 1.1 (A) Timeline showing where each research chapter falls on the post-fire soil microbial timeline and broadly what the research addresses. (B) Map overviewing soil sample locations for research presented in **Chapter 2, Chapter 3,** and **Chapter 4**.

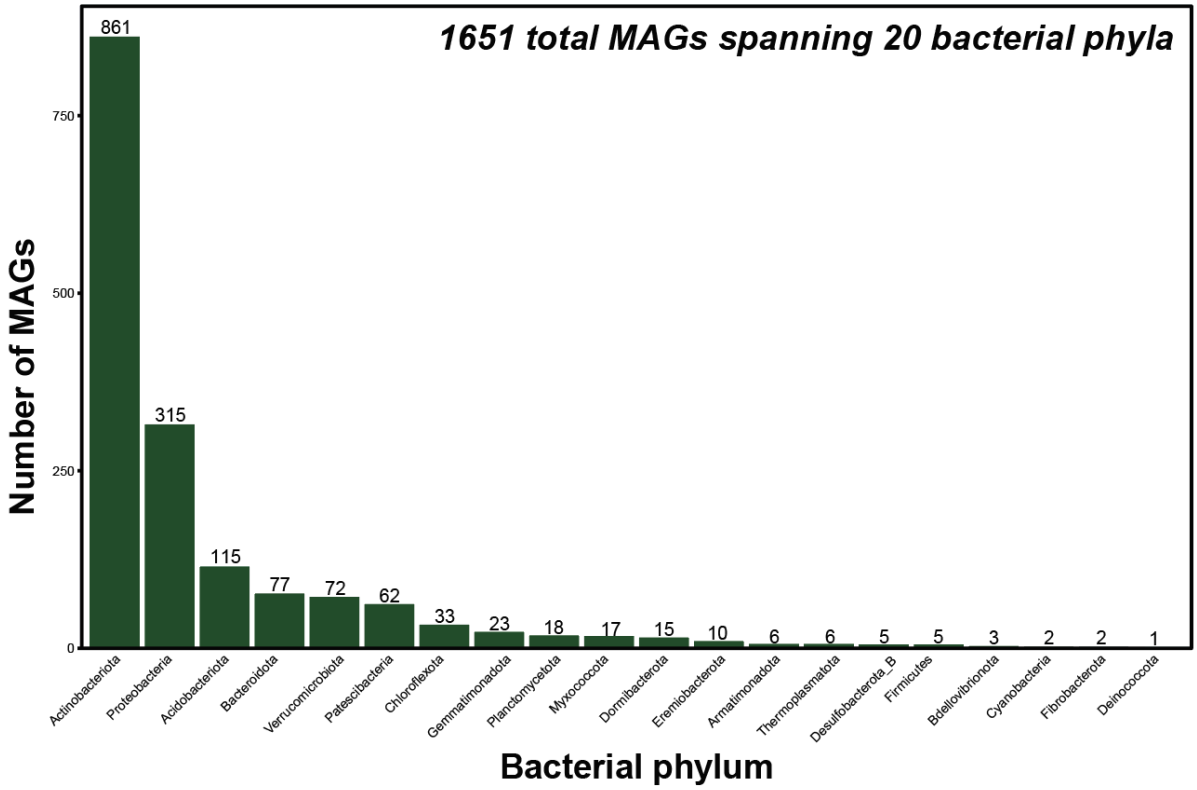

Figure 1.2 Overview of all bacterial MAGs reconstructed from the sequencing efforts carried out for this doctoral research.

Chapter 1 References

1. Aragão, L. E. O. C. *et al.* 21st Century drought-related fires counteract the decline of Amazon deforestation carbon emissions. *Nat. Commun.* **9**, 536 (2018).

2. Parente, J., Pereira, M. G., Amraoui, M. & Fischer, E. M. Heat waves in Portugal: Current regime, changes in future climate and impacts on extreme wildfires. *Sci. Total Environ.* **631–632**, 534–549 (2018).

3. Ruffault, J., Curt, T., Martin-StPaul, N. K., Moron, V. & Trigo, R. M. Extreme wildfire events are linked to global-change-type droughts in the northern Mediterranean. *Nat. Hazards Earth Syst. Sci.* **18**, 847–856 (2018).

4. Rovithakis, A. *et al.* Future climate change impact on wildfire danger over the Mediterranean: the case of Greece. *Environ. Res. Lett.* **17**, 045022 (2022).

5. Dutta, R., Das, A. & Aryal, J. Big data integration shows Australian bush-fire frequency is increasing significantly. *R. Soc. Open Sci.* **3**, 150241 (2016).

6. Bradstock, R. A., Cohn, J. S., Gill, A. M., Bedward, M. & Lucas, C. Prediction of the probability of large fires in the Sydney region of south-eastern Australia using fire weather. *Int. J. Wildland Fire* **18**, 932–943 (2009).

7. Cattau, M. E., Wessman, C., Mahood, A. & Balch, J. K. Anthropogenic and lightning-started fires are becoming larger and more frequent over a longer season length in the U.S.A. *Glob. Ecol. Biogeogr.* **29**, 668–681 (2020).

8. Pausas, J. G. & Keeley, J. E. Wildfires and global change. *Front. Ecol. Environ.* **19**, 387–395 (2021).

9. Allen, C. D. *et al.* ECOLOGICAL RESTORATION OF SOUTHWESTERN PONDEROSA PINE ECOSYSTEMS: A BROAD PERSPECTIVE. *Ecol. Appl.* **12**, (2002).

10. Swetnam, T. W. *et al.* Multiscale perspectives of fire, climate and humans in western North America and the Jemez Mountains, USA. *Philos. Trans. R. Soc. B Biol. Sci.* **371**, 20150168 (2016).

11. Gallardo, M., Gómez, I., Vilar, L., Martínez-Vega, J. & Martín, M. P. Impacts of future land use/land cover on wildfire occurrence in the Madrid region (Spain). *Reg. Environ. Change* **16**, 1047–1061 (2016).

12. Bowman, D. M. J. S. *et al.* Vegetation fires in the Anthropocene. *Nat. Rev. Earth Environ.* **1**, 500–515 (2020).

13. Schoennagel, T., Veblen, T. T. & Romme, W. H. The Interaction of Fire, Fuels, and Climate across Rocky Mountain Forests. *BioScience* **54**, 661–676 (2004).

14. Westerling, A. L. Increasing western US forest wildfire activity: sensitivity to changes in the timing of spring. *Philos. Trans. R. Soc. B Biol. Sci.* **371**, 20150178 (2016).

15. Higuera, P. E. & Abatzoglou, J. T. Record-setting climate enabled the extraordinary 2020 fire season in the western United States. *Glob. Change Biol.* gcb.15388 (2020) doi:10.1111/gcb.15388.

16. Bayham, J., Yoder, J. K., Champ, P. A. & Calkin, D. E. The Economics of Wildfire in the United States. *Annu. Rev. Resour. Econ.* **14**, 379–401 (2022).

17. Kabeshita, L. *et al.* Pathways framework identifies wildfire impacts on agriculture. *Nat. Food* **4**, 664–672 (2023).

18. Pausas, J. G. & Keeley, J. E. Wildfires as an ecosystem service. *Front. Ecol. Environ.* **17**, 289–295 (2019).

19. Certini, G. Effects of fire on properties of forest soils: a review. *Oecologia* **143**, 1–10 (2005).

20. Ebel, B. A. Impacts of Wildfire and Slope Aspect on Soil Temperature in a Mountainous Environment. *Vadose Zone J.* **11**, vzj2012.0017 (2012).

21. Imeson, A. C., Verstraten, J. M., van Mulligen, E. J. & Sevink, J. The effects of fire and water repellency on infiltration and runoff under Mediterranean type forest. *CATENA* **19**, 345–361 (1992).

22. Mataix-Solera, J., Cerdà, A., Arcenegui, V., Jordán, A. & Zavala, L. M. Fire effects on soil aggregation: A review. *Earth-Sci. Rev.* **109**, 44–60 (2011).

23. Hohner, A. K., Rhoades, C. C., Wilkerson, P. & Rosario-ortiz, F. L. Wildfires alter forest watersheds and threaten drinking water quality. *Acc. Chem. Reserach* (2019) doi:10.1021/acs.accounts.8b00670.

24. Dahm, C. N., Candelaria-Ley, R. I., Reale, C. S., Reale, J. K. & Van Horn, D. J. Extreme water quality degradation following a catastrophic forest fire. *Freshw. Biol.* **60**, 2584–2599 (2015).

25. Li, J. *et al.* Spatiotemporal variability of fire effects on soil carbon and nitrogen: A global meta-analysis. *Glob. Change Biol.* gcb.15742 (2021) doi:10.1111/gcb.15742.

26. Adkins, J., Sanderman, J. & Miesel, J. Soil carbon pools and fluxes vary across a burn severity gradient three years after wildfire in Sierra Nevada mixed-conifer forest. *Geoderma* **333**, 10–22 (2019).

27. Wagner, S. *et al.* Questions remain about the biolability of dissolved black carbon along the combustion continuum. *Nat. Commun.* **12**, 4281 (2021).

28. Zhang, Q. *et al.* Temperature Thresholds of Pyrogenic Dissolved Organic Matter in Heating Experiments Simulating Forest Fires. *Environ. Sci. Technol.* **57**, 17291–17301 (2023).

29. Wan, S., Hui, D. & Luo, Y. Fire effects on nitrogen pools and dynamics in terrestrial ecosystems: A meta-analysis. *Ecol. Appl.* **11**, 1349–1365 (2001).

30. Roth, H. K. *et al.* Effects of burn severity on organic nitrogen and carbon chemistry in high-elevation forest soils. *Soil Environ. Health* **1**, 100023 (2023).

31. Rhoades, C. C. *et al.* The Legacy of a Severe Wildfire on Stream Nitrogen and Carbon in Headwater Catchments. *Ecosystems* **22**, 643–657 (2019).

32. Fernández-García, V. *et al.* Impact of burn severity on soil properties in a Pinus pinaster ecosystem immediately after fire. *Int. J. Wildland Fire* **28**, 354 (2019).

33. Dove, N. C., Safford, H. D., Bohlman, G. N., Estes, B. L. & Hart, S. C. High-severity wildfire leads to multi-decadal impacts on soil biogeochemistry in mixed-conifer forests. *Ecol. Appl.* **30**, eap.2072 (2020).

34. Fierer, N. Embracing the unknown: Disentangling the complexities of the soil microbiome. *Nat. Rev. Microbiol.* **15**, 579–590 (2017).

35. Crowther, T. W. *et al.* The global soil community and its influence on biogeochemistry. *Science* **365**, eaav0550 (2019).

36. Wang, B., An, S., Liang, C., Liu, Y. & Kuzyakov, Y. Microbial necromass as the source of soil organic carbon in global ecosystems. *Soil Biol. Biochem.* **162**, 108422 (2021).

37. Wang, C. *et al.* Large-scale importance of microbial carbon use efficiency and necromass to soil organic carbon. *Glob. Change Biol.* **27**, 2039–2048 (2021).

38. van der Heijden, M. G. A., Bardgett, R. D. & van Straalen, N. M. The unseen majority: soil microbes as drivers of plant diversity and productivity in terrestrial ecosystems. *Ecol. Lett.* **11**, 296–310 (2008).

39. Anthony, M. A. *et al.* Forest tree growth is linked to mycorrhizal fungal composition and function across Europe. *ISME J.* 1–10 (2022) doi:10.1038/s41396-021-01159-7.

40. Pressler, Y., Moore, J. C. & Cotrufo, M. F. Belowground community responses to fire: meta-analysis reveals contrasting responses of soil microorganisms and mesofauna. *Oikos* **128**, 309–327 (2019).

41. Dove, N. C. & Hart, S. C. Fire reduces fungal species richness and in situ mycorrhizal colonization: A meta-analysis. *Fire Ecol.* **13**, 37–65 (2017).

42. Neary, D. G., Klopatek, C. C., DeBano, L. F. & Ffolliott, P. F. Fire effects on belowground sustainability: a review and synthesis. *For. Ecol. Manag.* **122**, 51–71 (1999).

43. Sáenz de Miera, L. E., Pinto, R., Gutierrez-Gonzalez, J. J., Calvo, L. & Ansola, G. Wildfire effects on diversity and composition in soil bacterial communities. *Sci. Total Environ.* **726**, 138636 (2020).

44. Ammitzboll, H., Jordan, G. J., Baker, S. C., Freeman, J. & Bissett, A. Diversity and abundance of soil microbial communities decline, and community compositions change with severity of post-logging fire. *Mol. Ecol.* mec.15900 (2021) doi:10.1111/mec.15900.

45. Caiafa, M. V. *et al.* Distinct fungal and bacterial responses to fire severity and soil depth across a ten-year wildfire chronosequence in beetle-killed lodgepole pine forests. *For. Ecol. Manag.* **544**, 121160 (2023).

46. Weber, C. F., Lockhart, J. S., Charaska, E., Aho, K. & Lohse, K. A. Bacterial composition of soils in ponderosa pine and mixed conifer forests exposed to different wildfire burn severity. *Soil Biol. Biochem.* **69**, 242–250 (2014).

47. Pulido-Chavez, M. F., Alvarado, E. C., DeLuca, T. H., Edmonds, R. L. & Glassman, S. I. High-severity wildfire reduces richness and alters composition of ectomycorrhizal fungi in low-severity adapted ponderosa pine forests. *For. Ecol. Manag.* **485**, 118923 (2021).

48. Fox, S. *et al.* Fire as a driver of fungal diversity — A synthesis of current knowledge. *Mycologia* 1–27 (2022) doi:10.1080/00275514.2021.2024422.

49. Pulido-Chavez, M. F. *et al.* Rapid bacterial and fungal successional dynamics in first year after chaparral wildfire. *Mol. Ecol.* **32**, 1685–1707 (2023).

50. Whitman, T. *et al.* Soil bacterial and fungal response to wildfires in the Canadian boreal forest across a burn severity gradient. *Soil Biol. Biochem.* **138**, 107571 (2019).

51. Lucas-Borja, M. E. *et al.* Immediate fire-induced changes in soil microbial community composition in an outdoor experimental controlled system. *Sci. Total Environ.* **696**, (2019).

52. Glassman, S. I. *et al.* Prescribed versus wildfire impacts on exotic plants and soil microbes in California grasslands. *Appl. Soil Ecol.* **185**, 104795 (2023).

53. Whitman, T., Woolet, J., Sikora, M., Johnson, D. B. & Whitman, Ellen. Resilience in soil bacterial communities of the boreal forest from one to five years after wildfire

across a severity gradient | Elsevier Enhanced Reader. *Soil Biol. Biochem.* 108755 (2022) doi:10.1016/j.soilbio.2022.108755.

54. Xiang, X. *et al.* Rapid recovery of soil bacterial communities after wildfire in a Chinese boreal forest. *Sci. Rep.* **4**, 3829 (2015).

55. Sun, H. *et al.* Bacterial community structure and function shift across a northern boreal forest fire chronosequence. *Sci. Rep.* **6**, 32411 (2016).

56. Barbour, K. M., Weihe, C., Walters, K. E. & Martiny, J. B. H. Testing the contribution of dispersal to microbial succession following a wildfire. *mSystems* **0**, e00579-23 (2023).

57. Cobo-Díaz, J. F. *et al.* Metagenomic Assessment of the Potential Microbial Nitrogen Pathways in the Rhizosphere of a Mediterranean Forest After a Wildfire. *Microb. Ecol.* **69**, 895–904 (2015).

58. Fernández-González, A. J. *et al.* The rhizosphere microbiome of burned holm-oak: potential role of the genus Arthrobacter in the recovery of burned soils. *Sci. Rep.* **7**, 6008 (2017).

59. Dove, N. C., Taş, N. & Hart, S. C. Ecological and genomic responses of soil microbiomes to high-severity wildfire: linking community assembly to functional potential. *ISME J.* **16**, 1853–1863 (2022).

60. Johnson, D. B., Woolet, J., Yedinak, K. M. & Whitman, T. Experimentally determined traits shape bacterial community composition one and five years following wildfire. *Nat. Ecol. Evol.* **7**, 1419–1431 (2023).

61. Adkins, J., Docherty, K. M. & Miesel, J. R. Copiotrophic Bacterial Traits Increase With Burn Severity One Year After a Wildfire. *Front. For. Glob. Change* **5**, (2022).

62. Bruns, T. D., Chung, J. A., Carver, A. A. & Glassman, S. I. A simple pyrocosm for studying soil microbial response to fire reveals a rapid, massive response by Pyronema species. *PLOS ONE* **15**, e0222691 (2020).

63. Fischer, M. S. *et al.* Pyrolyzed Substrates Induce Aromatic Compound Metabolism in the Post-fire Fungus, Pyronema domesticum. *Front. Microbiol.* **12**, (2021).

64. Arora, P. K. & Sharma, A. New metabolic pathway for degradation of 2-nitrobenzoate by Arthrobacter sp. SPG. *Front. Microbiol.* **06**, 1–6 (2015).

65. Gkorezis, P. *et al.* Draft Genome Sequence of Arthrobacter sp. Strain SPG23, a Hydrocarbon-Degrading and Plant Growth-Promoting Soil Bacterium. *Genome Announc.* **3**, 14–15 (2015).

66. Westerberg, K., Elväng, A. M., Stackebrandt, E. & Jansson, J. K. Arthrobacter chlorophenolicus sp. nov., a new species capable of degrading high concentrations of 4-chlorophenol. *Int. J. Syst. Evol. Microbiol.* **50**, 2083–2092 (2000).

67. Mongodin, E. F. *et al.* Secrets of soil survival revealed by the genome sequence of Arthrobacter aurescens TC1. *PLoS Genet.* **2**, 2094–2106 (2006).

68. Dsouza, M., Taylor, M. W., Turner, S. J. & Aislabie, J. Genomic and phenotypic insights into the ecology of Arthrobacter from Antarctic soils. *BMC Genomics* **16**, 36 (2015).

69. Harris, N. L. *et al.* Global maps of twenty-first century forest carbon fluxes. *Nat. Clim. Change* **11**, 234–240 (2021).

70. Coop, J. D. *et al.* Wildfire-Driven Forest Conversion in Western North American Landscapes. *BioScience* **XX**, 1–15 (2020).

71. Pingree, M. R. A. & DeLuca, T. H. Function of Wildfire-Deposited Pyrogenic Carbon in Terrestrial Ecosystems. *Front. Environ. Sci.* **5**, 1–7 (2017).

72. Flanagan, N. E., Wang, H., Winton, S. & Richardson, C. J. Low-severity fire as a mechanism of organic matter protection in global peatlands: Thermal alteration slows decomposition. *Glob. Change Biol.* **26**, 3930–3946 (2020).

73. Adkins, J. & Miesel, J. R. Post-fire effects of soil heating intensity and pyrogenic organic matter on microbial anabolism. *Biogeochemistry* **154**, 555–571 (2021).

74. Bostick, K. W. *et al.* Biolability of Fresh and Photodegraded Pyrogenic Dissolved Organic Matter From Laboratory-Prepared Chars. *J. Geophys. Res. Biogeosciences* **126**, e2020JG005981 (2021).

75. Roller, B. R. K. & Schmidt, T. M. The physiology and ecological implications of efficient growth. *ISME J.* **9**, 1481–1487 (2015).

76. Tas, N. *et al.* Impact of fire on active layer and permafrost microbial communities and metagenomes in an upland Alaskan boreal forest. *ISME J.* 1904–1919 (2014) doi:10.1038/ismej.2014.36.

77. Jansson, J. K. & Hofmockel, K. S. The soil microbiome — from metagenomics to metaphenomics. *Curr. Opin. Microbiol.* **43**, 162–168 (2018).

78. Hall, E. K. *et al.* Understanding how microbiomes influence the systems they inhabit. *Nat. Microbiol.* **3**, 977–982 (2018).

79. Nelson, A. R. *et al.* Wildfire-dependent changes in soil microbiome diversity and function. *Nat. Microbiol.* **7**, 1419–1430 (2022).

Chapter 2: Wildfire-dependent changes in soil microbiome diversity and function[1]

2.1 Summary

Forest soil microbiomes have crucial roles in carbon storage, biogeochemical cycling, and rhizosphere processes. Wildfire season length, and the frequency and size of severe fires, have increased owing to climate change. Fires affect ecosystem recovery and may modify soil microbiomes and microbially-mediated biogeochemical processes. To study wildfire-dependent changes in soil microbiomes, we characterized functional shifts in the soil microbiota (bacteria, fungi, and viruses) across burn severity gradients (low, moderate, and high severity) one-year post-fire in coniferous forests in Colorado and Wyoming, USA. We found severity-dependent increases of Actinobacteria encoding genes for heat resistance, fast growth and pyrogenic carbon utilization that might enhance post-fire survival. We report that increased burn severity led to the loss of ectomycorrhizal fungi and less tolerant microbial taxa. Viruses remained active in post-fire soils, and likely influenced carbon cycling and biogeochemistry via turnover of biomass and ecosystem-relevant auxiliary metabolic genes. Our genome-resolved analyses link post-fire soil microbial taxonomy to functions and reveal the complexity of post-fire soil microbiome activity.

[1] This chapter was reproduced verbatim from "Nelson et al. Wildfire-dependent changes in soil microbiome and diversity. Nature Microbiology (2022)". The text benefitted from writing and editing contributions from contributing authors and reviewers selected by the publisher. The ordering of the materials in this dissertation are consistent with the content available online but have been renumbered to reflect incorporation into this dissertation.

2.2 Introduction

Changes in climate coupled with the effects of long-term fire suppression and shifting land use patterns have increased the frequency, severity, and season length of wildfires in the western US[1–3]. In 2020 and 2021, the western US experienced severe, record-breaking wildfires[2]. High severity wildfires cause greater erosion[4], soil carbon (C) and nitrogen (N) losses[5], and nutrient and sediment export in stream water[6], so the increasing occurrence of severe wildfires may have important consequences for both terrestrial and aquatic ecosystems. Shifting wildfire patterns have also been linked to slow post-fire revegetation and tree seedling recruitment[7] and thus delayed watershed recovery[8] in western US forests. Although ecosystem recovery from severe wildfires is closely linked to belowground biological processes, little is known about the impact of high severity fire on soil microbiome function in high elevation, coniferous ecosystems.

The soil microbiome regulates soil organic matter (SOM) decomposition and stabilization[9], soil nutrient dynamics[10], and rhizosphere function[11]. During wildfires, the soil microbiome can be impacted immediately by the loss of heat-sensitive taxa and after by lasting changes in soil chemistry and vegetation shifts[12]. Wildfires reduce soil microbial biomass and community diversity in numerous ecosystems[13–16] and such changes likely influence and inhibit post-fire plant recovery[17].

Post-fire shifts in soil microbiome composition[14,18,19] and assembly processes[20–22] are relatively well-characterized across different ecosystems, with some studies explicitly linked with corresponding shifts in microbially-mediated C and N cycling[23–26]. This work has been complemented by laboratory studies with pure cultures of pyrophilous taxa that demonstrate their ability to persist during stressful conditions[27,28] and utilize aromatic C[29–

[32]. Metagenomic approaches can bridge insights between field-based compositional analyses and more controlled laboratory studies. To date, two studies have applied gene-resolved metagenomic analyses to post-fire soils[23,33]. Genome-resolved metagenomic tools can link potential pyrophilous traits (e.g., fast growth rate, heat resistance) to specific organisms that thrive in burned soils and support laboratory observations[34]. Furthermore, this approach enables a broader understanding of microbiome function, through identification of co-occurring functional traits, potential interspecies interactions, and viral-host dynamics.

Here, we bridge laboratory studies and field-based compositional investigations through a genome-resolved multi-omic approach to characterize wildfire impacts on soil microbiome function. Furthermore, the work represents a holistic understanding of the post-fire soil microbiome, including comprehensive characterization of interacting bacterial, fungal, and viral communities. We studied burn severity gradients in two recent forest wildfires to characterize how fire severity influences C composition and the intimately connected soil microbiome. We hypothesized that higher severity wildfire results in an increasingly altered soil microbiome and that taxa colonizing burned soils would encode functional traits that favor their persistence. These analyses advance the understanding of linkages between the soil microbiome and post-fire forest biogeochemistry.

2.3 Results & Discussion

2.3.1 Fire decreases soil microbiome diversity and shifts composition

Near surface soils (0-5 cm depth) were collected approximately one-year post-fire from four burn severity gradient transects (control, low, moderate, and high burn severity)

at two wildfires that occurred in 2018 along the Colorado-Wyoming border. Bacterial and fungal communities were profiled using marker gene analyses, while a subset of twelve samples (low or high severity-impacted Ryan fire soils) were additionally interrogated with metagenomic and metatranscriptomic sequencing. Bacterial and fungal communities were significantly different between burned (*n*=144) and unburned (*n*=32) soils (bacterial ANOSIM R=0.57, p<0.05; fungal ANOSIM R=0.72, p<0.05) (**Figure 2.1**).

While shifts in community composition with burn were observed in both surface (0-5 cm) and deep (5-10 cm) soils (**Figure 2.2**), surface soils were impacted to a greater extent. Microbial diversity generally decreased with increasing severity in surface soils, although differences between moderate and high severity were statistically indistinct (**Figure 2.3**). Similarly, as fungal and bacterial diversity decreased with burn severity, beta dispersion ('distance to centroid') calculations revealed increasingly similar bacterial communities (**Figure 2.4**) with less complex community structures (via WGCNA; **Table 2.1**). These shifts resulted in significant dissimilarity between microbial communities in surface soils impacted by either low (*n*=24) and high (*n*=24) severity wildfire (bacterial ANOSIM R=0.15, p<0.05; fungal ANOSIM R=0.25, p<0.05). In contrast, deep soils displayed an opposite effect, with increasing beta dispersion after wildfire signifying greater bacterial community dissimilarity (**Figure 2.4**). Stochastic community shifts in deep soils may follow wildfire, potentially due to spatially heterogeneous changes in soil chemistry and nutrient availability. Combined amplicon sequencing data analyses highlight the susceptibility of surface soils to wildfire, resulting in less diverse and inter-connected microbial communities. In contrast, the microbiome in deep soil displays a

more muted response to wildfire, potentially due to insulation from soil heating (dependent on soil moisture).

2.3.2 Microbiome community compositional shifts with burn

Reflecting observations from prior studies[3–6], bacterial communities in burned soils were characterized by lower diversity and were enriched in Actinobacteria and Bacteroidetes relative to unburned controls (**Figure 2.2**). The Actinobacteria genera *Arthrobacter, Modestobacter, Blastococcus, and Actinomadura* had the largest increases in relative abundance in burned soils relative to control soils and were discriminant taxa for burned soils. The diversity of fungal communities in surface soils also decreased with fire (**Figure 2.3**) and, similar to previous studies[7–9], shifted from Basidiomycete- to Ascomycete-dominated with the Basidiomycota relative abundance decreasing by ~58% (**Figure 2.2**). Discriminant fungal taxa included ASVs from the *Sordariomycetes*, *Saccharomycetes*, and *Dothideomycetes*, taxa also found in previous fire studies[6,9].

The pyrophilous *Ascomycetes* increased in relative abundance by 118% between unburned and burned surface soils (~34% to 75%; **Figure 2.2**); dominant genera included *Calyptrozyma* (~30% relative abundance in burned surface soil), *Tricharina* (~13%), and *Geopyxis* (~7%). *Geopyxis* has been previously documented as a pyrophilous taxa and is identified as an endophyte, which would aid in their persistence through the fire event and proliferation thereafter[10,11]. The two most abundant *Ascomycete* orders in burned surface soils were *Helotiales* (~31% relative abundance), which have been found in other post-fire soils [12,13] and lab pyrocosm experiments[14] and *Pezizales* (~28%), which is a common post-fire soil taxa[7,8,15] known for producing resistant structures like spores[16]. The second most dominant *Ascomycetes* family *Pyronemataceae* (~21% relative abundance

in burned surface soil) has been found to grow in soils heated in the laboratory to 70°C, to increase in forest soil samples post-fire, and to readily degrade aromatic compounds in the presence of pyrolyzed OM[8,17]. The *Ascomycotes* displayed a higher fire tolerance than the *Basidiomycota*, which had a decrease in relative abundance by ~58% between unburned and burned surface soils, dropping from 50% to 21% relative abundance (**Figure 2.2**).

2.3.3 Soil chemistry shifts across burn severity and depth

Similar to the microbial data, we found that wildfire had a greater effect on surface soil chemistry (**Appendix A**). Surface soil pH was 7.8 on average in moderate and high severity plots; both were significantly higher than unburned samples (average pH of 7.2; pairwise t-test, $p<0.05$). Total soil C was significantly lower in the high/moderate (3.3%) than the low (13.3%) and unburned surface soils (15.7%) (pairwise t-test; all burn severity comparisons $p<0.05$). Interestingly, there were no significant changes in DOC, NH_4-N, NO_3-N, or %N, potentially because of small sample sizes. Average DOC was 148 mg/L in control plots, compared to 131, 58 and 43 mg/L in low, moderate, and high severity plots, respectively, though the pattern was not statistically significant. Only NH_4-N had significant changes in deep samples, with significantly higher concentrations in burned (average 0.76 mg/L) vs. unburned (0.19 mg/L) samples (pairwise t-test; $p<0.05$).

2.3.4 A comprehensive dataset from fire-impacted soils

While myriad studies have reported changes in microbial community membership following wildfire[14,18,35], the functional implications of these shifts are difficult to infer from compositional data. We used genome-resolved metagenomics to generate a

comprehensive, publicly accessible catalog of post-fire bacterial, fungal, and viral genomes from coniferous forest soils. From metagenomic sequencing of burned (low and high severity) soils we reconstructed 637 medium- and high-quality bacterial metagenome assembled genomes (MAGs) (**Figure 2.5**) that represent taxa shown to increase following wildfire in complementary 16S rRNA gene sequencing data (e.g., *Blastococcus*, *Arthrobacter*;). The dataset spans 21 phyla and encompasses 237 MAGs from taxa within the Actinobacteria, 167 from the Proteobacteria, 62 from the Bacteroidota, and 52 from the Patescibacteria. Furthermore, we recovered 2 fungal genomes from the Ascomycota, affiliated with *Leotiomycetes* and *Coniochaeata lignaria*. We additionally recovered 2,399 DNA and 91 RNA viral populations (vMAGs) (**Appendix A**).

2.3.5 Actinobacteria respond strongly to high severity wildfire

Based on consistent high relative abundances across surface soils impacted by high severity wildfire ('High S') that mirrored 16S rRNA gene data, forty MAGs were selected for further genomic analyses. Combined, these MAGs accounted for an average relative abundance of ~60% in High S samples and ~34% in low severity-impacted surface soils ('Low S'), and collectively represent the most abundant MAGs responding to altered soil conditions, one-year post-wildfire. Metatranscriptomic read mapping revealed activity of these MAGs in High S samples, accounting for an average of ~50% of total gene expression and 90% of differentially expressed genes in High S vs Low S soils (**Appendix A**). These MAGs were also active in Low S samples, albeit to a lesser extent (accounting for ~30% of gene expression). Most of these MAGs (28 of 40) were affiliated with the Actinobacteria phyla, specifically the genera *Arthrobacter* (8 MAGs),

Blastococcus (5), and *SCTD01* (5) (**Appendix A**). Ten of these MAGs (**Appendix A**), including 9 Actinobacteria, were significantly enriched in High S relative to Low S samples (pairwise t-test, $p < 0.05$; **Figure 2.6**), indicating a positive response one year following high severity wildfire. In general, Actinobacteria dominated the microbiome in burned surficial soils; all 237 Actinobacteria MAGs were responsible for ~56% of gene expression in High S samples and ~47% in Low S samples. Dominant MAGs in high severity-impacted deep samples ('High D') were more diverse (representing Actinobacteria, Eremiobacterota, Acidobacteriota, and Proteobacteria), reflecting the likely more heterogeneous impact of wildfire on deeper soils.

The heat produced during wildfire exerts a pulse disturbance on soils and as such the relative abundance of two groups of thermal resistance genes, sporulation and heat shock, increased significantly (Welch's t-test, $p < 0.05$) from Low S to High S soils (42.8% and 20.4% increase, respectively). Nearly all the aforementioned MAGs (38/40) encoded sporulation genes, indicating that spore formation is likely a trait supporting survival and post-fire colonization. Many genomes (31/40) encoded heat shock proteins and molecular chaperones to further facilitate thermal resistance. In 16 MAGs, thermal resistance was complimented by genes for mycothiol biosysnthesis, a compound produced by Actinobacteria that aids in oxidative stress tolerance[36]. Genes for osmoprotectant (trehalose, *otsAB*, *treZY*[37]; glycine betaine, *betAB*[38]) synthesis were widespread among these 40 MAGs (17 and 38 MAGs encoded trehalose and glycine betaine synthesis genes, respectively), which could facilitate cell viability under low soil moisture conditions post-fire. We recognize that many well-studied soil taxa encode genes for similar traits, but note that combinations of these traits is likely an emergent property of fire disturbance

supporting post-fire dominance of these taxa. Further, MAGs recovered from High S samples also had significantly higher guanine-cytosine (GC) content, which has been linked to thermal stability[39,40], than MAGs from fire-impacted deeper soils (**Figure 2.7**; pairwise t-test, $p<0.05$). The lysing of microorganisms during soil heating represents sources of labile organic C and N associated with necromass[41]. All 40 featured MAGs expressed peptidase genes (2721 total) in High S soils, of which approximately 41 were differentially expressed ($p<0.05$) between High S vs Low S samples. These included genes responsible for peptidoglycan degradation (component of bacterial cell walls), suggesting that taxa enriched post-fire actively utilize microbial necromass.

The ability to grow quickly and occupy newly available niches is likely a key trait for microorganisms colonizing or growing in burned soils[18,42]. We inferred maximum growth rates using codon usage bias (CUB) across our bacterial MAGs to determine whether colonizing taxa encoded the potential for rapid growth[43,44] (**Appendix A**). After removal of MAGs with doubling times >5 hours due to model inaccuracies at slower growth rates[43], the average doubling time within our MAG dataset was ~3.2 hours. Twenty-two of the 40 MAGs of interest in High S samples had doubling times faster than the dataset average (ranging from ~0.3 to 4.7 hours). Further, there was a significant negative correlation (Spearman's $\rho = -0.18$, $p<0.05$) between MAG relative abundance in High S samples and growth rate, indicating that High S conditions may select for microorganisms that can grow quickly (**Figure 2.8**). These insights suggest that abundant bacteria sampled one-year post-wildfire occupied niches in the immediate aftermath of wildfire through strategies likely including rapid growth. In contrast, these patterns were absent from MAGs recovered from other conditions (**Figure 2.8**). Emphasizing the

importance of fast growth for colonizing severely burned soils, only 19 MAGs from High S samples had growth rates too slow to accurately estimate (249 MAGs with growth rates >5 hours). To determine whether these same microorganisms were growing rapidly at the time of sampling (one-year post-wildfire), we investigated gene expression associated with rapid growth[45,46] (ribosomes, central metabolism) through MAG abundance-normalized transcripts (**Appendix A**). Results suggested diminished growth rates for the dominant High S bacteria at time of sampling, relative to other Actinobacteria MAGs that were highly expressing ribosomal and TCA cycle genes in High S samples. Together, these analyses indicate that potential rapid growth could enable these microorganisms to occupy free niche space in soil immediately following wildfire, but this strategy may not be maintained once those niches are filled.

2.3.6 Deeper burned soils are dominated by distinct microbial membership

Only 13 MAGs had an average relative abundance > 0.5% and a standard deviation less than the average relative abundance in High D soils, as compared to the 40 MAGs in High S. This is likely due to the heterogeneity of wildfire impact on deep soils as compared to the homogenizing influence wildfire has on surface soils. These 13 MAGs were affiliated with Actinobacteria, Eremiobacterota, Acidobacteriota, and Proteobacteria (**Appendix A**). Like the surface soil, the Actinobacteria dominated, with 10/13 of the MAGs being Actinobacteria, representing the genera *Streptomyces*, *SCTD01*, and *Palsa-744*. These 13 MAGs accounted for ~18% of the High D community composition, and 14.3% of total MAG gene expression. The 13 MAGs were also active in Low D samples, albeit to a lesser extent (accounting for ~5% of total expression). Of these 13 MAGs, there were two (RYN_267, RYN_347) that were significantly enriched (pairwise t-test; $p < 0.05$)

in High D relative to Low D conditions, representing the Actinobacteria and Eremiobacterota.

Genes associated with thermal resistance were again common in the dominant High D MAGs. Four of these MAGs (R110.16, R86.130, R86.18, R94.45) had metabolic potential to synthesize the environmental stress protectant mycothiol[18]. All MAGs discussed here encoded at least one sporulation gene, and one of the MAGs (RYN_220) was affiliated with the *Streptomyces* which have been shown to form sporogenic structures (aerial hyphae) in response to adverse conditions (i.e., high temperatures, nutrient depletion)[19]. These stress response traits, common to the *Streptomyces*, likely facilitate their dominance on soils one year following high severity wildfire.

Associated with the enrichment (16S data: 155% relative abundance increase from control to High D) and activity of *Streptomyces* in High D samples, we observed high expression of genes encoding the biosynthesis of cobalamin (vitamin B12, *cob* genes), an important coenzyme involved in gene regulation and the synthesis of nucleotides and amino acids. Cobalamin production is conserved within a relatively small group of microorganisms – including *Streptomyces* – and can serve as a keystone function within ecosystems[20]. The entire aerobic cobalamin biosynthesis pathway was expressed in Low D and High D samples (**Figure 2.9**; pathway adapted[20,21]). Here, a *Streptomyces* MAG (RYN_220) was responsible for 13% of MAG gene expression linked to cobalamin biosynthesis in High D samples. In total, the MAGs mentioned above were responsible for nearly 35% of the total cobalamin biosynthesis MAG gene expression in High D samples. These observations contrast directly with High S samples; the general absence of *Streptomyces* in these samples resulted in limited expression of this pathway.

Cobalamin biosynthesis gene expression was ~175% greater in High D samples, and 2 of the aforementioned MAGs (RYN_225, RYN_347) differentially expressed *cobN* and *btuB* (cobalamin transporter gene) in High D samples relative to High S. In the deep soil, the increased transcription of genes for cobalamin synthesis could be a beneficial consequence of wildfire enriching taxa that encode this trait (i.e., *Streptomyces*). Given the noted importance of this cofactor in mediating a range of critical soil microbiome functions, this process could potentially aid in plant reestablishment[22] and enhance ecosystem function across trophic levels[23].

2.3.7 Broad functional shifts with burn severity

To analyze broad shifts in functional potential and gene expression between Low and high severity conditions within both soil depths, we categorized genes using DRAM gene headers. There were 885,498 genes annotated with DRAM in the metagenomic dataset and 146,894 transcripts annotated with DRAM that had counts of at least 10 across all 12 samples. A DESeq2 analysis of the DRAM-annotated transcripts revealed 352 differentially expressed genes between Low S and High S samples and 26 between Low D and High D samples (**Appendix A**). Most of the differential expression in High S and High D was attributed to the Actinobacteria phyla (97.9% and 50% of differentially expressed genes, respectively). There were genera and family-level differences between the activity in both soil depths, with *Actinobacteriota* genera *Blastococcus* (69.1%), *SCTD01* (10.4%) *Arthrobacter* (4.8%) and *Modestobacter* (2.7%) as the large players in High S and the family *Streptosporangiaceae* (35%) being the biggest player in High D. Outside of the *Actinobacteriota* phylum, the *Proteobacteria* genus *Palsa-1478* was responsible for 45% of differentially expressed genes in High D samples. Thus, the

metatranscriptomics data additionally reflects the increased susceptibility of surface soil to fire relative to deep soils.

There was a large change in broad functional potential between Low S and High S samples; of the 28 DRAM gene headers analyzed, 22 were significantly different in coverage between the severity conditions (**Figure 2.10**). Though there is a large shift in microbiome functional potential, the metatranscriptomics data reveals that there is less of a change in gene expression between Low S and High S conditions, exhibiting potential functional redundancy. Thirteen DRAM gene headers have differentially expressed genes, and 7 of these were genes only differentially expressed in high severity conditions (**Figure 2.10**). In total, there were 288 genes differentially expressed in High S and 64 genes differentially expressed in Low S. Reflecting the large role of *Actinobacteriota* in high severity-impacted soils mentioned above, the majority of differentially expressed genes in High S were from the *Actinobacteriota* phyla (97.9% of differentially expressed genes). Specifically, the *Actinobacteriota* genera *Blastococcus* (69.1%), *SCTD01* (10.4%) *Arthrobacter* (4.8%) and *Modestobacter* (2.7%)

Contrastingly, the microbiome of deep soils exhibited a much smaller shift in functional potential with only 4/28 DRAM gene headers having a significant change in coverage between Low D and High D (peptidase, information systems, CAZY, and CRISPR; **Figure 2.10**). There was also little change in gene expression; there were 6 DRAM headers (26 total genes) with differentially expressed genes, 20 that were differentially expressed in High D and 6 in Low D (**Figure 2.10**). The *Actinobacteriota* phyla was responsible for the largest proportion of differentially expressed genes following high-severity fire (50%) and the family *Streptosporangiaceae* and was

responsible for 35% of the differentially expressed genes. The *Proteobacteria* genera *Palsa-1478* was also responsible for a large amount of differentially expressed genes (45%).

2.3.8 Actinobacteria process pyrogenic organic matter

During wildfire, SOM may be transformed to increasingly aromatic molecular structures that are commonly considered less available for microbial utilization[47]. Similar to other studies[48], mass spectrometry analyses of DOM revealed severity-dependent aromaticity increases in surface soils one year post-fire (**Figure 2.11**). These aromaticity index trends were absent in DOM from more insulated deep soils (**Figure 2.12**). Low severity wildfire drives an increase in DOM aromaticity but also an accumulation of other unique compounds likely from incomplete combustion of SOM[49,50], whereas moderate and high severity wildfire in surface soils resulted in formation of unique aromatic organic compounds (**Figure 2.11**). The microbial transformation of these compounds is constrained by solubility and thermodynamic thresholds established by available electron acceptors[51] (e.g., oxygen). To estimate the potential thermodynamic favorability of this DOM, we calculated the Nominal Oxidation State of Carbon (NOSC); higher NOSC values theoretically yield a lower ΔG_{Cox} (i.e., more favorable) when coupled to reduction of an electron acceptor[52]. Unique formulas in High S samples had significantly higher NOSC values, indicating increasing thermodynamic favorability for oxidation of DOM following severe wildfire (**Figure 2.11**; pairwise t-test, $p<0.05$). Thus, thermodynamic limitations likely do not influence the lability of pyrogenic DOM in this system and other factors such as solubility or microbial community function likely govern compound processing.

We focused on microbial processing of catechol and protocatechuate, two intermediate products formed during aerobic degradation of diverse aromatic compounds[53]. The genomic potential for these reactions was present across severities and soil depths, and was dominated by Actinobacteria and Proteobacteria (**Figure 2.13**); 80 and 226 MAGs encoded >50% of the catechol and protocatechuate ortho-cleavage pathways, respectively, including most of the featured High S and High D MAGs (**Figure 2.13**). Meta-cleavage pathways were also broadly represented within the MAGs (**Figure 2.14**). In High S samples, the *Arthrobacter* MAG RYN_101 alone was responsible for ~44% of *catA* (catechol 1,2-dioxygenase) gene expression, and therefore likely plays a key role in catechol degradation. Contrastingly, in High D samples, the *Streptosporangiaceae* MAG RYN_225 was responsible for ~46% and 23% of expression of *pcaGH* (protocatechuate 3,4-dioxygenase) and *pcaC* (4-carboxymuconolactone decarboxylase) that catalyzes protocatechuate degradation (**Figure 2.13**). However, no MAGs of interest from High S or High D samples encoded the entire catechol or protocatechuate ortho-cleavage pathway (**Figure 2.13**), indicating that metabolic handoffs between community members are likely important for complete compound degradation. Outside of catechol and protocatechuate, there was genomic evidence for the benzoyl-CoA and phenylacetyl-CoA oxidation pathways (**Figure 2.15**). These data indicate that post-fire soils support microbiomes that actively degrade some fire-derived aromatic compounds and has implications for C storage in wildfire-impacted ecosystems, since pyrogenic C compounds are considered largely resistant to decay and contribute to C storage[54]. Further work should integrate multi-omics data from field and laboratory studies into ecosystem models to refine the quantification of post-fire C fluxes.

2.3.9 Viruses impact burned soil microbiome structure and function

We recovered 2399 distinct DNA and 91 distinct RNA viral populations (vMAGs) from the metagenomic and metatranscriptomic assemblies. Of these, 945 were previously undescribed (only clustering with other vMAGs from this study) and 92 were taxonomically assigned, with the majority (*n*=86) within the *Caudovirales* order (**Appendix A**). DNA and RNA viral communities mirrored beta diversity trends observed in bacterial and fungal communities; those in deep soils were less homogenous compared to communities in surface soils, further highlighting the homogenizing influence of wildfire (**Figure 2.16**). Additionally, although DNA and RNA viral community composition was indistinct between low and high severity-impacted soils (ANOSIM R=0.007 and -0.12, respectively; $p > 0.1$), we did measure significant differences between the two soil depths (ANOSIM R=0.59 and 0.57, respectively; $p<0.05$).

Given the importance of viral activity on soil microbiomes[55], we identified potential virus-host linkages that could offer insights into how viruses target bacteria. Many abundant and active MAGs (*n*=94) – including 32 from the Actinobacteria – encoded CRISPR-Cas arrays with an average of ~18 spacers (max 210 spacers; **Appendix A**). By matching CRISPR spacers to protospacers in vMAGs, we linked 9 vMAGs with 4 bacterial hosts (RYN_115, RYN_242, RYN_436, RYN_542) from the Actinobacteria, Planctomycetota, and Proteobacteria. While each of these MAGs were active (expressing transcripts), the RYN_242 MAG (*Solirubrobacteraceae*) was among the top 3% most active MAGs across all conditions, suggesting that viruses are targeting active bacteria. We expanded upon potential virus-host linkages using VirHostMatcher[56] (d_2^* value < 0.25), revealing higher numbers of viral linkages with more abundant host MAGs (**Figure**

2.17). For example, the High S and High D MAGs of interest had above average numbers of putative viral linkages (average of 278 compared to dataset-wide average of 196). Moreover, 129 vMAGs were linked to all 28 featured Actinobacteria MAGs from High S samples, potentially due to conserved nucleotide frequencies. These shared 129 vMAGs comprised ~7.6% of the viral community in High S samples, again suggesting that abundant and active bacteria in burned soils are actively targeted by abundant phage, potentially impacting soil C cycling via release of labile cellular components following cell lysis (i.e., viral shunt)[57]. There is also evidence for the "piggyback-the-winner" viral strategy, where lysogenic lifestyles are favored at high microbial abundances and growth rates[58]. Of our 2399 DNA vMAGs, 185 had putative lysogenic lifestyles based on gene annotations for integrase, recombinase, or excisionase genes, and 25 of these had nucleotide frequency-based linkages to all the featured High S Actinobacteria MAGs.

To investigate potential viral roles in post-fire soil C cycling, we characterized the putative AMG repertoire of the vMAGs. Viruses use AMGs to "hijack" and manipulate host metabolism; one permafrost soil study found AMGs associated with SOM degradation and central C metabolism, suggesting that viruses play a direct role in augmenting soil C cycling[55]. There were 773 total putative AMGs detected in 445 vMAGs, including 138 CAZymes targeting diverse substrates (e.g., cellulose, chitin, pectin; **Appendix A**). Additionally, the AMGs included 105 genes related to growth (e.g., ribosomal proteins, ribonucleoside-diphosphate reductase), 21 central C metabolism genes, and 21 peptidases. Over 50 of these genes – including some related to SOM and necromass processing (e.g., glycoside hydrolases, polysaccharide lyases) and cell growth (pyrimidine ribonucleotide biosynthesis) – were encoded within viral genomes linked to

all 28 of the featured High S Actinobacteria MAGs. Furthermore, metatranscriptomic analyses indicate that 13 of these AMGs were being actively transcribed, suggesting that prophage manipulate SOM degradation and potential cell growth in active bacteria in High S samples (**Appendix A**).

2.3.10 Fungi are active across burn conditions

Two fungal Ascomycota MAGs from known pyrophilous taxa, *Leotiomycetes* (R113-184) and *Coniochaeata ligniaria* (R110-5)[59–61], were reconstructed from metagenomes. These taxa were prominently represented in our ITS amplicons; the *Leotiomycetes* class increased in relative abundance by ~215% between control and High S samples (14% to 45%) and the *Coniochaeta* genus relative abundance increased from 0.003% to 1% from control to High D samples.

Complementing observations from bacterial MAGs, the fungal MAGs encoded and expressed genes for degrading aromatic compounds. Both expressed genes for degrading salicylate (salicylate hydroxylase), phenol (phenol 2-monooxygenase), and catechol (catechol 1,2-dioxygenase), and expression of all three genes increased with fire severity. The MAGs also encoded laccases, which are enriched in pyrophilous fungal genomes[62] and act on aromatic substrates[63]. The *Coniochaeta* MAG additionally encoded hydrophobic surface binding proteins (*hsbA*; PF12296) which may facilitate the degradation of fire-derived hydrophobic compounds and be critical to soil recovery[62]. To compare the fungal and bacterial contribution to catechol degradation, we compared normalized transcriptomic reads recruited to the gene encoding catechol 1,2-dioxygenase, *catA*. In High S samples, the fungal MAGs generated more than twice the number of transcripts per gene compared to bacterial MAGs, indicating the important role

that fungi likely play in aromatic DOM degradation in burned soils. Both fungal MAGs also expressed diverse peptidases (**Figure 2.18**), with increased expression from low to high fire severity in both surface and deep samples (~40.4% and 235%, respectively), which could degrade necromass from lysed microorganisms.

2.3.11 Fungal MAGs encode secondary metabolite clusters

The *Coniochaeta* MAG (R110-5) encoded 26 secondary metabolite clusters, including 12 PolyKetide Synthase (PKS) clusters and 4 Non-Ribosomal Peptide Synthetase (NRPS) clusters. This trait appears to be conserved across the *Coniochaeta* genera, as the other four *Coniochaeta* genomes deposited on JGI MycoCosm encode an average of ~36, ranging from 25-66. Both polyketide and non-ribosomal peptide secondary metabolites display a diverse array of biological uses and properties including antibiotic synthesis[25], siderophore production[26], and fungal developmen[27] (e.g., sporulation factors), and may give organisms a competitive edge, especially under stressful conditions. The other fungal MAG (R113-184; *Leotiomycetes*) may persist following wildfire due to an endophytic lifestyle; 36 *Leotiomycetes* ESV's were classified as endophytes by FUNGuild. Pyrophilous endophytic fungi have been found to occur survive fire events in small-scale refugia then, triggered by the fire, produce reproductive sporocarps [10].

2.3.12 Ecosystem implications of soil microbiome changes

We observed short-term (one-year post-fire) differences in microbiome composition and function that likely alter biogeochemical cycling and initial post-fire vegetation recovery. We found no expression of the gene catalyzing N fixation (*nifH*),

despite the key role that N-fixing bacteria play in augmenting plant-available soil N pools[10] following disturbance, the pre- and post-fire abundance of actinorhizal shrubs (*Ceanothus velutinus, Shepherdia canadensis*), and the numerous leguminous forb species that form symbioses with N-fixing bacteria in these ecosystems. Nitrification is another key microbially-mediated process that generally increases in post-fire soils due to an influx of ash-derived ammonium (also found here; **Appendix A)**[25,64]. Ammonia monooxygenase (*amoA*) transcripts were detected in deep soils but were absent in burned surface soils. Moreover, transcript abundances for both *amoA* and nitrite oxidoreductase (*nxrAB*) were significantly higher in Low D vs. High D samples (Welch's t-test; $p<0.05$) (**Appendix A**), potentially due to the inability of ammonia-oxidizing bacteria (e.g., *Nitrospira*) to withstand post-fire soil conditions. Indeed, *Nitrospira* was present in both control and burned deep soils but absent in moderate and high severity-impacted surface soils. These observations are supported by other studies; short-term, post-fire decreases in the abundances of genes catalyzing N-fixation and ammonia-oxidization have been noted in a conifer forest following wildfire[65].

While pyrophilous taxa were enriched post-wildfire, the loss of other soil microorganisms may impact biogeochemical processes and associated soil health. Increasing wildfire severity (from low to high) resulted in large decreases in the relative abundances of both Acidobacteria and Verrucomicrobia in surface soils (**Figure 2.2**; relative abundance decreases of 37.6% and 63.6%, respectively). Members of the Acidobacteria frequently play an active role in soil C cycling via decomposition[66–68] and are considered a keystone taxa for SOM degradation[69]. Here, representative MAGs affiliated with Acidobacteria (RYN_25, RYN_26) from the *Pyrinomonadaceae* family (16S

rRNA gene data; -94.9% from Low S to High S) and Verrucomicrobia from the *Verrucomicrobiaceae* family (16S rRNA gene data; -82.35% Low S to High S) all encoded CAZYmes for targeting complex plant-derived carbohydrate polymers (e.g., cellulose, beta-mannans, beta-galactans, xylan). Furthermore, Acidobacteria MAGs RYN_25 and RYN_26 both encoded genes (e.g., *epsH*) for synthesis of exopolysaccharides that play critical roles in soil aggregate formation and SOM stabilization as mineral-associated OM[70]. The loss of these taxa following severe wildfire may reduce the potential for SOM degradation and stabilization in surface soils.

Ectomycorrhizal fungi (EMF) facilitate plant access to limiting nutrients and water in return for photosynthetically-derived carbohydrates[71]. We observed a 99% decrease in EMF relative abundances across the burn severity gradient (**Table 2.2**), which could be due to heat-induced fungal mortality or plant host death[14]. This has implications for the reestablishment of obligate ectomycorrhizal host plants such as *P. contorta*, the dominant tree species in these forests. For example, *Cenoccum geophilum*, a known EMF symbiont of *P. contorta*[72] that is indicative of fast conifer growth[73], was present in unburned sites but absent after fire. Inoculation of *P. contorta* and most conifers with EMF is a standard forest nursery production and reforestation practice[74], but inoculating seedlings destined for post-fire landscapes[75] with a mixture of local EMF species[72] may increase lost soil microbial diversity.

2.4 Conclusions

Here we present a genome-resolved multi-omics analysis of the impact of wildfire on the soil microbiome of conifer forest ecosystems, providing functional context to

previously observed post-fire shifts in soil microbiome structure. Our results suggest that a combination of life strategies, including heat tolerance, fast growth, and the utilization of pyrogenic substrates allow microorganisms to occupy available post-fire niche space. We found the widespread microbial processing of aromatic compounds that were likely generated during wildfire, which has implications for the residence time of pyrogenic C. Carbon processing in burned soils is also influenced by active viruses that target key bacterial community members through viral-mediated cell lysis and activity of AMGs. This rich genome-resolved multi-omic dataset provides invaluable insight into the impact of severe wildfire on the soil microbiome of western US forest ecosystems, which continue to experience unprecedented wildfire disturbances.

2.5 Materials & Methods

2.5.1 Field campaign

Sampling was conducted in old-growth, lodgepole pine-dominated (*Pinus contorta*) forests burned by Badger Creek (8215 ha) and Ryan (11567 ha) fires during 2018 in the Medicine Bow National Forest. The average return interval for wildfire within these forests is about 200 years[76] and the even-aged lodgepole pine stands sampled regenerated from stand-replacing wildfires. Total annual precipitation averages 467 mm and mean annual temperature is 1.9°C with average annual minima and maxima of -12.1°C and 17.1°C, respectively (Cinnabar Park, SNOTEL site 1046). Soils are formed in metamorphic and igneous parent material and are well-drained with moderate to rapid permeability. The most abundant soil types are loamy-skeletal, Ustic Haplocryepts and fine-loamy, Ustic Haplocryalfs (**Appendix A**). The plots were at similar elevation (2480-2760 m) and on

mainly gentle slopes (10/15 plots; little aspect influence). Microbial communities were not statistically different between gentle and moderate sloping plots (ANOSIM; $p<0.05$) and north or south facing plots when slope was moderate (>10°; ANOSIM; $p<0.05$). Four burn severity gradients comprised of low, moderate, and high severity sites and an unburned control were selected based on remotely sensed comparisons of pre and post-fire greenness[77], and then field validated prior to sampling (early August 2019) using US Forest Service guidelines[78,79]. Low, moderate, and high severity sites had >85%, 20-85%, and <20% surficial organic matter cover, respectively[78], which we quantified visually within each plot using a point-intercept approach (**Figure 2.19**). Low severity plots had sparse grass and low shrub (*Vaccinium myrtillu*) cover, which we avoided to ensure we sampled root-free soil. Low severity sites also had a very small litter layer to a depth of <1 mm and Site #4 had live trees remaining, but all were >2 m away from the sampling plot. Samples were collected on August 16 and 19 of 2019, two days without any precipitation events, approximately one year following containment of both fires. At each sampling site, a 3 m x 5 m sampling grid with six m^2 subplots was laid out perpendicular to the dominant slope (**Figure 2.19**). Surface (0-5 cm depth) and deeper soil (5-10 cm depth) was collected with a sterilized trowel in each subplot for DNA and RNA extractions and subsequent microbial analyses. Surface soil samples included thin O-horizon at control and low severity plots and charred mineral soil at moderate and high severity plots. Deeper (5-10 cm) samples were mineral soils. In three subplots of each plot, additional material was collected for chemical analyses. Samples for RNA analyses were immediately flash-frozen using an ethanol-dry ice bath and placed on dry ice to remain frozen in the field. Samples for DNA extractions and chemical analyses were immediately

placed on ice and all samples were transported to the laboratory at Colorado State University (CSU). Soils for DNA and RNA extractions were stored at -80°C in the laboratory until processing. A total of 176 soil samples were collected (**Appendix A**).

2.5.2 Soil chemistry

We evaluated soil nutrients and chemistry to gauge changes across a gradient of wildfire severity and to consider the implications of those conditions on microbial activity or substrate quality. Analyses of inorganic forms of soil N (NO_3–N and NH_4–N) were conducted on a subset of deep soil samples (*n* = 12 each for low, moderate, and high severity, *n* = 8 for control). Samples were passed through a 4 mm mesh sieve and extracted with 2 M KCl within 24 h of sampling. Extracts were analyzed for NO_3–N and NH_4–N by colorimetric spectrophotometry[80] (Lachat Company, Loveland, CO). A subset of surface (*n* = 15) and deep soil samples (*n* = 45) were dried (48 h at 60°C), ground to a fine powder and analyzed for total C and N by dry combustion (LECO Corporation, St. Joseph, MI, USA). We analyzed the NO_3–N and NH_4–N and dissolved organic C (DOC) and total dissolved N (TDN) released during warm water extracts[81] using ion chromatography (NH4-N and NO3-N; Thermo-Fisher Corporation, Waltham, MA) and TOC-VCPN total organic carbon analyzer (DOC and TDN; Shimadzu Corporation, Columbia, MD, USA). Soil pH was analyzed in a 1:1 soil to deionized water slurry after one hour of agitation[82] using a temperature-corrected glass electrode (Hach Scientific, Loveland, CO, USA). Soil chemistry data is included in **Appendix A**.

2.5.3 High-resolution carbon analyses: FTICR-MS

Water extractions were completed on a subset of 47 samples from the Ryan Fire for high-resolution C analyses using Fourier Transform Ion Cyclotron Resonance Mass Spectrometry (FTICR-MS) to analyze dissolved organic matter (DOM). Briefly, 100 mL of milliQ water (> 18 mΩ) was added to 50 g of sample in an acid-washed and combusted (400°C for 6 hours) 250 mL Erlenmeyer flask. These were placed on a shaker table for 10 hours at 170 rpm. Following shaking, liquid was poured off into a 50 mL centrifuge tube and centrifuged for 10 min at 7500 g and supernatant was filtered through a polypropylene 0.2 µm filter (polypropylene material). The extracts were acidified to pH 2 and additionally pre-treated with solid-phase extractions (SPE) using Agilent Bond Elut-PPL cartridges (3 mL, 200 mg) (Agilent Technologies, DE, USA) following standard lab protocol[83] and subsequently diluted to 50 ppm. A 12 Tesla (12T) Bruker SolariX FTICR-MS located at the Environmental Molecular Sciences Laboratory in Richland, WA, USA was used to collect DOM high-resolution mass spectra from each DOM sample. Samples were injected into the instrument using a custom automated direction infusion cart that performed two offline blanks between each sample and using an Apollo II electrospray ionization (ESI) source in negative ion mode with an applied voltage of -4.2kV. Ion accumulation time was optimized between 50 and 80 ms. One hundred and forty-four transients were co-added into a 4MWord time domain (transient length of 1.1 s) with a spectral mass window of m/z 100-900, yielding a resolution at 400K at m/z 381. Spectra were internally recalibrated in the mass domain using homologous series separated by 14 Da (CH_2 groups). The mass measurement accuracy was typically within 1 ppm for singly charged ions across a broad m/z range (100 m/z - 900 m/z). Bruker Daltonics

DataAnalysis (version 4.2) was used to convert mass spectra to a list of m/z values by applying the FTMS peak picking module with a signal-to-noise ratio (S/N) threshold set to 7 and absolute intensity threshold to the default value of 100. Chemical formulae were assigned with Formularity[84] based on mass measurement error < 0.5 ppm, taking into consideration the presence of C, H, O, N, S and P and excluding other elements. This open-access software was also used to align peaks with a 0.5 ppm threshold. Raw FTICR-MS data is provided in archive (doi:10.5281/zenodo.5182305). The R package ftmsRanalysis[85] was then used to remove peaks that either were outside the desired m/z range (200 m/z – 900 m/z) or had a more abundant isotopologue, assign Van Krevelen compound classes, and calculate nominal oxidation state of carbon (NOSC) and aromaticity index (AI) based on the number of different atoms using equations 1 and 2 below:

$$NOSC = 4 - \frac{5C+H-3N-20-2S}{C}$$

(1)

$$AI = 4 - \frac{1+C-O-S-0.5H}{C-O-S-N-P}$$

(2)

2.5.4 DNA extraction, 16S rRNA gene and ITS amplicon sequencing

DNA was extracted from soil samples using the Zymobiomics Quick-DNA Fecal/Soil Microbe Kits (Zymo Research, CA, USA). 16S rRNA genes in extracted DNA were amplified and sequenced at Argonne National Laboratory on the Illumina MiSeq using 251-bp paired-end reads and the primers 515F/806R[86], targeting the V4 region of the 16S rRNA gene. For fungal community composition, the DNA was PCR amplified

targeting the first nuclear ribosomal internal transcribed spacer region (ITS) using the primers (ITS1f/ITS2) and sequenced on the Illumina MiSeq platform at the University of Colorado using 251-bp paired-end reads.

For taxonomic assignment, we used the SILVA[87] (release 132) and UNITE[88] (v8.3) databases for bacteria and fungi, respectively. We employed the QIIME2 environment[89] (release 2018.11) for processing of reads, which are both deposited and available at NCBI under BioProject #PRJNA682830. DADA2[90] was used to filter, learn error rates, denoise, and remove chimeras from reads. Following this step, 16S rRNA gene and ITS amplicon sequencing reads retained on average 48,379 and 34,004 reads per sample, respectively. Taxonomy was assigned using the QIIME2 scikit-learn classifier trained on the SILVA and UNITE databases for bacteria and fungi, respectively. Ecological guilds were assigned to fungal ASVs using FUNGuild[91] (v1.2). Similar to FUNGuild creator recommendations, we accepted guild assignments classified as “highly probable” or “probable” to avoid possible overinterpretation and discarded any ASVs classified as multiple guilds.

To characterize how microbial populations differed across burn severities and depths, we used the R[92] vegan[93] (v2.5-7) and phyloseq[94] (v1.28.0) packages. Nonmetric multidimensional scaling (NMDS) was conducted on Bray-Curtis dissimilarities to examine broad differences between microbial communities. Analyses of similarity (ANOSIM, vegan) was utilized to test the magnitude of dissimilarity between microbial communities. Mean species diversity of each sample (alpha diversity) was calculated based on species abundance, evenness, or phylogenetic relationships using Shannon’s Diversity Index (H), Faith’s Phylogenetic Diversity (pd), and Pielou’s Evenness (J). Linear

discriminant analysis (LDA) with a score threshold of 2.0 was used to determine ASVs discriminant for unburned or burned soil[95].

2.5.5 Metagenomic assembly and binning

A subset of 12 Ryan Fire samples from a single transect representing low and high severity burn from surface and deep soils was selected for metagenomic sequencing to analyze changes in microbial community functional potential (*n*=3 per condition). The four different conditions are hereafter referred to as 'Low S' (low severity surface soil), 'High S' (high severity surface soil), 'Low D' (low severity deep soil), and 'High D' (high severity deep soil). Libraries were prepared using the Tecan Ovation Ultralow System V2 and were sequenced on the NovaSEQ6000 platform on a S4 flow cell using 151-bp paired-end reads at Genomics Shared Resource, Colorado Cancer Center, Denver, CO, USA. Sequencing adapter sequences were removed from raw reads using BBduk (https://jgi.doe.gov/data-and-tools/bbtools/bb-tools-user-guide/bbduk-guide/) and reads were trimmed with Sickle[96] (v1.33). For each sample, trimmed reads were assembled into contiguous sequences (contigs) using the de novo de Bruijn assembler MEGAHIT v1.2.9 using kmers[97] (minimum kmer of 27, maximum kmer of 127 with step of 10). Assembled contigs shorter than 2500bp were discarded for all downstream usages, including gene-resolved analyses for inorganic N cycling and binning into genomes. These assembled contigs (> 2500bp) were binned using MetaBAT2 with default parameters[98] (v2.12). Metagenome-assembled genome (MAG) quality was estimated using checkM[99] (v1.1.2) and taxonomy was assigned using GTDB-Tk[100] (R05-RS95, v1.3.0). MAGs from all metagenomes were dereplicated using dRep[101] (default parameters, v2.2.3) to create a non-redundant MAG dataset. Low quality MAGs (<50% completion and >10%

contamination) were excluded from further analysis[102]. Reads from all samples were mapped to the dereplicated MAGs using BBMap with default parameters (version 38.70, https://sourceforge.net/projects/bbmap/). Per-contig coverage across each sample was calculated using CoverM contig (v0.3.2) (https://github.com/wwood/CoverM) with the 'Trimmed Mean' method, retaining only those mappings with minimum percent identity of 95% and minimum alignment length of 75%. Coverages were scaled based on library size and scaled per-contig coverages were used to calculate the mean per-bin coverage and relative abundance in each sample (**Appendix A**The quality metrics and taxonomy of the subsequent 637 medium- and high-quality MAGs discussed here are included in the supplementary material (**Appendix A**) and are deposited at NCBI (BioProject ID PRJNA682830). Maximum cell doubling times were calculated from codon usage bias (CUB) patterns in each MAG with >10 ribosomal proteins using gRodon[43] (**Appendix A**). Bacterial MAGs with an average relative abundance > 0.5% across triplicates (with a standard deviation less than the average relative abundance) in both High S and High D were selected as MAGs of interest for further genome-resolved discussion and insight into the function of the post-fire microbiome in surface and deep soils (**Appendix A**).

Fungal MAGs (R113-184 and R110-5) were identified because they were abnormally large for bacterial MAGs and were confirmed as eukaryotic origin based on mmseqs2 searches for all available ORFs in their contigs against the NCBI NR and MycoCosm database, with best hits to *Coniochaeta ligniaria* and the *Leotiomycetes*/*Helotiales* clade. To identify taxonomy and precisely place the MAGs in the fungal tree (**Figure 2.20**), we used 867 single-copy orthogroups from OrthoFinder v2.5.4[103] using default parameters. The protein sequences in each orthogroup were

aligned with MAFFT[104] (--maxiterate 1000 --globalpair) and trimmed with TrimA1 v1.4.rev22[105] (-automated1). All the filtered MSAs were concatenated. The phylogenetic tree was built using iqtree v1.6.9[106] detecting the best model for each gene partition, 10000 ultrafast bootstrap, and 10000 SH-like approximate likelihood ratio test (-m MFP -bb 10000 -alrt 10000 -safe). The tree was visualized using FigTree 1.4.4 (http://tree.bio.ed.ac.uk/software/figtree/) and the support values represent the ultrafast bootstraps/SH-aLRT. Completeness for both MAGs was assessed using BUSCO v4.0.6[107] and CEGMA[108].

2.5.6 Metagenome-assembled genome annotation

Eukaryotic MAGs were annotated using the JGI Annotation Pipeline analyzed with complementary metatranscriptomics assemblies[109] (RnaSPAdes, v3.13.0) and are deposited on MycoCosm[110] (https://mycocosm.jgi.doe.gov/ColoR110_1 and https://mycocosm.jgi.doe.gov/ColoR113_1). Bacterial MAGs were annotated using DRAM[111] (v1.0). In addition to the DRAM annotations, we used HMMER[112] against Kofamscan HMMs[113] to identify genes for catechol and protocatechuate meta- and ortho-cleavage, naphthalene transformations, and inorganic N cycling (**Appendix A**).

2.5.7 Metatranscriptomics

RNA was extracted from the subset of 12 samples utilized for metagenomics using the Zymobiomics DNA/RNA Mini Kit (Zymo Research, CA, USA) and RNA was cleaned, DNase treated, and concentrated using the Zymobiomics RNA Clean & Concentrator Kit (Zymo Research, CA, USA). The Takara SMARTer Stranded Total RNA-Seq Kit v2 (Takara Bio Inc, Shiga, Japan) was used to remove ribosomal RNA from total RNA and

construct sequencing libraries. Samples were sequenced on the NovaSEQ6000 platform on a S4 flow cell using 151-bp paired-end reads at Genomics Shared Resource, Colorado Cancer Center, Denver, CO, USA. Adapter sequences were removed from raw reads using Bbduk (https://jgi.doe.gov/data-and-tools/bbtools/bb-tools-user-guide/bbduk-guide/) and sequences were trimmed with Sickle v1.33[96]. Trimmed reads were mapped to metagenome assemblies using BBMap (parameters: ambiguous=random, idfilter=0.95; v38.70). Mappings were filtered to 95% identity and counts were generated using HTSeq[114]. For differential expression analysis, the dataset was filtered to transcripts which were successfully annotated by DRAM (*n*=132,665) and DESeq2[115] was used to identify transcripts that were differentially expressed in any condition (**Appendix A**). The same analysis was also run on the combined HMM output described above (1,189 total transcripts). We normalized our dataset by calculating the gene length corrected trimmed mean of M values[116] (geTMM) using edgeR[117] to normalize for library depth and gene length (**Appendix A**). To identify transcripts that were highly expressed in any given condition, we filtered the data to transcripts that were in the upper 20% of TMM for 2 of the 3 samples in any one condition (**Table 2.3**). To compare bacterial and fungal expression data for individual genes, we normalized the number of either fungal or bacterial transcript reads to the gene coverage in each sample to compare the number of transcripts recruited per gene.

2.5.8 Viruses

Viral contigs were recovered from the metagenomic assemblies using VirSorter2[118] (v2.2.2) and only contigs >/= 10kb with a VirSorter2 score > 0.5 were retained. Viral contigs were trimmed using checkV[119] (v0.4.0) and the final contigs were

clustered using the CyVerse app ClusterGenomes (v1.1.3) requiring an average nucleotide identity of 95% or greater over at least 80% of the shortest contig. The final DNA viral metagenome-assembled genome (vMAG) dataset was manually curated using the checkV, VIRSorter2, and DRAM-v annotation outputs according to protocol[120]. RNA vMAGs were also recovered from metatranscriptome assemblies using VIRSorter2[118] (v2.2.2). The resulting sequences were clustered using ClusterGenomes (v1.1.3) on CyVerse using the aforementioned parameters. To quantify relative abundance of DNA and RNA vMAGs across the 12 samples, we mapped the metagenomic and metatranscriptomic reads to the vMAGs using BBMap with default parameters (v38.70). To determine vMAGs that had reads mapped to at least 75% of the vMAG, we used CoverM (v0.6.0) in contig mode to find vMAGs that passed this 75% threshold (--min-covered-fraction 75). We then used CoverM (v0.6.0) in contig mode to output reads per base and used this to calculate final DNA and RNA vMAG relative abundance in each metagenome and metatranscriptome. vConTACT2 (v0.9.8; CyVerse) was used to determine vMAG taxonomy. Final viral sequences are deposited on NCBI (BioProject ID #PRJNA682830 - BioSamples SAMN20555178, SAMN20555179; **Appendix A**). We used DRAM-v[111] (v1.2.0) to identify auxiliary metabolic genes (AMGs) within the final viral dataset (**Appendix A**).

CRISPR-Cas protospacers were found and extracted from MAG sequences using the CRISPR Recognition Tool[121] (CRT, minimum of 3 spacers and 4 repeats) in Geneious (v2020.0.3) and CRisprASSembler[122] with default parameters (v1.0.1). BLASTn was used to compare MAG protospacer sequences with protospacer sequences in vMAGs with matches only retained if they were 100% or contained ≤1 bp mismatch with an e-

value ≤1e-5. To identify putative vMAG-MAG linkages, we used an oligonucleotide frequency dissimilarity measure (VirHostMatcher v1.0.0) and retained only linkages with a d_2^* value < 0.25[56] (**Appendix A**).

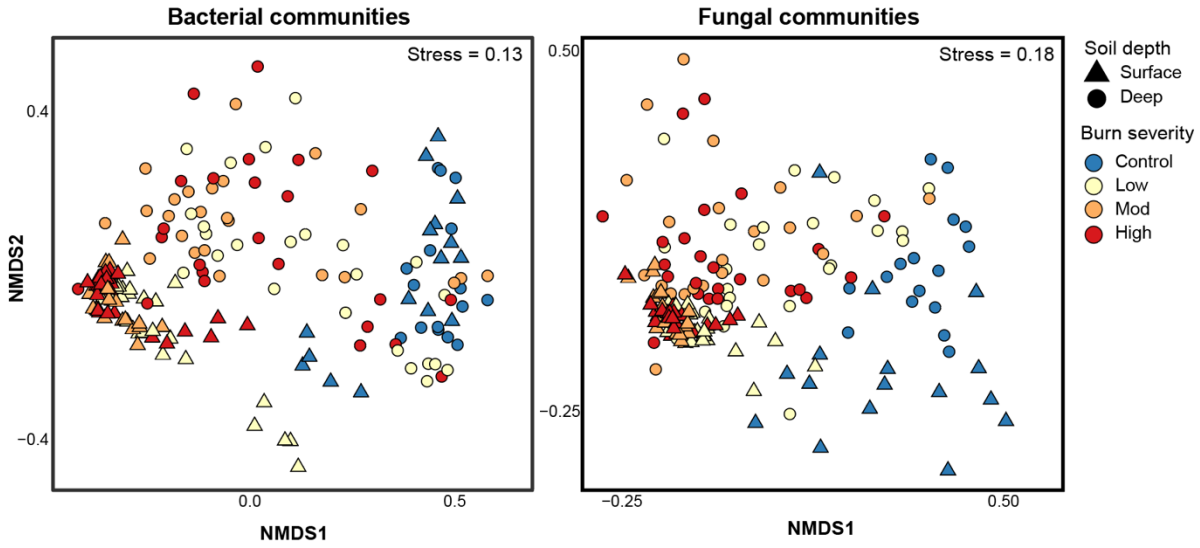

Figure 2.1 Non-metric multidimensional scaling (NMDS) ordination of all bacterial (left) and fungal (right) communities shaped by soil depth and colored by burn severity.

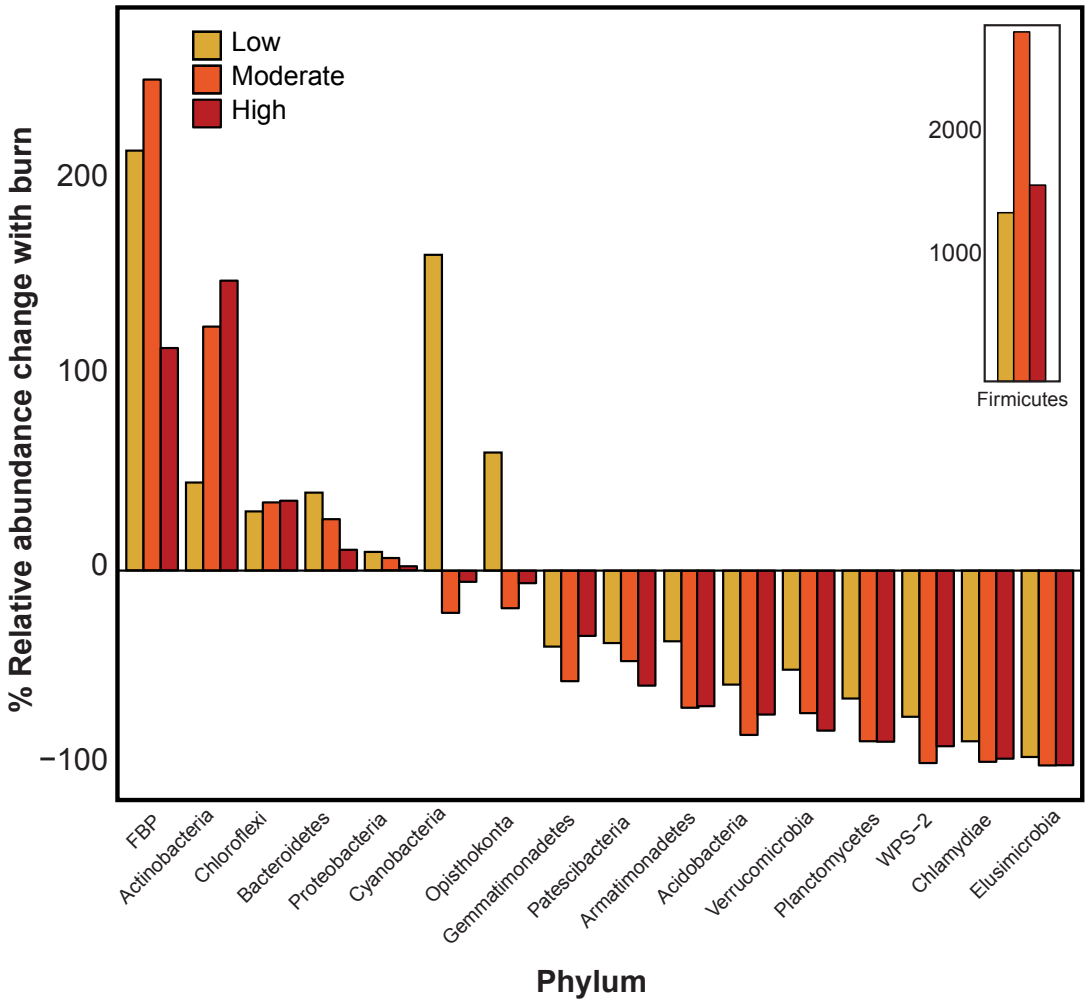

Figure 2.2 The percent change in relative abundance from control to low, moderate, and high severity in surface soil of each main bacterial and fungal phylum. Phyla with relative abundance less than 0.5% were discarded for this analysis. Note that although the Firmicutes have the largest increase with burn (inset) their overall relative abundance in burned samples is still low relative to Actinobacteria (1.21% vs 25.6% relative abundance). Phyla with significant (one-sided pairwise t-test; $p < 0.05$) differences in relative abundance between the unburned and burned conditions are denoted with an asterisk.

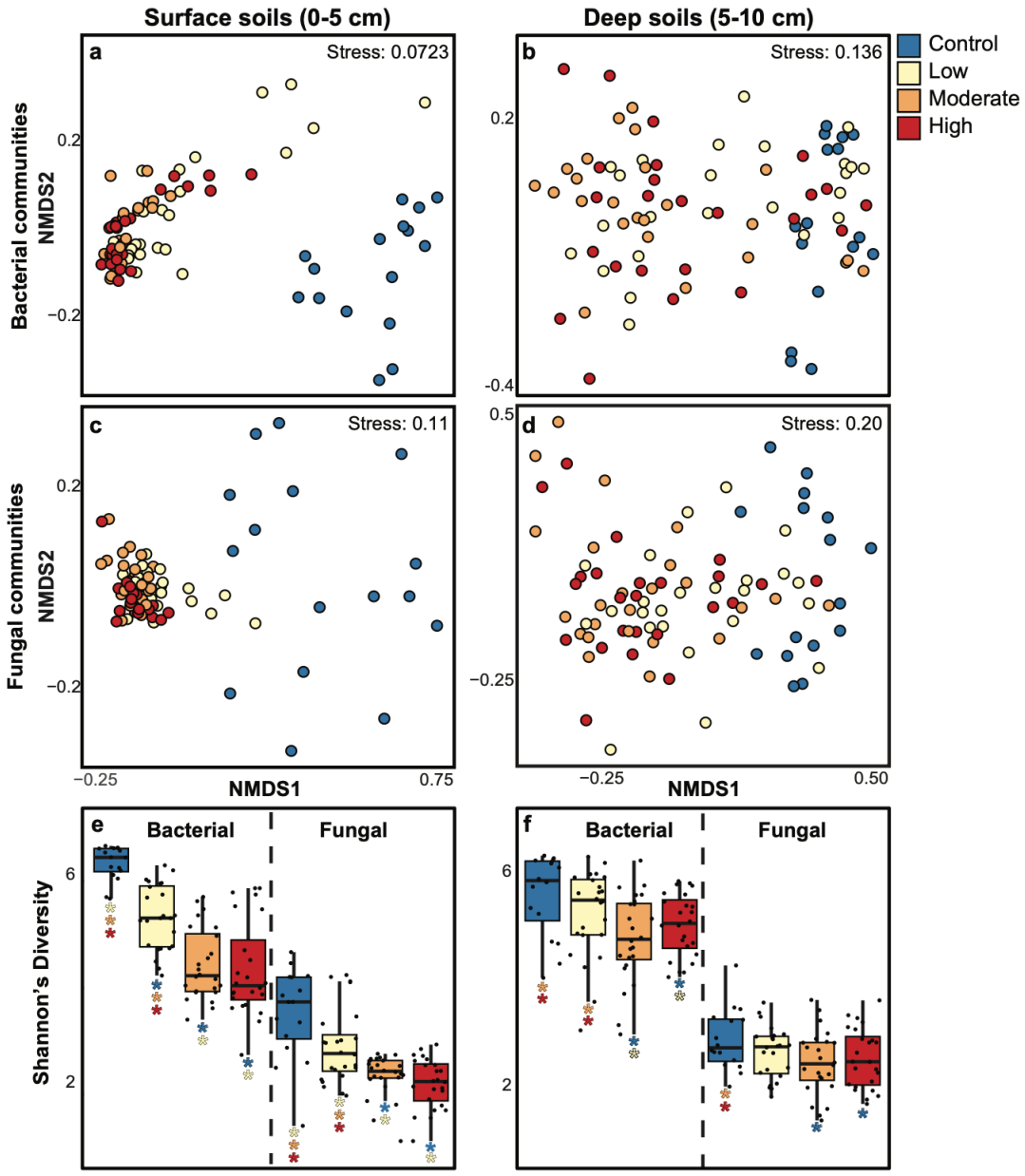

Figure 2.3 a–d, NMDS of surface (0–5 cm) (a,c) and deeper (5–10 cm) soil (b,d) bacterial (a,b) and fungal (c,d) communities shows increased separation of burned and unburned microbial communities in surface soils relative to deep soil communities. e,f, Shannon's diversity (H) calculated from 16S rRNA and ITS gene sequencing in surface (e) and deep soils (f) further shows the increased susceptibility of microbiomes in surface soils to wildfire. Asterisks in e and f denote significant differences (pairwise t-test; $P < 0.05$) between conditions ($n = 16$ for control S and D, $n = 24$ for low, moderate, and high severity-impacted S and D samples). Corresponding P values are listed in Supplementary Table 1. The lower and upper hinges of the boxplots represent the 25th

and 75th percentiles, respectively, and the middle line is the median. The whiskers extend from the median by 1.5× the interquartile range. Data points represent outliers.

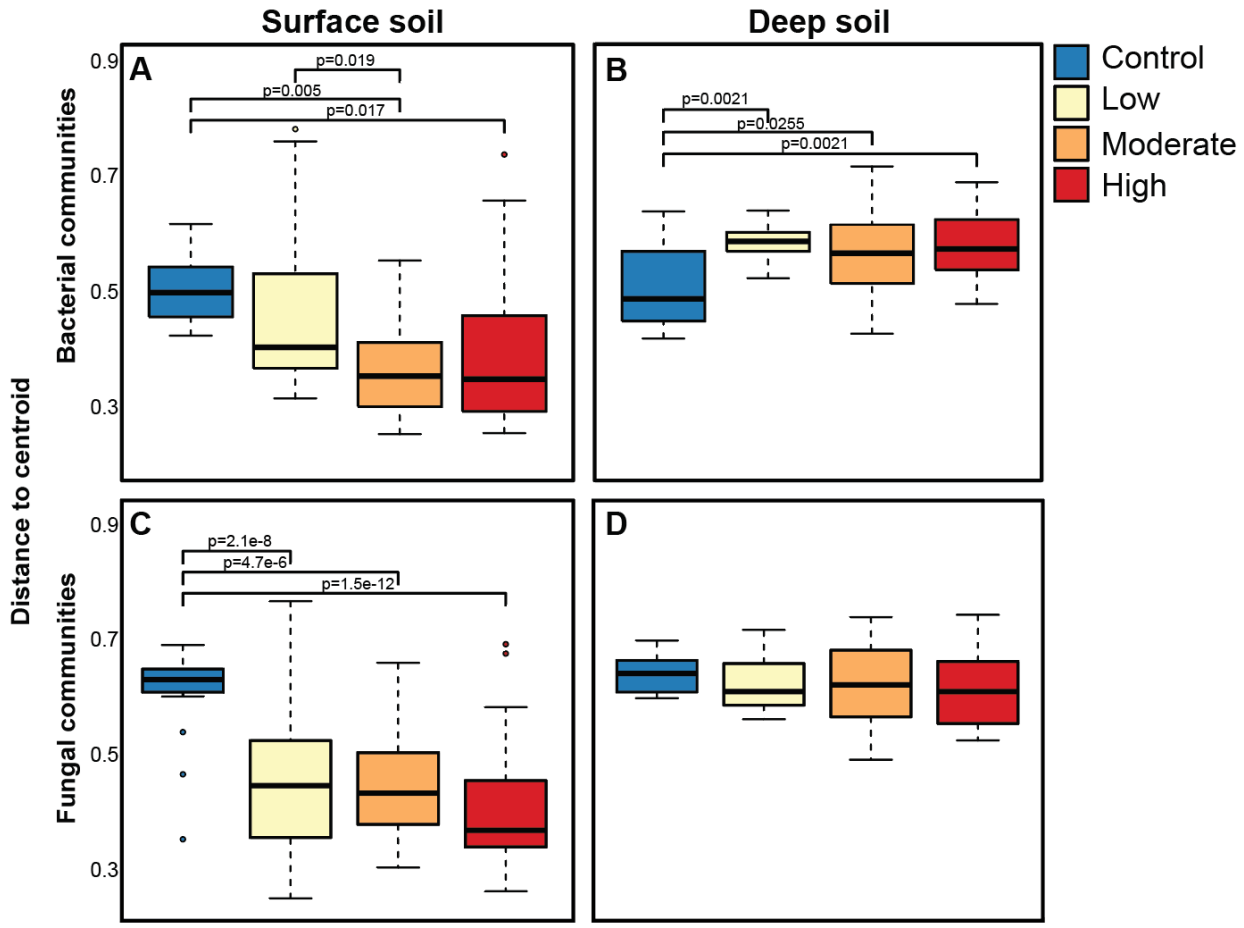

Figure 2.4 Distance to centroid calculations of the NMDS ordinations of surface (A, C) and deep (B, D) soil bacterial (A, B) and fungal (C, D) communities by burn severity (*n* = 16 for control S and D, *n* = 24 for low, moderate, and high severity-impacted S and D samples). P-values are indicated if comparisons are significantly different (one-sided pairwise t-test, $p<0.05$) between conditions. The lower and upper hinges of the boxplots represent the 25th and 75th percentile and the middle line is the median. The upper whisker extends to the median plus 1.5x interquartile range and the lower whisker extends to the median minus 1.5x interquartile range.

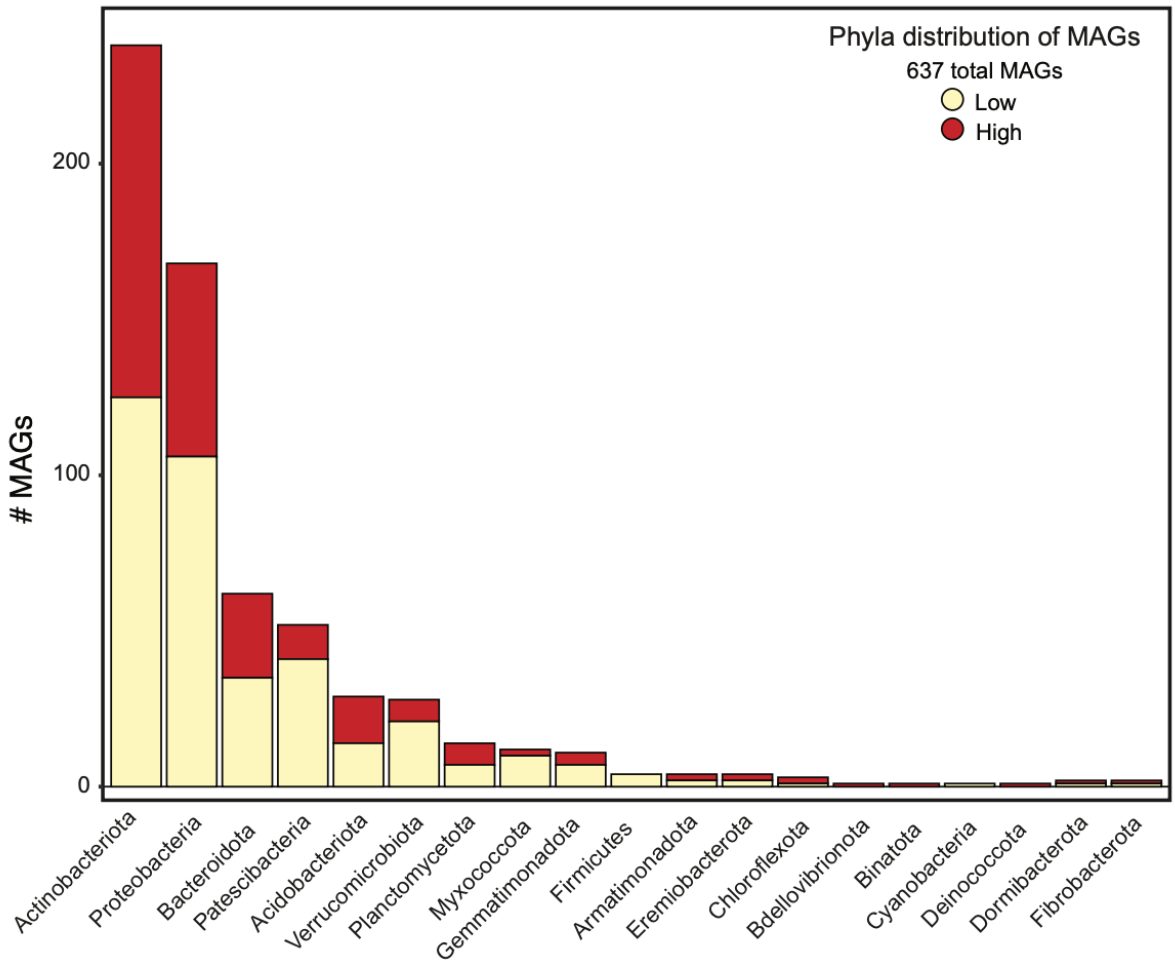

Figure 2.5 Phyla distribution of the 637 medium- and high-quality MAGs (> 50% completion, <10% contamination) from burned surface and deep soils.

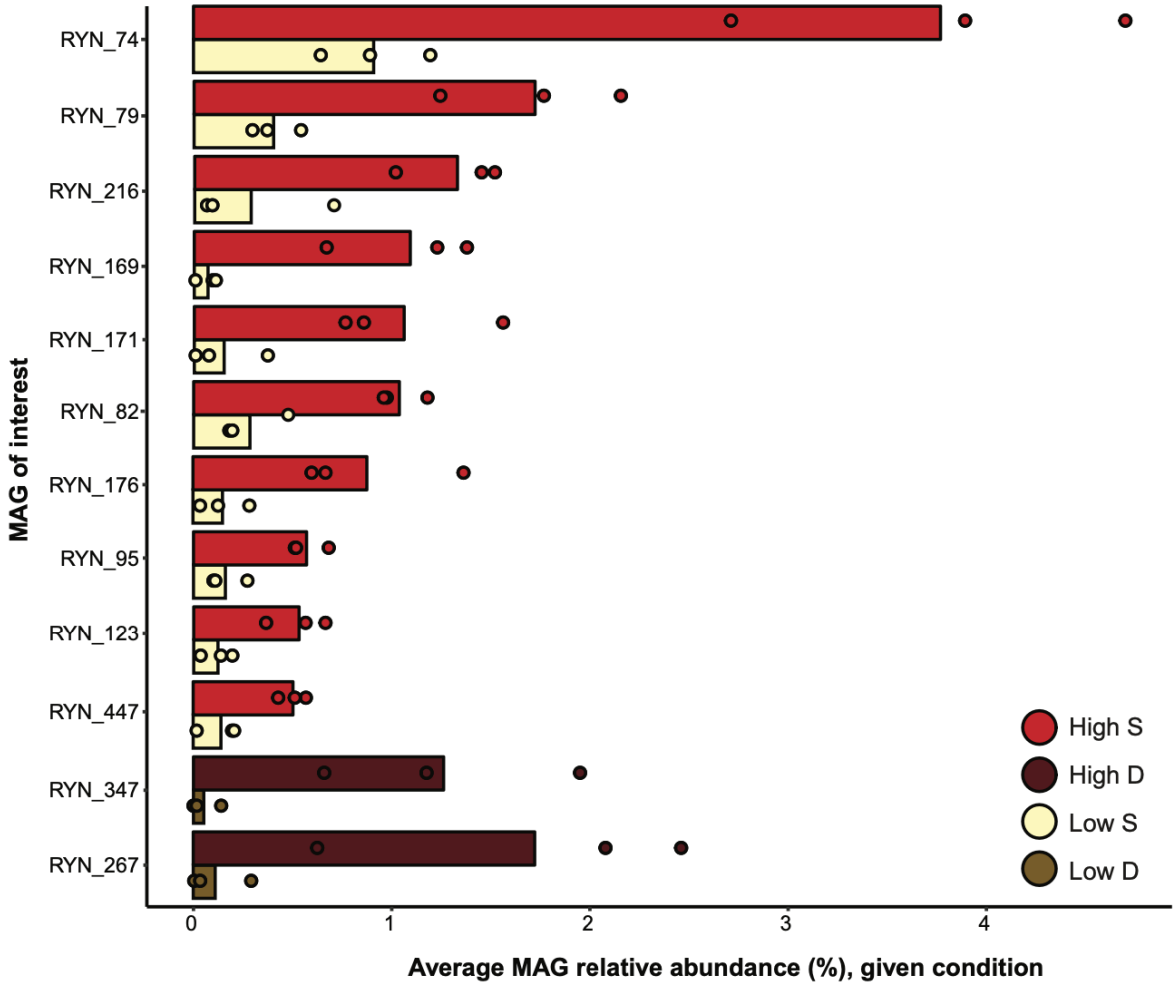

Figure 2.6 The relative abundances in Low and high severity of MAGs that are significantly enriched (one-sided pairwise t-test; $p < 0.05$; p-values in Supplementary Data 2) in High S vs. Low S (7 MAGs) or High D vs. Low D (2 MAGs) that match the designated criteria for discussion in the text (average relative abundance > 0.05% and standard deviation less than average relative abundance). Overlayed points show relative abundance of MAGs in each samples (n = 3 for each condition).

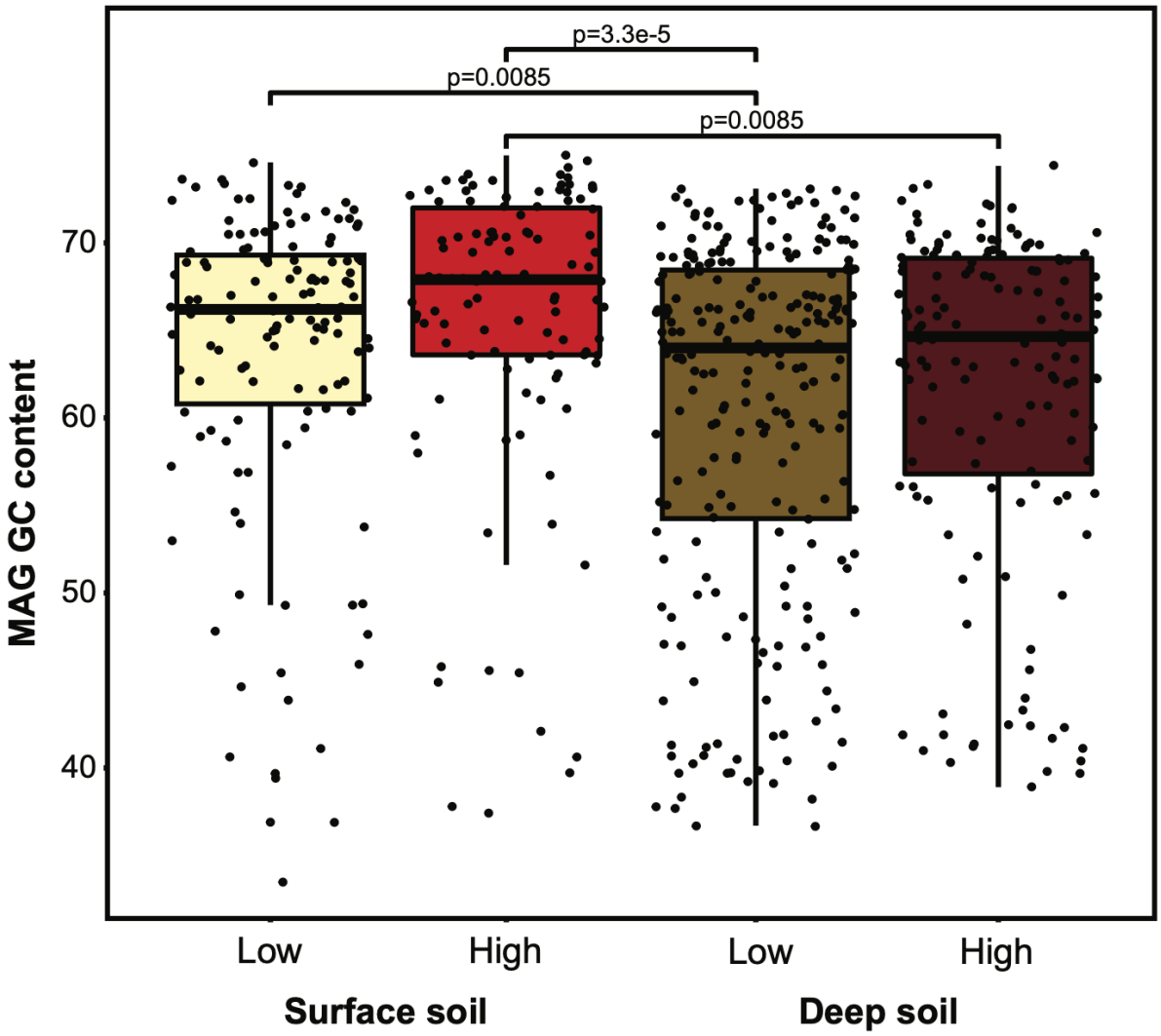

Figure 2.7 GC content of MAGs reconstructed from each condition. P-values are indicated between conditions if there are significant differences (one-sided pairwise t-test, $p < 0.05$). The lower and upper hinges of the boxplots represent the 25th and 75th percentile and the middle line is the median. The upper whisker extends to the median plus 1.5x interquartile range and the lower whisker extends to the median minus 1.5x interquartile range. Jittered points represent individual MAGs (n = 131 reconstructed from Low S samples, n = 111 from High S, n = 247 from Low D, n = 148 from High D).

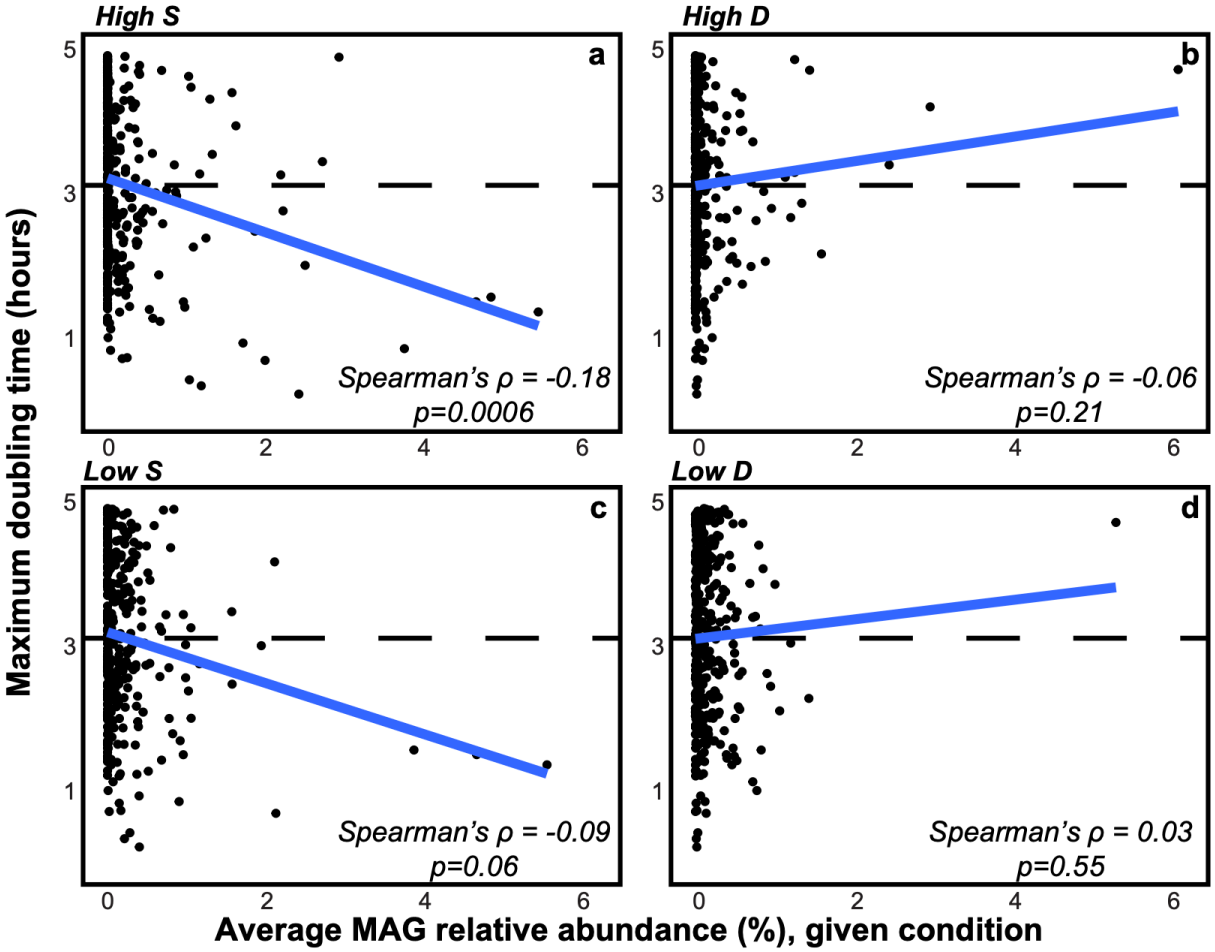

Figure 2.8 a–d, High S conditions (a) favour MAGs from organisms with faster potential growth rates (lower maximum doubling time, estimated using gRodon), indicated here by a significant negative correlation (two-sided Spearman's rho test; Spearman's $\rho = -0.18$, $P < 0.05$). This trend is not present in the other three conditions (b–d). MAG average maximum doubling time is shown by the dashed line.

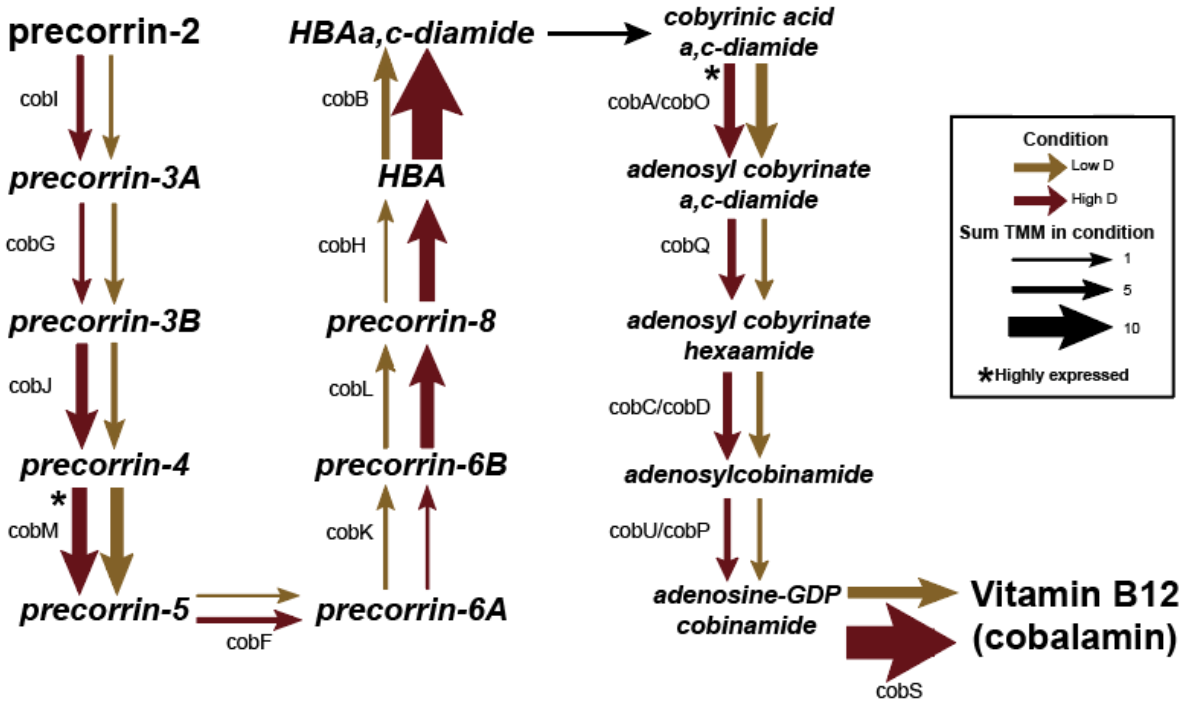

Figure 2.9 The aerobic cobalamin (Vitamin B12) biosynthesis pathway (adapted from Doxey et al., 2015 and Lu et al., 2020) with arrows indicating the summed TMM in the colored condition.

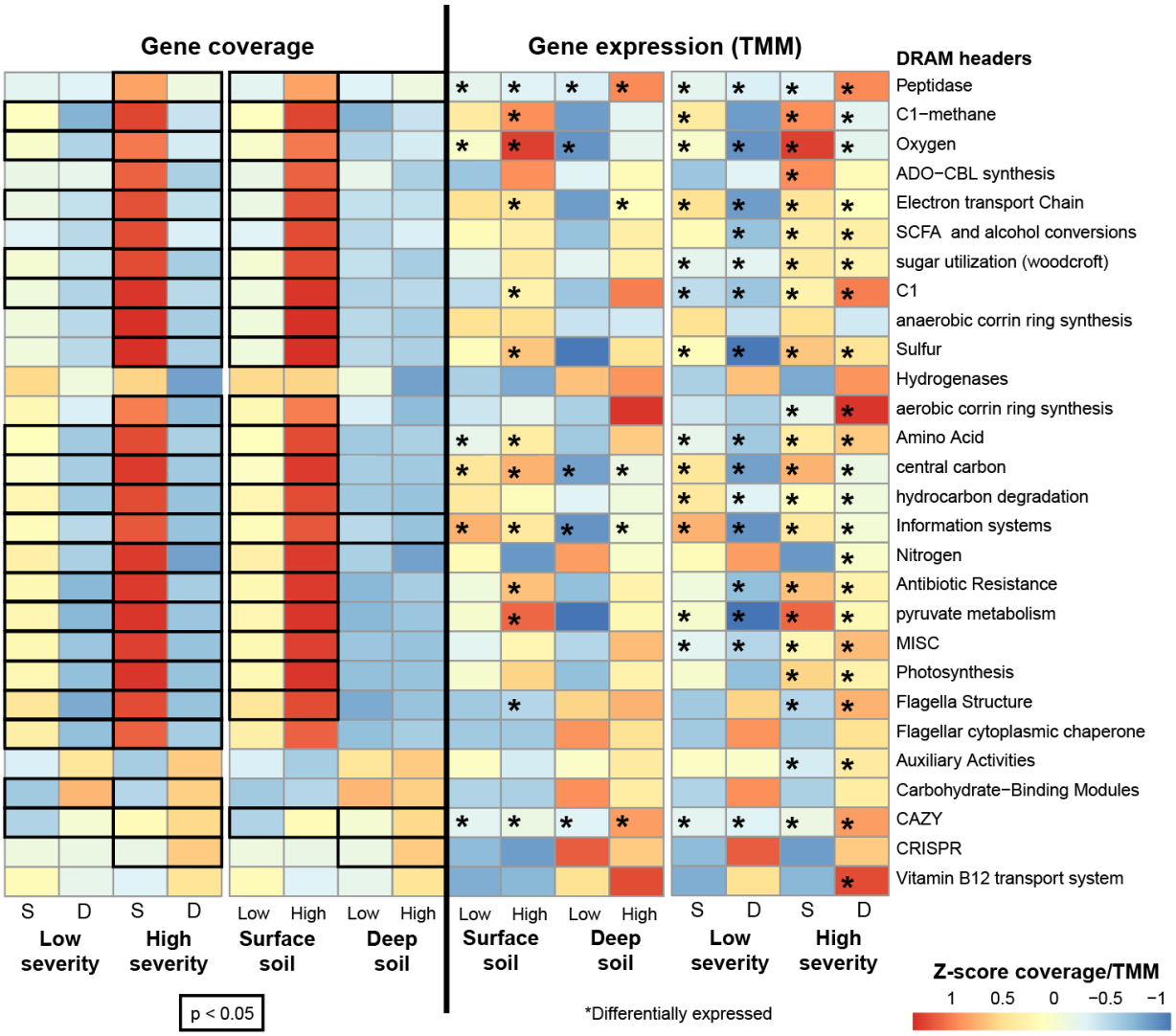

Figure 2.10 Overall trends between low and high severity surface and deep soils in the gene coverage (left) and gene expression (right) of the different DRAM gene headers. In the gene coverage heat maps, a bolded box indicates that the two conditions are significantly different from one another (pairwise t-test, $p<0.05$). In the gene expression data, stars indicate whether there are genes within that DRAM header that are differentially expressed in that condition relative to the other.

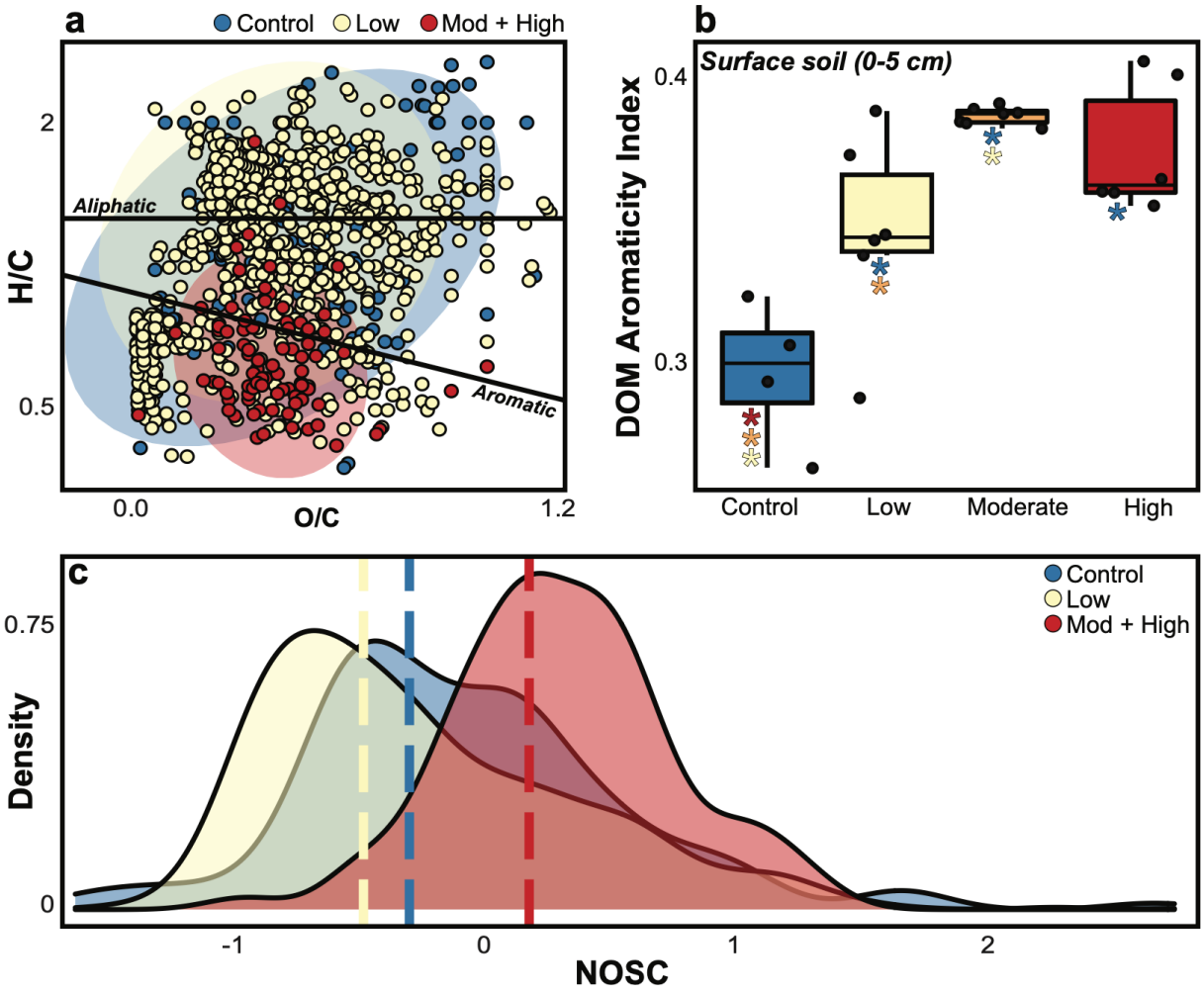

Figure 2.11 a, Van Krevelen diagram showing unique formulas in unburned, low, and moderate and high (combined) surface soils. b, Aromaticity index of DOM pools extracted from surface soils across the burn severity gradient (n = 4 for control, 6 for low, 5 for moderate and 6 for high severity). Corresponding P values are shown in Supplementary Fig. 4b from one-sided pairwise t-test. The lower and upper hinges of the boxplot represent the 25th and 75th percentiles, respectively, and the middle line is the median. The whiskers extend from the median by 1.5× the interquartile range. Data points represent outliers. Coloured asterisks indicate significant difference between the two conditions (pairwise t-test, $P < 0.05$). c, Density plot of unique formula NOSC value distributions between different conditions. Dashed line shows NOSC median for each condition.

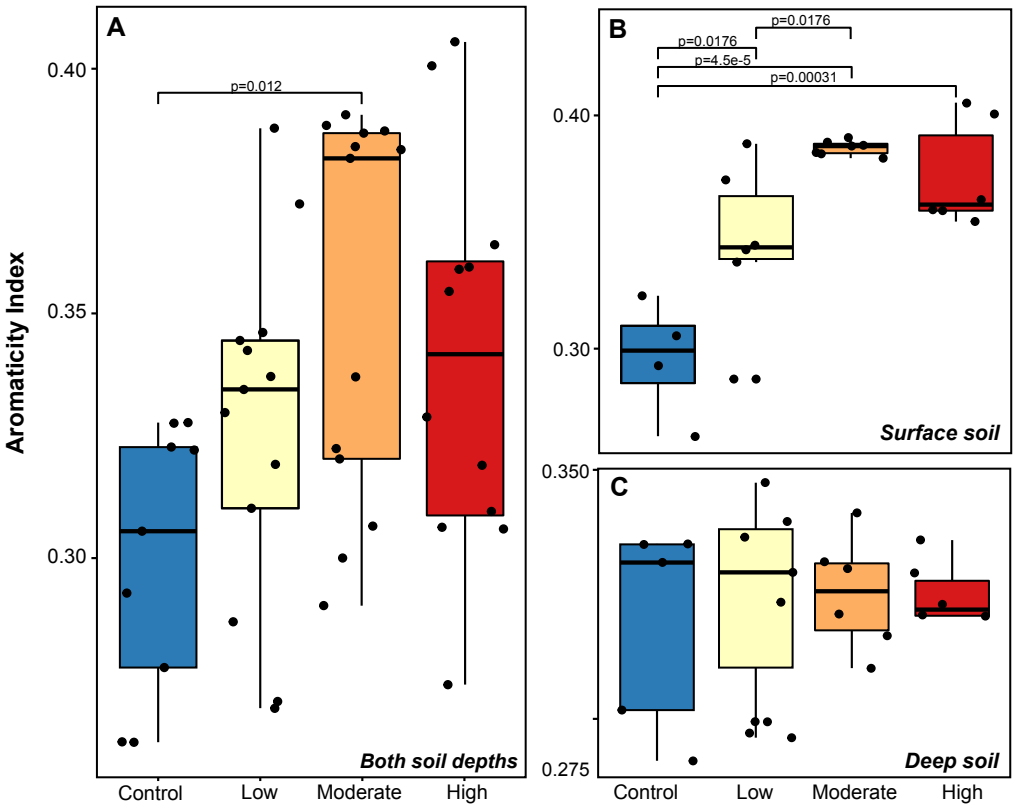

Figure 2.12 DOM aromaticity index trends across soil depths. Aromaticity index of DOM pools across burn severity conditions for all samples combined (A; *n* = 9 for control, 12 for low, 11 for moderate, and 12 for high severity), and shallow (B; *n* = 4 for control, 6 for low, 5 for moderate, and 6 for high severity) and deep (C; *n* = 5 for control, 6 for low, moderate, and high severity) samples. P-values are shown if there is significant differences between conditions (one-sided pairwise t-test, $p<0.05$). The lower and upper hinges of the boxplots represent the 25th and 75th percentile and the middle line is the median. The upper whisker extends to the median plus 1.5x interquartile range and the lower whisker extends to the median minus 1.5x interquartile range. Data points represent outliers.

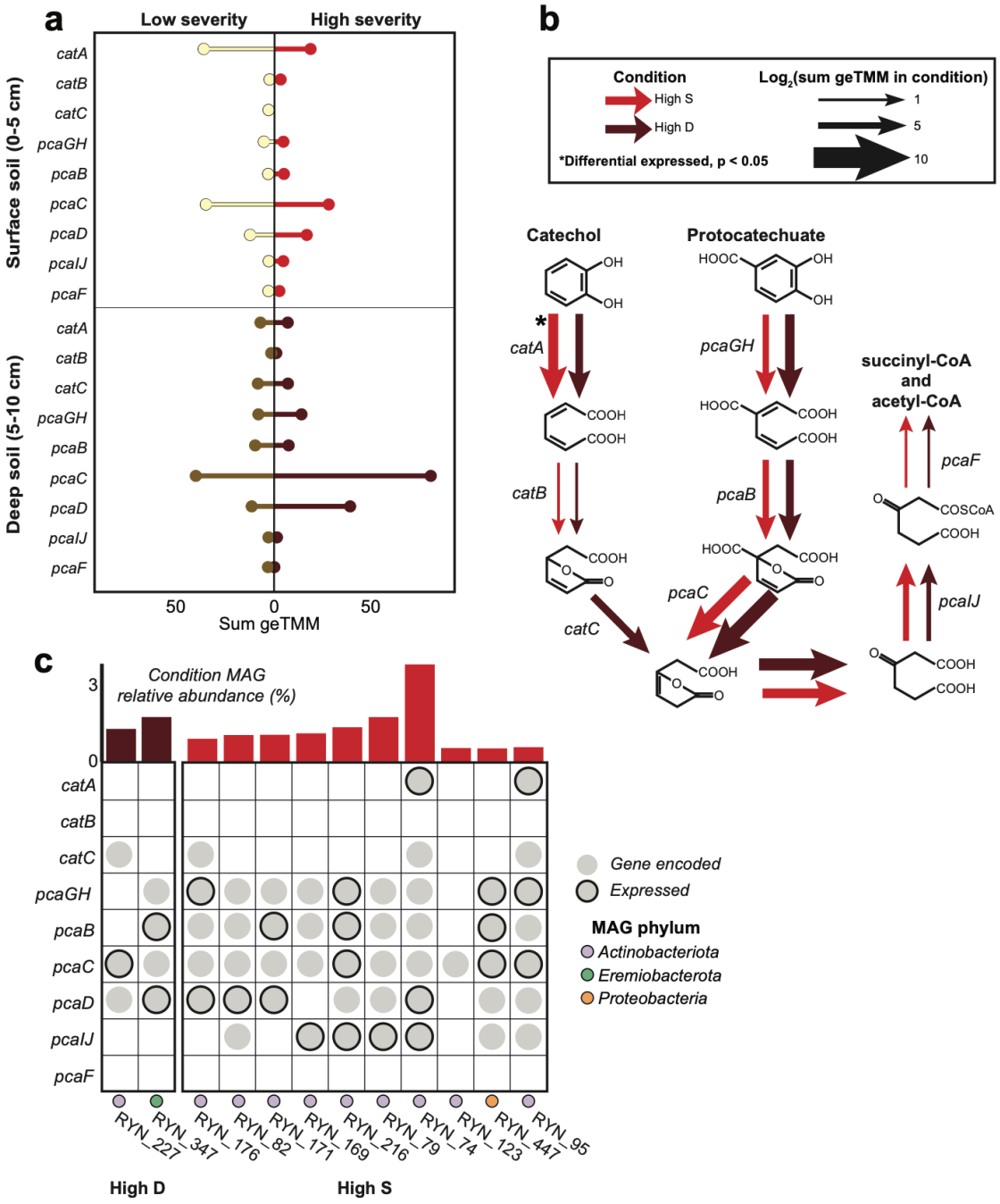

Figure 2.13 a, The summed geTMM of each gene for catechol and protocatechuate ortho-cleavage in each condition. b, The pathway for catechol and protocatechuate ortho-cleavage, with arrows indicating the log normalized sum geTMM of the gene for high severity surface and deep soils. Asterisk indicates genes that are differentially expressed in the condition (Wald's test in DESeq2; P = 0.0055 for catA in High S). c, The genomic potential and expression of each gene in the pathway for the MAGs of interest in High S and High D samples. The bar chart at the top shows the featured MAG relative abundance in that condition, coloured by featured condition.

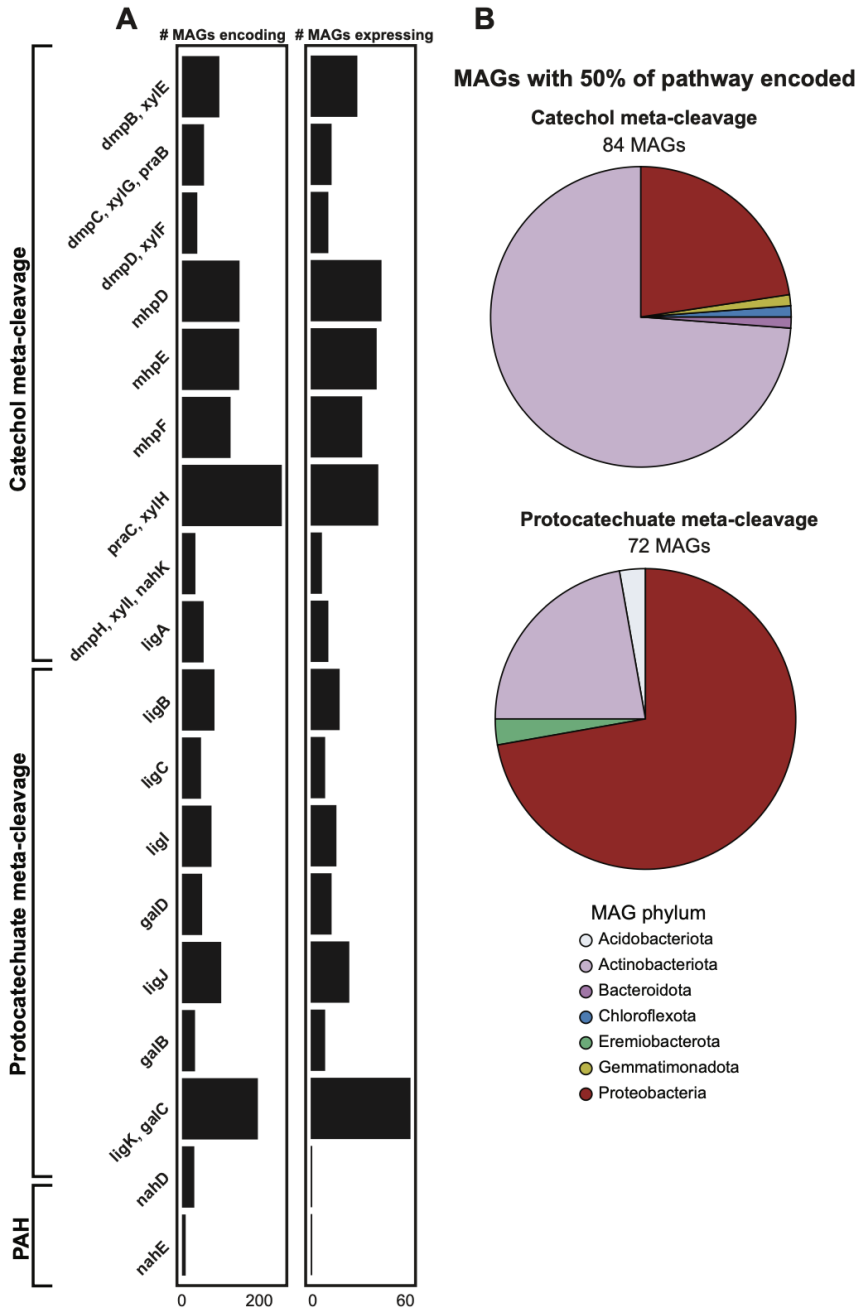

Figure 2.14 (a) Number of MAGs encoding and expressing each gene of the catechol and protocatechuate meta-cleavage pathways. (b) Phyla distribution of MAGs encoding 50% of either pathway.

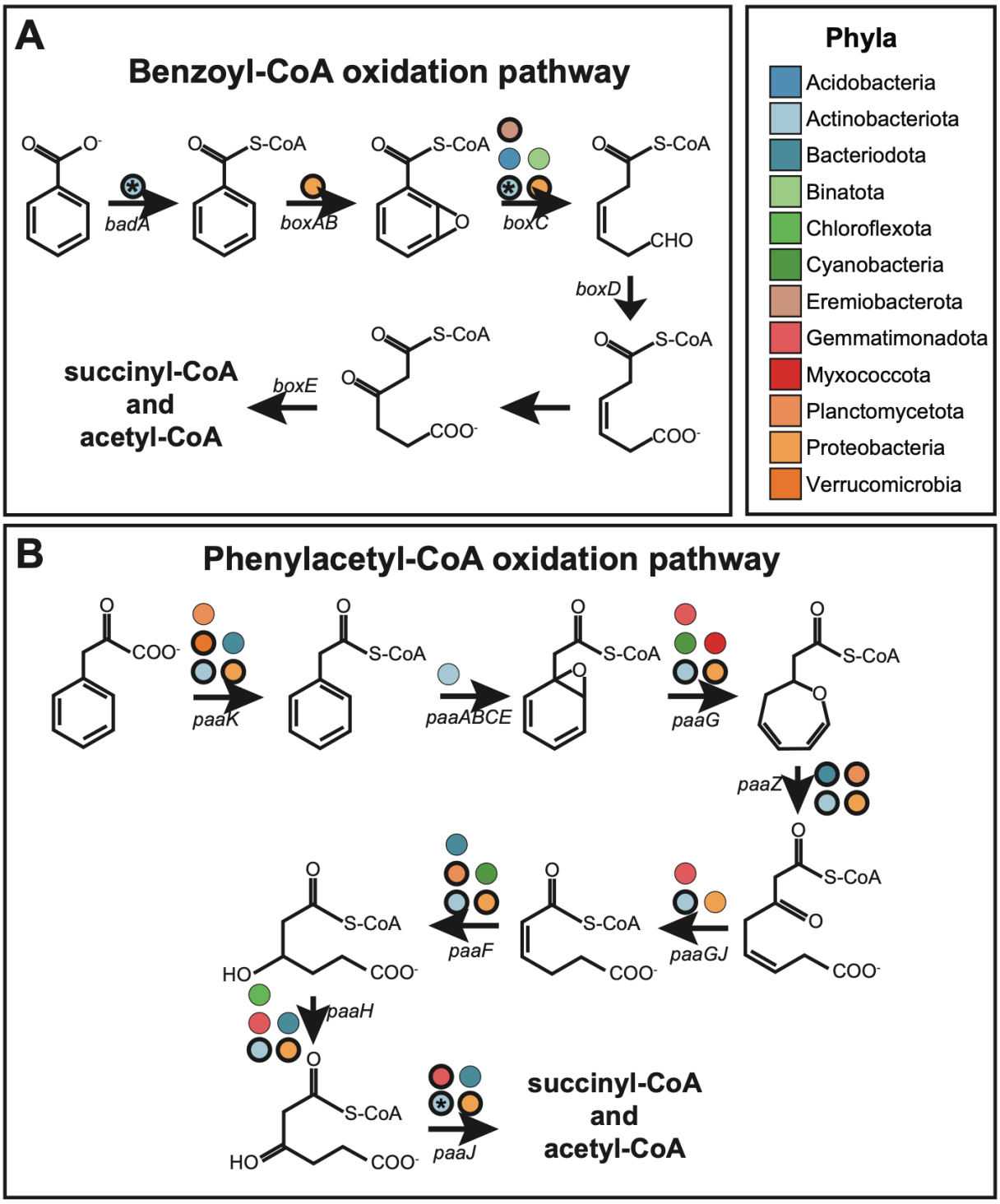

Figure 2.15 The benzoyl-CoA oxidation pathway (a) and phenylacetyl-CoA oxidation pathway (b) with overlaid gene names and whether there was encoded or expressed evidence of these genes. Colored circles indicate whether a MAG from that phyla encoded that gene, bolded circles indicate that metatranscriptomic reads mapped to the gene, and asterisks indicate the gene was being highly expressed in any given condition.

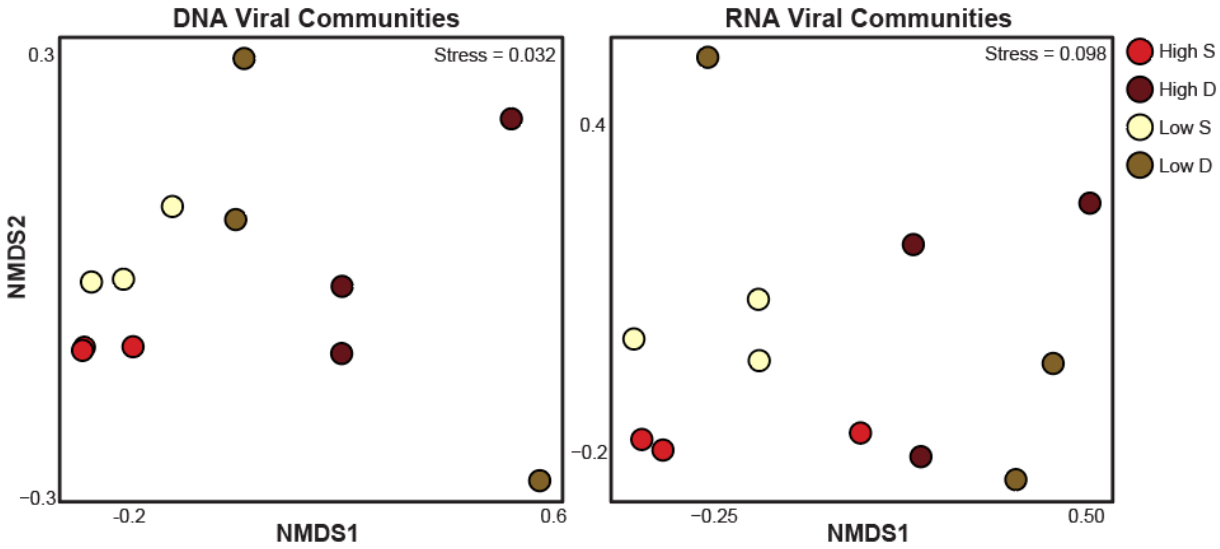

Figure 2.16 DNA and RNA viral community dynamics. NMDS of DNA (left) and RNA (right) vMAG abundance across all four conditions.

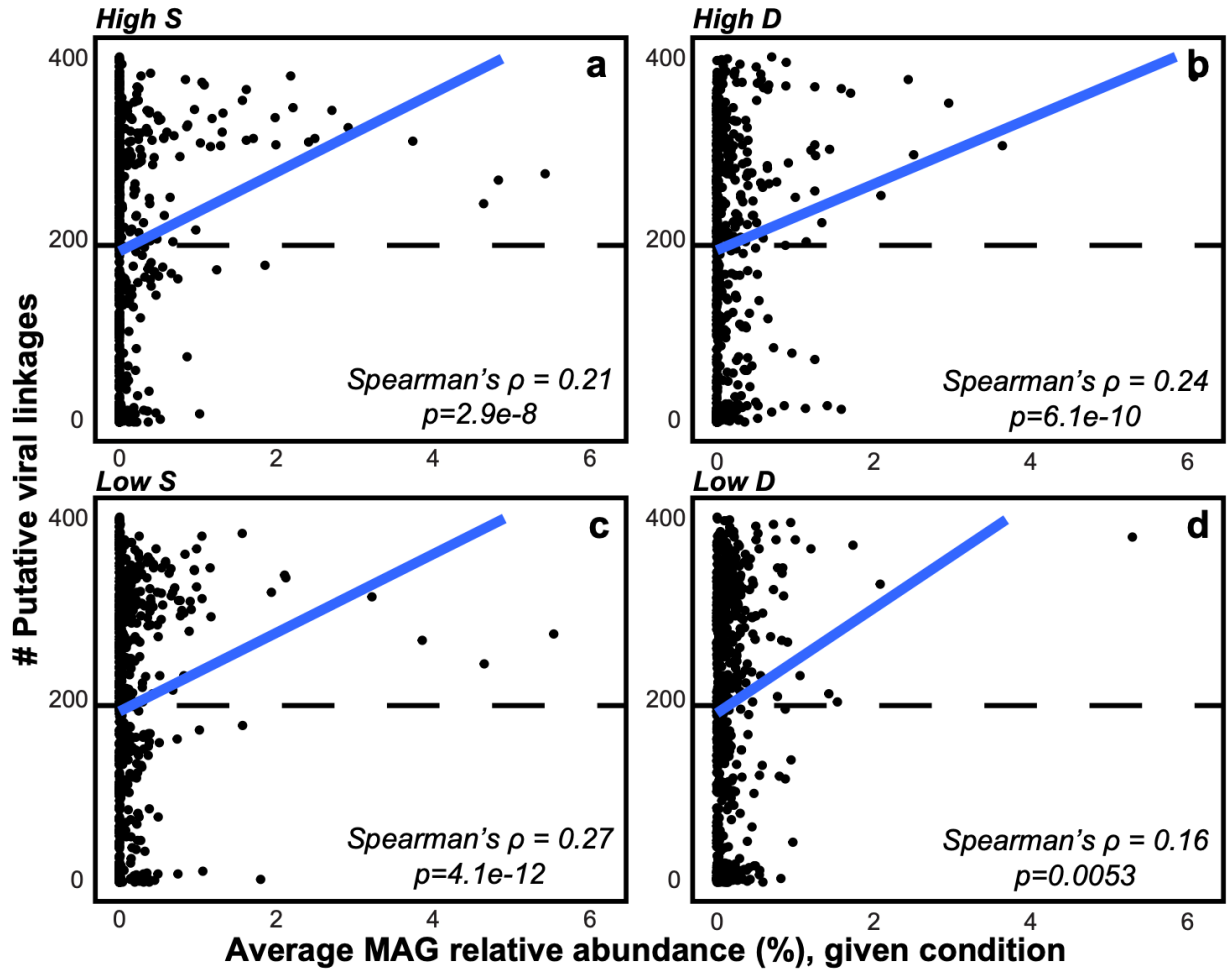

Figure 2.17 Each MAG's relative abundance within (a) High S and (b) D and (c) Low S and (d) D conditions plotted against the number of putative viral linkages identified by VirHostMatcher. Dashed line indicates the dataset average of 196 virus-host linkages. Correlation and significance between MAG relative abundance and number of putative viral linkages were assessed using the two-sided Spearman rho test.

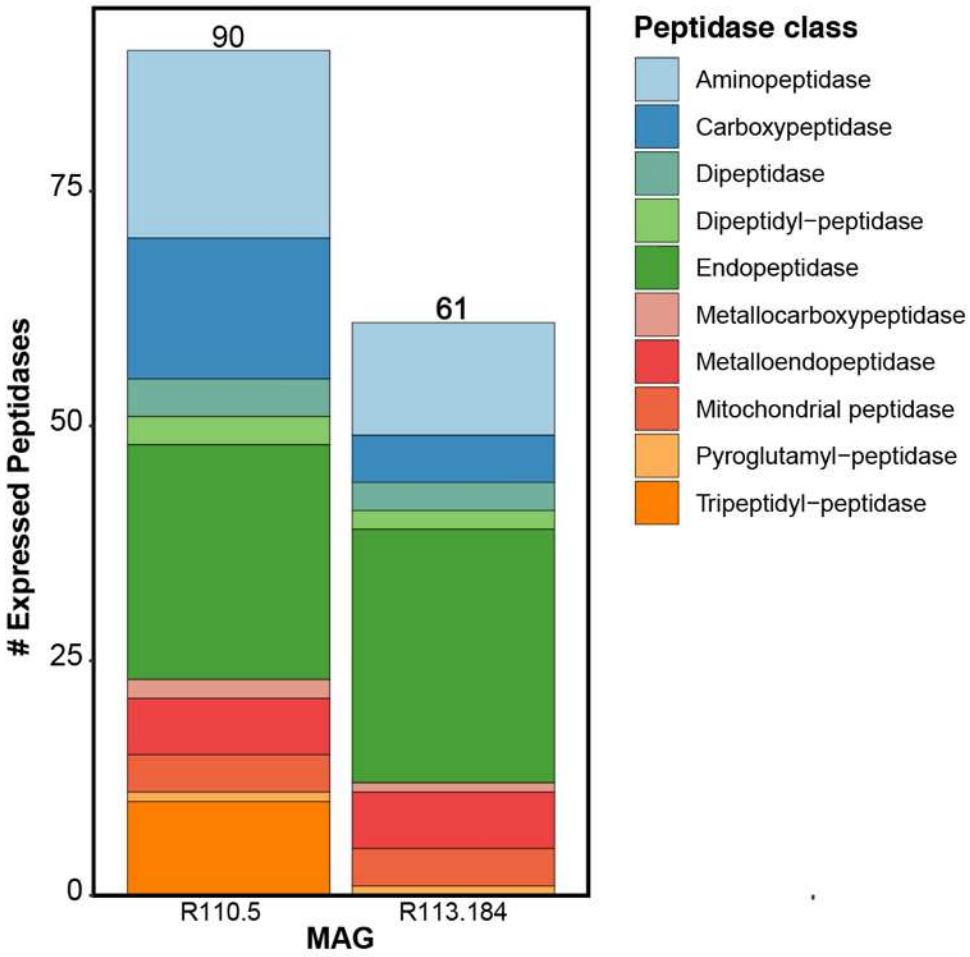

Figure 2.18 Peptidase expression prevalent in fungal MAGs. The diversity of all peptidases expressed by each fungal MAG across all 4 conditions.

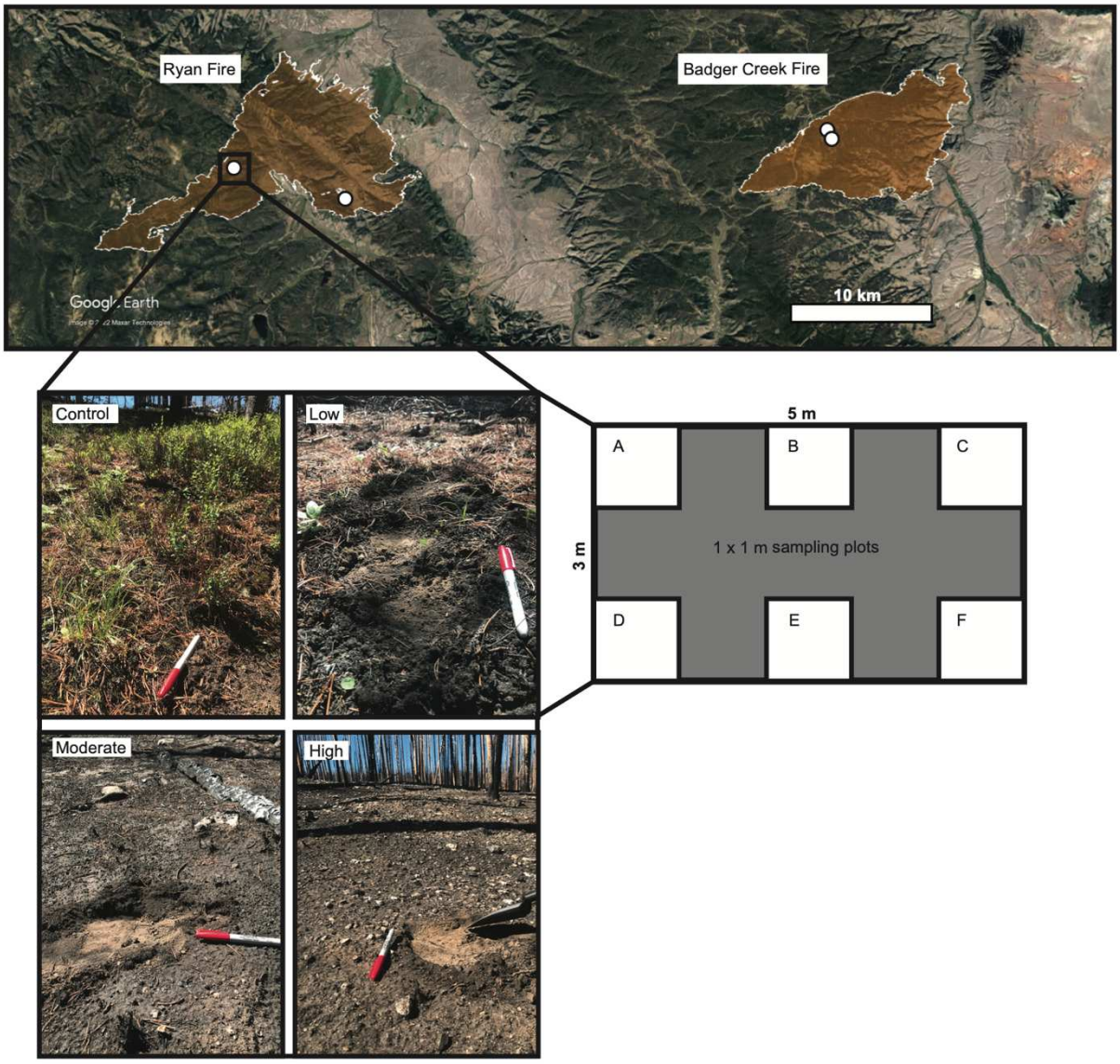

Figure 2.19 There were four replicate burn severity gradients (two at Ryan Fire and two At Badger Creek Fire; six subsamples were collected in each burn condition at each gradient.

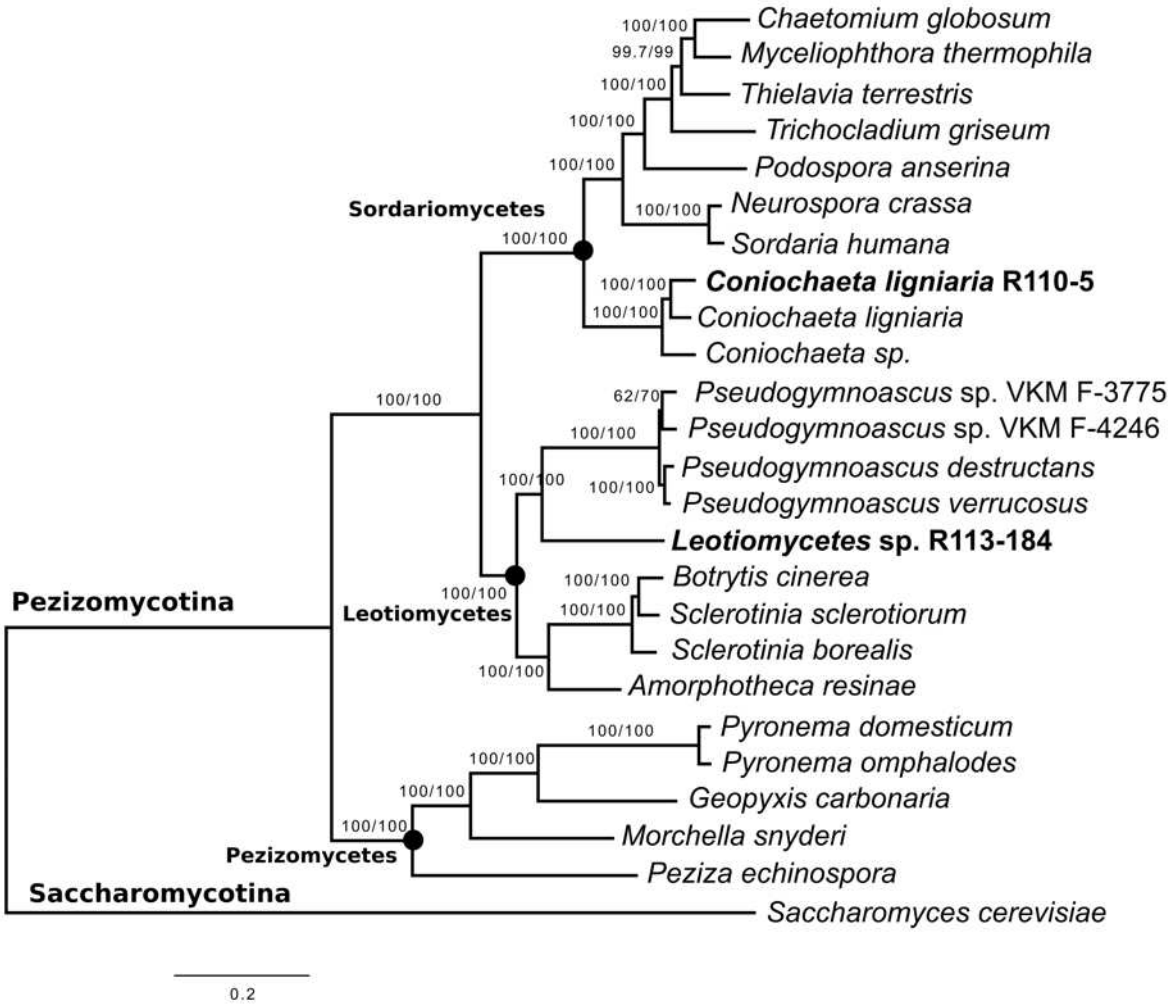

Figure 2.20 Fungal phylogenetic tree. Maximum likelihood tree showing the phylogenetic relationship of the 2 fungal MAGS (bold) based on 867 single-copy orthogroups.

Chapter 2 Tables

Table 2.1 Characteristics of WGCNA networks created from 16S rRNA gene sequencing data from each condition.

Condition	Nodes	Edges	Edge:node	Modules	N samples
Bacterial communities					
Control, surface	10426	3662534	351.3	16	16
Low, surface	6234	1194870	191.7	22	24
Moderate, surface	2442	196930	80.6	11	24
High, surface	2193	277073	126.3	11	24
Control, deep	9452	2769191	292.9	16	16
Low, deep	9132	1904471	208.5	21	24
Moderate, deep	5916	1376628	232.7	18	24
High, deep	6415	1151930	179.6	19	24
Fungal communities					
Control, surface	2491	271323	108.9	12	16
Low, surface	1548	126698	81.8	11	24
Moderate, surface	238	14366	60.3	2	24
High, surface	260	17026	65.5	2	24
Control, deep	1569	145649	92.8	9	16
Low, deep	681	48389	71.1	5	24
Moderate, deep	242	14558	60.1	3	24
High, deep	374	23626	63.1	3	24

Table 2.2 Percent change in relative abundance from control to low, moderate, and high severity in surface soils of all ASVs assigned to each ecological guild by FUNguild. Data shown here only includes guilds with greater than 30 classified ASVs.

Guild	# ESVs	% Change with Low	% Change with Mod	% Change with High
Ectomycorrhizal	321	-99.7	-99.9	-99.9
Endophyte	39	-94.2	-95.9	-99.9
Epiphyte	31	-81.1	-99.3	-98.8
Fungal parasite	132	-19.5	-41.1	-65.2
Plant pathogen	528	122.0	24.4	-65.2
Undefined saprotroph	1292	231.0	290.9	298.7
Wood saprotroph	133	-34.2	-99.5	-99.2

Table 2.3 The geTMM cutoff values for high expression analysis in each sample. Values correspond to the 20th percentile value TMM. Transcripts were highly expressed if the TMM was above this value for 2/3 samples in any one condition.

Sample	geTMM high expression cutoff
R85	1.68
R86	3.26
R89	1.47
R90	3.16
R93	1.68
R94	3.28
R109	1.68
R110	2.24
R113	1.68
R114	2.11
R117	1.61
R118	1.87

.

Chapter 2 References

1. Dennison, P. E., Brewer, S. C., Arnold, J. D. & Moritz, M. A. Large wildfire trends in the western United States, 1984-2011. *Geophys. Res. Lett.* **41**, 2928–2933 (2014).
2. Higuera, P. E. & Abatzoglou, J. T. Record-setting climate enabled the extraordinary 2020 fire season in the western United States. *Glob. Chang. Biol.* gcb.15388 (2020). doi:10.1111/gcb.15388
3. Parks, S. A. & Abatzoglou, J. T. Warmer and Drier Fire Seasons Contribute to Increases in Area Burned at High Severity in Western US Forests From 1985 to 2017. *Geophys. Res. Lett.* **47**, 1–10 (2020).
4. Benavides-Solorio, J. D. D. & MacDonald, L. H. Measurement and prediction of post-fire erosion at the hillslope scale, Colorado Front Range. *Int. J. Wildl. Fire* **14**, 457 (2005).
5. Pierson, D. N., Robichaud, P. R., Rhoades, C. C. & Brown, R. E. Soil carbon and nitrogen eroded after severe wildfire and erosion mitigation treatments. *Int. J. Wildl. Fire* **28**, 814 (2019).
6. Rhoades, C. C., Entwistles, D. & Butler, D. The influence of wildfire extent and severity on streamwater chemistry, sediment and temperature following the Hayman Fire , Colorado. *Int. J. Wildl. Fire* 430–442 (2011).
7. Chambers, M. E., Fornwalt, P. J., Malone, S. L. & Battaglia, M. A. Patterns of conifer regeneration following high severity wildfire in ponderosa pine – dominated forests of the Colorado Front Range. *For. Ecol. Manage.* **378**, 57–67

(2016).

8. Rhoades, C. C. *et al.* The Legacy of a Severe Wildfire on Stream Nitrogen and Carbon in Headwater Catchments. *Ecosystems* **22**, 643–657 (2019).
9. Strickland, M. S., Lauber, C., Fierer, N. & Bradford, M. A. Testing the functional significance of microbial community composition. *Ecology* **90**, 441–451 (2009).
10. van der Heijden, M. G. A., Bardgett, R. D. & van Straalen, N. M. The unseen majority: soil microbes as drivers of plant diversity and productivity in terrestrial ecosystems. *Ecol. Lett.* **11**, 296–310 (2008).
11. Mendes, R. *et al.* Deciphering the Rhizosphere Microbiome for Disease-Suppressive Bacteria. *Science (80-.).* **332**, 1097–1100 (2011).
12. Hart, S. C., DeLuca, T. H., Newman, G. S., MacKenzie, M. D. & Boyle, S. I. Post-fire vegetative dynamics as drivers of microbial community structure and function in forest soils. *For. Ecol. Manage.* **220**, 166–184 (2005).
13. Pressler, Y., Moore, J. C. & Cotrufo, M. F. Belowground community responses to fire: meta-analysis reveals contrasting responses of soil microorganisms and mesofauna. *Oikos* **128**, 309–327 (2019).
14. Pulido-Chavez, M. F., Alvarado, E. C., DeLuca, T. H., Edmonds, R. L. & Glassman, S. I. High-severity wildfire reduces richness and alters composition of ectomycorrhizal fungi in low-severity adapted ponderosa pine forests. *For. Ecol. Manage.* **485**, 118923 (2021).
15. Villadas, P. J. *et al.* The Soil Microbiome of the Laurel Forest in Garajonay National Park (La Gomera, Canary Islands): Comparing Unburned and Burned Habitats after a Wildfire. *Forests* **10**, 1051 (2019).

16. Dove, N. C. & Hart, S. C. Fire reduces fungal species richness and in situ mycorrhizal colonization: A meta-analysis. *Fire Ecol.* **13**, 37–65 (2017).

17. Ibáñez, T. S., Wardle, D. A., Gundale, M. J. & Nilsson, M.-C. Effects of Soil Abiotic and Biotic Factors on Tree Seedling Regeneration Following a Boreal Forest Wildfire. *Ecosystems* (2021). doi:10.1007/s10021-021-00666-0

18. Whitman, T. *et al.* Soil bacterial and fungal response to wildfires in the Canadian boreal forest across a burn severity gradient. *Soil Biol. Biochem.* **138**, 107571 (2019).

19. Brown, S. P. *et al.* Context dependent fungal and bacterial soil community shifts in response to recent wildfires in the Southern Appalachian Mountains. *For. Ecol. Manage.* **451**, 117520 (2019).

20. Ferrenberg, S. *et al.* Changes in assembly processes in soil bacterial communities following a wildfire disturbance. *ISME J.* **7**, 1102–1111 (2013).

21. Knelman, J. E., Schmidt, S. K., Garayburu-Caruso, V., Kumar, S. & Graham, E. B. Multiple, compounding disturbances in a forest ecosystem: Fire increases susceptibility of soil edaphic properties, bacterial community structure, and function to change with extreme precipitation event. *Soil Syst.* **3**, 1–16 (2019).

22. Zhang, L. *et al.* Habitat heterogeneity induced by pyrogenic organic matter in wildfire-perturbed soils mediates bacterial community assembly processes. *ISME J.* **5**, (2021).

23. Tas, N. *et al.* Impact of fire on active layer and permafrost microbial communities and metagenomes in an upland Alaskan boreal forest. *ISME J.* 1904–1919 (2014). doi:10.1038/ismej.2014.36

24. Yang, S. *et al.* Fire affects the taxonomic and functional composition of soil microbial communities, with cascading effects on grassland ecosystem functioning. *Glob. Chang. Biol.* **26**, 431–442 (2020).

25. Dove, N. C., Safford, H. D., Bohlman, G. N., Estes, B. L. & Hart, S. C. High-severity wildfire leads to multi-decadal impacts on soil biogeochemistry in mixed-conifer forests. *Ecol. Appl.* **30**, eap.2072 (2020).

26. Pérez-Valera, E., Goberna, M. & Verdú, M. Fire modulates ecosystem functioning through the phylogenetic structure of soil bacterial communities. *Soil Biol. Biochem.* **129**, 80–89 (2019).

27. SantaCruz-Calvo, L., González-López, J. & Manzanera, M. Arthrobacter siccitolerans sp. nov., a highly desiccation-tolerant, xeroprotectant-producing strain isolated from dry soil. *Int. J. Syst. Evol. Microbiol.* **63**, 4174–4180 (2013).

28. Mongodin, E. F. *et al.* Secrets of soil survival revealed by the genome sequence of Arthrobacter aurescens TC1. *PLoS Genet.* **2**, 2094–2106 (2006).

29. Bourguignon, N., Isaac, P., Alvarez, H., Amoroso, M. J. & Ferrero, M. A. Enhanced polyaromatic hydrocarbon degradation by adapted cultures of actinomycete strains. *J. Basic Microbiol.* **54**, 1288–1294 (2014).

30. Fischer, M. S. *et al.* Pyrolyzed Substrates Induce Aromatic Compound Metabolism in the Post-fire Fungus, Pyronema domesticum. *Front. Microbiol.* **12**, (2021).

31. Arora, P. K. & Sharma, A. New metabolic pathway for degradation of 2-nitrobenzoate by Arthrobacter sp. SPG. *Front. Microbiol.* **06**, 1–6 (2015).

32. Ren, L. *et al.* Insight Into Metabolic Versatility of an Aromatic Compounds-

Degrading Arthrobacter sp. YC-RL1. *Front. Microbiol.* **9**, 1–15 (2018).

33. Cobo-Díaz, J. F. *et al.* Metagenomic Assessment of the Potential Microbial Nitrogen Pathways in the Rhizosphere of a Mediterranean Forest After a Wildfire. *Microb. Ecol.* **69**, 895–904 (2015).

34. Dove, N. C., Taş, N. & Hart, S. C. Ecological and genomic responses of soil microbiomes to high-severity wildfire: linking community assembly to functional potential. *ISME J.* 1–11 (2022). doi:10.1038/s41396-022-01232-9

35. Adkins, J., Docherty, K. M., Gutknecht, J. L. M. & Miesel, J. R. How do soil microbial communities respond to fire in the intermediate term? Investigating direct and indirect effects associated with fire occurrence and burn severity. *Sci. Total Environ.* **745**, 140957 (2020).

36. Newton, G. L., Buchmeier, N. & Fahey, R. C. Biosynthesis and Functions of Mycothiol, the Unique Protective Thiol of Actinobacteria. *Microbiol. Mol. Biol. Rev.* **72**, 471–494 (2008).

37. Reina-Bueno, M. *et al.* Role of trehalose in heat and desiccation tolerance in the soil bacterium Rhizobium etli. *BMC Microbiol.* **12**, 207 (2012).

38. Schimel, J. P. Life in Dry Soils: Effects of Drought on Soil Microbial Communities and Processes. *Annu. Rev. Ecol. Evol. Syst.* **49**, 409–432 (2018).

39. Musto, H. *et al.* Correlations between genomic GC levels and optimal growth temperatures in prokaryotes. *FEBS Lett.* **573**, 73–77 (2004).

40. Yakovchuk, P. Base-stacking and base-pairing contributions into thermal stability of the DNA double helix. *Nucleic Acids Res.* **34**, 564–574 (2006).

41. Mooshammer, M. *et al.* Decoupling of microbial carbon, nitrogen, and phosphorus

cycling in response to extreme temperature events. *Sci. Adv.* **3**, e1602781 (2017).

42. Pérez-Valera, E., Goberna, M. & Verdú, M. Fire modulates ecosystem functioning through the phylogenetic structure of soil bacterial communities. *Soil Biol. Biochem.* **129**, 80–89 (2019).

43. Weissman, J. L., Hou, S. & Fuhrman, J. A. Estimating maximal microbial growth rates from cultures, metagenomes, and single cells via codon usage patterns. *PNAS* **118**, 1–10 (2020).

44. Long, A. M., Hou, S., Ignacio-Espinoza, J. C. & Fuhrman, J. A. Benchmarking microbial growth rate predictions from metagenomes. *ISME J.* **15**, 183–195 (2021).

45. Karlin, S., Mrázek, J., Campbell, A. & Kaiser, D. Characterizations of Highly Expressed Genes of Four Fast-Growing Bacteria. *J. Bacteriol.* **183**, 5025–5040 (2001).

46. Scott, M., Gunderson, C. W., Mateescu, E. M., Zhang, Z. & Hwa, T. Interdependence of Cell Growth and Gene Expression: Origins and Consequences. *Science (80-.).* **330**, 1099–1102 (2010).

47. Faria, S. R. *et al.* Wildfire-induced alterations of topsoil organic matter and their recovery in Mediterranean eucalypt stands detected with biogeochemical markers. *Eur. J. Soil Sci.* **66**, 699–713 (2015).

48. Chen, H., Rhoades, C. C. & Chow, A. T. Characteristics of soil organic matter 14 years after a wildfire: A pyrolysis-gas-chromatography mass spectrometry (Py-GC-MS) study. *J. Anal. Appl. Pyrolysis* **152**, 104922 (2020).

49. Knicker, H. Pyrogenic organic matter in soil: Its origin and occurrence, its

chemistry and survival in soil environments. *Quat. Int.* **243**, 251–263 (2011).

50. Bahureksa, W. *et al.* Nitrogen Enrichment during Soil Organic Matter Burning and Molecular Evidence of Maillard Reactions. *Environ. Sci. Technol.* acs.est.1c06745 (2022). doi:10.1021/acs.est.1c06745

51. Boye, K. *et al.* Thermodynamically controlled preservation of organic carbon in floodplains. *Nat. Geosci.* **10**, 415–419 (2017).

52. LaRowe, D. E. & Van Cappellen, P. Degradation of natural organic matter: A thermodynamic analysis. *Geochim. Cosmochim. Acta* **75**, 2030–2042 (2011).

53. Fuchs, G., Boll, M. & Heider, J. Microbial degradation of aromatic compounds-From one strategy to four. *Nat. Rev. Microbiol.* **9**, 803–816 (2011).

54. Pingree, M. R. A. & DeLuca, T. H. Function of Wildfire-Deposited Pyrogenic Carbon in Terrestrial Ecosystems. *Front. Environ. Sci.* **5**, 1–7 (2017).

55. Trubl, G. *et al.* Soil Viruses Are Underexplored Players in Ecosystem Carbon Processing. *mSystems* **3**, 1–21 (2018).

56. Ahlgren, N. A., Ren, J., Lu, Y. Y., Fuhrman, J. A. & Sun, F. Alignment-free d_2^* oligonucleotide frequency dissimilarity measure improves prediction of hosts from metagenomically-derived viral sequences. *Nucleic Acids Res.* **45**, 39–53 (2017).

57. Kuzyakov, Y. & Mason-Jones, K. Viruses in soil: Nano-scale undead drivers of microbial life, biogeochemical turnover and ecosystem functions. *Soil Biol. Biochem.* **127**, 305–317 (2018).

58. Knowles, B. *et al.* Lytic to temperate switching of viral communities. *Nature* **531**, 466–470 (2016).

59. Hewelke, E. *et al.* Soil Functional Responses to Natural Ecosystem Restoration of a Pine Forest Peucedano-Pinetum after a Fire. *Forests* **11**, 286 (2020).

60. Mahoney, D. P. & LaFavre, J. S. Coniochaeta extramundana, with a Synopsis of Other Coniochaeta Species. *Mycologia* **73**, 931 (1981).

61. Yang, T. *et al.* Distinct fungal successional trajectories following wildfire between soil horizons in a cold-temperate forest. *New Phytol.* **227**, 572–587 (2020).

62. Steindorff, A. S. *et al.* Comparative genomics of pyrophilous fungi reveals a link between fire events and developmental genes. *Environ. Microbiol.* **23**, 99–109 (2021).

63. Viswanath, B., Rajesh, B., Janardhan, A., Kumar, A. P. & Narasimha, G. Fungal Laccases and Their Applications in Bioremediation. *Enzyme Res.* **2014**, 1–21 (2014).

64. Bouskill, N. J., Mekonnen, Z., Zhu, Q., Grant, R. & Riley, W. J. Microbial contribution to post-fire tundra ecosystem recovery over the 21st century. *Commun. Earth Environ.* **3**, 26 (2022).

65. Yeager, C. M., Northup, D. E., Grow, C. C., Barns, S. M. & Kuske, C. R. Changes in nitrogen-fixing and ammonia-oxidizing bacterial communities in soil of a mixed conifer forest after wildfire. *Appl. Environ. Microbiol.* **71**, 2713–2722 (2005).

66. Ward, N. L. *et al.* Three Genomes from the Phylum Acidobacteria Provide Insight into the Lifestyles of These Microorganisms in Soils. *Appl. Environ. Microbiol.* **75**, 2046–2056 (2009).

67. García-Fraile, P., Benada, O., Cajthaml, T., Baldrian, P. & Lladó, S. Terracidiphilus gabretensis gen. nov., sp. nov., an Abundant and Active Forest

Soil Acidobacterium Important in Organic Matter Transformation. *Appl. Environ. Microbiol.* **82**, 560–569 (2016).

68. Eichorst, S. A., Kuske, C. R. & Schmidt, T. M. Influence of Plant Polymers on the Distribution and Cultivation of Bacteria in the Phylum Acidobacteria. *Appl. Environ. Microbiol.* **77**, 586–596 (2011).

69. Banerjee, S. *et al.* Network analysis reveals functional redundancy and keystone taxa amongst bacterial and fungal communities during organic matter decomposition in an arable soil. *Soil Biol. Biochem.* **97**, 188–198 (2016).

70. Costa, O. Y. A., Raaijmakers, J. M. & Kuramae, E. E. Microbial Extracellular Polymeric Substances: Ecological Function and Impact on Soil Aggregation. *Front. Microbiol.* **9**, 1–14 (2018).

71. Smith, S. E. & Read, D. Mycorrhizal Symbiosis. *Soil Sci.* **137**, 204 (1984).

72. Douglas, R. B., Parker, V. T. & Cullings, K. W. Belowground ectomycorrhizal community structure of mature lodgepole pine and mixed conifer stands in Yellowstone National Park. *For. Ecol. Manage.* **208**, 303–317 (2005).

73. Anthony, M. A. *et al.* Forest tree growth is linked to mycorrhizal fungal composition and function across Europe. *ISME J.* 1–10 (2022). doi:10.1038/s41396-021-01159-7

74. Marx, D. H., Bryan, W. C. & Cordell, C. E. Survival and Growth of Pine Seedlings with Pisolithus Ectomycorrhizae after Two Years on Reforestation Sites in North Carolina and Florida. *For. Sci.* **23**, 363–373 (1977).

75. Franco, A. R., Sousa, N. R., Ramos, M. A., Oliveira, R. S. & Castro, P. M. L. Diversity and Persistence of Ectomycorrhizal Fungi and Their Effect on Nursery-

Inoculated Pinus pinaster in a Post-fire Plantation in Northern Portugal. *Microb. Ecol.* **68**, 761–772 (2014).

76. Kipfmueller, K. F. & Baker, W. L. A fire history of a subalpine forest in south-eastern Wyoming, USA. *J. Biogeogr.* **27**, 71–85 (2000).

77. Key, C. H. & Benson, N. C. Landscape Assessment (LA) sampling and analysis methods. *USDA For. Serv. - Gen. Tech. Rep. RMRS-GTR* (2006).

78. Parson, A., Robichaud, P. R., Lewis, S. A., Napper, C. & Clark, J. T. *Field guide for mapping post-fire soil burn severity*. *USDA Forest Service - General Technical Report RMRS-GTR* (2010). doi:10.2737/RMRS-GTR-243

79. Miesel, J. R., Hockaday, W. C., Kolka, R. K. & Townsend, P. A. Soil organic matter composition and quality across fire severity gradients in coniferous and deciduous forests of the southern boreal region. *J. Geophys. Res. Biogeosciences* **120**, 1124–1141 (2015).

80. Bundy, L. G. & Meisinger, J. J. Nitrogen Availability Indices. in *Methods of Soil Analysis: Part 2 Microbiological and Biochemical Properties* 951–984 (Macmillan Education UK, 2018). doi:10.2136/sssabookser5.2.c41

81. McDowell, W. H. *et al.* A comparison of methods to determine the biodegradable dissolved organic carbon from different terrestrial sources. *Soil Biol. Biochem.* **38**, 1933–1942 (2006).

82. Thomas, G. W. Soil pH and soil acidity. *Methods soil Anal. Part 3* 475–490 (1996).

83. Dittmar, T., Koch, B., Hertkorn, N. & Kattner, G. A simple and efficient method for the solid-phase extraction of dissolved organic matter (SPE-DOM) from seawater.

Limnol. Oceanogr. Methods **6**, 230–235 (2008).

84. Tolić, N. *et al.* Formularity: Software for Automated Formula Assignment of Natural and Other Organic Matter from Ultrahigh-Resolution Mass Spectra. *Anal. Chem.* **89**, 12659–12665 (2017).

85. Bramer, L. M. *et al.* ftmsRanalysis: An R package for exploratory data analysis and interactive visualization of FT-MS data. *PLOS Comput. Biol.* **16**, e1007654 (2020).

86. Caporaso, J. G. *et al.* Ultra-high-throughput microbial community analysis on the Illumina HiSeq and MiSeq platforms. *ISME J.* **6**, 1621–1624 (2012).

87. Quast, C. *et al.* The SILVA ribosomal RNA gene database project: improved data processing and web-based tools. *Nucleic Acids Res.* **41**, D590–D596 (2012).

88. Kõljalg, U. *et al.* UNITE: a database providing web-based methods for the molecular identification of ectomycorrhizal fungi. *New Phytol.* **166**, 1063–1068 (2005).

89. Bolyen, E. *et al.* Reproducible, interactive, scalable and extensible microbiome data science using QIIME 2. *Nat. Biotechnol.* **37**, 852–857 (2019).

90. Callahan, B. J. *et al.* DADA2: High-resolution sample inference from Illumina amplicon data. *Nat. Methods* **13**, 581–583 (2016).

91. Nguyen, N. H. *et al.* FUNGuild: An open annotation tool for parsing fungal community datasets by ecological guild. *Fungal Ecol.* **20**, 241–248 (2016).

92. Team, R. C. R: A language and environment for statistical computing. *R Found. Stat. Comput. Vienna, Austria* (2021).

93. Oksanen, J. *et al.* Package 'vegan'. in (Springer Netherlands, 2013).

doi:10.1007/978-94-024-1179-9_301576

94. McMurdie, P. J. & Holmes, S. phyloseq: An R Package for Reproducible Interactive Analysis and Graphics of Microbiome Census Data. *PLoS One* **8**, e61217 (2013).

95. Segata, N. *et al.* Metagenomic biomarker discovery and explanation. *Genome Biol.* **12**, R60 (2011).

96. Joshi, N. & Fass, J. Sickle: A sliding-window, adaptive, quality-based trimming tool for FastQ files. (2011).

97. Li, D., Liu, C.-M., Luo, R., Sadakane, K. & Lam, T.-W. MEGAHIT: an ultra-fast single-node solution for large and complex metagenomics assembly via succinct de Bruijn graph. *Bioinformatics* **31**, 1674–1676 (2015).

98. Kang, D. D. *et al.* MetaBAT 2: an adaptive binning algorithm for robust and efficient genome reconstruction from metagenome assemblies. *PeerJ* **7**, e7359 (2019).

99. Parks, D. H., Imelfort, M., Skennerton, C. T., Hugenholtz, P. & Tyson, G. W. CheckM: assessing the quality of microbial genomes recovered from isolates, single cells, and metagenomes. *Genome Res.* **25**, 1043–1055 (2015).

100. Chaumeil, P.-A., Mussig, A. J., Hugenholtz, P. & Parks, D. H. GTDB-Tk: a toolkit to classify genomes with the Genome Taxonomy Database. *Bioinformatics* **36**, 1925–1927 (2019).

101. Olm, M. R., Brown, C. T., Brooks, B. & Banfield, J. F. dRep: a tool for fast and accurate genomic comparisons that enables improved genome recovery from metagenomes through de-replication. *ISME J.* **11**, 2864–2868 (2017).

102. Bowers, R. M. *et al.* Minimum information about a single amplified genome (MISAG) and a metagenome-assembled genome (MIMAG) of bacteria and archaea. *Nat. Biotechnol.* **35**, 725–731 (2017).

103. Emms, D. M. & Kelly, S. OrthoFinder: phylogenetic orthology inference for comparative genomics. *Genome Biol.* **20**, 238 (2019).

104. Katoh, K. MAFFT: a novel method for rapid multiple sequence alignment based on fast Fourier transform. *Nucleic Acids Res.* **30**, 3059–3066 (2002).

105. Capella-Gutierrez, S., Silla-Martinez, J. M. & Gabaldon, T. trimAl: a tool for automated alignment trimming in large-scale phylogenetic analyses. *Bioinformatics* **25**, 1972–1973 (2009).

106. Nguyen, L. T., Schmidt, H. A., Von Haeseler, A. & Minh, B. Q. IQ-TREE: A fast and effective stochastic algorithm for estimating maximum-likelihood phylogenies. *Mol. Biol. Evol.* **32**, 268–274 (2015).

107. Seppey, M., Manni, M. & Zdobnov, E. M. BUSCO: Assessing Genome Assembly and Annotation Completeness. in *Methods in Molecular Biology* 227–245 (Humana Press Inc., 2019). doi:10.1007/978-1-4939-9173-0_14

108. Parra, G., Bradnam, K. & Korf, I. CEGMA: a pipeline to accurately annotate core genes in eukaryotic genomes. *Bioinformatics* **23**, 1061–1067 (2007).

109. Bushmanova, E., Antipov, D., Lapidus, A. & Prjibelski, A. D. RnaSPAdes: A de novo transcriptome assembler and its application to RNA-Seq data. *Gigascience* **8**, 1–13 (2019).

110. Grigoriev, I. V. *et al.* MycoCosm portal: Gearing up for 1000 fungal genomes. *Nucleic Acids Res.* **42**, 699–704 (2014).

111. Shaffer, M. *et al.* DRAM for distilling microbial metabolism to automate the curation of microbiome function. *Nucleic Acids Res.* **48**, 8883–8900 (2020).

112. Eddy, S. R. Accelerated profile HMM searches. *PLoS Comput. Biol.* **7**, (2011).

113. Aramaki, T. *et al.* KofamKOALA: KEGG Ortholog assignment based on profile HMM and adaptive score threshold. *Bioinformatics* **36**, 2251–2252 (2020).

114. Anders, S., Pyl, P. T. & Huber, W. HTSeq--a Python framework to work with high-throughput sequencing data. *Bioinformatics* **31**, 166–169 (2015).

115. Love, M. I., Huber, W. & Anders, S. Moderated estimation of fold change and dispersion for RNA-seq data with DESeq2. *Genome Biol.* **15**, 550 (2014).

116. Smid, M. *et al.* Gene length corrected trimmed mean of M-values (GeTMM) processing of RNA-seq data performs similarly in intersample analyses while improving intrasample comparisons. *BMC Bioinformatics* **19**, 236 (2018).

117. Robinson, M. D., McCarthy, D. J. & Smyth, G. K. edgeR: a Bioconductor package for differential expression analysis of digital gene expression data. *Bioinformatics* **26**, 139–140 (2010).

118. Guo, J. *et al.* VirSorter2: a multi-classifier, expert-guided approach to detect diverse DNA and RNA viruses. *Microbiome* **9**, 37 (2021).

119. Nayfach, S. *et al.* CheckV assesses the quality and completeness of metagenome-assembled viral genomes. *Nat. Biotechnol.* **39**, 578–585 (2021).

120. Guo, J., Vik, D., Pratama, A. A., Roux, S. & Sullivan, M. B. Viral sequence identification SOP with VirSorter2. (2021). doi:10.17504/protocols.io.btv8nn9w

121. Bland, C. *et al.* CRISPR recognition tool (CRT): a tool for automatic detection of clustered regularly interspaced palindromic repeats. *BMC Bioinformatics* **8**, 209

(2007).

122. Skennerton, C. T., Imelfort, M. & Tyson, G. W. Crass: identification and reconstruction of CRISPR from unassembled metagenomic data. *Nucleic Acids Res.* **41**, e105–e105 (2013).

Chapter 3: Genomic evidence of altered life history strategies in the post-wildfire soil microbiome

3.1 Summary

The soil microbiome plays a vital role in biogeochemical cycling and ecosystem function and is an important player in terrestrial carbon cycling, but its complexity makes it challenging to understand post-disturbance soil microbiome successional dynamics and resulting impact on emergent ecosystem function. The application of conceptual life history strategy frameworks, like Grimes' C-S-R for plant communities, to environmental microbial communities can distill their complexity, enabling enhanced predictability of soil microbiome recovery following disturbances and the simplification of microbe representation in models. Various conceptual frameworks have been developed for the soil microbiome; the Y-A-S framework is a rendition of Grimes' C-S-R that broadly overviews soil microbiome life history strategies. In contrast, others have proposed frameworks specific to different disturbances (e.g., the traits-based fire ecology framework for predicting post-wildfire soil microbiome succession). Here, we test the applicability of conceptual life history strategy frameworks to the soil microbiome using wildfire as a model disturbance. Wildfires, which are increasing in both frequency and severity with climate change, reduce soil microbial biomass and alter the community composition of the soil microbiome, selecting for consistent "pyrophilous" taxa that persist and thrive in burned soil across numerous post-wildfire ecosystems. We utilize a comprehensive metagenome-assembled genome catalog from post-wildfire soil samples representing 1, 3, 5, and 11 years following low- and high-severity wildfire (CO, USA) to identify whether specific fitness traits enable the persistence of microbial taxa in post-

wildfire soils. We broadly found that high severity wildfire initially selects for fast growing microbial taxa and, up to a decade post-fire, those that invest in genes for acquiring diverse resources from the external environment (i.e., resource acquisition strategy of the Y-A-S framework), which likely has implications for post-wildfire soil carbon cycling. Together, this work begins to disentangle how trait-based frameworks can inform post-disturbance microbial ecology and enhance predictability of how environmental disturbance influence the function of the soil microbiome.

3.2 Introduction

The soil microbiome, like the soils it inhabits, is extremely complex and heterogeneous and is one of the most diverse microbial ecosystems on the planet with an estimated ~10^{11} bacterial cells per gram of soil[1]. This diversity coupled with the vast number of soil microorganisms unable to be cultured – termed microbial dark matter – makes studying the soil microbiome very challenging. The relatively recent advent of metagenomics[2,3], coupled with other 'omics tools (e.g., metatranscriptomics, metaproteomics), has greatly expanded our understanding of the taxonomic and functional breadth of the soil microbiome and revealed its importance in mediating various ecosystem services (e.g., fostering plant productivity[4], regulating soil carbon transformation and storage[5,6]).

Ecosystem disturbances, like permafrost thaw or wildfire, influence the function of the soil microbiome and sequencing tools have offered insight into the longevity and magnitude of these impacts[7–10]. However, the widespread use of sequencing tools to understand the effects of such a disturbance on the soil microbiome can be costly to

researchers computationally and financially and it is often difficult to conduct representative sampling to fully capture temporal and intrasite variability[11]. This complexity makes it challenging to both understand and predict post-disturbance soil microbiome dynamics and cascading impacts on ecosystem processes (e.g., carbon fluxes).

In plant communities, ecologists have addressed this difficulty by developing conceptual life history strategy frameworks to summarize key plant fitness traits that govern post-disturbance successional trajectories. One such framework, Grimes' C-S-R framework[12], categorizes plants as three primary life history strategies: Competitors (C), Stress tolerators (S), and Ruderal (R) species, with tradeoffs between traits that represent each strategy. Competitors excel at maximizing resource capture in productive or undisturbed systems (e.g., perennials), stress tolerators are associated with continuously low resource conditions (e.g., cacti), and ruderal species are successful in recently disturbed systems and have traits like shade intolerance or fast growth. These three strategies have been shown to apply broadly across ecosystems, adequately represent and distill the taxonomic diversity in plant communities[13], and help predict post-disturbance plant succession[14,15].

The success of conceptual life history strategy frameworks in plant ecology for predicting post-disturbance succession has led microbial ecologists to adapt these ideas for the complex soil microbiome; a microbe that is classified as a competitor might have a large genome and high catabolic diversity, a stress tolerator microbe is proposed to encode stress tolerant genes or be slow growers, and a ruderal microbial species might be a spore former that can grow quickly[16]. Malik et al (2020)[17] further proposed a new

framework, the Y-A-S framework, as a rendition of Grimes' C-S-R specifically modified to represent the soil microbiome. Here, the three microbial life history strategies are suggested to be high yield (Y), or taxa that maximize growth efficiency and thrive in resource-abundant conditions, resource acquisition (A), taxa that primarily invest in resource acquisition machinery (e.g., extracellular enzymes) and thrive in conditions where resources are complex or depleted, and stress tolerators (S) that invest energy into genes for persisting during fluctuating soil conditions (e.g., osmolyte production, desiccation). Importantly, all three life history strategies are proposed to be linked to emergent carbon cycling, making it valuable for not only predicting post-disturbance microbial succession but also impacts to carbon fluxes.

In contrast to the proposed Y-A-S framework, others suggest conceptual frameworks specific to the disturbance. One such example is wildfire, which is a unique soil disturbance as it causes distinct pulse and press disturbance impacts; the initial pulse disturbance exerts heat on the forest floor and death of aboveground vegetation, while the longer-term press disturbance is defined by lasting impacts to soil chemistry (e.g., increased pH, altered soil carbon quality and quantity)[18–20]. Wildfire depletes soil microbial biomass[21] and diversity[9,22], alters microbially mediated carbon and nitrogen functionality[9,10,18], and selects for putative pyrophilous microbial taxa (e.g., Actinobacteria *Arthrobacter* and Proteobacteria *Massilia*) that are proposed to exhibit specific traits that enable their persistence in post-wildfire soils. To explain the drivers of post-wildfire soil microbial succession, Johnson et al. (2023) proposed the traits-based framework of bacterial responses to wildfire[23] which includes microbial life history traits specific to soil impacts unique to wildfire: heat resistance, ability to degrade fire-transformed soil carbon,

and ability to withstand high soil pH induced by burning. If such frameworks effectively represent soil microbes, they serve as valuable tools to the field of microbial ecology, helping to predict post-disturbance soil microbial successional trajectories, distill complex environmental datasets, and aid in representing microbes in models aimed at predicting post-disturbance ecosystem carbon fluxes.

Here, we use wildfire as a model disturbance to analyze soil microbiome life history strategies as it is increasingly pertinent to understand post-wildfire ecosystem processes; with climate change, wildfire is increasing in frequency, severity, and extent across the globe[24–26]. We use a comprehensive soil metagenome-assembled genome (MAG) catalog from northern CO (USA) post-wildfire coniferous forests to assess the representation of proposed microbial life history strategies and identify potential selection of taxa based on their genomic investment into fitness traits. The utilized sample set represents an 11-year chronosequence post-wildfire, including soils that represent low and high burn severity, along with unburned controls. Previous work has characterized key soil microbiome compositional shifts along the chronosequence[22], with burned soils enriched in the aforementioned putative pyrophilous taxa that are cosmopolitan across different post-fire ecosystems (e.g., boreal forest[27], California chaparral[28]). We broadly hypothesized that there would be distinct life history strategy shifts across burn severity and with time post-fire, with wildfire selecting for taxa that invest in traits for tolerating the stress induced by fire (e.g., high heat, lower soil moisture) that recedes over time to be replaced by taxa that largely invest in resource acquisition due to the structural complexity of fire-transformed, or pyrogenic, carbon.

3.3 Results & Discussion

3.3.1 MAG catalog representing diverse soil bacterial taxa across time following wildfire

To characterize bacterial traits and functional potential across a wildfire burn severity chronosequence, we performed shotgun metagenomic sequencing on 36 surface (0-5 cm depth) soil samples from a 2021 sampling campaign. Samples were collected across a 1-11 year post-wildfire chronosequence in northern CO and southern WY, and included varying burn severities (low and high severity) and unburned control soils (**Table 3.1**). The chronosequence encompassed a series of natural wildfires at 1 (2020 Mullen fire), 3 (2018 Ryan fire), 5 (2016 Beaver Creek fire), and 11 (2010 Church's Park fire) years post-fire in subalpine coniferous forests dominated by lodgepole pine (**Figure 3.1**). Metagenome-assembled genomes (MAGs) reconstructed from this sequencing effort were combined with a MAG catalog (*n* = 637 MAGs) from previous work conducted 1 year post-fire in the Ryan fire[9]. The final dereplicated, medium and high-quality MAG dataset used here contained 825 MAGs, including MAGs representing the bacterial phyla Actinobacteria (*n* = 311), Proteobacteria (*n* = 212), and Bacteroidota (*n* = 73) along with putative pyrophilous taxa identified in previous post-wildfire studies[9,27,28] (*Arthrobacter*, *n* = 12; *Blastococcus*, *n* = 9; Massilia, *n* = 9) (**Figure 3.2**). This comprehensive collection of MAGs was used to investigate the impact of wildfire on soil microbiome functional profiles and life history strategies across both time (1-11 years post-fire) and disturbance severity (low and high severity) in the Colorado Rockies.

3.3.2 Broad overview of life history trait profiles in MAG catalog

The variation and distribution of life history traits across the MAG catalog was investigated using *microTrait*[29], a tool that to uses genes and predicted metabolic

pathways to infer microbial process that are ecologically-relevant for soil carbon cycling[17]. The identified traits can be associated with three broad categories; resource acquisition (A), resource use (energy generating; Y), or stress tolerance (S), known broadly as the Y-A-S conceptual framework[17]. Y-A-S was proposed as an alternative to Grime's C-S-R framework for plant communities[30] to summarize the three key life history strategies of soil microbes[17]. Y-strategists allocate resource use to cellular growth by investing in assimilatory pathways, A-strategists invest into acquiring resources via production of extracellular enzymes or specialized membrane transporters, and S-strategists invest energy into stress tolerant enzymes aiding in biomolecular damage repair, desiccation protection, thermal resistance, or osmolyte production. While this conceptual framework has critiques[31,32], it has been widely used to characterize soil microbiomes across ecosystems[33–36] and inferred from MAG data[37,38].

Of the profiled traits by *microTrait* (*n* = 189), 29 were encoded by the majority of MAGs (80% or >661 MAGs). These traits largely fell under the A strategy (18 of the 29), including functions for complex carbohydrate depolymerization (e.g., xylan, chitin, and cellulose). The trait most widely encoded in the MAG catalog (824 of the 825 MAGs) was for protein degradation, likely reflecting abundant microbial necromass in soil C (estimated at ~30-40% of SOM) and the likely ubiquitous degradation of microbial necromass by active soil microbes. The remaining 11 widely encoded functions were all associated with S strategies, including genes for enduring temperature fluctuations (both high and low temperatures), desiccation, and pH stress. S strategy traits were also more widely distributed within the MAG catalog (**Figure 3.3**; average of 489 MAGs encoding each trait vs. 304 MAGs for A traits), indicating the evolutionary importance of

environmental responsiveness to fluctuating conditions within soils. Combined, these data shows that functional potential with the soil microbial communities broadly aligns with A and S life history strategies. Moreover, this results aligns with a large-scale biogeography analysis revealing that the soil microbiome of coniferous forests generally fall within these life history strategies with variation caused by soil pH[37]. The forests studied here were also greatly impacted by severe mountain pine beetle outbreak in ~2005, with control sites having ~75% average overstory tree mortality[42,43], potentially contributing to overall lower resource availability in these soils[44] and resulting in increased genomic investment into acquiring diverse resources (A strategy).

Visualizing differences in MAG trait allocations in multivariate space, we observed separation largely based on taxonomy, with much of the dissimilarity explained by bacterial phyla (PERMANOVA $R^2 = 0.45$, $p = 0.001$) and class (PERMANOVA $R^2 = 0.54$, $p = 0.001$) (**Figure 3.4**). Here, despite recent critiques[32], bacterial taxonomy to the class level is a large driver of genomic trait allocation. MAGs affiliated with the Proteobacteria and Actinobacteria had among the highest number of encoded traits (normalized by number of phyla MAGs in dataset; **Figure 3.5**) for both A and S strategies, likely lending to their general high abundance in soils[16]. In contrast, MAGs affiliated with the Acidobacteria preferentially encoded S traits over A traits, while Verrucomicrobia MAGs displayed the opposite trend. Overall, these analyses point to fine-scale interphylum differences in genomic allocation to various life history strategies which may influence wildfire-induced changes to the soil microbiome.

3.3.3 Wildfire drives soil microbiome community composition

A marker gene study on this sample set found that fire severity drove depleted microbial biomass and altered community structure marked by the enrichment of putative pyrophilous taxa (e.g., Actinobacteria *Blastococcus*, Proteobacteria *Massilia*) and subsequent decrease in Acidobacteria and Verrucomicrobia in recently burned soils[22]. The data presented here complements the previously described trends in biomass (via qPCR) and compositional shifts (via marker gene) overviewing these sites.

Phospholipid fatty acid (PLFA) profiling revealed the long-term (11 year) depletion of microbial biomass in burned surface soils, with greater impacts in high severity-impacted soils and negligible recovery over the chronosequence (**Figure 3.6**). Bacterial compositional shifts inferred from metagenomic read mapping to the MAG catalog confirmed the broad compositional trends found via 16S rRNA gene sequencing[22], with time post-fire significantly driving community composition (PERMANOVA R^2=0.10994, p=0.008; **Figure 3.7**) and the effect of fire treatment waning with time (**Table 3.2**). Further mirroring the corresponding marker gene data, metagenomic sequencing revealed a general fire-induced loss of Verrucomicrobia and Acidobacteria accompanied by a dominance of Actinobacteria (**Figure 3.8**).

3.3.4 Signature of wildfire on soil microbiome life history strategies

To investigate the impact of wildfire on dominant life history strategies encoded within the soil microbiome, we selected the top 50 most abundant MAGs (via coverage) within each treatment (e.g., 1 year post-fire high severity), generally representing at least 80% of the total metagenome coverage. Subsetting the MAG catalog to the most abundant retained 320 MAGs but still preserved many of the compositional shifts seen in

the entire MAG catalog (e.g., loss of Acidobacteria and Verrucomicrobia from unburned to high severity; **Figure 3.9**). There was overlap between the dominant MAGs across treatments (**Figure 3.10a**), with more shared dominant MAGs between high severity-impacted sites that were closer in time (**Figure 3.10b**). This trend was absent in low severity-impacted sites, revealing the stronger selective pressure of high severity wildfire that wanes with time.

High severity wildfire selected for MAGs that had higher genomic investment into A strategy traits over the entire 11 year chronosequence (**Figure 3.11**); these trends were absent for both Y and S strategy traits (**Figure 3.12**). The increased dominance of A-strategists up to 11 years post-high severity wildfire could be caused by fire-induced resource scarcity or complexity, resulting in the selection for taxa that increase investment into resource capture[17]. Increased A traits included encoded carbohydrate-active enzymes (CAZymes), with an increase of encoded CAZymes in high severity soils 1 year post-fire, and variability in the enrichment of different CAZymes over the chronosequence (**Figure 3.13**). In the immediate aftermath of fire (1 year), the active recruitment of resources from the external environment was highlighted by the enrichment of CAZymes likely localized to the cellular periplasm or extracellular space (via PSORTb[45]; **Figure 3.13**).

Genes encoding for aminopeptidases and metalloendopeptidases, enzymes that cleave peptide bonds in proteins and peptides, were also enriched in the high severity-impacted soil microbiome (**Figure 3.14**). Microbial necromass has been hypothesized to increase following burning[9,23] and the enrichment of aminopeptidases suggests that the use of necromass is an important process supporting microbial activity following wildfire.

Mirroring the burning-induced increase in soil inorganic N (**Figure 3.15**), caused by the release of NH_4^+ from combustion of forest biomass and surface organic matter and decreased plant uptake post-fire[46], many of the enriched A strategy traits were related to inorganic N uptake and transformation. These included assimilatory nitrate reduction and more widely encoded transport systems for various N species (e.g., amide, nitrate, nitrite, urea). Along with inorganic N, functions for substrate uptake were more widely encoded in the dominant soil microbiome 1 year following high severity wildfire (**Figure 3.16**).

The increased genomic investment of the high severity-impacted soil microbiome into A traits suggests resource scarcity in burned soils. Resource scarcity was also supported by selection for decreased genome size across soils from all high severity-impacted timepoints (**Figure 3.17**); decreased genome size has been previously found to be caused by both resource scarcity[47] and thermal stress[48] in soils.

3.3.5 Prevalence of putative pyrophilous traits in post-wildfire soil microbiome

In contrast to the Y-A-S framework, others have proposed conceptual frameworks specific to different disturbances (e.g., wildfire). Wildfire causes distinct short- and long-term alterations to soil, like the initial increase in soil temperature caused by heating and lasting burning-induced alterations to soil chemistry (e.g., increased pH, increase in aromaticity of soil carbon)[49]. Because of the unique signature of wildfire on soils, there are particular functional traits hypothesized to drive post-wildfire soil microbial succession[23]. These traits, termed the traits-based fire ecology framework, include the ability to persist during the initial heat pulse disturbance (*fire survival*, e.g., heat shock proteins), the ability to grow quickly and fill in newly unoccupied niche space following wildfire-induced loss of microbial biomass (**Figure 3.6**; *fast growth*), and capacity to

withstand the longer-term press disturbance of wildfire-altered soil chemistry (*post-fire environmental affinity*; e.g., ability to degrade aromatic carbon). To identify the applicability of this trait framework across this wildfire chronosequence, we assessed these traits across the dominant 50 MAGs from each condition along with a subset of 23 MAGs that represented previously hypothesized putative pyrophilous taxa of the Actinobacteria *Blastococcus* (*n* = 8) and *Arthrobacter* (*n* = 10) and Proteobacteria *Massilia* (*n* = 5). This subset of 23 putative pyrophilous MAGs had overlap with condition dominant MAGs and all 23 were dominant in at least one of the high severity treatments, confirming the importance of these taxa in post-wildfire soils.

There was no clear enrichment of S strategy traits (**Figure 3.12**), including S traits for persisting during wildfire-induced high soil temperatures (e.g., heat shock proteins, ATP-dependent proteases for repairing denatured proteins; **Figure 3.18a**) and for tolerating desiccation stress due to short-term decreased soil moisture (**Figure 3.15**). In the high severity-impacted soil microbiome, the lack of enriched *fire survival* traits could be due to the relatively narrow extent of the purported *Goldilocks zone* – the depth layer in the soil where temperatures increase just enough to select for cells that encode heat resistance genes without killing them[50]. Here, the use of surface (0-5 cm) soils for analyses likely sampled the *necromass zone*[50], or the region of the soil profile where temperatures lyse cells, causing increases in labile carbon and nitrogen for colonizing microorganisms to use and proliferate post-fire and the aforementioned enrichments of A traits (e.g., aminopeptidases, **Figure 3.11**, **Figure 3.14**). Although most heat resistance functions had similar prevalence across the dataset, dominant MAGs in 1 year post-fire low severity impacted soils more widely encoded heat-induced transcription factors than

MAGs dominant in high severity samples (38 vs. 32 MAGs), potentially indicating microbial survival in surface soils impacted by low severity fire where more muted heating occurred. Importantly however, these functions were common across the MAG dataset, including MAGs from control soils.

With the hypothesized influx of bioavailable necromass-derived C and N, the ability to grow quickly and utilize these substrates should lead to initial (i.e., 1 year post fire) dominance of putative copiotrophs that decreases over time. Here, we used *gRodon*[51] to estimate individual MAG maximum growth rates via codon usage bias (CUB) to assess whether these patterns persisted in the environment. We detected a clear impact of increasingly severe wildfire on the selection for taxa that could grow quickly, with more dominant MAGs in burned soils with maximum growth rates <5 hours (**Figure 3.18b**). Further, we observed faster average growth rates (of d<5 hours) in these MAGs and those representing putative pyrophilous taxa (**Figure 3.18b**). Combined, these data highlight the importance of fast growth in the immediate post-fire soil microbial that diminishes by ~11 years post-fire.

Post-fire environmental affinity, or the ability to tolerate altered soil chemistry conditions, was evaluated by assessing the genomic potential to persist in high pH soil environments and degrade aromatic molecules, which largely makes up pyrogenic carbon. To quantify and compare MAG pH preferences, we used a machine learning model using 56 predictor genes found to be predictive of bacterial pH cell preferences[52]. Overall, there was evidence of severe wildfire long-term (>11 years) selection for taxa that could tolerate elevated soil pH (**Figure 3.15**, **Figure 3.18c**). This trait was also

present across the putative pyrophilous MAGs, with a median pH preference similar to that calculated for dominant MAGs from 1 and 3 years post-fire high severity soils.

In contrast to the selection of bacteria with higher pH preferences, there was no immediate impact of wildfire on the functional potential of the soil microbiome to degrade aromatic C, both in the dominant MAGs and the MAGs representing putative pyrophilous taxa (**Figure 3.18d**). However, by 5 years post-fire, MAGs encoding more genes for degrading aromatics were enriched in high severity soil samples (**Figure 3.18d**). This supports previous work[53] hypothesizing that more labile pyrogenic C fractions (i.e., oxygenated or low molecular weight components[54]) are initially mineralized and depleted, resulting in later use of more aromatic pyrogenic carbon. Together, this dataset confirms the importance of fast growth and affinity for high pH soils in the post-wildfire soil microbiome. Given that the putative pyrophilous taxa studied here (e.g., *Blastococcus*, *Arthrobacter*, *Massilia*) have been documented across diverse fire-adapted ecosystems, including CO coniferous forests[9,22], CA chaparral[28], boreal forests[27], and Mediterranean holm oak forests[55,56], we propose that these conserved life history strategies drive post-wildfire soil microbiome successional trajectories across diverse ecosystems. Thus, these traits have global relevance in shaping the soil microbiome of post-wildfire ecosystems.

3.3.6 Implications of post-wildfire trait selection for ecosystem carbon cycling

Accurately quantifying post-wildfire ecosystem carbon budgets is challenging due to heterogeneity across ecosystems, difficulties upscaling field-generated data, and key knowledge gaps introducing uncertainty (e.g., wildfire impacts to feedbacks between above- and belowground processes relevant to carbon fluxes)[57]. This is especially pertinent as climate change and human intervention is causing an increase in severity,

frequency, and extent of wildfires across the globe[24–26], resulting in hampered ecosystem resilience[58,59] that can lead to ecosystem conversions[60]. Classifying key pyrophilous soil microbial taxa and identifying traits that define post-wildfire soil microbial succession across ecosystems, especially as microbial life history strategies can influence soil carbon cycling[17], could help distill complex microbial data and increase predictability of post-wildfire soil microbial dynamics and their biogeochemical consequences.

Here, we show that wildfire initially selects for taxa that are copiotrophic and can grow quickly to fill in the newly unoccupied niche space (**Figure 3.18b**) and, up to a decade post-fire, taxa that invest in resource acquisition strategies (**Figure 3.11**). Copiotrophs are hypothesized to grow less efficiently (i.e., lower carbon use efficiency, CUE) than oligotrophs[61,62], leading to greater carbon loss from the soils and less stable carbon accumulation via formation of microbial biomass. Further, microbial investment into resource acquisition (e.g., producing extracellular enzymes) is hypothesized to lead to soil carbon loss due to inefficient growth (i.e., lower CUE)[63]. Understanding the linkages between wildfire, soil microbial life history strategies, and CUE is imperative as microbial growth efficiency is negatively correlated with soil carbon stocks[64] and wildfire-induced shifts in community CUE could influence the post-wildfire ecosystem carbon budget. Combined, this work suggests that severe wildfire selects for a soil microbiome that largely encodes traits that could lead to increased soil carbon losses over time.

3.4 Conclusions

The use of conceptual life history strategy frameworks in microbial ecology would further the field, enhancing predictability of post-disturbance environmental microbial

succession and enable the simplification of complex microbiomes in ecosystem models. Here, we use a comprehensive MAG catalog representing a post-wildfire coniferous forest soil microbiome over time (1-11 years) and disturbance severity (low and high severity wildfire), along with control forest soils, to identify whether trait frameworks help delineate post-wildfire soil microbiome succession. Application of the Y-A-S framework showed that severe wildfire selected for MAGs that were enriched in resource acquisition life history strategy traits over the 11-year chronosequence, while the traits-based fire ecology framework helped identify traits encoded in dominant MAGs that are more specific to wildfire (e.g., fast growers, preference for higher soil pH). There was minor overlap between frameworks, with the *fire survival* traits of the traits-based fire ecology framework broadly fitting into the stress tolerance strategists of Y-A-S, but the combined application of both helped elucidate the reason for pyrophilous taxa selection following wildfire. This unique and comprehensive dataset provides support for the application of conceptual life history strategy frameworks to soil microbiomes, which help provide invaluable insight and predictability into complex post-disturbance soil microbial successional dynamics.

3.5 Materials & Methods

3.5.1 Field campaign and sample set

Soil samples were collected in July 29 and 30 of 2021 across a chronosequence of wildfire burn scars in northern CO (USA). Wildfire burn scars sampled included the 2010 Church's Park fire (representing 11 years post-fire), 2016 Beaver Creek fire (5 years post-fire), 2018 Ryan fire (3 years post-fire), and the 2020 Mullen fire (1 year post-fire)

(**Figure 3.1**). At each burn scar, soil samples were taken from the 0-5 cm depth from three separate transects that included both low and high severity impacted soils, along with an unburnt control. Burn severities were determined using US Forest Service guidelines[65]; low and high severity sites had >85% and <20% surficial organic matter, respectively, which we quantified visually with each 1m^2 sampling plot. See Caiafa et al. (2023) for more details on the sampling campaign[22]. Along with the aforementioned samples, we also used metagenomes from shallow soil samples described in Nelson et al (2022)[9], which included Ryan fire sites sampled one year following the fire in 2019. The entire sample set utilized here includes 42 total samples representing both low and high severity-impacted soils up to 11 years following burning (**Table 3.1**). All sample metadata included in **Appendix B**.

3.5.2 Soil chemistry and microbial biomass

We evaluated soil chemistry and microbial biomass on a subset of samples to gauge changes the chronosequence. To analyze inorganic forms of soil N (NO3–N and NH4–N), samples were passed passed through a 4 mm mesh sieve and extracted with 2 M KCl. Extracts were analyzed for NO3–N and NH4–N by colorimetric spectrophotometry[66] (Lachat Company, Loveland, CO). We analyzed the NO3–N and NH4–N and dissolved organic C (DOC) and total dissolved N (TDN) released during warm water extracts[67] using ion chromatography (NH4-N and NO3-N; Thermo-Fisher Corporation, Waltham, MA) and TOC-VCPN total organic carbon analyzer (DOC and TDN; Shimadzu Corporation, Columbia, MD, USA). Soil pH was analyzed in a 1:1 soil to deionized water slurry after one hour of agitation[68] using a temperature-corrected glass electrode (Hach Scientific, Loveland, CO, USA). A subset of 27 samples were sent to the

Soil Health Assessment Center at the University of Missouri for phospholipid and neutral lipid fatty acid analysis (PLFA and NLFA) using the Buyer and Sasser (2012)[69] extraction method with a Bligh-Dyer extraction[70] and MIDI Sherlock software (v6.3; MIDI, Inc., Newark, DE). All data included in **Appendix B**.

3.5.3 DNA extractions and metagenomic sequencing processing

Total DNA was extracted from all bulk soil and rhizosphere samples (*n* = 36) using the Zymobiomics Quick-DNA Fecal/Soil Microbe Kits (Zymo Research, CA, USA). Samples were sequenced at the Joint Genome Institute (JGI) using an Illumina library (2x151) and the Illumnina NovaSeq S4 platform. Sequencing depth ranged from 10-93 Gbp (**Appendix B**). Sequencing adapter sequences were removed from raw reads using BBduk (https://jgi.doe.gov/data-and-tools/bbtools/bb-tools-user-guide/bbduk-guide/) and reads were trimmed with Sickle[71] (v1.33). For each sample, trimmed reads were assembled into contiguous sequences (contigs) using the *de novo* de Bruijn assembler MEGAHIT v1.2.9 using kmers[72] (minimum kmer of 27, maximum kmer of 127 with step of 10). Assembled contigs (>2,500 bp) were binned using MetaBAT[73] with default parameters (v2.12.1). Metagenome-assembled genome (MAG) quality was estimated using checkM[2] (v1.1.2) and taxonomy was assigned using GTDB-Tk[74] (v2.1.1). MAGs from these metagenomes were combined with MAGs presented in Nelson et al (2022)[9] and dereplicated using dRep[75] (default parameters, v3.0.0) to create a non-redundant MAG dataset. Low quality MAGs (<50% completion and >10% contamination) were excluded from further analysis[76], resulting in 825 final MAGs (620 from Nelson et al. 2022[9], 205 from new sequencing campaign; **Appendix B**). Because of the large range of sample sequencing depth, reads > 15Gbp were rarefied to 15Gbp for mapping and

estimating coverage of MAGs across samples. Rarefied reads were mapped to MAGs using Bowtie2[77] (v2.3.5) and MAG coverage across samples was calculated using coverM genome (v0.6.0) with the 'Trimmed Mean' (hereafter referred to as TMM) method.

To identify traits encoded within the genomes, microTrait[29] was run using R v4.1.2. To identify putative pyrogenic C degraders, we used HMMER[78] against Kofamscan HMMs[79] and HMMs from the CANT-HYD[80] database. Maximum genome doubling times of genomes were estimated via codon usage bias using gRodon[51] (v2.0.0). We used a threshold of 5 hours to delineate putative fast and slow growers because, when using *gRodon*, there is no longer a signal of growth optimization via CUB with estimated growth rates >5 hours[51]. A machine learning model was used to estimate pH preference of MAGs based on profiles of 56 genes encoded within the MAGs[52].

To focus on MAGs most representative of the different treatments, we subset the MAG catalog to the top 50 most abundant MAGs (via coverage) in each treatment (e.g., 3 year post-fire high severity) that resulted in >80% read recruitment for all samples, with an exception of Ryan fire high severity (65% read recruitment). This is likely due to the large number of MAGs from samples collected from the Ryan fire. The MAG list is included in **Appendix B**.

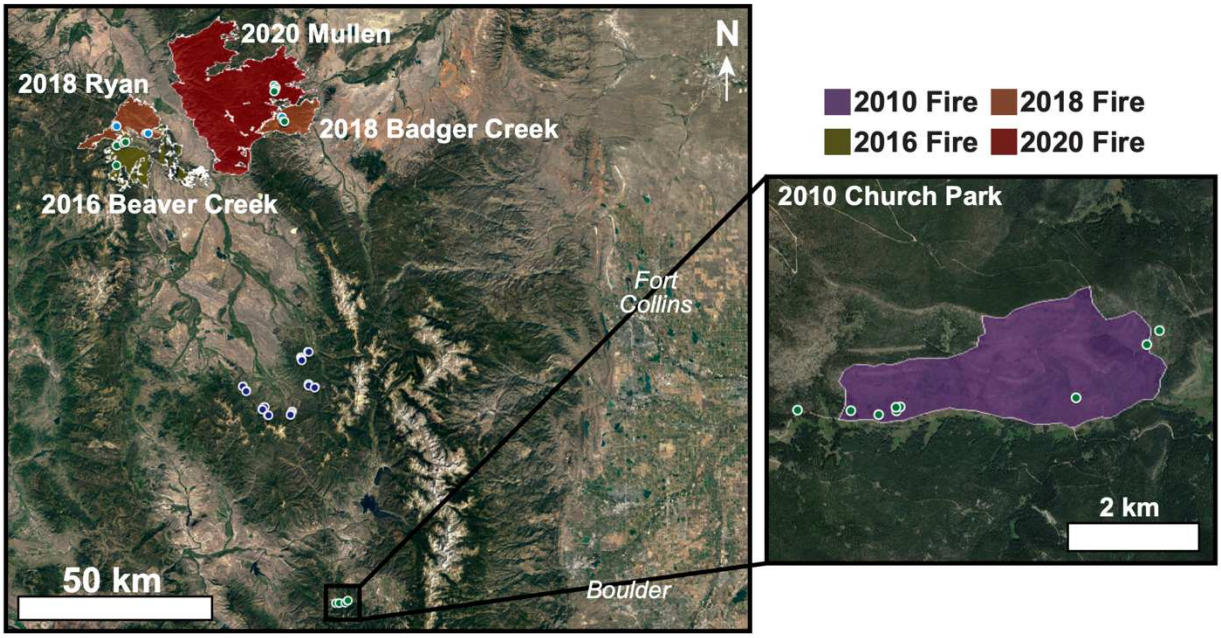

Figure 3.1 Map of sampled burn scars (summer 2021), including burned area of all five sampled wildfires in northern Colorado representing 1-11 years post-wildfire.

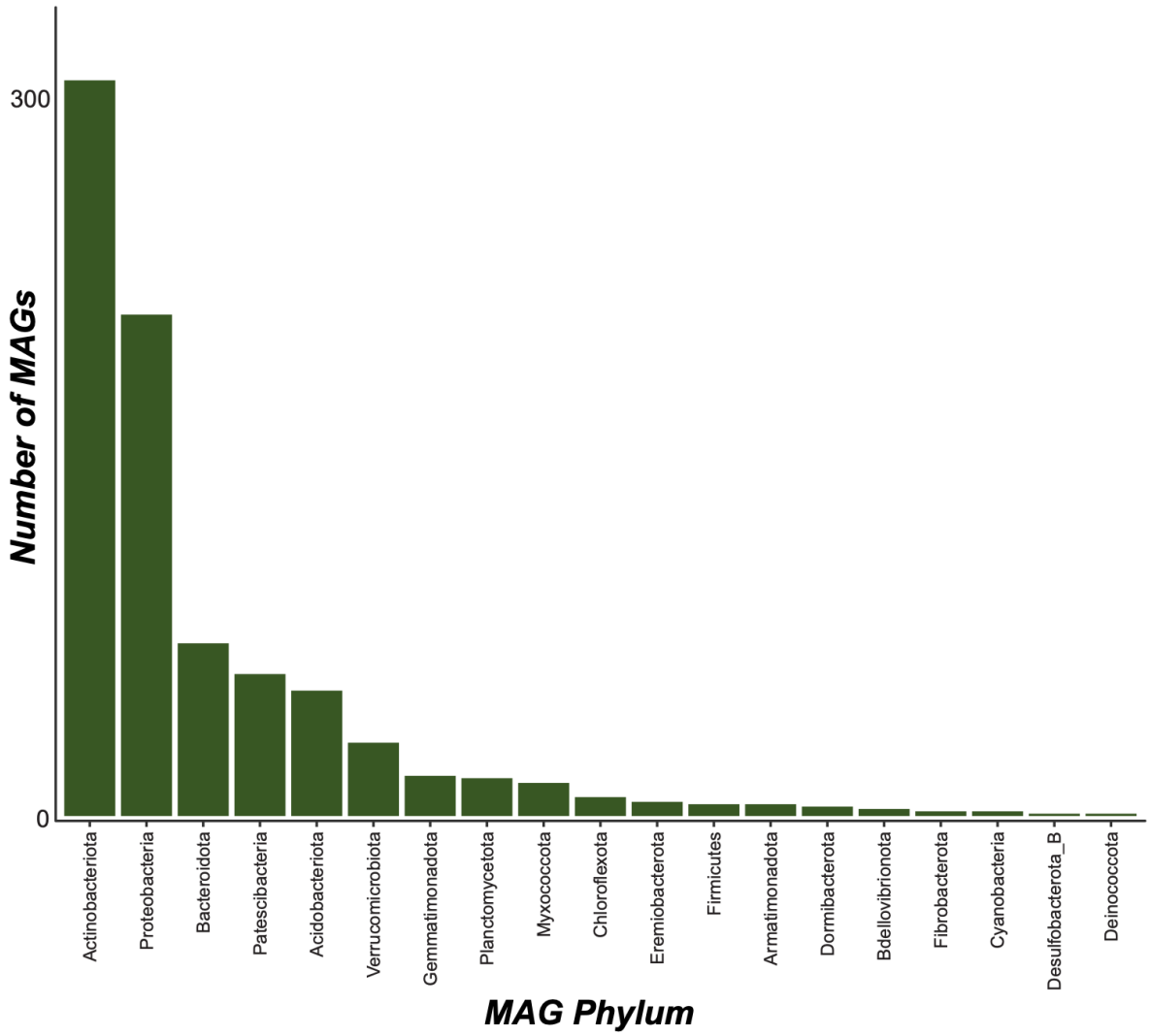

Figure 3.2 Bacterial phyla overview of metagenome-assembled genomes (MAGs) (*n* = 825).

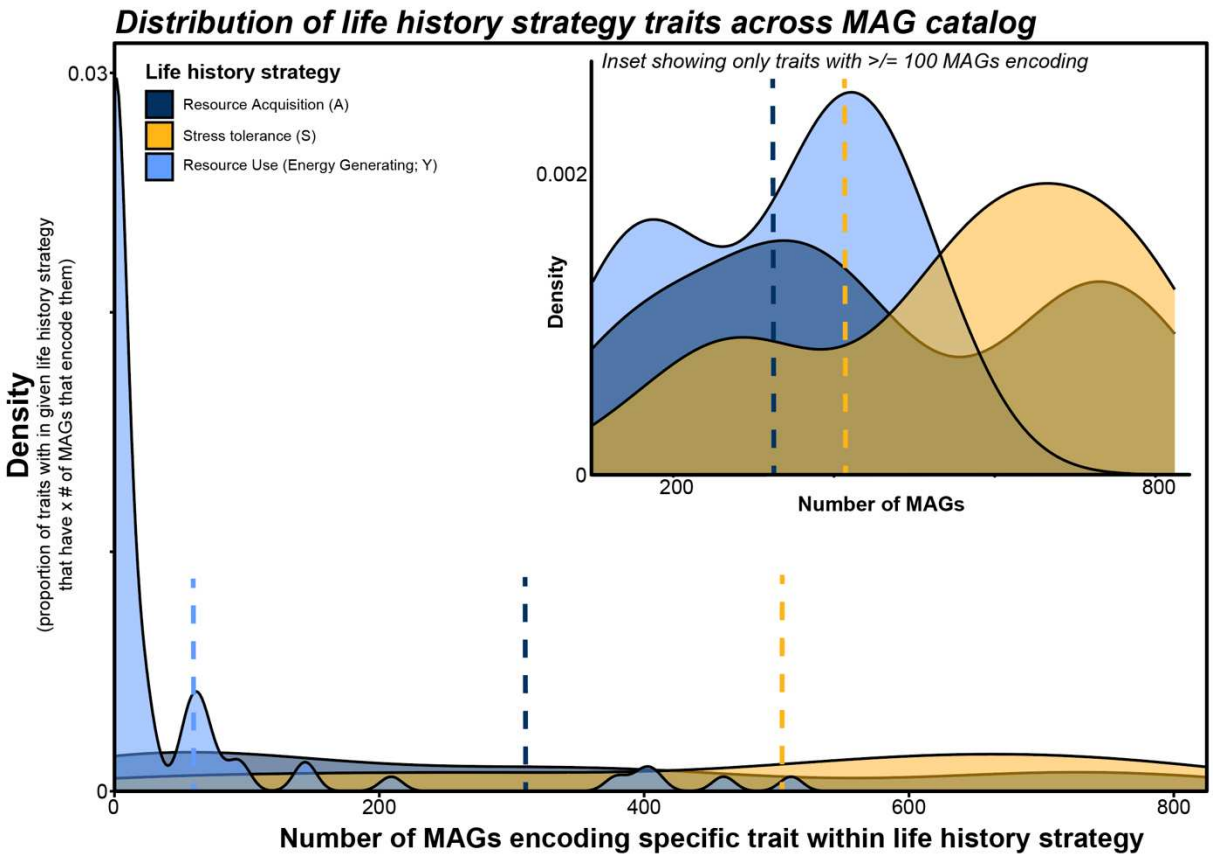

Figure 3.3 Density plot showing the number of traits within a given life history strategy (Y, A, S) that have a given number of MAGs that encode them. Dashed lines show average number of MAGs that encode each trait within the given life history strategy.

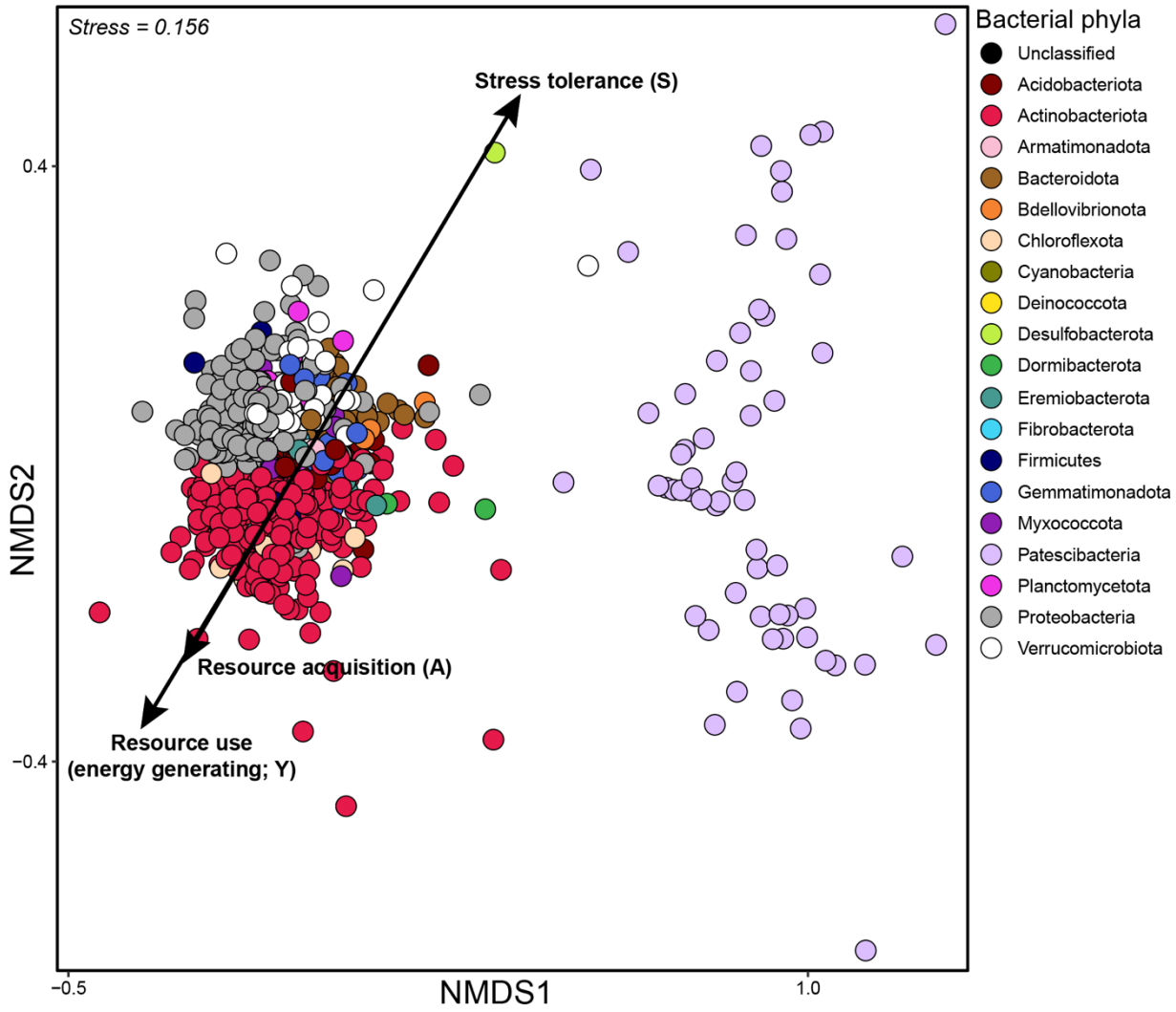

Figure 3.4 Non-metric multidimensional scaling (NMDS) ordination of Bray-Curtis dissimilarity between MAGs based on MAG Y-A-S profiles generated from *microTrait*. Arrows indicate life history strategies largely driving differences.

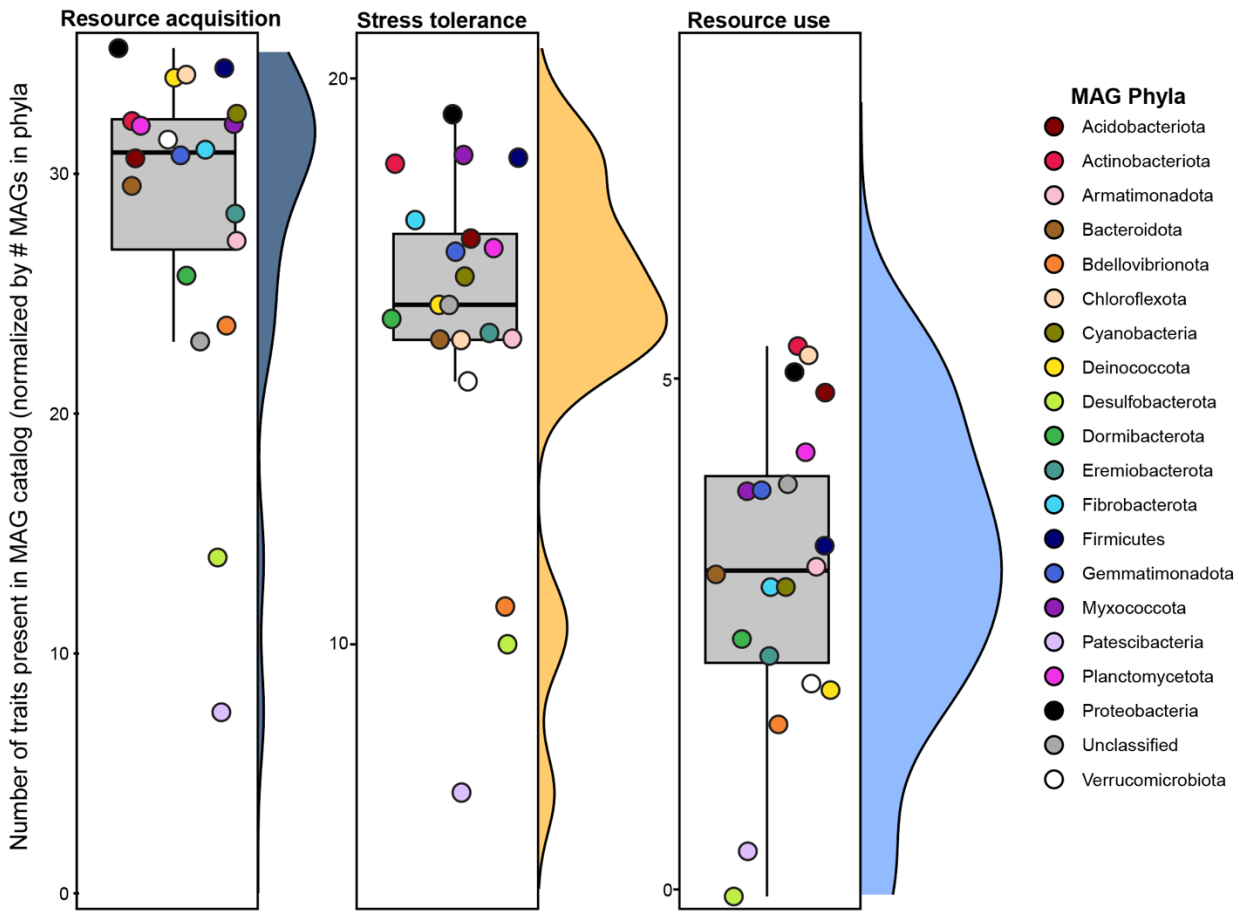

Figure 3.5 Boxplots showing number of traits (via *microTrait*) encoded by MAGs classified as each bacterial phyla in each life history strategy, normalized by number of MAGs within each phylum for comparison across all phyla. The lower and upper hinges of the boxplots represent the 25th and 75th percentiles, respectively, and the middle line is the median. The whiskers extend from the median by 1.5× the interquartile range. Density plots that represent data to the right of each boxplot.

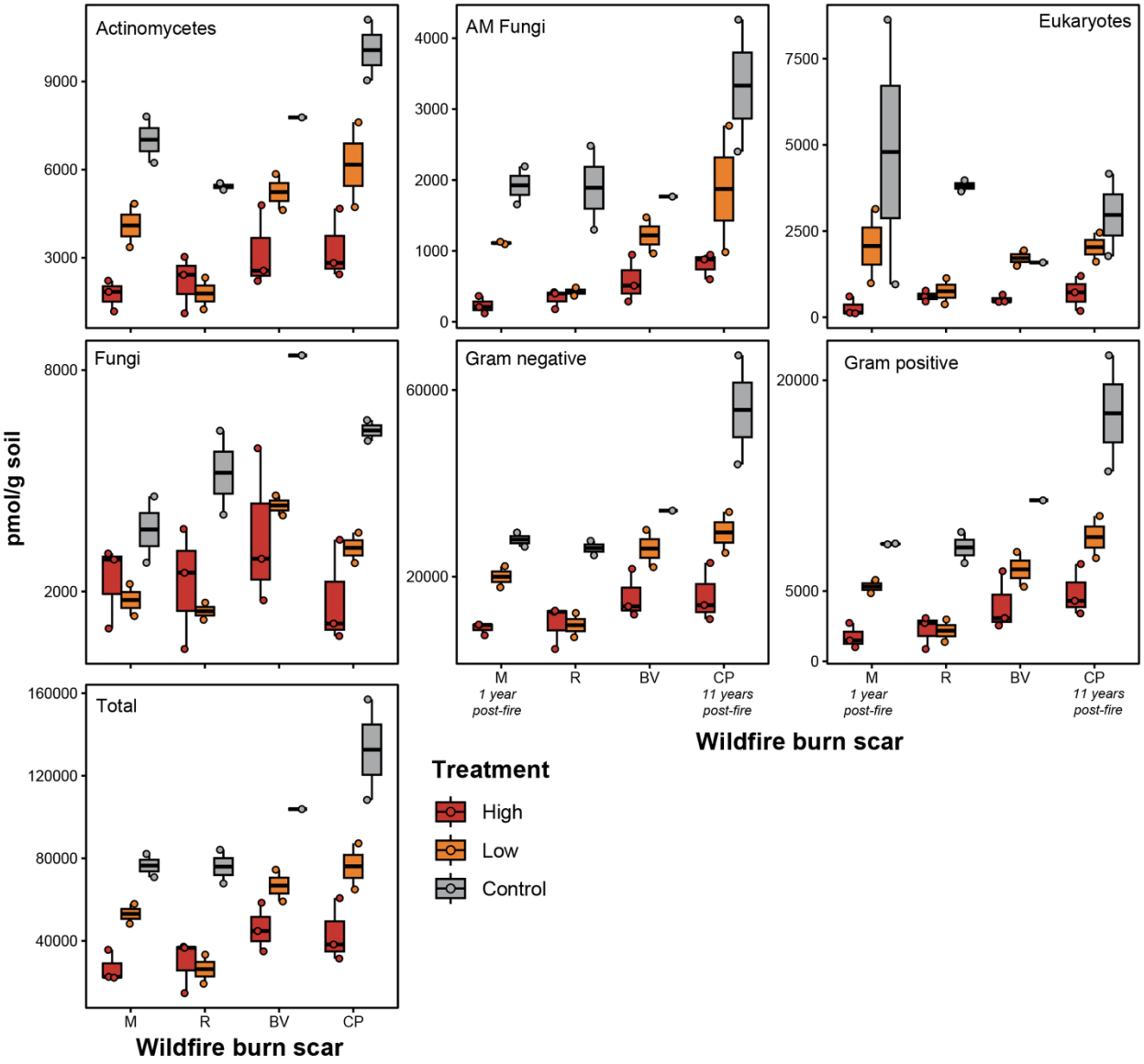

Figure 3.6 Microbial biomass (from PLFA analyses) from across treatments and time post wildfire. M = Mullen fire (sampled 1 year post-fire), R = Ryan fire (3 years), BV = Beaver Creek fire (5 years), and CP = Church's Park fire (11 years). The lower and upper hinges of the boxplots represent the 25th and 75th percentiles, respectively, and the middle line is the median. The whiskers extend from the median by 1.5x the interquartile range.

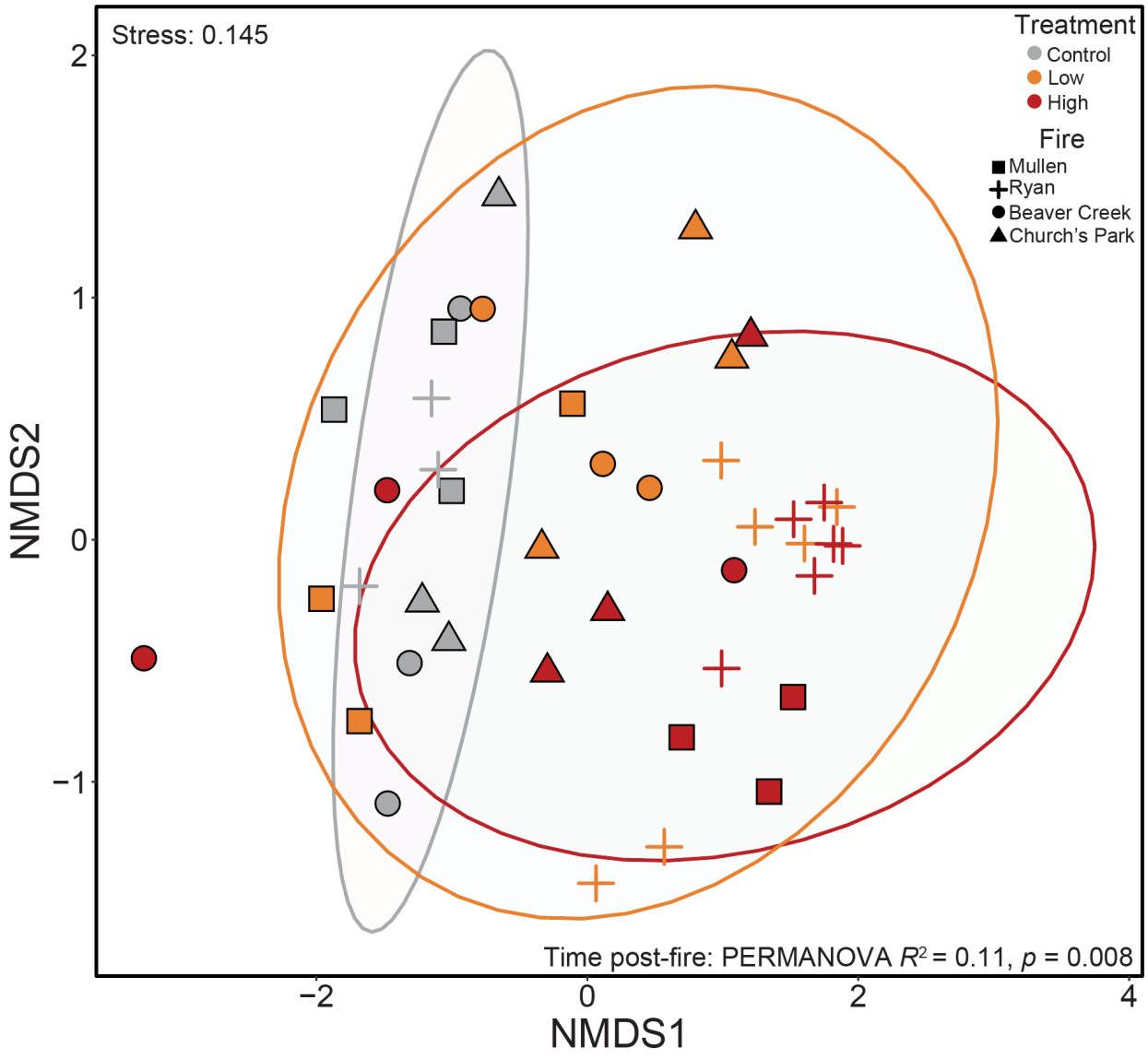

Figure 3.7 Non-metric multidimensional scaling (NMDS) ordination of Bray-Curtis dissimilarity between samples based on MAG relative abundance profiles.

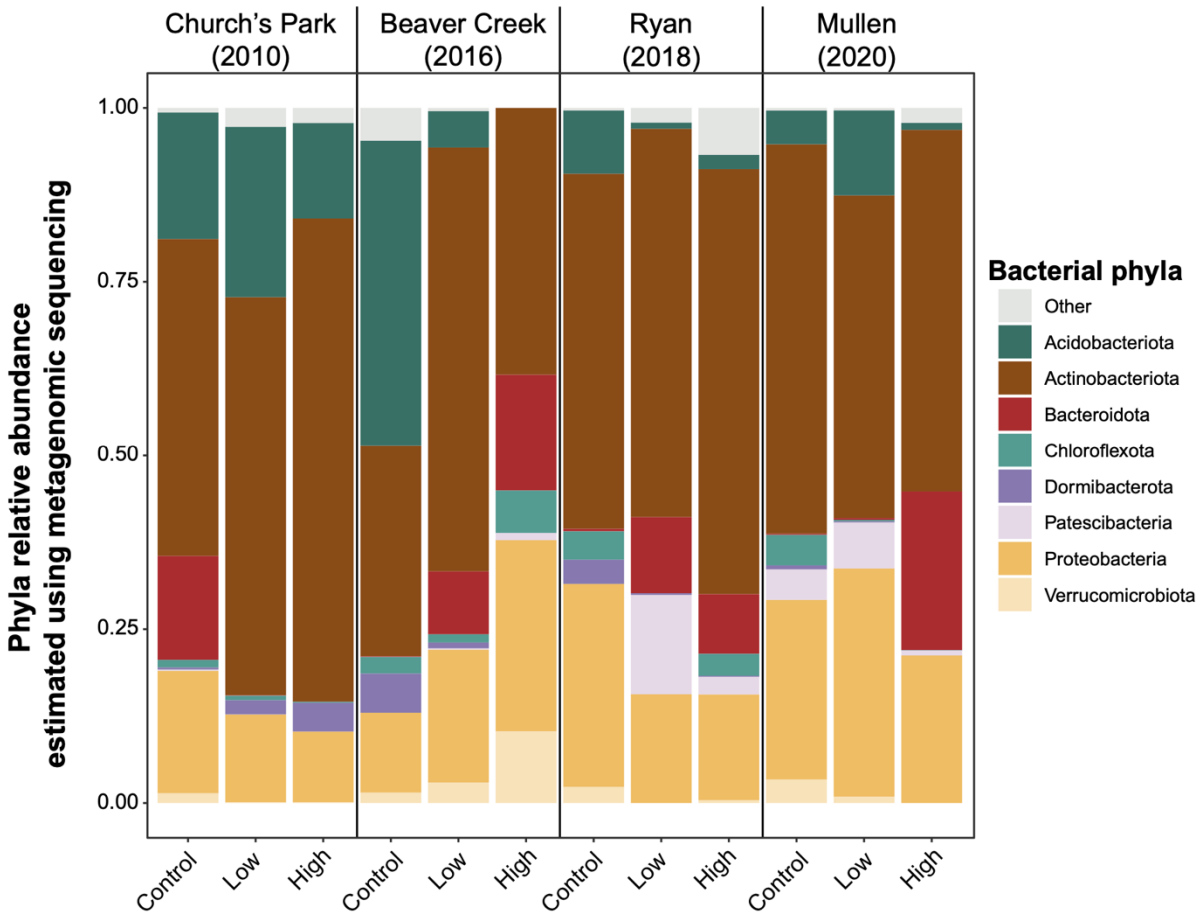

Figure 3.8 Relative abundance of bacteria phyla across treatments, averaged by triplicate, estimated by mapping metagenomic reads to MAG catalog.

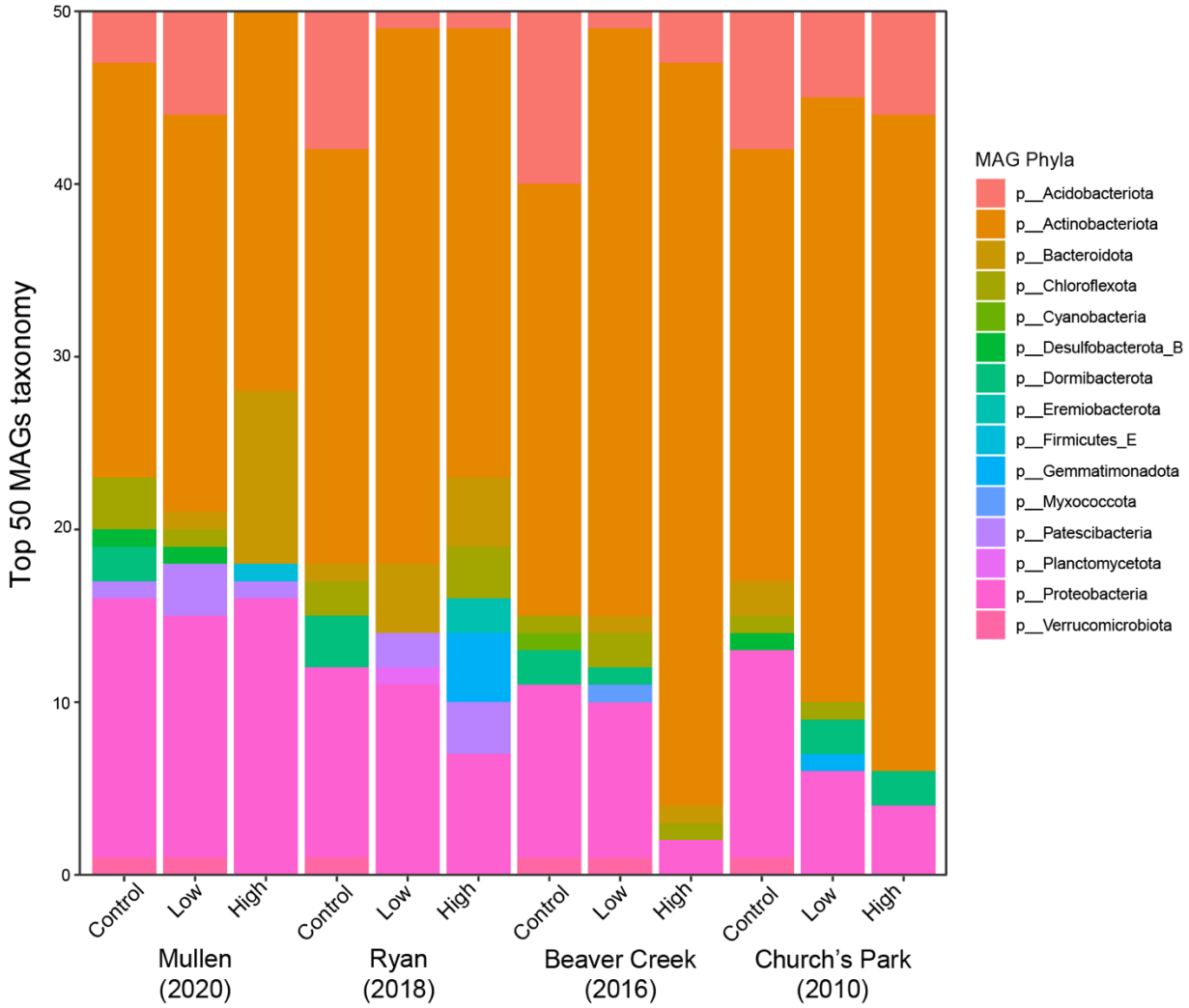

Figure 3.9 Phyla distribution of MAGs that were the top 50 most abundant in each condition (determined via read mapping to MAG catalog).

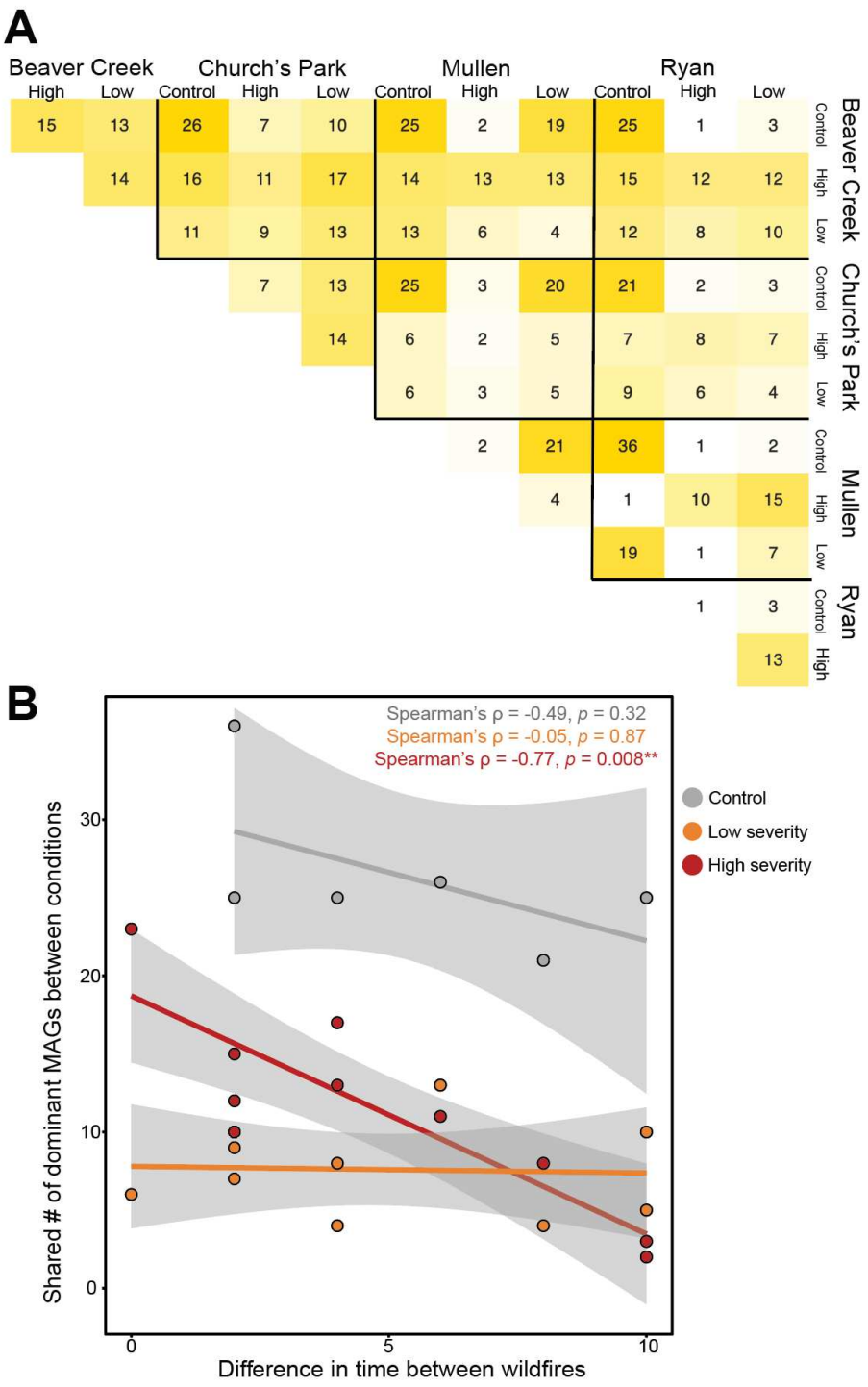

Figure 3.10 (A) Number of dominant MAGs shared between each condition. (B) Number of shared dominant MAGs between conditions plotted against the difference in time between treatment of wildfires. For example, the high severity points plotted at 10 years are showing the number of shared dominant MAGs between the Mullen (2020) and Church's Park fire (2010). Correlation and significance were assessed using the two-sided Spearman rho test.

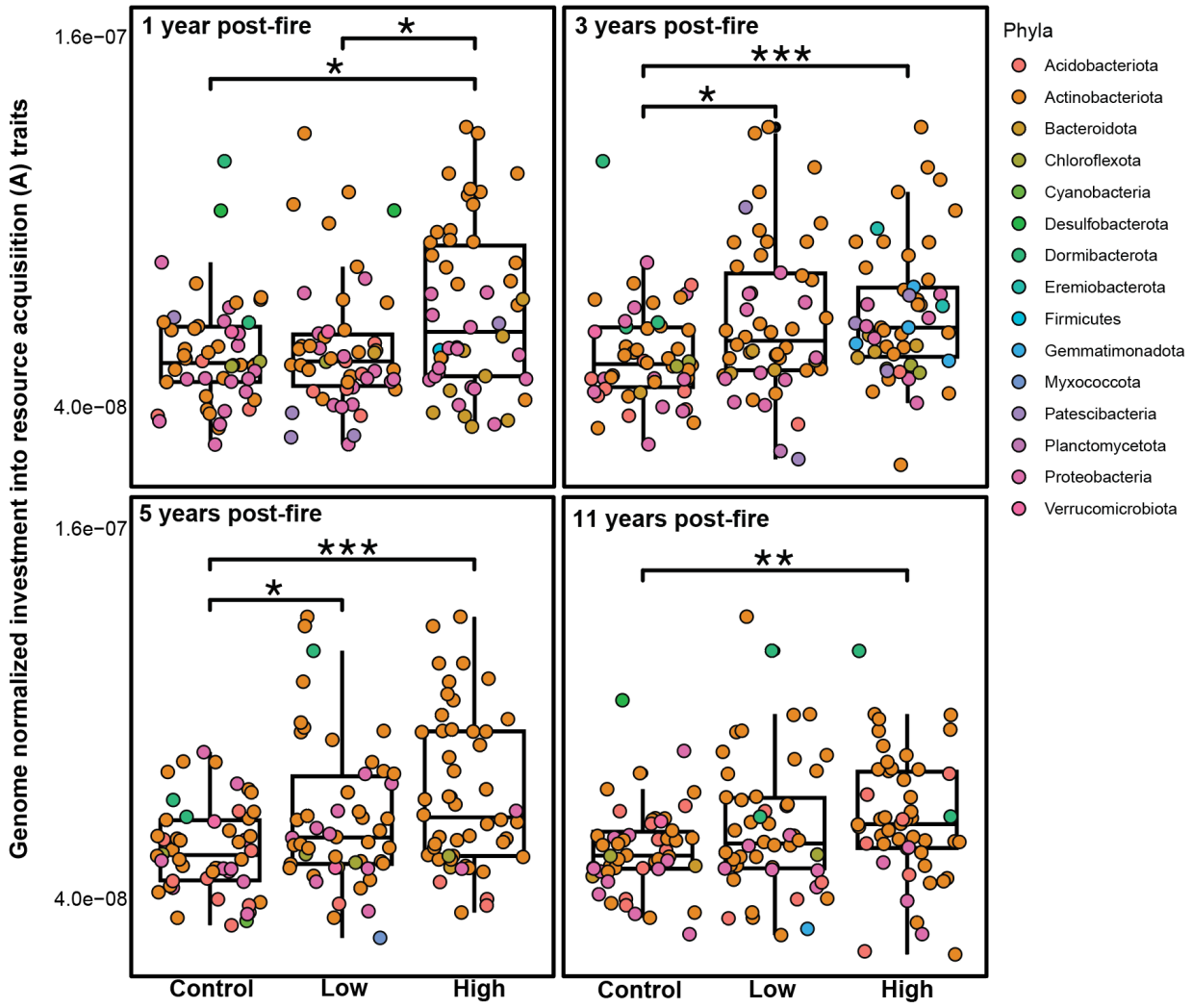

Figure 3.11 Genome sized normalized investment into *microTrait* assigned resource acquisition traits of top 50 most dominant MAGs across conditions. The lower and upper hinges of the boxplots represent the 25th and 75th percentiles, respectively, and the middle line is the median. The whiskers extend from the median by 1.5x the interquartile range. Points represent individual MAGs. Significant differences between conditions indicated with asterisks as indicated by Wilcoxon rank-sum test. *p<0.05, **p<0.01, ***p<0.001.

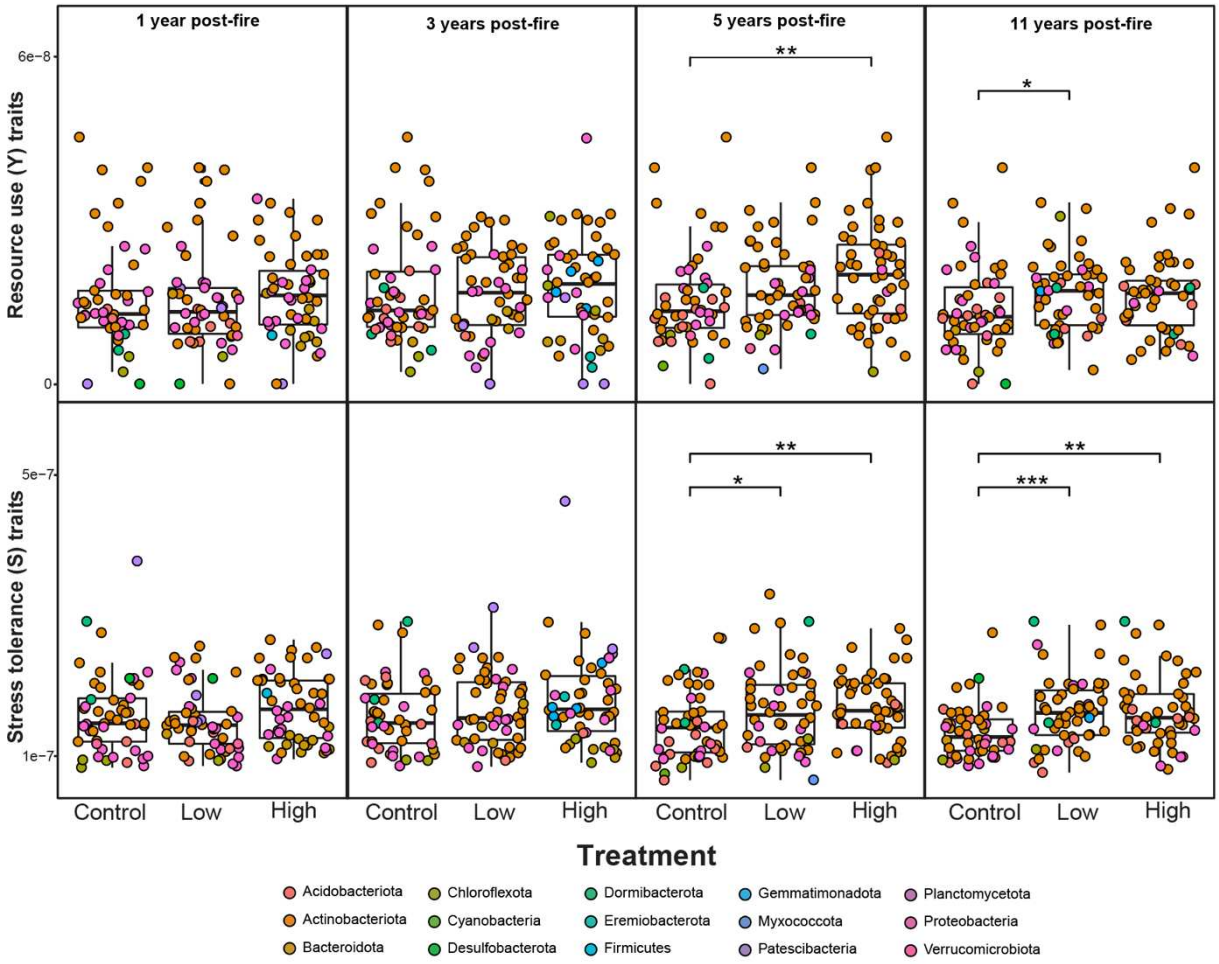

Figure 3.12 Genome sized normalized investment into *microTrait* assigned resource use (Y; top) and stress tolerance (S; bottom) traits of top 50 most dominant MAGs across conditions. The lower and upper hinges of the boxplots represent the 25th and 75th percentiles, respectively, and the middle line is the median. The whiskers extend from the median by 1.5x the interquartile range. Points represent individual MAGs. Significant differences between conditions indicated with asterisks as indicated by Wilcoxon rank-sum test. *p<0.05, **p<0.01.

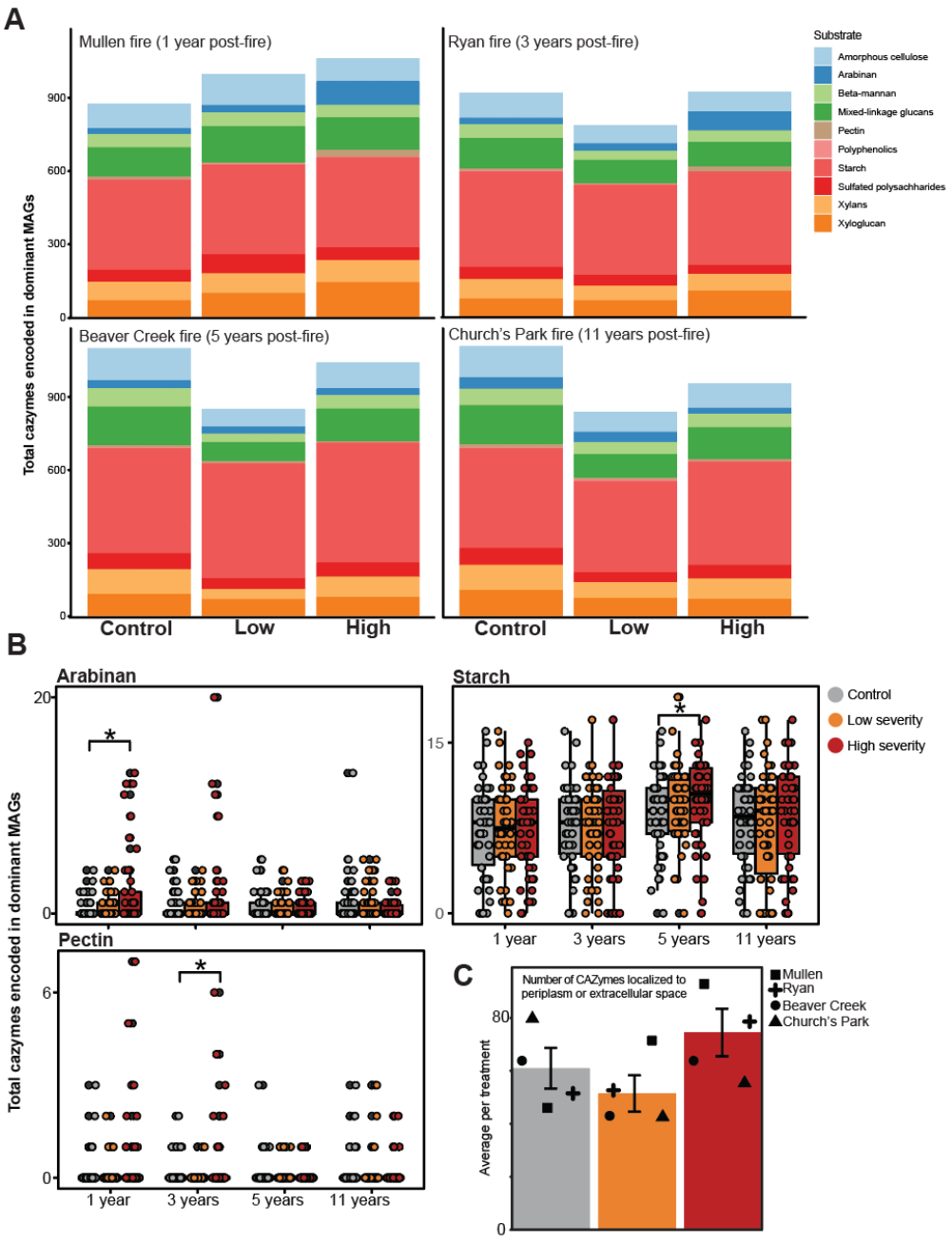

Figure 3.13 (A) Total number of CAZymes encoded in all 50 dominant MAGs across conditions, colored by substrate that CAZyme acts upon. **(B)** Boxplot of CAZymes for targeting specific substrates encoded in dominant MAGs across treatments. The lower and upper hinges of the boxplots represent the 25th and 75th percentiles, respectively, and the middle line is the median. The whiskers extend from the median by 1.5x the interquartile range. Points represent individual MAGs. Significant differences between conditions indicated with asterisks as indicated by Wilcoxon rank-sum test. *p<0.05, **p<0.01. **(C)** Average number of CAZymes localized to periplasm or extracellular space, with individual points representing number from each wildfire site.

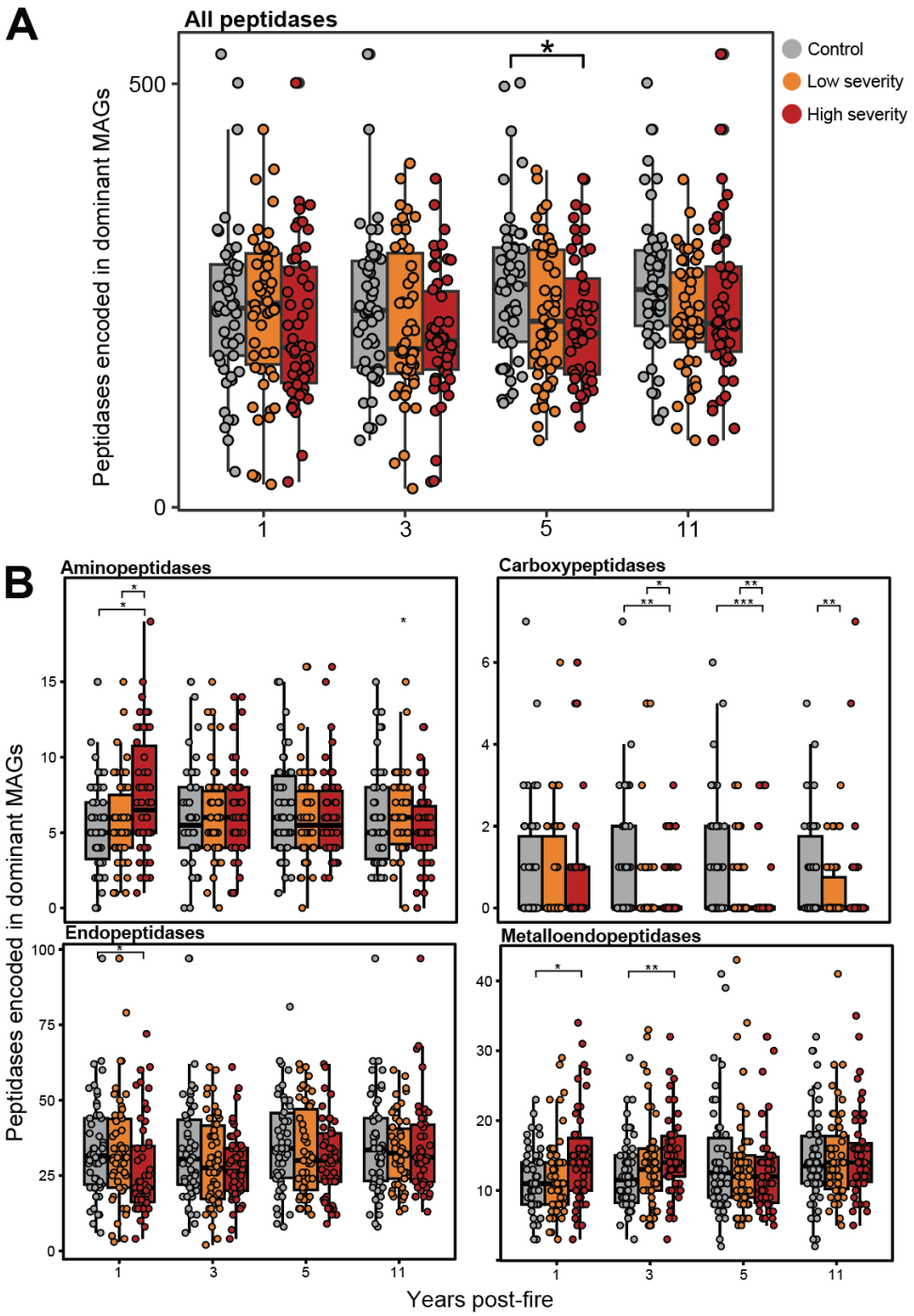

Figure 3.14 (A) Total number of peptidases encoded in all 50 dominant MAGs across conditions. **(B)** Boxplot specific types of peptidases across treatments. The lower and upper hinges of the boxplots represent the 25th and 75th percentiles, respectively, and the middle line is the median. The whiskers extend from the median by 1.5x the interquartile range. Points represent individual MAGs. Significant differences between conditions indicated with asterisks as indicated by Wilcoxon rank-sum test. *p<0.05, **p<0.01.

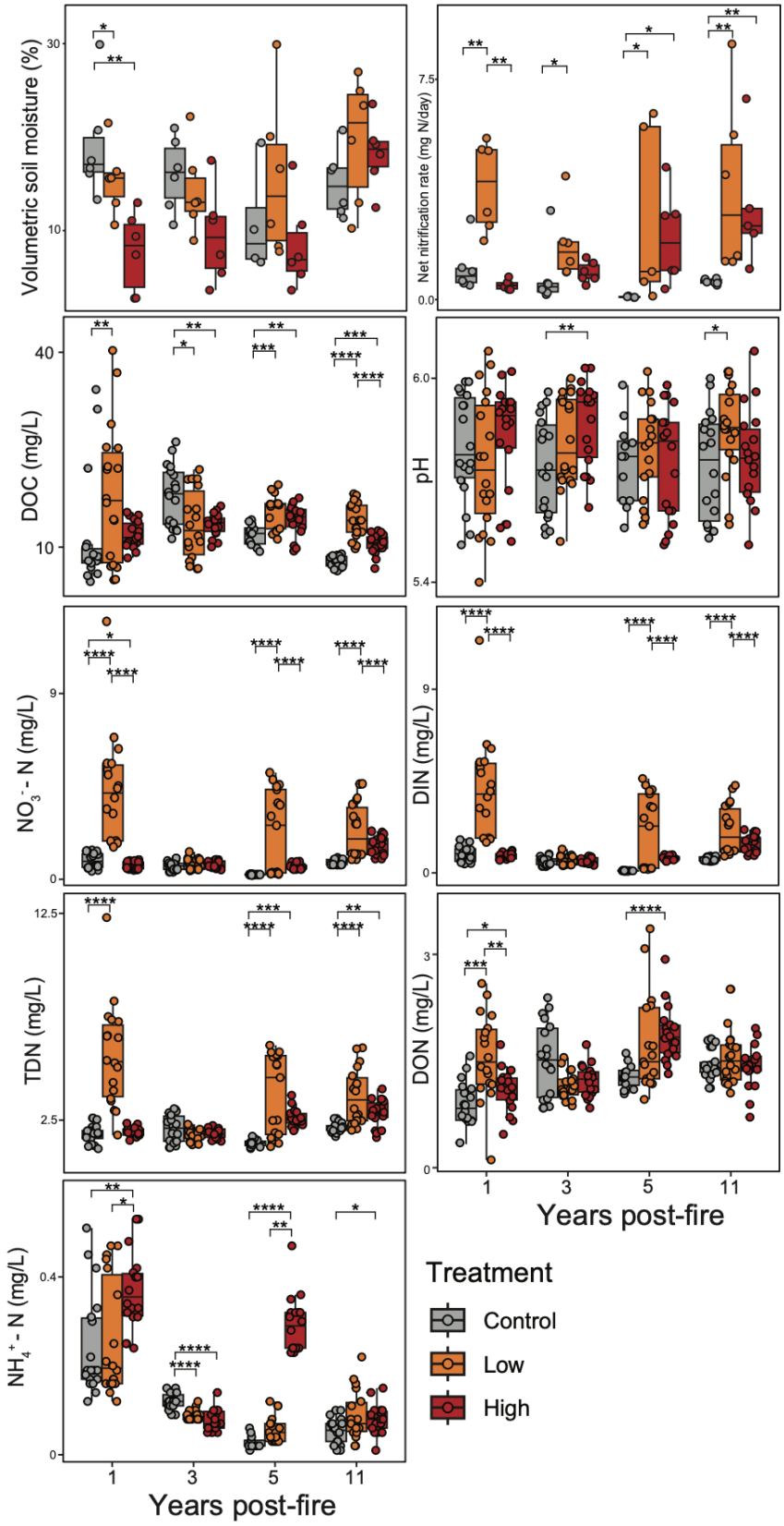

Figure 3.15 Bulk soil chemistry data from water extracts and laboratory incubations. The lower and upper hinges of the boxplots represent the 25th and 75th percentiles, respectively, and the middle line is the median. The whiskers extend from the median by 1.5x the interquartile range. Jittered points represent individual samples. Significant differences between conditions indicated with asterisks as indicated by Wilcoxon rank-sum test. **p*<0.05, ***p*<0.01, ****p*<0.001, *****p*<0.0001.

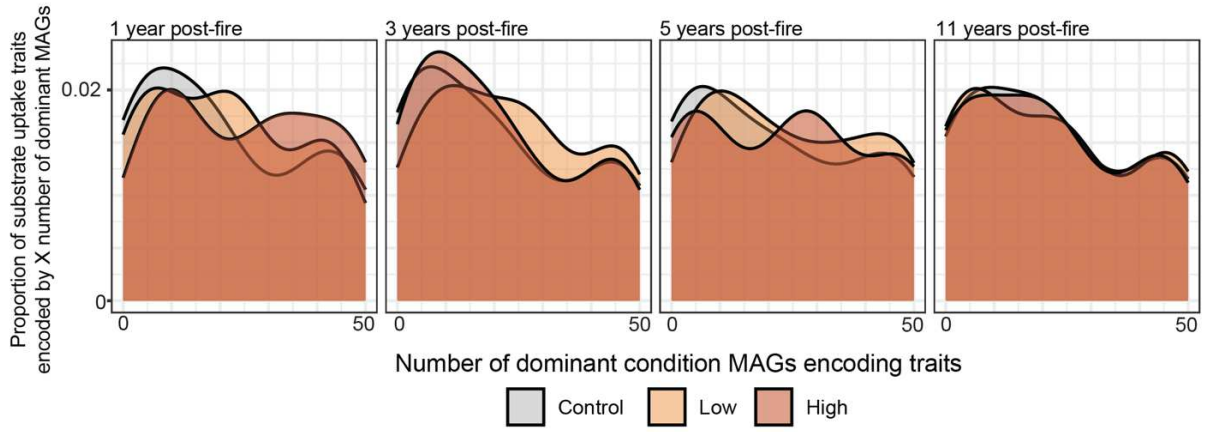

Figure 3.16 Density plot showing the number of resource acquisition 'substrate uptake' traits that have a given number of treatment dominant MAGs that encode them, showing the enrichment of these traits in the dominant soil microbiome 1 year post-high severity wildfire.

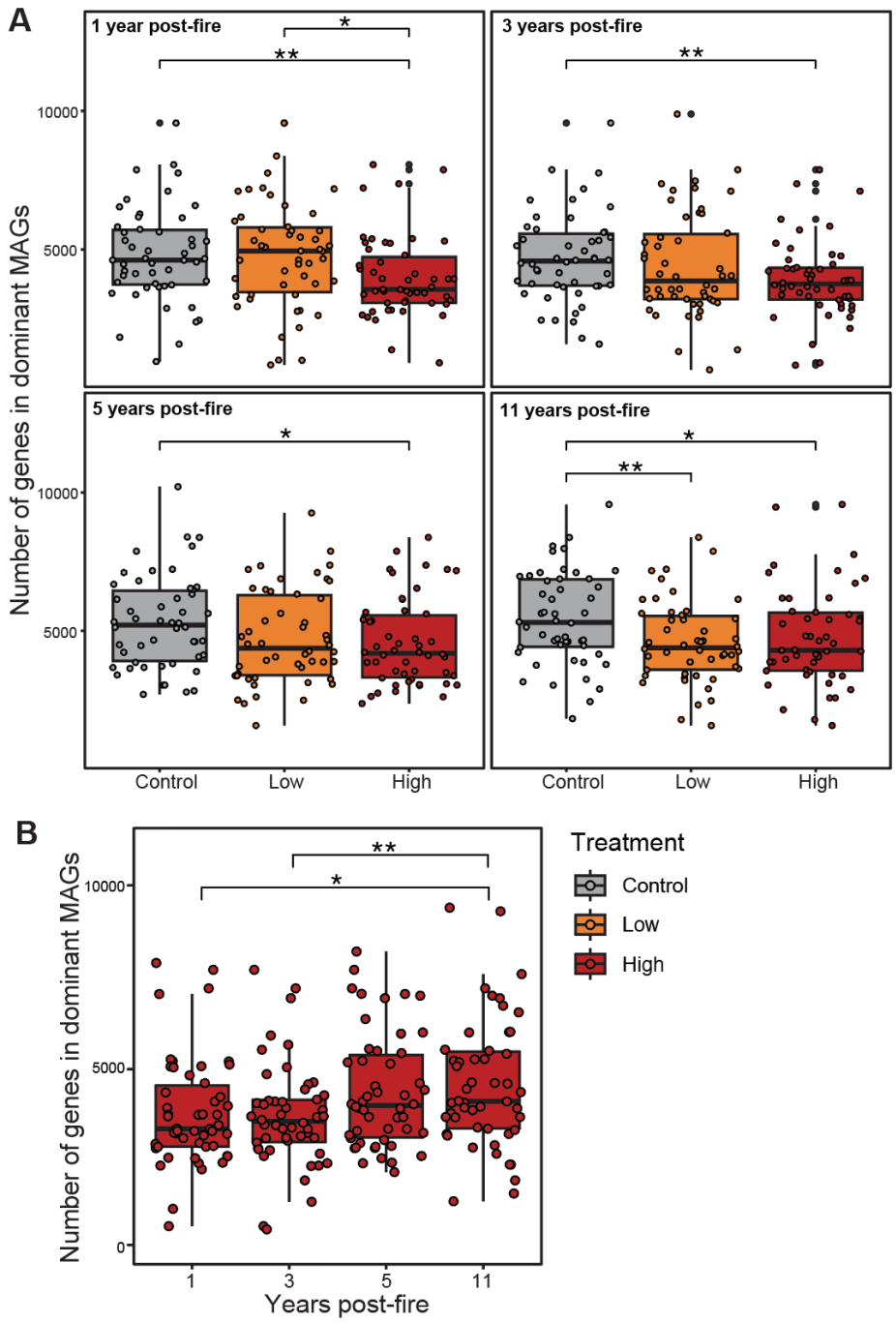

Figure 3.17 (A) Total number of encoded genes in dominant 50 MAGs across treatments. **(B)** Total number of encoded genes in dominant 50 MAGs across wildfires from only high severity sites. The lower and upper hinges of the boxplots represent the 25th and 75th percentiles, respectively, and the middle line is the median. The whiskers extend from the median by 1.5x the interquartile range. Points represent individual MAGs. Significant differences between conditions indicated with asterisks as indicated by Wilcoxon rank-sum test. *p<0.05, **p<0.01.

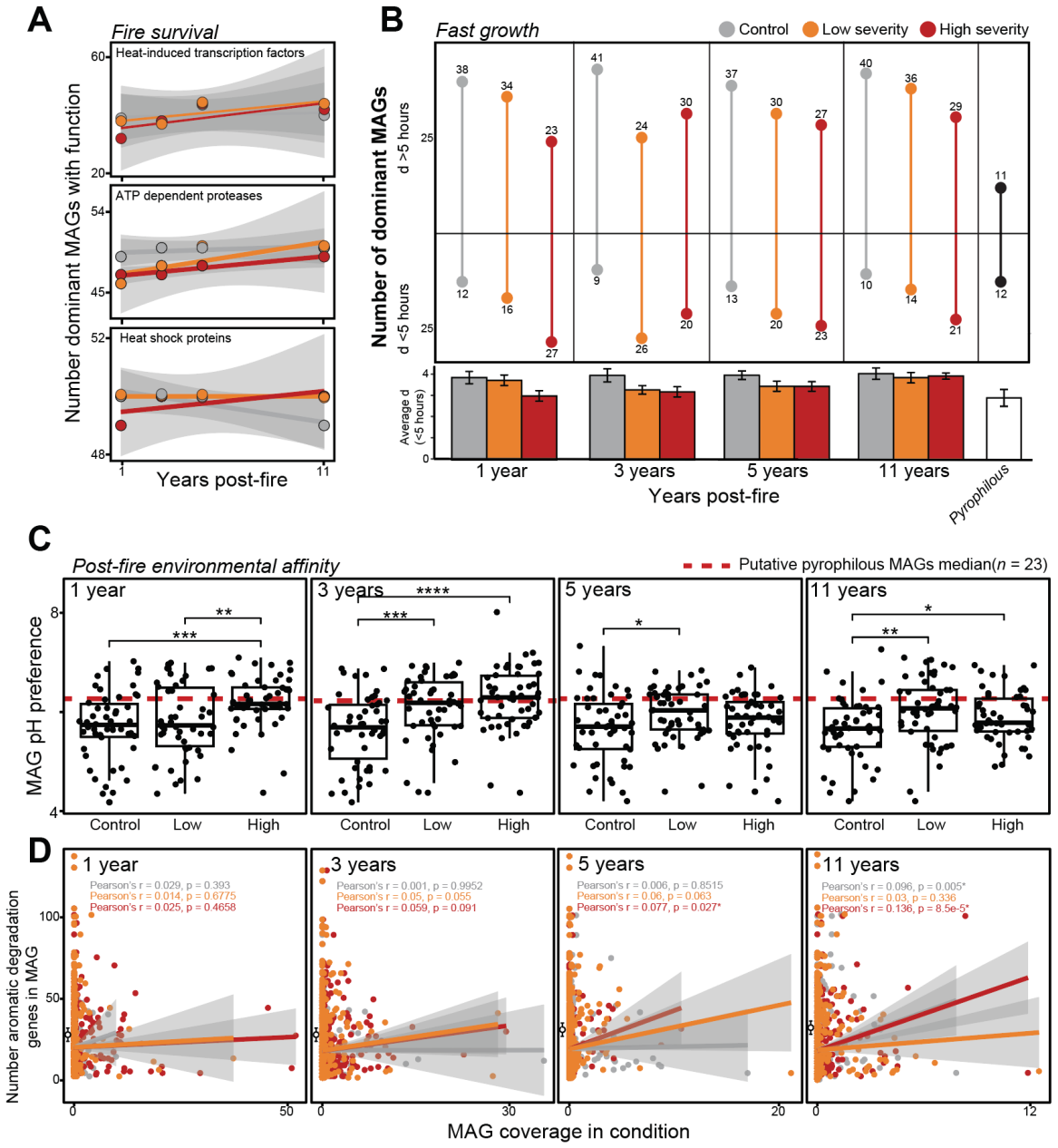

Figure 3.18 (A) Number of dominant MAGs for each treatment with specific "fire survival" high temperature stress resistant function plotted against the treatment's years post-fire (e.g., 1 year post-fire is samples from the Mullen fire) with linear regression lines colored by treatment. **(B)** Number of dominant MAGs (total *n* = 50) from each treatment and MAGs representing putative pyrophilous taxa (total *n* = 23) with gRodon estimated growth rate (d) > or < 5 hours, with average d of MAGs <5 hours indicated in below bar graphs. Error bars represent standard error of the mean. **(C)** MAG pH preference of dominant MAGs across treatments with red line indicating median MAG pH preference of the subset of putative pyrophilous taxa MAGs. The lower and upper hinges of the boxplots represent the 25th and 75th percentiles, respectively, and the middle line is the median. The whiskers extend from the median by 1.5x the interquartile range. Points represent individual MAGs. Significant differences between conditions

indicated with asterisks as indicated by Wilcoxon rank-sum test. *p<0.05, **p<0.01, ***p<0.001, ****p<0.0001. **(D)** Individual MAG coverage in treatment (e.g., 1 year post-fire low severity) plotted against the total number of aromatic degradation genes in MAG with Pearson's correlation coefficient indicated on plot. Black-outlined, white points on each subplot show average number of aromatic degradation genes in putative pyrophilous taxa MAGs with error bars showing standard error of the mean.

Chapter 3 Tables

Table 3.1 Details of samples used for metagenomic sequencing. Note that the 1 year post-fire time point has 6 more metagenomes due to the use of metagenomes from Nelson et al. (2022)[9].

Treatment	1 year	3 years	5 years	11 years
Control	*3*	*3*	*3*	*3*
Low	*9*	*3*	*3*	*3*
High	*9*	*3*	*3*	*3*

Table 3.2 PERMANOVA on Bray-Curtis dissimilarity testing effect of sampled burn treatment (control, low, high burn severity) on microbial community composition (via MAG relative abundances), separated by fire site.

Fire (time post-fire)	PERMANOVA
Mullen (1 yr)	R^2 = 0.4237 , p=0.014*
Ryan (3 yr)	R^2 = 0.41 , p=0.014*
Beaver Creek (5 yr)	R^2 = 0.26 , p=0.34
Church's Park (11 yr)	R^2 = 0.30508, p=0.108

Chapter 3 References

1. Horner-Devine, M. C., Carney, K. M. & Bohannan, B. J. M. An ecological perspective on bacterial biodiversity. *Proc. R. Soc. Lond. B Biol. Sci.* **271**, 113–122 (2004).

2. Parks, D. H., Imelfort, M., Skennerton, C. T., Hugenholtz, P. & Tyson, G. W. CheckM: assessing the quality of microbial genomes recovered from isolates, single cells, and metagenomes. *Genome Res.* **25**, 1043–1055 (2015).

3. Daniel, R. The metagenomics of soil. *Nat. Rev. Microbiol.* **3**, 470–478 (2005).

4. van der Heijden, M. G. A., Bardgett, R. D. & van Straalen, N. M. The unseen majority: soil microbes as drivers of plant diversity and productivity in terrestrial ecosystems. *Ecol. Lett.* **11**, 296–310 (2008).

5. Crowther, T. W. *et al.* The global soil community and its influence on biogeochemistry. *Science* **365**, eaav0550 (2019).

6. Clemmensen, K. E. *et al.* Roots and Associated Fungi Drive Long-Term Carbon Sequestration in Boreal Forest. *Science* **339**, 1615–1618 (2013).

7. Woodcroft, B. J. *et al.* Genome-centric view of carbon processing in thawing permafrost. *Nature* **560**, 49–54 (2018).

8. Singleton, C. M. *et al.* Methanotrophy across a natural permafrost thaw environment. *ISME J.* **12**, 2544–2558 (2018).

9. Nelson, A. R. *et al.* Wildfire-dependent changes in soil microbiome diversity and function. *Nat. Microbiol.* **7**, 1419–1430 (2022).

10. Dove, N. C., Taş, N. & Hart, S. C. Ecological and genomic responses of soil microbiomes to high-severity wildfire: linking community assembly to functional potential. *ISME J.* **16**, 1853–1863 (2022).

11. Lombard, N., Prestat, E., van Elsas, J. D. & Simonet, P. Soil-specific limitations for access and analysis of soil microbial communities by metagenomics. *FEMS Microbiol. Ecol.* **78**, 31–49 (2011).

12. Grime, J. P. Evidence for the Existence of Three Primary Strategies in Plants and Its Relevance to Ecological and Evolutionary Theory. *Am. Nat.* **111**, 1169–1194 (1977).

13. Pierce, S. *et al.* A global method for calculating plant CSR ecological strategies applied across biomes world-wide. *Funct. Ecol.* **31**, 444–457 (2017).

14. Li, T. *et al.* Community assembly during vegetation succession after metal mining is driven by multiple processes with temporal variation. *Ecol. Evol.* **12**, e8882 (2022).

15. Zanzottera, M., Dalle Fratte, M., Caccianiga, M., Pierce, S. & Cerabolini, B. E. L. Community-level variation in plant functional traits and ecological strategies shapes habitat structure along succession gradients in alpine environment. *Community Ecol.* **21**, 55–65 (2020).

16. Fierer, N. Embracing the unknown: Disentangling the complexities of the soil microbiome. *Nat. Rev. Microbiol.* **15**, 579–590 (2017).

17. Malik, A. A. *et al.* Defining trait-based microbial strategies with consequences for soil carbon cycling under climate change. *ISME J.* **14**, 1–9 (2020).

18. Dove, N. C., Safford, H. D., Bohlman, G. N., Estes, B. L. & Hart, S. C. High-severity wildfire leads to multi-decadal impacts on soil biogeochemistry in mixed-conifer forests. *Ecol. Appl.* **30**, eap.2072 (2020).

19. Francos, M., Úbeda, X., Pereira, P. & Alcañiz, M. Long-term impact of wildfire on soils exposed to different fire severities. A case study in Cadiretes Massif (NE Iberian Peninsula). *Sci. Total Environ.* **615**, 664–671 (2018).

20. Zhang, Q. *et al.* Temperature Thresholds of Pyrogenic Dissolved Organic Matter in Heating Experiments Simulating Forest Fires. *Environ. Sci. Technol.* **57**, 17291–17301 (2023).

21. Pressler, Y., Moore, J. C. & Cotrufo, M. F. Belowground community responses to fire: meta-analysis reveals contrasting responses of soil microorganisms and mesofauna. *Oikos* **128**, 309–327 (2019).

22. Caiafa, M. V. *et al.* Distinct fungal and bacterial responses to fire severity and soil depth across a ten-year wildfire chronosequence in beetle-killed lodgepole pine forests. *For. Ecol. Manag.* **544**, 121160 (2023).

23. Johnson, D. B., Woolet, J., Yedinak, K. M. & Whitman, T. Experimentally determined traits shape bacterial community composition one and five years following wildfire. *Nat. Ecol. Evol.* **7**, 1419–1431 (2023).

24. Tran, B. N., Tanase, M. A., Bennett, L. T. & Aponte, C. High-severity wildfires in temperate Australian forests have increased in extent and aggregation in recent decades. *PLOS ONE* **15**, e0242484 (2020).

25. Abatzoglou, J. T. & Williams, A. P. Impact of anthropogenic climate change on wildfire across western US forests. *Proc. Natl. Acad. Sci.* **113**, 11770–11775 (2016).

26. Rovithakis, A. *et al.* Future climate change impact on wildfire danger over the Mediterranean: the case of Greece. *Environ. Res. Lett.* **17**, 045022 (2022).

27. Whitman, T. *et al.* Soil bacterial and fungal response to wildfires in the Canadian boreal forest across a burn severity gradient. *Soil Biol. Biochem.* **138**, 107571 (2019).

28. Pulido-Chavez, M. F. *et al.* Rapid bacterial and fungal successional dynamics in first year after chaparral wildfire. *Mol. Ecol.* **32**, 1685–1707 (2023).

29. Karaoz, U. & Brodie, E. L. microTrait: A Toolset for a Trait-Based Representation of Microbial Genomes. *Front. Bioinforma.* **2**, (in press) (2022).

30. Grime, J. P. The C-S-R model of primary plant strategies — origins, implications and tests. in *Plant Evolutionary Biology* (eds. Gottlieb, L. D. & Jain, S. K.) 371–393 (Springer Netherlands, Dordrecht, 1988). doi:10.1007/978-94-009-1207-6_14.

31. Treseder, K. K. Ecological strategies of microbes: Thinking outside the triangle. *J. Ecol.* **111**, 1832–1843 (2023).

32. Stone, B. W. G. *et al.* Life history strategies among soil bacteria—dichotomy for few, continuum for many. *ISME J.* **17**, 611–619 (2023).

33. Wang, B. & Allison, S. D. Drought legacies mediated by trait trade-offs in soil microbiomes. *Ecosphere* **12**, e03562 (2021).

34. Shao, P., Lynch, L., Xie, H., Bao, X. & Liang, C. Tradeoffs among microbial life history strategies influence the fate of microbial residues in subtropical forest soils. *Soil Biol. Biochem.* **153**, 108112 (2021).

35. Ning, Q. *et al.* Tradeoffs of microbial life history strategies drive the turnover of microbial-derived organic carbon in coastal saline soils. *Front. Microbiol.* **14**, (2023).

36. Feng, J. *et al.* Soil microbial trait-based strategies drive metabolic efficiency along an altitude gradient. *ISME Commun.* **1**, 1–9 (2021).

37. Piton, G. *et al.* Life history strategies of soil bacterial communities across global terrestrial biomes. *Nat. Microbiol.* **8**, 2093–2102 (2023).

38. Barnett, S. E., Egan, R., Foster, B., Eloe-Fadrosh, E. A. & Buckley, D. H. Genomic Features Predict Bacterial Life History Strategies in Soil, as Identified by Metagenomic Stable Isotope Probing. *mBio* **14**, e03584-22 (2023).

39. Liang, C., Amelung, W., Lehmann, J. & Kästner, M. Quantitative assessment of microbial necromass contribution to soil organic matter. *Glob. Change Biol.* **25**, 3578–3590 (2019).

40. Wang, B., An, S., Liang, C., Liu, Y. & Kuzyakov, Y. Microbial necromass as the source of soil organic carbon in global ecosystems. *Soil Biol. Biochem.* **162**, 108422 (2021).

41. Angst, G. *et al.* Stabilized microbial necromass in soil is more strongly coupled with microbial diversity than the bioavailability of plant inputs. *Soil Biol. Biochem.* **190**, 109323 (2024).

42. Kayes, L. J. & Tinker, D. B. Forest structure and regeneration following a mountain pine beetle epidemic in southeastern Wyoming. *For. Ecol. Manag.* **263**, 57–66 (2012).

43. Rhoades, C. C. *et al.* Snagfall the first decade after severe bark beetle infestation of high-elevation forests in Colorado, USA. *Ecol. Appl.* **30**, e02059 (2020).

44. Trahan, N. A., Dynes, E. L., Pugh, E., Moore, D. J. P. & Monson, R. K. Changes in soil biogeochemistry following disturbance by girdling and mountain pine beetles in subalpine forests. *Oecologia* **177**, 981–995 (2015).

45. Yu, N. Y. *et al.* PSORTb 3.0: improved protein subcellular localization prediction with refined localization subcategories and predictive capabilities for all prokaryotes. *Bioinformatics* **26**, 1608–1615 (2010).

46. Li, J. *et al.* Spatiotemporal variability of fire effects on soil carbon and nitrogen: A global meta-analysis. *Glob. Change Biol.* gcb.15742 (2021) doi:10.1111/gcb.15742.

47. Chuckran, P. F. *et al.* Edaphic controls on genome size and GC content of bacteria in soil microbial communities. *Soil Biol. Biochem.* **178**, 108935 (2023).

48. Sorensen, J. W., Dunivin, T. K., Tobin, T. C. & Shade, A. Ecological selection for small microbial genomes along a temperate-to-thermal soil gradient. *Nat. Microbiol.* **4**, 55–61 (2019).

49. Roth, H. K. *et al.* Effects of burn severity on organic nitrogen and carbon chemistry in high-elevation forest soils. *Soil Environ. Health* **1**, 100023 (2023).

50. Bruns, T. D., Chung, J. A., Carver, A. A. & Glassman, S. I. A simple pyrocosm for studying soil microbial response to fire reveals a rapid, massive response by Pyronema species. *PLOS ONE* **15**, e0222691 (2020).

51. Weissman, J. L., Hou, S. & Fuhrman, J. A. Estimating maximal microbial growth rates from cultures, metagenomes, and single cells via codon usage patterns. *PNAS* **118**, 1–10 (2020).

52. Ramoneda, J. *et al.* Building a genome-based understanding of bacterial pH preferences. *Sci. Adv.* **9**, eadf8998 (2023).

53. Adkins, J., Docherty, K. M. & Miesel, J. R. Copiotrophic Bacterial Traits Increase With Burn Severity One Year After a Wildfire. *Front. For. Glob. Change* **5**, (2022).

54. Bostick, K. W. *et al.* Biolability of Fresh and Photodegraded Pyrogenic Dissolved Organic Matter From Laboratory-Prepared Chars. *J. Geophys. Res. Biogeosciences* **126**, e2020JG005981 (2021).

55. Cobo-Díaz, J. F. *et al.* Metagenomic Assessment of the Potential Microbial Nitrogen Pathways in the Rhizosphere of a Mediterranean Forest After a Wildfire. *Microb. Ecol.* **69**, 895–904 (2015).

56. Fernández-González, A. J. *et al.* The rhizosphere microbiome of burned holm-oak: potential role of the genus Arthrobacter in the recovery of burned soils. *Sci. Rep.* **7**, 6008 (2017).

57. Hudiburg, T. *et al.* Terrestrial carbon dynamics in an era of increasing wildfire. *Nat. Clim. Change* **13**, 1306–1316 (2023).

58. Rodman, K. C. *et al.* A changing climate is snuffing out post-fire recovery in montane forests. *Glob. Ecol. Biogeogr.* 1–13 (2020) doi:10.1111/geb.13174.

59. Stevens-Rumann, C. S., Kemp, K. B., Higuera, P. E. & Rother, M. T. Evidence for declining forest resilience to wildfires under climate change. *Ecol. Lett.* **21**, 243–252 (2018).

60. Coop, J. D. *et al.* Wildfire-Driven Forest Conversion in Western North American Landscapes. *BioScience* **XX**, 1–15 (2020).

61. Roller, B. R. K. & Schmidt, T. M. The physiology and ecological implications of efficient growth. *ISME J.* **9**, 1481–1487 (2015).

62. Roller, B. R. K., Stoddard, S. F. & Schmidt, T. M. Exploiting rRNA operon copy number to investigate bacterial reproductive strategies. *Nat. Microbiol.* **1**, 1–7 (2016).

63. Hagerty, S. B., Allison, S. D. & Schimel, J. P. Evaluating soil microbial carbon use efficiency explicitly as a function of cellular processes: implications for measurements and models. *Biogeochemistry* **140**, 269–283 (2018).

64. Wang, C. *et al.* Large-scale importance of microbial carbon use efficiency and necromass to soil organic carbon. *Glob. Change Biol.* **27**, 2039–2048 (2021).

65. Parson, A., Robichaud, P. R., Lewis, S. A., Napper, C. & Clark, J. T. *Field Guide for Mapping Post-Fire Soil Burn Severity*. *USDA Forest Service - General Technical Report RMRS-GTR* 1–49 https://www.fs.usda.gov/treesearch/pubs/36236 (2010) doi:10.2737/RMRS-GTR-243.

66. Bundy, L. G. & Meisinger, J. J. Nitrogen Availability Indices. in *Methods of Soil Analysis: Part 2 Microbiological and Biochemical Properties* 951–984 (Macmillan Education UK, London, 2018). doi:10.2136/sssabookser5.2.c41.

67. McDowell, W. H. *et al.* A comparison of methods to determine the biodegradable dissolved organic carbon from different terrestrial sources. *Soil Biol. Biochem.* **38**, 1933–1942 (2006).

68. Thomas, G. W. Soil pH and Soil Acidity. in *Methods of Soil Analysis* 475–490 (John Wiley & Sons, Ltd, 1996). doi:10.2136/sssabookser5.3.c16.

69. Buyer, J. S. & Sasser, M. High throughput phospholipid fatty acid analysis of soils. *Appl. Soil Ecol.* **61**, 127–130 (2012).

70. Bligh, E. G. & Dyer, W. J. A RAPID METHOD OF TOTAL LIPID EXTRACTION AND PURIFICATION. *Can. J. Biochem. Physiol.* **37**, 911–917 (1959).

71. Joshi, N. & Fass, J. Sickle: A sliding-window, adaptive, quality-based trimming tool for FastQ files. Preprint at (2011).

72. Li, D., Liu, C.-M., Luo, R., Sadakane, K. & Lam, T.-W. MEGAHIT: an ultra-fast single-node solution for large and complex metagenomics assembly via succinct de Bruijn graph. *Bioinformatics* **31**, 1674–1676 (2015).

73. Kang, D. D. *et al.* MetaBAT 2: an adaptive binning algorithm for robust and efficient genome reconstruction from metagenome assemblies. *PeerJ* **7**, e7359 (2019).

74. Chaumeil, P.-A., Mussig, A. J., Hugenholtz, P. & Parks, D. H. GTDB-Tk: a toolkit to classify genomes with the Genome Taxonomy Database. *Bioinformatics* **36**, 1925–1927 (2019).

75. Olm, M. R., Brown, C. T., Brooks, B. & Banfield, J. F. dRep: a tool for fast and accurate genomic comparisons that enables improved genome recovery from metagenomes through de-replication. *ISME J.* **11**, 2864–2868 (2017).

76. Bowers, R. M. *et al.* Minimum information about a single amplified genome (MISAG) and a metagenome-assembled genome (MIMAG) of bacteria and archaea. *Nat. Biotechnol.* **35**, 725–731 (2017).

77. Langmead, B. & Salzberg, S. L. Fast gapped-read alignment with Bowtie 2. *Nat. Methods* **9**, 357–359 (2012).

78. Eddy, S. R. Accelerated profile HMM searches. *PLoS Comput. Biol.* **7**, (2011).

79. Aramaki, T. *et al.* KofamKOALA: KEGG Ortholog assignment based on profile HMM and adaptive score threshold. *Bioinformatics* **36**, 2251–2252 (2020).

80. Khot, V. *et al.* CANT-HYD: A Curated Database of Phylogeny-Derived Hidden Markov Models for Annotation of Marker Genes Involved in Hydrocarbon Degradation. *Front. Microbiol.* **12**, 1–15 (2022).

Chapter 4: Soil microbiome feedbacks during disturbance-driven forest ecosystem conversion[2]

4.1 Summary

Disturbances cause rapid changes to forests, with different disturbance types and severities creating unique ecosystem trajectories that can impact the underlying soil microbiome. Pile burning – the combustion of logging residue on the forest floor – is a common fuel reduction practice that can have impacts on forest soils analogous to those following high severity wildfire. Further, pile burning following clear-cut harvesting can create persistent openings dominated by non-woody plants surrounded by dense regenerating conifer forest. A paired 60-year chronosequence of burn scar openings and surrounding regenerating forest after clear-cut harvesting provides a unique opportunity to assess whether belowground microbial processes mirror aboveground vegetation during disturbance-induced ecosystem shifts. Soil ectomycorrhizal fungal diversity was reduced the first decade after pile burning, which could explain poor tree seedling establishment and subsequent persistence of herbaceous species within the openings. Fine-scale changes in the soil microbiome mirrored aboveground shifts in vegetation, with short-term changes to microbial carbon cycling functions resembling a post-fire microbiome (e.g., enrichment of aromatic degradation genes) and respiration in burn scars decoupled from substrate quantity and quality. Broadly, however, soil microbiome composition and function within burn scar soils converged with that of the surrounding

[2] This chapter was reproduced verbatim from "Nelson et al. Soil microbiome feedbacks during disturbance-driven forest ecosystem conversion. In review (2024)". The text benefitted from writing and editing contributions from contributing authors.

regenerating forest six decades after the disturbances, indicating potential microbial resilience that was disconnected from aboveground vegetation shifts. This work begins to unravel the belowground microbial processes that underlie disturbance-induced ecosystem changes, which are increasing in frequency tied to climate change.

4.2 Introduction

Disturbances, such as wildfire or logging, are common factors that shape forests and leave legacies that can alter the trajectory of post-disturbance recovery. The subalpine forests of the southern Rockies (USA) are shaped by infrequent stand-replacing wildfire[1] that can release seed stored in cones of lodgepole pine, create seedbeds that favor tree and herbaceous seedling regeneration, reduce surface fuel loads, and alter carbon (C) and nitrogen (N) cycling[2,3]. Although these ecosystems are adapted to wildfire, climate change coupled with shifting land use patterns have increased the frequency and severity of wildfires in the western United States[4–6]. Further, the combination of wildfire and other disturbances (e.g., windthrow, drought, or bark beetle infestation) may hamper successful tree regrowth[7–9], which can result in the replacement of forests with non-forest vegetation[10]. Such forest conversions have been documented in response to shifting wildfire activity and compound disturbance especially near vegetation ecotone boundaries and in arid landscapes[11–14].

The microbial communities (bacteria, archaea, and fungi) that inhabit forest soils drive important biogeochemical processes that influence above-ground forest productivity[15] by providing N and P[16] via mycorrhizal relationships, governing organic matter transformation and C storage[17,18], and regulating plant diversity[19]. Following a

disturbance such as wildfire, changes in soil microbial community composition or function may directly influence ecosystem processes[20] and could modulate the resistance or resilience of a post-disturbance aboveground forest ecosystem[21].

One such disturbance, pile burning, is the combustion of logging residue on the forest floor, and is a common management practice to reduce surface fuels that can have impacts on forest soils analogous to those following severe wildfire[22,23]. The extreme soil heating (>300°C @ 5 cm depth[24]) and duration of smoldering combustion caused by pile burning[24,25] can result in long-lasting (years to decades) increases in soil pH and nutrient availability[26], loss of soil C, and depleted microbial biomass[24]. Prior research on a 5 decade chronosequence of burn pile scars revealed that pile burning could create persistent openings in the forest with a lack of pine tree regeneration and high cover of graminoids (e.g., grasses) and forbs (e.g., *Achillea millefolium*), in contrast to surrounding forest that was successfully regenerating after clear-cut harvesting[27]. Here, we leverage this multidecadal chronosequence of paired burn pile scars and surrounding regenerating forest to investigate the belowground microbial dynamics during divergent ecosystem recovery trajectories.

To identify the soil microbiome processes that underlie this multidecadal burning-induced vegetation-type conversion, we interrogated the soil bacterial and fungal communities using molecular approaches (16S rRNA gene, ITS amplicon, and metagenomic sequencing) to characterize the composition and functional potential of the soil microbiome within the aforementioned series of burn scars along a 5 decade chronosequence, along with soils collected from the surrounding regenerating forest and parallel pine seedling bioassay *in situ* and greenhouse experiments. This work advances

our understanding of the interplay between aboveground vegetation and belowground microbial processes that underpin ecosystem shifts following disturbances, which are predicted to increase in response to climate change. We broadly hypothesized that **(1)** burn scar soil microbial communities will diverge compositionally over the chronosequence as vegetation shifts over time, **(2)** differences in aboveground communities and plant inputs will result in altered soil microbiome function as related to C and N cycling, and **(3)** microbial traits associated with the legacy of fire in burn pile scars (e.g., genes for degrading pyrogenic C) will recede with time and be replaced by traits associated with herbaceous ecosystems.

4.3 Results & Discussion

4.3.1 Long-term shifts in aboveground vegetation and soil chemistry

Pile burning catalyzed the shift to a herbaceous-dominated plant community, with higher forb and graminoid cover and lower tree density (average of 366 trees ha^{-1} vs. ~3600 trees ha^{-1})[27] in the openings as compared to the surrounding regenerating pine forest. Changes in soil pH, sulfate, and chloride also persisted across most of the chronosequence (up to six decades post-disturbance; **Figure 4.1**). Various N species (e.g., NH_4^+, NO_3^-, TDN) were elevated in the most recently burned openings due to combustion of organic matter, reduced plant N uptake, and enrichment of ash-derived ammonium followed by subsequent microbial nitrification[27](**Figure 4.1**). Changes to belowground inputs associated with the shift from forest to herbaceous community combined with altered soil chemistry could influence the structure and function of the soil microbiome[28].

4.3.2 Soil microbiome compositional shifts reveal pulse and press disturbance

To track soil microbiome changes during ecosystem recovery along distinct ecological trajectories (i.e., post-clear cut forest regeneration and forest shift to herbaceous plant-dominance), we sequenced 16S rRNA genes and ITS amplicons from soil samples (0-15 cm depth) collected in burn pile scars that were burned over five decades (1960s-2000s; hereafter referred to as 'burn scar'), and adjacent unburned soils in lodgepole pine forest regenerating after clear cutting (hereafter referred to as 'regen forest'). Burn scar soil bacterial communities were generally compositionally distinct from regen forest soils across the chronosequence (**Figure 4.2**; PERMANOVA R^2 = 0.085, p = 0.001) with interactive effects with time post-disturbance (PERMANOVA R^2 = 0.062, p = 0.001). The soil bacterial communities in the older regenerating forest soils more closely resembled a nearby old-growth lodgepole pine forest than recently regenerated stands[20] (**Figure 4.2**). Soil communities were also statistically distinct between regen forest and burn scar samples, although less so than bacterial communities (**Figure 4.2**; PERMANOVA R^2 = 0.02, p = 0.001), with similar interactive effects with time post-disturbance and treatment (PERMANOVA R^2 = 0.066, p = 0.001). These patterns shifted with time since fire, with treatment having less of an effect on bacterial community composition over time and fungal communities becoming statistically indistinct after six decades post-disturbance (1960s; **Figure 4.3**). Broad soil microbiome compositional differences were correlated to soil pH, which remained elevated within the burn scars over the chronosequence (**Figure 4.1, Figure 4.3**). Thus, despite differences in aboveground vegetation in burn scars, with lodgepole pine generally replaced by

graminoids and forbs[27], the soil microbiome was broadly compositionally indistinct from that of the surrounding regenerating forest six decades post-disturbance.

Despite broad soil microbial community similarities, the burn scar soil microbiome harbored fine-scale compositional shifts likely associated with pile burning and the subsequent changes in vegetation. For example, soil communities within more recent burn scars displayed similar compositional traits to post-wildfire soils that lessened over time since burn. ASVs associated with the fire-responding Actinobacteria genera *Arthrobacter*[20,28–30], *Blastococcus*[20,30,31], *Modestobacter*[20], and *Massilia*[32,33] were all generally higher in relative abundance in burn scars relative to regen forest soil samples, with the relative abundance of both *Blastococcus* and *Modestobacter* decreasing over the chronosequence (i.e., recovery time since burning; **Figure 4.4**). In contrast, sequences affiliated with fire-sensitive *Verrucomicrobia*[20], were depleted in burn scars relative to regen forest soils, but steadily increased over the time series (**Figure 4.5**). Similar to other studies[31,33], more recently burned scar soils contained *Ascomycota*-dominated fungal communities (**Figure 4.5**) which reverted to *Basidiomycota*-dominance two decades post-burn. There was also a short-lived (three decade) post-burn enrichment of taxa within the fungal phyla *Mortierellomycota* (**Figure 4.5**), which display similar trends in the rhizosphere of aspen saplings colonizing severely burned soils[34].

Over time, some changes in the burn scar soil microbiome mirrored shifts observed in the soil microbiome of forests undergoing conversion to grassland. Crowther et al (2014)[35] characterized how deforestation influenced soil microbial communities across different biomes and found consistent compositional shifts, including a decrease in *Basidiomycota*. In the herbaceous-plant dominated burn scar soils, the relative

abundance of *Basidiomycota* remained low compared to the regen forest soils after six decades (**Figure 4.5**). In contrast to persistent low EMF diversity in burn scar soils throughout the chronosequence, regen forest soils experienced temporal increases in EMF diversity concurrent with the reestablishment of lodgepole pine[27], resulting in significant differences in EMF diversity between regen forest and burn scar soils 50 years following disturbance (**Figure 4.6**). Similar to patterns observed after deforestation[36], the relative abundance of *Cyanobacteria* was elevated by pile burning and remained higher in burn scar soils over the chronosequence (**Figure 4.5**). Together, these compositional data reveal that despite broad compositional convergence between burn scar and regen forest soil microbiomes, there are compositional differences likely initiated by aboveground disturbances; burning caused an enrichment of pyrophilous taxa that, as graminoids and forbs established within the burn scar, transitioned to communities with greater compositional similarities to those observed in herbaceous-plant dominated ecosystems.

4.3.3 Disturbances govern soil microbiome assembly

To determine how assembly processes governing soil bacterial community structure differed over time and across treatments (i.e., pile burning vs clear cutting), two null modeling analyses, β-nearest taxon index (βNTI) and Raup-Crick (Bray-Curtis) (RC_{BC}) were performed. These approaches use randomized community structures to identify whether measured communities are more similar or dissimilar to one another than would be expected by random chance. If |βNTI| is greater than 2, deterministic processes drive community assembly. Communities with a βNTI > 2 are more different than would be expected by random chance due to variable selection, whereas communities with a

βNTI < -2 are more similar than would be expected by random chance due to homogenizing selection. These assembly processes are driven by environmental conditions, where a homogenous environment (e.g., spatially or temporally) might result in homogenizing selection and heterogeneous conditions (e.g., variable soil pH) might cause variable selection processes[37]. If |βNTI| is less than 2, communities are as different as expected by random chance and stochastic processes dictate community structure. These stochastic processes can be distinguished using RC_{BC} analyses as dispersal limitation (RC_{BC} > 0.95) where there is a decreased ability for communities to mix, and homogenizing dispersal (RC_{BC} < -0.95) where a system experiences high exchange rates. If $|RC_{BC}|$ is less than 0.95, there is no single assembly process strong enough to control community structure and an undominated signal is observed.

Combined, βNTI and RC_{BC} results revealed a diminishing impact of pile burning on soil bacterial community assembly over time. Burn scar soil bacterial communities experienced more homogenizing selection (i.e., communities are more like one another than expected by random chance) when they were more similar in age (**Figure 4.7)**. These data suggest that burn scars follow very similar recovery trajectories over time, as within-decade community comparisons (e.g., all 2000s-2000s, 1990s-1990s, etc.) are dominated by homogenizing selection. With greater time between comparisons (e.g., a 1960s-2000s burn comparison vs. a 1960s-1960s burn comparison), the influence of both variable selection and dispersal limitation increased. The observed shift in processes governing soil bacterial community structure with time indicates the lessening of fire influence and the role of additional environmental factors (e.g., differing plant carbon soil

inputs) in shaping community assembly during ecosystem shift from forest to herbaceous plant-dominated.

Null model analyses between burn scar and regen forest soils also revealed evidence for the decreasing influence of fire on bacterial communities with time. Within-decade treatment comparisons (**Figure 4.7)** highlighted greater variable selection (i.e., communities are more different than one another than expected by random chance) in the 2000s, which greatly decreased over time to be replaced by predominantly homogenizing selection processes. Thus, these data indicate that following the fire pulse disturbance, the resulting press disturbance of altered soil physicochemical conditions and altered aboveground vegetation exerted significant control on soil bacterial community assembly for up to three decades. Beyond this, dispersal limitation and homogenizing selection (**Figure 4.7**) influenced soil bacterial community structure within the two conditions. Therefore, under many situations in burn scar and regen forest soils disturbed between 30 and 60 years ago, the communities experience sufficiently similar environmental conditions to develop homogenously (e.g., subject to homogenizing selection). However, if selection is too weak, these communities proceed to develop due to dispersal limitation due to the lack of strong dispersal capabilities between burn scar and regen locations.

4.3.4 Fire legacy soil microbiome traits differ in prevalence at longer timescales

Previous studies focusing on the post-fire soil microbiome have identified prevalent traits that allow specific taxa to thrive and become dominant in soils with altered physicochemical characteristics[20,29,38]. Using our extensive gene dataset from 56 metagenomes from both burn scar and regen forest soils across a multidecadal

chronosequence, we inventoried three recurring traits to assess their importance within the burn scar soil microbiome over multidecadal timescales. These traits included (1) fast growth rates to enable quick occupation of newly available niche space following disturbance, (2) stress response genes to allow their survival within the altered post-burn soils, and (3) the ability to degrade fire-transformed pyrogenic carbon with increased aromaticity.

Previous studies have found that fast growth potential is a key characteristic that governs soil successional dynamics one year following wildfire[20,38] but that its significance may wane after five years[39]. In contrast, another fire chronosequence study performed in the Sierra Nevada found that communities had relatively fast growth rates multiple decades post-fire due to an increase in microbial metabolic substrates[29]. Here, we investigated whether fast growth was a dominant trait within the burn scars via estimates of maximum growth rates of bulk soil metagenomes[40]. Following the removal of 3 samples that had a maximum growth rate >5 hours, the average maximum growth rates for soil microbiomes within burn scar and regen forest soils were 3.67 and 3.25 hours, respectively. Over the chronosequence, there was no evidence that the burned soil microbiome harbored faster maximum growth rates relative to regen forest soils, indicating that this trait plays a lesser role in structuring microbial communities across decadal timescales post-fire (**Figure 4.8**). Here, we suggest that altered vegetative successional dynamics following slash pile burning likely influences the substrates available for microbial growth and may account for observed differences with natural wildfires.

Stress response is another important trait that allows taxa to persist in burned soils that generally have lower moisture due to loss of overstory causing increased temperatures and fire-induced soil hydrophobicity. The genomic potential for biosynthesis of two such stress protectants, mycothiol and ectoine, is enriched in MAGs in early post-fire soils[29] (i.e., 4 years post-fire). Mycothiol is produced by Actinobacteria for oxidative stress tolerance[41], which is likely high following burning due to increased hydrophobicity and decreased water holding capacity of soils, and ectoine aids in rapid temperature fluctuations and ionizing radiation damage[42]. Here, genes for synthesizing ectoine were more abundant in burn scar vs. regen forest soils over nearly the entire chronosequence (**Figure 4.8**). The enrichment of ectoine synthesis genes is likely due to the long-term loss of overstory within the burn scars, which remain depleted in shade-producing pine species and become graminoid- and forb-dominated[43]. In contrast, genes for mycothiol synthesis were not significantly more abundant in burn scar vs. regen forest soils, revealing that oxidative stress tolerance is no longer an important trait decades following burning. We additionally inventoried the gene dataset for genes necessary for trehalose and glycine betaine synthesis, heat shock, and sporulation, and found that these stress response genes were not consistently enriched in burn scar soils relative to regen forest (**Figure 4.8**), indicating that the enrichment of stress response genes with wildfire is no longer prevalent decades following wildfire. Instead, differences in the abundances of these genes here (e.g., ectoine synthesis) are likely due to the divergent ecological trajectories between burn scars and regen forest soils.

Another important trait for the soil microbiome that colonizes and persists in soils following high temperature burning is the ability to utilize pyOM, which is generally

increased in aromaticity as compared to unburned soils[44]. Briefly, we found that genes associated with the bacterial degradation of PAHs and benzene were enriched in more recently burned scars relative to regen forest soils (**Figure 4.9**). These enriched genes decline by 30 years following pile burning, likely due to decreasing pyOM concentrations over time since burn. Benzene degradation genes also remain enriched within burned soils over much of the chronosequence (**Figure 4.9**). This metagenomic sequencing data reveals that the trait for pyOM utilization in the burned soil microbiome is important within burn pile systems decades following burning.

Combined, these data reveal that key traits governing soil microbial dynamics in the immediate aftermath of fire are either not important over these multidecadal timescales (fast growth rates), differ due to the ecosystem conversion of the burn scars to herbaceous plant-dominated ecosystems (stress response), or show waning importance over time since burn (pyrogenic C utilization).

4.3.5 Ecosystem trajectories alter microbiome functional potential for C and N cycling

To identify impacts of ecosystem conversion on soil microbial functional potential for C and N cycling, we leveraged a gene database derived from 56 metagenomes from burn scar and regen forest soils for genes associated with aromatic catabolism (e.g., polyaromatic degradation, b-ketoadipate pathway; *n* = 26,241 genes), the processing of alkanes (*n* = 814), carbohydrate degradation (CAZymes; *n* = 275,398), and the cycling of inorganic N (*n* = 6,686). Pile burning and clear cutting both reduced soluble soil C (i.e., dissolved organic C, DOC; **Figure 4.1**) which then recovers as herbaceous plant or tree roots proliferate and forest litter inputs increase. Soil DOC concentrations increased over time in both treatments, likely following two different mechanisms: in burn scars, DOC

increase may derive from degradation of bulkier, low solubility fire-derived polyaromatic hydrocarbons (PAHs) into smaller water-soluble compounds and root exudation from quickly establishing grasses. In regen forest soils, DOC increase followed the reestablishment and growth of lodgepole pine through litter and root exudate inputs. Burn scar soils generally had higher DOC, supporting previous work showing increased total C in burn scar soils relative to regen forest[27]. However, relative soil respiration and inferred soil organic matter bioavailability was generally lower in burn scars soils relative to regen forest soils (**Figure 4.10**), potentially due to limited pine reestablishment within burn scars and lower C release via root exudation of annuals relative to perennials[45]. As expected, respiration was positively correlated to %C, C:N, and initial soil moisture in regen forest soils, whereas these trends were absent in burn scar soils (**Figure 4.9)**. This suggests that other factors such as microbial access to substrates or the genomic potential to utilize available C may exert a greater influence on soil respiration within the burn scar soils.

To investigate whether the metagenome-encoded potential for utilizing C substrates differed between burn scar and regen forest soils, we quantified the relative abundance of specific genes over time and between treatments. Burning can transform soil organic matter (SOM) to increasingly aromatic molecular structures[44], like PAHs, which become more aromatic with increased burn severity. Because of the prevalence of aromatic pyrogenic organic matter (pyOM) within burned soils[44,46] and studies indicating microbial potential for degrading pyOM in burned soils[20] we identified genes targeting both PAHs and monoaromatic compounds (e.g., benzene). We found that genes for bacterial degradation of PAHs and benzene were enriched in the most recent burn scars

relative to regen forest soils, likely due to residual pyOM from slash pile burning (**Figure 4.9**). PAH degradation genes were linked to MAGs that represented the Proteobacteria family *Xanthobacteraceae* (BP_680, BP_689, BP_693, BP_694), the Actinobacteria genus *Mycobacterium* (e.g., BP_237), the Desulfobacterota family *Binataceae* (e.g., BP_616), and the Myxococcota genus *Labilitrix* (BP_638), revealing diverse community members that encode the functional potential for degrading PAHs within burn scar soils. The relative abundance of PAH degradation genes quickly declined 30 years following pile burning (1990s) and continued to mirror gene relative abundance profiles in regen forest soils throughout the remainder of the chronosequence (**Figure 4.9**). In contrast, genes encoding benzene degradation remained enriched within burned soils through much of the chronosequence, likely because monoaromatic compounds can also be derived from root and plant litter inputs, revealing a longer-term legacy that follows the impact of burning (e.g., altered plant inputs). Combined, these data reveal clear pyrophilous traits encoded by the soil microbiome that persisted for several decades following burning (more detailed in *Section 2.3.4*). In contrast to these trends, genes encoding pathways for the degradation of alkanes (representing more simple aliphatic compounds) were enriched in regen forest soils up to 60 years post-disturbance (1960s soils; **Figure 4.9**), representing the likely greater concentrations of more simple bioavailable substrates within regen forest soils.

Relative abundance profiles of CAZymes further indicated altered genomic potential in more recently disturbed soils, with burn scar and regen forest soils becoming more similar ~60 years post-disturbance (1960s samples). For example, polysaccharide lyases, which catalyze the decomposition of acidic polysaccharides (e.g., starch and

chitin), were enriched in recently burned soils with many differentially abundant genes (via DESeq2, $p<0.05$; n = 147 genes enriched in 2000s burn scar vs 81 in regen forest; **Figure 4.11**). In contrast, carbohydrate esterases, which include enzymes involved in hemicellulose and pectin metabolism, displayed opposite trends and were enriched in regen forest soils (**Figure 4.11**). Carbohydrate esterase normalized abundance was significantly correlated with time since disturbance (Spearman's $\rho = 1$, $p = 0.0167$; **Figure 4.11**), recovering to resemble regen forest soils by the 1960s. Polysaccharide lyases also recovered to similar normalized abundances as regen forest soils by six decades post-disturbance, suggesting that some substrate pools are equally abundant after six decades post-disturbance. In contrast to conifer forests burned by high severity wildfire in California[29], where glycoside hydrolases were enriched in burned soils and attributed to C limitations, we identified no clear difference in their relative abundances over time between the two treatments.

Inorganic N was elevated the first decade following pile burning due to combustion and release of NH_4^+ from forest biomass and surface organic matter combustion and increased potential for nitrification (**Figure 4.1**). The influx of NH_4^+ is associated with a short-term (< 10 year) post-fire increase in nitrification[29,47]. We measured higher diversity of putative nitrifiers in burn scar relative to regen forest soils over the chronosequence (**Figure 4.12**), although genes encoding nitrification (*amoABC*; n = 50) were less abundant over the same samples (**Figure 4.12**). In contrast, denitrification gene profiles (e.g., *nirK*, *nirS*, *narG*, *nosZ*; n = 4235) did not differ between burn scar and regen forest soils (**Figure 4.12**), potentially reflecting the broad distribution of this functional trait across diverse bacterial lineages[48]. The only inorganic N function enriched in burned soils

was N fixation (*nifH*; *n* = 22) which was elevated in the 2000s burn scars (**Figure 4.12**). These *nif* genes were linked to 3 MAGs all associated with the Actinobacteria order *Actinomycetia* (BP_140, BP_141, BP_201), which have been found to play an important role as diazotrophs in desert soils[49]. Mirroring trends observed with C cycling functions, the normalized abundances of genes encoding microbially mediated N cycling (apart from nitrification) converged over time across both treatments.

Together, these data highlight the strong filtering effect of burning, which exerts combined pulse and press disturbances on soils that last multiple decades and are detected through significant differences in the functional potential of the soil microbiome. However, despite divergent ecological trajectories between regen forest and burn scar sites, and long-term differences in vegetation and associated soil carbon inputs, the longer-term convergence in functional potential for C and N cycling indicates the weakening of environmental filtering processes that drive differences in the soil microbiome functions over time.

4.3.6 Burn scars have lasting impacts on key soil functions

Functional potential between the burn scar and regen forest soil microbiomes generally converged over the chronosequence, with the number of differentially abundant genes between the two treatments (via DESeq2[50]; $p<0.01$) decreasing from 433,526 to 80,941 from the 2000s to 1960s (**Table 4.1**). However, there were still long-lasting influences of burning on certain ecologically relevant functions encoded within the burned soil microbiome (**Figure 4.13**; **Figure 4.14**). One such process is the biosynthesis of cobalamin (vitamin B12, *cob* genes), an important coenzyme involved in gene regulation and the synthesis of nucleotides and amino acids. Cobalamin production is conserved

within a relatively small group of microorganisms and serves as a keystone function within ecosystems[51]. Genes encoding the bacterial synthesis of cobalamin from cobinamide displayed greater relative abundances in regen forest soils across the entire time series with no convergence after six decades (**Figure 4.14**). Further, samples from regen forest soils also contained more differentially abundant genes associated with this process (*n* = 13 in 1960s regen forest) that linked to MAGs (via BLAST) affiliated with the Actinobacteria genera *Mycobacterium* (BP_728 and BP_240) and *Pseudonocardia* (BP_325), along with the Proteobacteria genera *Caballeronia* (BP_718) and *Aliidongia* (BP_649). Indeed, all noted genera associated with cobalamin synthesis had lower relative abundances in burn scar soils relative to regen forest soils over the entire chronosequence. Given the reliance of many soil bacteria on exogenous cobalamin[52] and its role as a cofactor in a broad array of bacterial enzymes[51], the trends observed here could influence soil microbiome activity and influence plant recovery within the burn scars[53].

In soils, where proteinaceous compounds are the most abundant form of soil organic N[54], peptidases degrade high molecular weight peptide N to simpler forms (e.g., amino acids) as part of a critical strategy used by microbes to gain bioavailable N in N-limited conditions. The depolymerization of peptide N is additionally considered a rate-limiting step for terrestrial N cycling, as it increases bioavailable N for both plants and microorganisms[55,56]. Here, we found greater relative abundances of genes encoding peptidases in regen forest soils relative to burn scar soils in the later decades following disturbance (i.e., 1980s, 1970s, 1960s; **Figure 4.14**). Although inorganic N chemical profiles converge over the chronosequence (**Figure 4.1**), these data suggest that burn

scar soils are more limited by available sources of organic N than regen forest soils six decades following disturbance.

Other broad functions that were more abundant in regen forest soils six decades following the disturbances are general transporters, sulfur (within DRAM summary output, 'energy'), short-chain fatty acid (SCFA) and alcohol conversions, and the DRAM header 'oxygen', which mainly includes genes encoding for cytochromes (e.g., *coxA*; cytochrome c oxidase subunit I [EC:1.9.3.1]) (**Figure 4.14**). Increased relative abundances of transporters indicates the prevalence of resource acquisition strategies within the regen forest microbiome and an increased investment in extracellular enzymatic machinery for resource capture, potentially at the expense of growth yield[57]. Increased relative abundances of genes encoding for electron transport chain cytochromes (*n* = 43,249 genes) might indicate increased respiratory activity and ATP yield, and the increased relative abundance of genes participating in sulfur cycling – the majority of which are for assimilatory sulfate reduction (20,704 of the 26,627 genes) – could also indicate increased microbial activity and growth in regen forest soils.

4.3.7 Altered soil microbiomes may contribute to limited pine establishment following pile burning

Pine seedlings require key soil microbial symbionts in the rhizosphere for optimal survival and growth. Despite the dense regeneration of lodgepole pine surrounding the burn scars, tree colonization is rare within the burn scars and they become graminoid- and forb-dominated over the chronosequence[27]. To investigate the belowground processes that may influence tree regeneration within the burn scar openings, we

conducted greenhouse pine bioassay growth experiments with soils collected from the sites and sampled the rhizosphere of *in situ* lodgepole pine seedlings planted within the burn pile scars in summer of 2017 (n = 9 per decade). An earlier study on this series of pile burn scars found that seedling survival and EMF colonization was lowest in the most recently burned scars although overall seedling growth and survival in the burn scars was high[26]. Here, in greenhouse pine seedling bioassay seedling experiments, we observed lower EMF relative abundance in root nodules on pine seedlings grown in recently burned soils (i.e., 2000s; **Figure 4.15**) that corroborated the low colonization of EMF found on pine seedling roots in the earlier study[26]. Despite overall high tree mortality and low root colonization (**Appendix C**), the few EMF that did colonize greenhouse pine seedling root nodules included *Rhizopogon*, *Suillus*, *Cenoccocum*, and *Wilcoxina,* all common spore bank fungi known to persist in post-fire soils[58–61] (**Figure 4.15**). Thus, in spite of the persistence of some well-known EMF, overall the results suggest that pile burning depletes pine-associated EMF spore banks that are abundant in most soils[61].

In corresponding *in situ* lodgepole pine seedling rhizosphere samples (i.e., seedlings planted within the burn pile scars), we found significant decreases in rhizosphere EMF community diversity in pines planted in more recent burn scars (2000s; **Figure 4.16**). Although some of the aforementioned post-fire spore bank fungi – *Rhizopogon*, *Suillus*, and *Wilcoxina*[58–61] – were generally present in the pine seedling rhizosphere across the chronosequence, there was a lack of other known EMF symbionts for lodgepole pine. For example, the Basidiomycota genera *Cortinarius* remained depleted in burn scar soils over the chronosequence (average 0.8% relative abundance) whereas it rebounded in regen forest soils (7.3% relative abundance in 1960s regen

forest) and was completely absent in rhizosphere samples. Although lodgepole pine regeneration is typically stimulated by clear cutting, the combination with pile burning appears to have depleted the local EMF recolonization potential. Further inhibiting seedling success and growth, rhizosphere samples from seedlings planted *in-situ* also hosted a significantly higher diversity of plant pathogenic fungi, relative to analogous samples from older burn scars (**Figure 4.16**). Dove et al. (2021)[34] reported an increased relative abundance of plant pathogens in the rhizosphere and leaf phyllosphere of aspen saplings in wildfire burn scars just one year post-fire, and our findings suggest that such effects may persist for extended time periods in soils impacted by high severity fire. Combined, data from greenhouse pine bioassay experiments and *in situ* lodgepole pine seedings suggests that pile burning has an adverse effect on vital EMF partners for lodgepole pine. A subsequent increase in plant pathogenic fungi might hinder the early success of pine within the burn scars, allowing the persistence of understory species (i.e., graminoids and forbs) and facilitating the conversion to a herbaceous plant-dominated ecosystem (**Figure 4.16**).

4.4 Conclusions

Within subalpine conifer forests of the Southern Rockies, the increase in compound disturbances can catalyze conversion from forest to non-forest vegetation. Here, we use pile burns as a surrogate of severe wildfire to investigate changes in the soil microbiome over the course of six decades following a compound disturbance comprised of pile burning following clear cut harvesting. We used paired comparisons of post-fire changes in soil beneath non-forest burn scars and lodgepole pine regrowth

following clear cut harvesting. Initial loss of lodgepole pine EMF partners following burning and increased plant pathogen abundance in addition to other factors (i.e., low seed availability, high seed predation) likely contributed to low tree seedling establishment within the scars. We also report a loss of ecologically relevant microbial functions (e.g., peptidases) that may further inhibit successful seedling reestablishment. Despite these short-term impacts (i.e., two decades), after six decades the soil microbiome within the burn scars recovered to generally resemble regen forest soils in both composition and function, revealing belowground resilience in response to disturbance-induced ecosystem conversions. The recovery of the soil microbiome described here might be influenced by the small spatial extent of the burn scars (~10 m in diameter) surrounded by closed canopy forest and further analyses of larger scale ecosystem conversions are needed to advance understanding. This unique dataset provides invaluable insight into the belowground microbial dynamics that underly aboveground ecosystem shifts within these vital and vulnerable terrestrial ecosystems.

4.5 Materials & Methods

4.5.1 Field sampling campaign

A chronosequence of burn pile scars that represented pile burning conducted in five separate decades (1960s, 1970s, 1980s, 1990s, 2000s) were sampled July 20 and 21, 2020 and are a subset of burn pile scars utilized in previous studies[26,27]. This chronosequence of burn pile scars represents pile burns ranging from 2 to 6 decades post-burning. The burn pile scars were located in northern Colorado on USFS land within the Medicine Bow-Routt National Forest. Lodgepole pine (*Pinus contorta*) is the dominant

tree species in the area in relatively even-aged stands. The most abundant soil types are loamy-skeletal, Typic Cryoboralfs and sandy-skeletal, Typic Cryochrepts, and are formed in sandstone, siltstone, and conglomerate residuum and colluvium, and are moderate deep and well-drained to excessively well-drained. See previous studies for an in-depth site description and explanation of site selection[26,27]. Briefly, USFS stand activity records, which extend back to the 1960s for the Medicine Bow-Routt National Forest, were used to locate harvest units where pile burn operations had been conducted. Selected pile burn openings were identified on aerial photographs and sites were limited to clear cut, even-age lodgepole pine stands and piles that were burned following clear cut, were not rehabilitated by the USFS, used a similar amount of fuel, and were roughly the same size (~10-15 m diameter). Additionally, site selection was limited to piles made within harvest units as opposed to larger burn piles created on logging decks where the large pile size and soil compaction may change the impact of burning. Trees with open cones were found in regenerating forests across all sites. The final selected chronosequence of burn pile scars represented pile burning that occurred over five decades, from the 1960s to the 2000s. For each decade (60s, 70s, 80s, 90s, and 2000s), there were three units with three piles each (n = 9 piles per decade), where we collected depth-resolved (0-10 cm and 10-15 cm) bulk soil samples (n = 18 bulk soil samples per decade; **Table 4.2**). At one pile per unit, we also collected depth-resolved samples from just outside the burn scar, which represented regenerating forest after clear cut that happened at the same time pile burning occurred (e.g., 1960s regen forest sample was clear cut in the 1960s). Each soil sample was collected with a 10 cm bulb corer, cleaned with ethanol between samples, after brushing away surficial litter and duff. Samples were immediately placed on ice and

transported back to the laboratory at Colorado State University (CSU). Soils for DNA extractions were stored at −80 °C in the laboratory until processing.

We additionally collected rhizosphere material from lodgepole pine seedlings that were planted within burn pile scars in 2017 for a previous study[26]. We collected rhizosphere material from one seedling within each pile (*n* = 9 per decade) to understand how different times since burn impacts rhizosphere microbiome recruitment and development. To collect rhizosphere material, we dug up the seedling, shook off loose soil not attached to roots, and sampled only soil directly connected to the root system. Samples were immediately placed on ice and transported back to the laboratory at Colorado State University and stored at −80 °C in the laboratory until processing. A total of 154 bulk soil and rhizosphere samples were collected (detailed in **Appendix C**; **Table 4.2**).

Because of outlier vegetation (i.e., more dense grass and fewer forbs and woody plants), for all analyses presented herein we've removed one unit from the 90s (unit 26) so that the 90s have only 6 rhizosphere samples, 4 control samples, and 12 burned soil samples, plus 8 of these samples utilized for metagenomic sequencing (**Table 4.2**).

4.5.2 Soil chemistry

We evaluated soil nutrients and chemistry to gauge changes caused by burning and shifting vegetation and to consider the implications of these changes on microbial communities. A subset of 60 bulk soil samples (30 burned, 30 unburned), which included 1 pile per unit per decade, with both burned and unburned shallow and deep samples (*n* = 12 samples per decade, 4 per unit), were selected for chemistry analyses. We analyzed the NO_3–N and NH_4–N and dissolved organic C (DOC) and total dissolved N (TDN)

released during warm water extracts[62] using ion chromatography (NH4-N and NO3-N; Thermo-Fisher Corporation, Waltham, MA) and TOC-VCPN total organic carbon analyzer (DOC and TDN; Shimadzu Corporation, Columbia, MD, USA). Soil pH was analyzed in a 1:1 soil to deionized water slurry after one hour of agitation[63] using a temperature-corrected glass electrode (Hach Scientific, Loveland, CO, USA). A set of soils were sieved (2 mm) and dried for 48 hours at 60°C and analyzed for total C and N by dry combustion on a LECO 1000 CHN analyzer (LECO Corporation, St. Joseph, MI, USA). C:N ratios were calculated with %C and %N from the LECO 1000 CHN analyzer data. Soil chemistry data is included in **Appendix C** and, for all analyses, depths were combined to represent the bulk soil chemistry.

4.5.3 Aerobic metabolism bioassays

Organic matter bioavailability in the soils was determined via laboratory incubations and measuring the production of CO_2 in sealed bottles over time. Soil incubation experiments were performed in October and November 2020 at Colorado College from soils collected from burn piles approximately two weeks after the primary field campaign explained above. To measure soil organic matter bioavailability via soil respiration, incubations were done in triplicate for each whole soil sample. For incubations, approximately 30 grams of unsieved soil, excluding large rocks or roots, was placed in a glass jar (pre-combusted at 500 °C for 5 hours) and left open to the atmosphere at room temperature between incubation time points. At 0, 1, 3, 7, and 14 days, airtight lids were placed on each jar for room temperature incubations (~22 °C). MilliQ water was added to samples before incubating on days 1, 3, 7 and 14 to return to original mass (day 0) and offset moisture losses due to evaporation. After 2-3 hours of

incubation, 10 ml of gas from the jar's headspace was analyzed using the SRI-8610C gas chromatograph (GC). Calibration of the GC was performed using 100 ppm, 1,000 ppm, and 10,000 ppm CO_2 standard gases, and ambient lab air was used to determine the background CO_2 (i.e., the concentration of CO_2 in the jar before the lid was closed) for each incubation. To estimate soil moisture, ~20 grams was dried at 50-60°C for approximately 24 hours and reweighed to obtain soil moisture content gravimetrically. Method adapted from previously published method[64]. Data included in **Appendix C**.

4.5.4 DNA extraction, 16S rRNA gene and ITS amplicon sequencing

Total DNA was extracted from all bulk soil and rhizosphere samples (*n* = 154 total) using the Zymobiomics Quick-DNA Fecal/Soil Microbe Kits (Zymo Research, CA, USA). 16S rRNA genes in extracted DNA were amplified and sequenced at Argonne National Laboratory on the MiSeq System (Illumina) using 251-bp paired-end reads and the Earth Microbiome Project primers 515F/806R[65], which targets the V4 region of the 16S rRNA gene. To characterize fungal community composition, the DNA was also PCR amplified targeting the first nuclear ribosomal internal transcribed spacer region (ITS) using the primers (ITS1f/ITS2)[66] and sequenced on the Illumina MiSeq platform at the Argonne National Laboratory using 251-bp paired-end reads.

We employed the QIIME2 environment[67] (release 2019.10) for read processing and began from the raw 16S rRNA gene and ITS amplicon sequencing reads, which are both deposited and available at NCBI under BioProject #PRJNA682830. DADA2[68] was used to filter, learn error rates, denoise, and remove chimeras from reads and, following DADA2, the 16S rRNA gene and ITS amplicon sequencing reads retained on average 23,226 and 19,585 reads per sample, respectively. Taxonomy was assigned using the

QIIME2 scikit-learn classifier trained on the SILVA[69] (release 138) and UNITE[70] (v8.3) databases for bacteria and fungi, respectively, resulting in 45,009 bacterial and 8,708 fungal ASVs. We chose not to rarefy to avoid discarding information, but instead converted all data to relative abundance for analysis and rarefaction curves were made for both 16S rRNA gene and ITS amplicon sequencing data to assess whether sequencing was sufficient for comparing alpha diversity between samples (**Figure 4.17**). Ecological guilds were assigned to fungal ASVs using FUNGuild[71] (v1.2). In accordance with FUNGuild creator recommendations[71], we only accepted guild assignments classified as "highly probable" or "probable" to avoid possible overinterpretation and did not retain any ASVs classified as multiple guilds.

All statistical analyses and data visualization were performed in the R environment[72] (v3.6.1). To characterize how microbial populations differed across burn severities and soil horizons, we used the vegan[73] (v2.5-7) and phyloseq (v1.28.0) packages. Nonmetric multidimensional scaling (NMDS) was conducted using Bray-Curtis dissimilarities to examine broad differences between microbial communities. Analyses of similarity (ANOSIM, vegan) was additionally utilized to statistically test the magnitude of dissimilarity between microbial communities from the different burn severity conditions and soil horizons. Mean species diversity of each sample (alpha diversity) was calculated based on species abundance and evenness using Shannon's Index (H). Linear discriminant analysis (LDA) with a score threshold of 2.0 was used to determine ASVs discriminant for specific conditions[75].

Surface and deeper microbial community compositions did not significantly differ from one another at most timepoints (**Figure 4.18**), so for all analyses presented we

combine ‘surface’ and ‘deep’ soils to represent the bulk burn scar and regen forest mineral soil column. The similar responses across the depth resolved samples is likely due to the consistent impacts of slash pile burning on surface and deeper soils that have been reported in other studies[76] due to high fuel loads which can cause large increases in temperature (up to ~300°C), even at 10 cm depth[76,77], which is in contrast to the lower soil temperatures reached in natural wildfires[78].

4.5.5 Greenhouse bioassay experiments

To assess the diversity of EMF fungi in the spore bank at each plot we performed *Pinus contorta* pine seedling bioassays using established methods[61] from soils collected from each burn pile and surrounding unburned regen forest soils. Seedlings were grown in a common ambient temperature glasshouse at the University of California, Riverside (CA, USA) and stratified *P. contorta* seeds were provided by the Forest Service Rocky Mountain Station (Fort Collins, CO, USA). Seeds were surface sterilized with 30% Hydrogen peroxide and then soaked in water for 48 h[79]. Seeds were germinated on a wetted filter paper for 7–10 days. Pine seedlings were planted in 50-ml Cone-tainers (Super ‘Stubby’ Cell Cone-tainer; Stuewe & Sons Inc., Tangent, OR, USA) using a 1:1 ratio of dried native soil and autoclaved coarse yellow sand to improve drainage. Plants were watered every three days and grown in the glasshouse without fertilizer for approximately 7 months before harvesting. Treatments were randomized among trays during initial planting and trays were further randomized every other week.

In total, 155 seedlings were planted (5 decades x 3 piles x 2 treatments x 5 replicates) plus 5 aerial controls which consisted only of sterilized potting soil (heated 1 hour at 123°C). Plants were harvested by removing the whole plant from the containers

and rinsing the soils from the roots with water. Roots were inspected under the dissecting microscope and EMF root tips were collected with sterilized forceps. EMF root tips from an individual seedling were combined into a single tube, flash-frozen, and kept at -80°C until processing.

Frozen EMF root tips were lyophilized, and genomic DNA was extracted using a modified version[61] of the QIAGEN DNAesy Blood and Tissue kit QIAGEN, Germantown, MD, USA). To identify EMF fungi present in the root tips, amplification of the rDNA internal transcribed spacer region 2 (ITS2) was done using the primers ITS3-2024F and ITS4-2409R[66]. PCR, library preparation and NovaSeq PE250 sequencing (Illumina) were performed by Novogene Corporation Inc., and are deposited and available at NCBI under BioProject #PRJNA682830. Note that only 32 root tips were used for DNA extractions and ITS amplicon sequencing as only 32 trees had present root nodules and enough DNA extracted for sequencing.

Illumina NovaSeq PE250 sequencing data were processed using QIIME2 version 2020.8[80]. Denoising was done using DADA2 to remove chimeric sequences and low-quality regions and to produce ASVs. Taxonomic assignments were done using Qiime2 Naïve Bayes Blast + and the reference database UNITE version 8.3 for fungi[70]. Sequences not assigned to the Kingdom Fungi were removed from the ASV tables before subsequent analysis. We assigned functional ecological guilds to each fungal ASV using FUNGuild[81]. All greenhouse bioassay data included in **Appendix C**.

4.5.6 Community ecological modeling

Two null modeling analyses, β-nearest taxon index (βNTI) and Raup-Crick (Bray-Curtis) (RC_{BC}), were performed on the 16S rRNA gene sequencing data to determine how

assembly processes governing bacterial community structure differed across treatments and over time[82–84]. A phylogenetic tree was created using the QIIME 2 phylogeny plugin's "align_to_tree_mafft_fasttree" action. The β-mean nearest taxon distance (βMNTD) was calculated for each possible pairwise sample comparison to find underlying phylogenic contributions to community structure. Using 999 community randomizations to generate a null distribution of βMNTD values, βNTI was calculated to observe the deviation of the observed βMNTD values from the null βMNTD values (*comdistnt,* "picante" R package v1.8). If the resulting |βNTI| was greater than 2, deterministic processes drive community assembly. Communities with a βNTI > 2 are more different than would be expected by random chance due to variable selection, whereas communities with a βNTI < -2 are more similar than would be expected by random chance due to homogenizing selection. Differentiating between these processes allows insight into how environmental conditions (e.g., recovery time since burning, vegetation shift) influence phylogenetic turnover of soil bacterial communities.

If the |βNTI| is less than 2, communities are as different as expected by random chance and stochastic processes dictate community structure. These stochastic processes can be distinguished using RC_{BC} analyses as dispersal limitation ($RC_{BC} > 0.95$) where there is a decreased ability for communities to mix, and homogenizing dispersal ($RC_{BC} < -0.95$) where a system experiences high exchange rates. If $|RC_{BC}|$ is less than 0.95, there is no single assembly process strong enough to control community structure and an undominated signal is observed. Because RC_{BC} values are only useful when βNTI indicates stochastic processes, RC_{BC} values are only presented when |βNTI| is less than 2. Here, RC_{BC} was calculated according to Stegen et al. [85]. Briefly, we used 9,999

iterations per pairwise comparison and probabilistically generated null communities based upon microbial abundances from the 16S rRNA gene sequencing data. From these null communities, a null distribution of Bray-Curtis values was calculated and compared to observed Bray-Curtis values and the resulting deviation of the observed values from the null values was normalized from 1 to -1 to calculate the final RC_{BC} value.

For all ecological modeling analyses, the ASV table was rarefied to 15,000 counts due to difficulties processing a feature table with more than 20,000 ASVs with the *cophenetic* command in the picante R package[86]. R code utilized in Danczak et al. (2020) was used here and can be found at https://github.com/danczakre/ShaleViralEcology[87]. Note that these analyses were only conducted on the 16S rRNA gene sequencing data because ITS amplicon sequencing data lacks the resolution for these analyses. All ecological modeling analyses are presented in **Appendix C**.

4.5.7 Metagenomic assembly, annotation, and binning

A subset of 56 bulk soil samples (28 burn scar, 28 regen forest) were selected for metagenomic sequencing to analyze how microbiome functional potential shifts with recovery post-burn. These 56 samples included 1 pile per unit per decade, with both burn and unburned shallow and deep samples (n = 12 samples per decade, 4 per unit). To maximize funding utilization, 46 samples were sequenced at the Joint Genome Institute (JGI) and 10 were sequenced at Genomics Shared Resource, Colorado Cancer Center, Denver, CO. At CU-Denver, libraries were prepared using the Tecan Ovation Ultralow System V2 and were sequenced on the NovaSeq 6000 (Illumnia) platform on an S4 flow cell using 151 bp paired-end reads. For samples sequenced at JGI, an Illumina library was constructed and sequenced 2x151 using the NovaSeq S4 platform (Illumina).

Sequencing depth ranged from 14-25 Gbp from the Colorado Cancer Center and 22-77 Gbp from JGI (**Appendix C**). Sequencing adapter sequences were removed from raw reads using BBduk (https://jgi.doe.gov/data-and-tools/bbtools/bb-tools-user-guide/bbduk-guide/) and low quality reads were trimmed with Sickle[88] (v1.33). For each sample, trimmed reads were assembled into contiguous sequences (contigs) using the *de novo* de Bruijn assembler MEGAHIT v1.2.9 using kmers[89] (minimum kmer of 27, maximum kmer of 127 with step of 10). Genes were predicted from contigs greater than 2500bp using Prodigal[90] (ref) (option '-p meta' for metagenome mode; V2.6.2). Predicted genes were clustered at ≥ 95% identity with MMseqs2[91], resulting in a final catalog of 16,683,787 non-redundant genes. Trimmed reads were rarefied to 14 Gbp due to a wide range of sequencing depth (14-77 Gbp) and mapped to the gene catalog using Bowtie2[92] (v2.3.5). Gene coverage across samples was calculated using coverM contig (v0.6.0; https://github.com/wwood/CoverM) with the 'Trimmed Mean' (hereafter referred to as TMM) method, retaining only those mappings with minimum percent identity of 95% and minimum alignment length of 75%. Genes were annotated using DRAM[93] (v1.4.0). In addition to the DRAM annotations, HMMER[94] against Kofamscan HMMs[95] (**Appendix C**) and HMMs from the CANT-HYD database[96] were also used to further identify genes for catechol and protocatechuate meta- and ortho-cleavage, naphthalene transformations, inorganic N cycling, and aromatic hydrocarbon metabolisms . Maximum community doubling times were calculated from codon usage bias (CUB) using gRodon[98] (v2.0.0; metagenome mode) and gene coverage data (via Bowtie2, v2.3.5).

Assembled contigs (>2,500 bp) were binned using MetaBAT2[99] with default parameters (v2.12.1). Metagenome-assembled genome (MAG) quality was estimated

using checkM[100] (v1.1.2) and taxonomy was assigned using GTDB-Tk[101] (v2.1.1). MAGs from all metagenomes were dereplicated using dRep[102] (default parameters, v3.0.0) to create a non-redundant MAG dataset. Low quality MAGs (<50% completion and >10% contamination) were excluded from further analysis[103], resulting in 786 final MAGs (**Appendix C**).

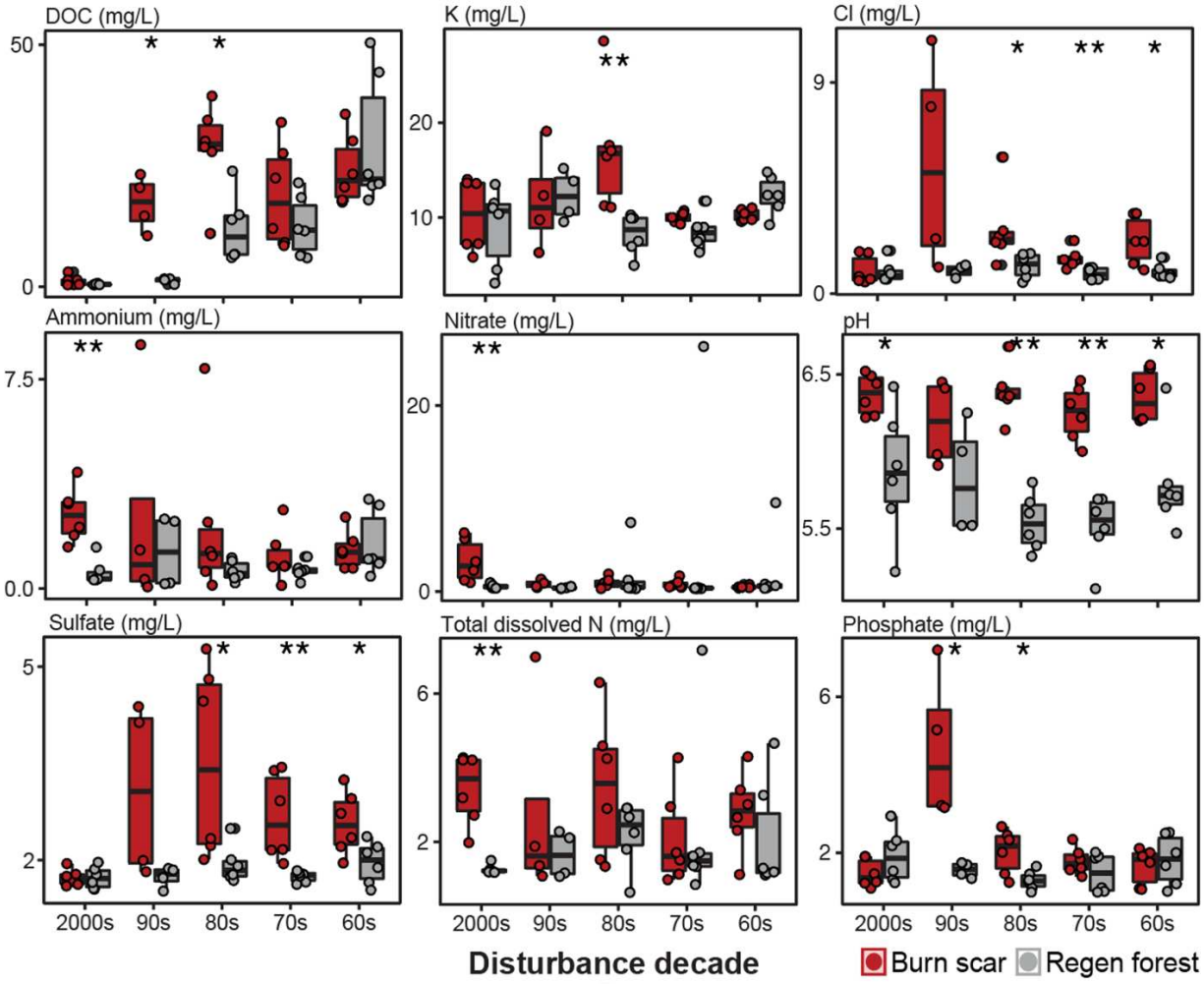

Figure 4.1 Soil chemistry data from water extracts of a subset of samples (n = 60). Points indicate individual sample data. The lower and upper hinges of the boxplots represent the 25th and 75th percentile and the middle line is the median. The upper whisker extends to the median plus 1.5x interquartile range and the lower whisker extends to the median minus 1.5x interquartile range. Significant differences between burn scar and regen forest samples indicated with asterisks as indicated by Wilcoxon rank-sum test. *p<0.05, **p<0.01.

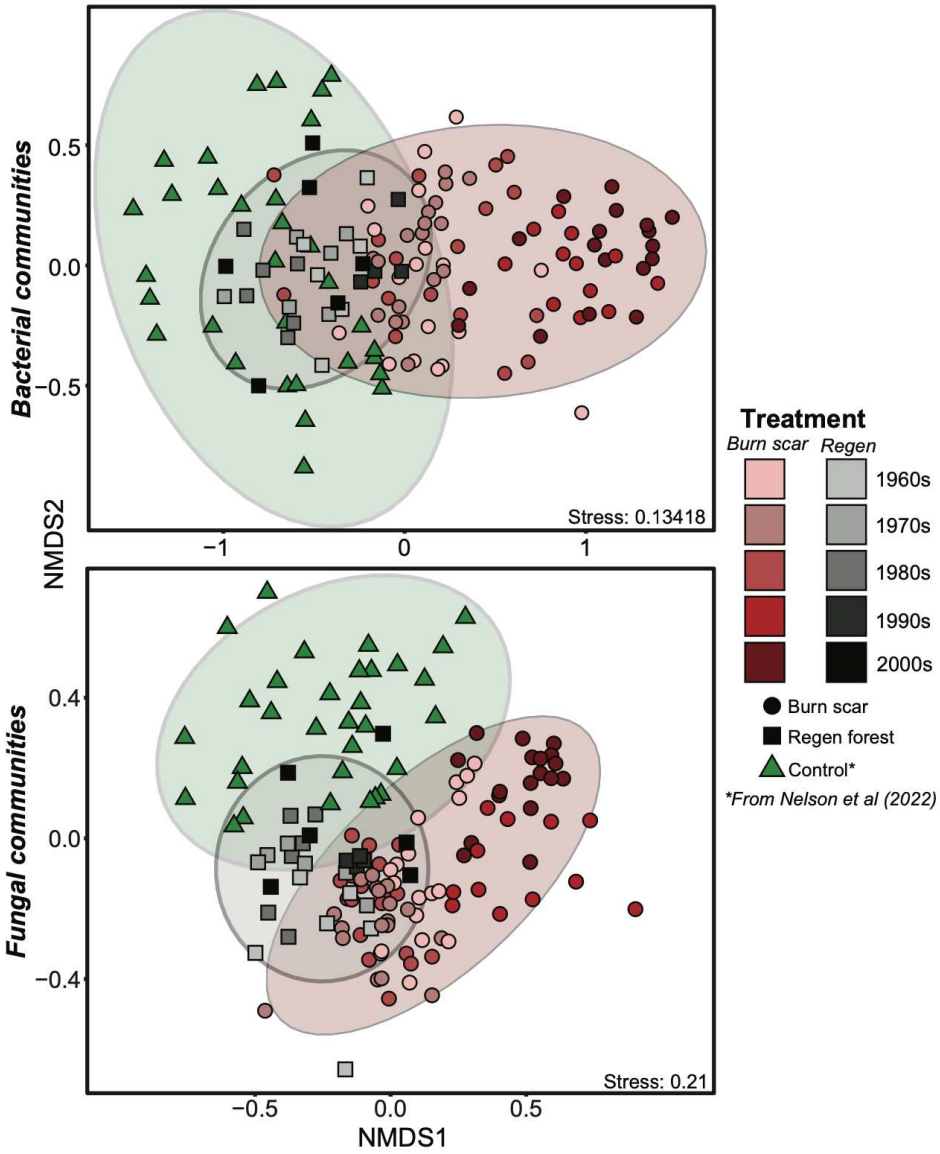

Figure 4.2 Non-metric multidimensional scaling (NMDS) of bacterial (above) and fungal (below) communities shows separation of burn scar and regen forest communities that decrease over time. Sequencing data from a recent study conducted in a nearby uncut, unburned lodgepole pine forest were included here as representative control soil bacterial and fungal communities[20]. Ellipses show ninety-five confidence intervals around each treatment.

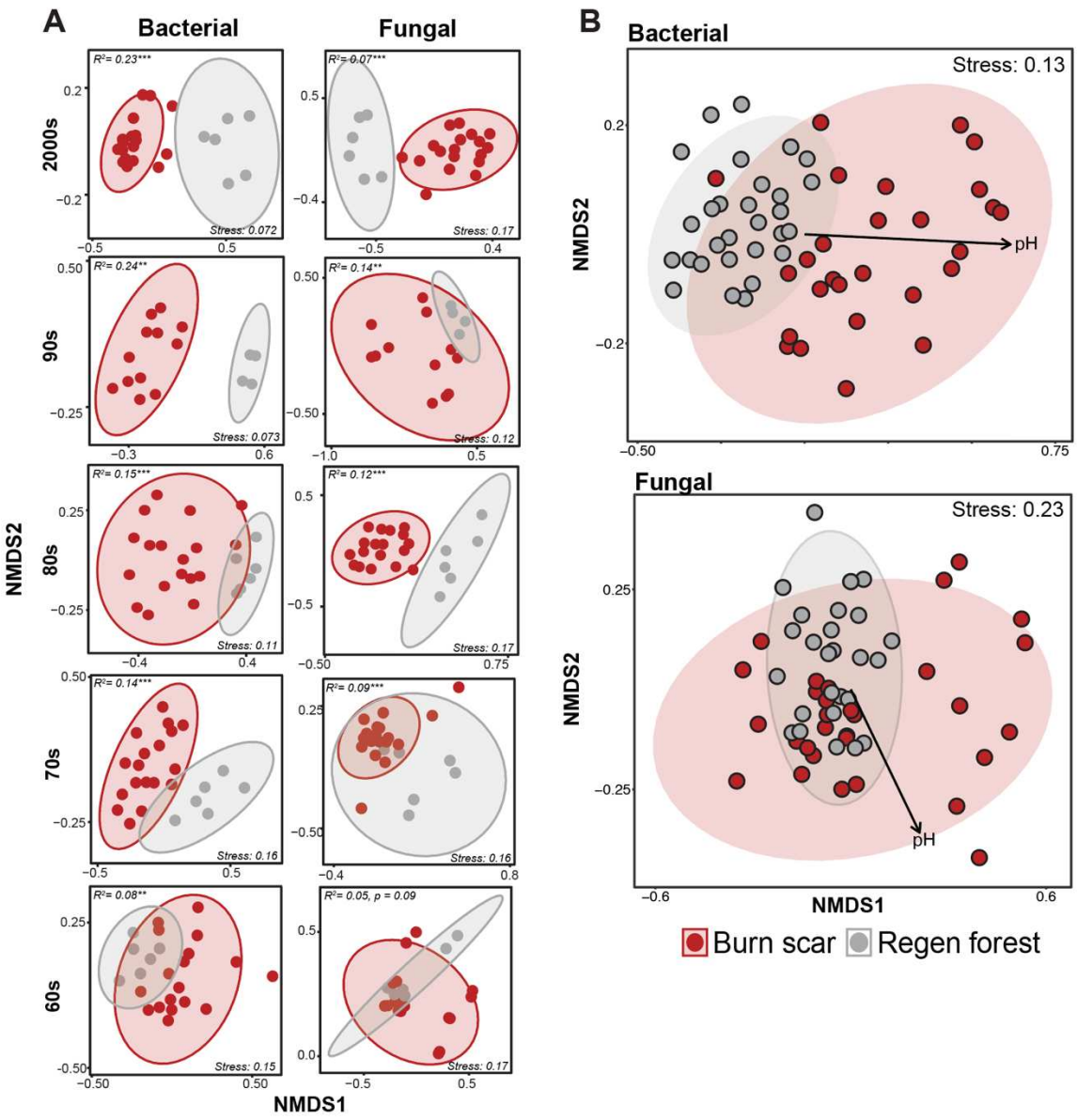

Figure 4.3 (A) Non-metric multidimensional scaling (NMDS) ordinations of bacterial and fungal communities over time since disturbance, with corresponding PERMANOVA values indicating whether burn scar and regen forest sample communities are significantly different from one another. **(B)** NMDS of all bacterial and fungal communities with overlaying vectors indicating which measured soil chemistry variables significantly drive compositional shifts (via *envfit*; $p < 0.05$, corrected for multiple testing using Bonferroni's correction). Vector length indicates the magnitude of effect, and proximity of points to vectors indicates correlation. Note that, in Panel B, only the subset of samples from which there is corresponding soil chemistry data are included. All ellipses show ninety-five confidence intervals for each treatment.

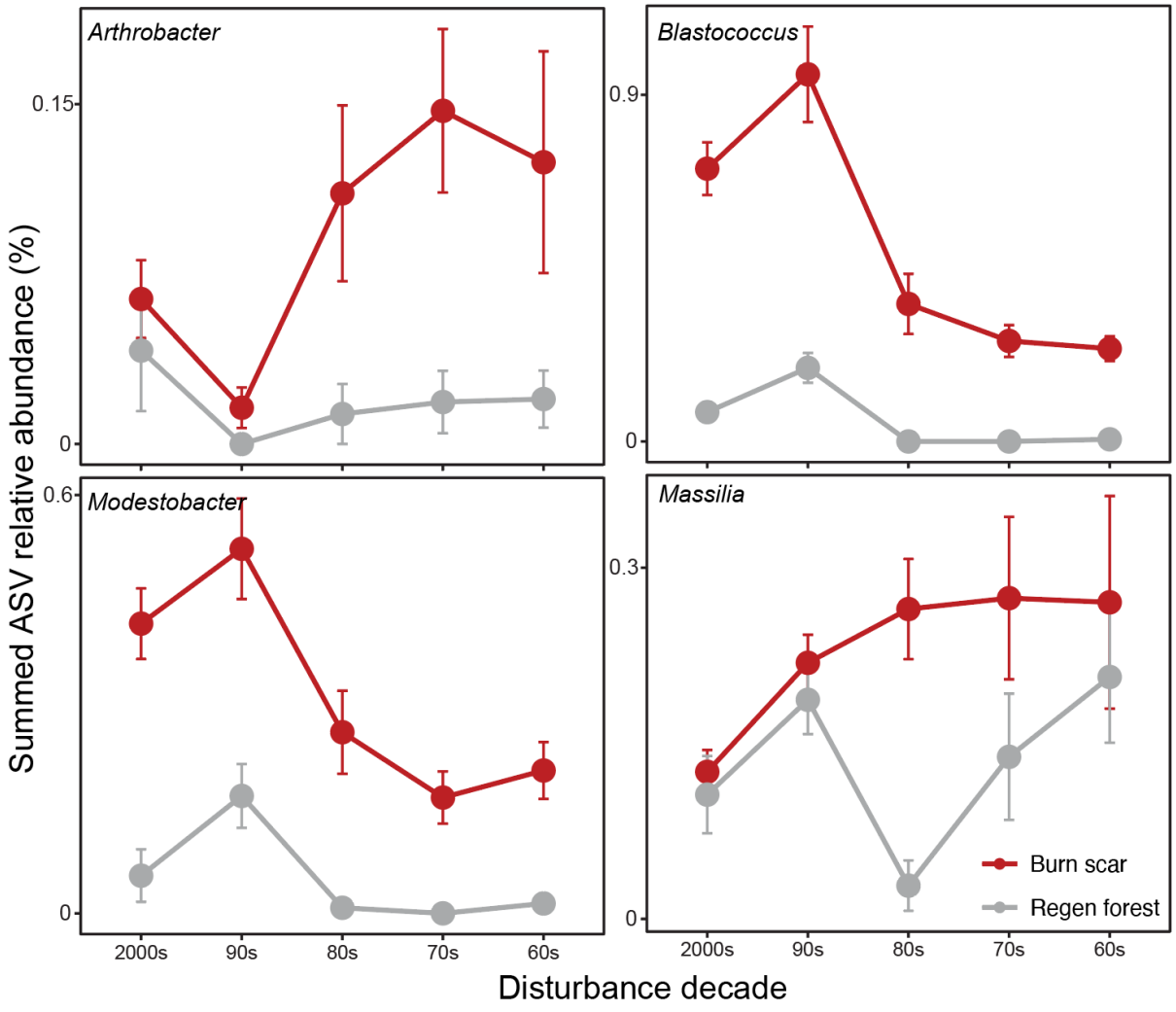

Figure 4.4 Summed ASV relative abundance of putative pyrophilous taxa, including the Actinobacteria genera *Arthrobacter* (*n* = 9 ASVs), *Blastococcus* (*n* = 22 ASVs), and *Modestobacter* (*n* = 9 ASVs), and the Proteobacteria genera *Massilia* (*n* = 22 ASVs). Error bars indicate the standard error of the mean.

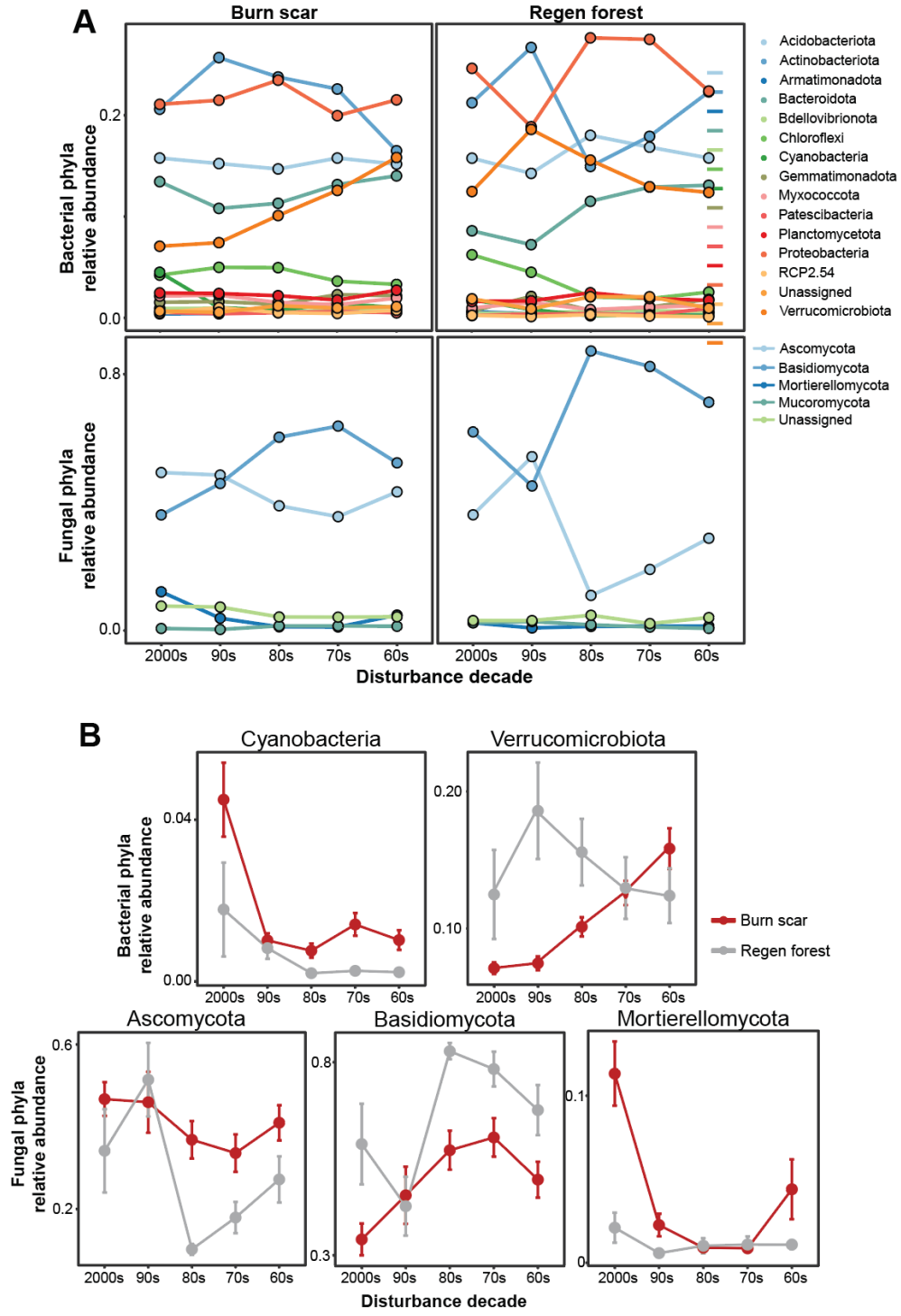

Figure 4.5 (A) Dominant bacterial (top) and fungal (bottom) phyla in burn scar and regen forest soils over time. Phyla with average relative abundances <0.5% across samples were discarded. (**B**) Bacterial and fungal phyla of interest relative abundance over time between burn scar and regen forest soils. Error bars indicate the standard error of the mean.

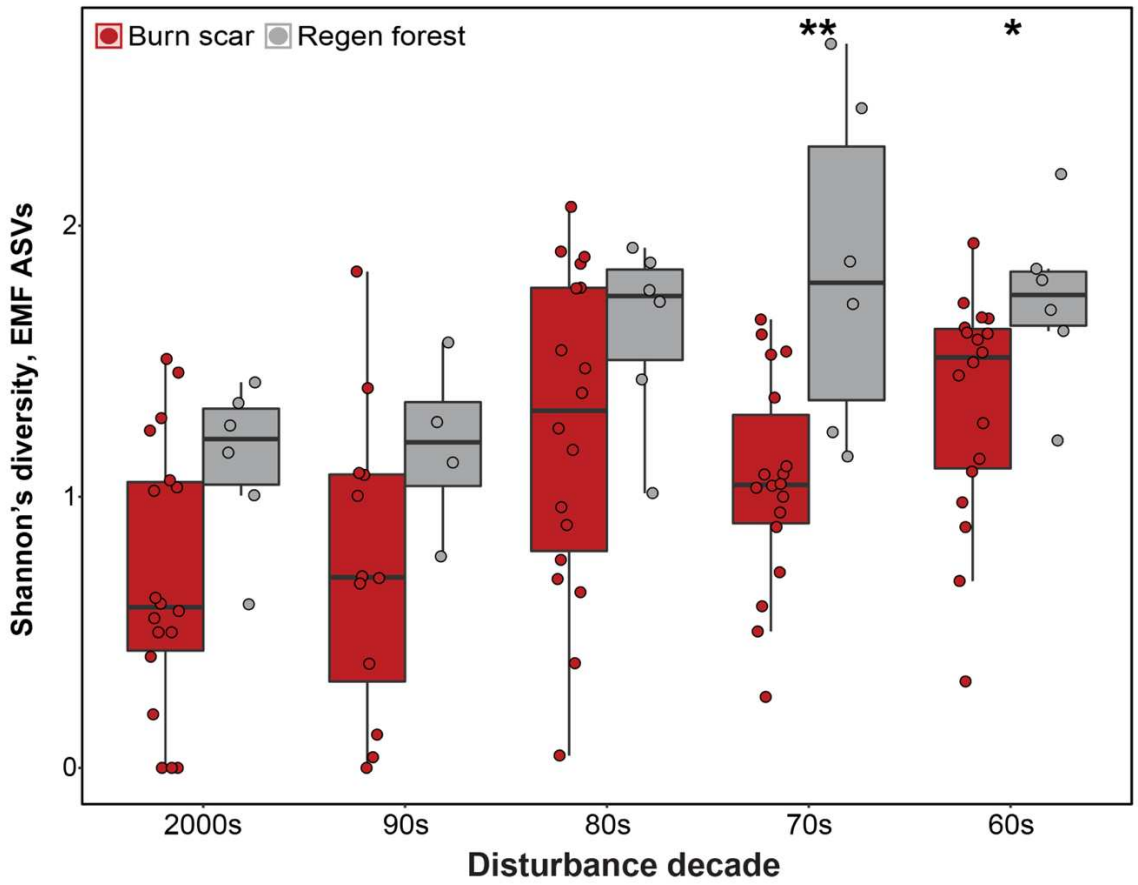

Figure 4.6 Shannon's diversity of EMF communities in burn scar and regen forest soils. The lower and upper hinges of the boxplots represent the 25th and 75th percentile and the middle line is the median. The upper whisker extends to the median plus 1.5x interquartile range and the lower whisker extends to the median minus 1.5x interquartile range. Significant differences between burn scar and regen forest samples indicated with asterisks as indicated by Wilcoxon rank-sum test. *p<0.05, **p<0.01.

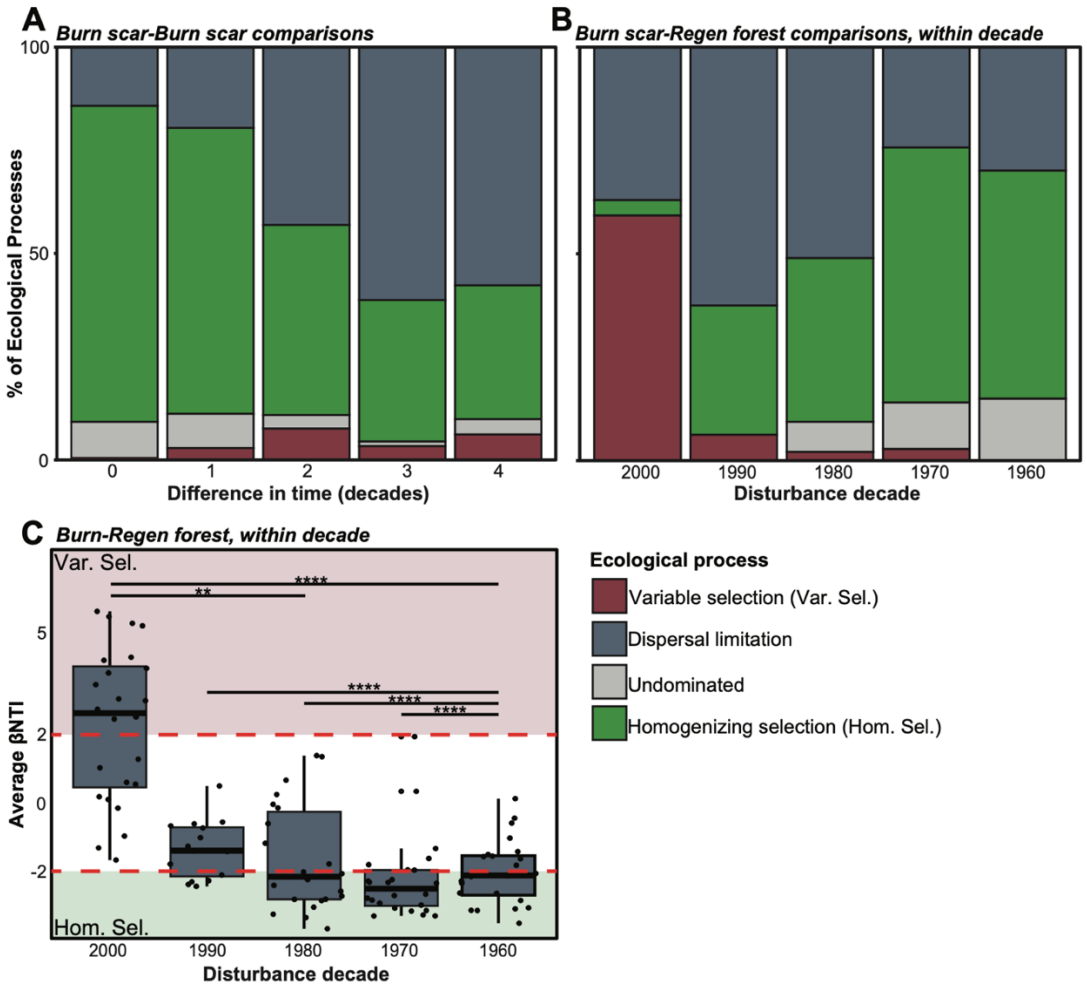

Figure 4.7 (A) Proportion of assembly processes, derived from βNTI and RC_{BC} analyses, dictating community structure from within-treatment (burn scar) comparisons plotted by difference in time between burn scars (e.g., 2000s-1970s comparison, 3-decade difference). These data show that burn scar bacterial communities are more similar to one another when closer in disturbance age. **(B)** Proportion of assembly processes from within-decade comparisons of treatments (e.g., 2000s burn compared to 2000s regen forest), which indicate that the burn scar and regen forest microbiomes are more different to one another with less recovery time post-disturbance. **(C)** Average βNTI from within-decade comparisons of treatments, showing that, over time post-disturbance, burn scar and regen forest microbiomes become more similar to one another than expected by random chance. The lower and upper hinges of the boxplots represent the 25th and 75th percentile and the middle line is the median. The upper whisker extends to the median plus 1.5x interquartile range and the lower whisker extends to the median minus 1.5x interquartile range. Significant differences between burn scar and regen forest samples indicated with asterisks as indicated by Wilcoxon rank-sum test. *p<0.05, **p<0.01, ***p<0.001, ****p<0.0001. Note that homogenizing dispersal was not observed in this system.

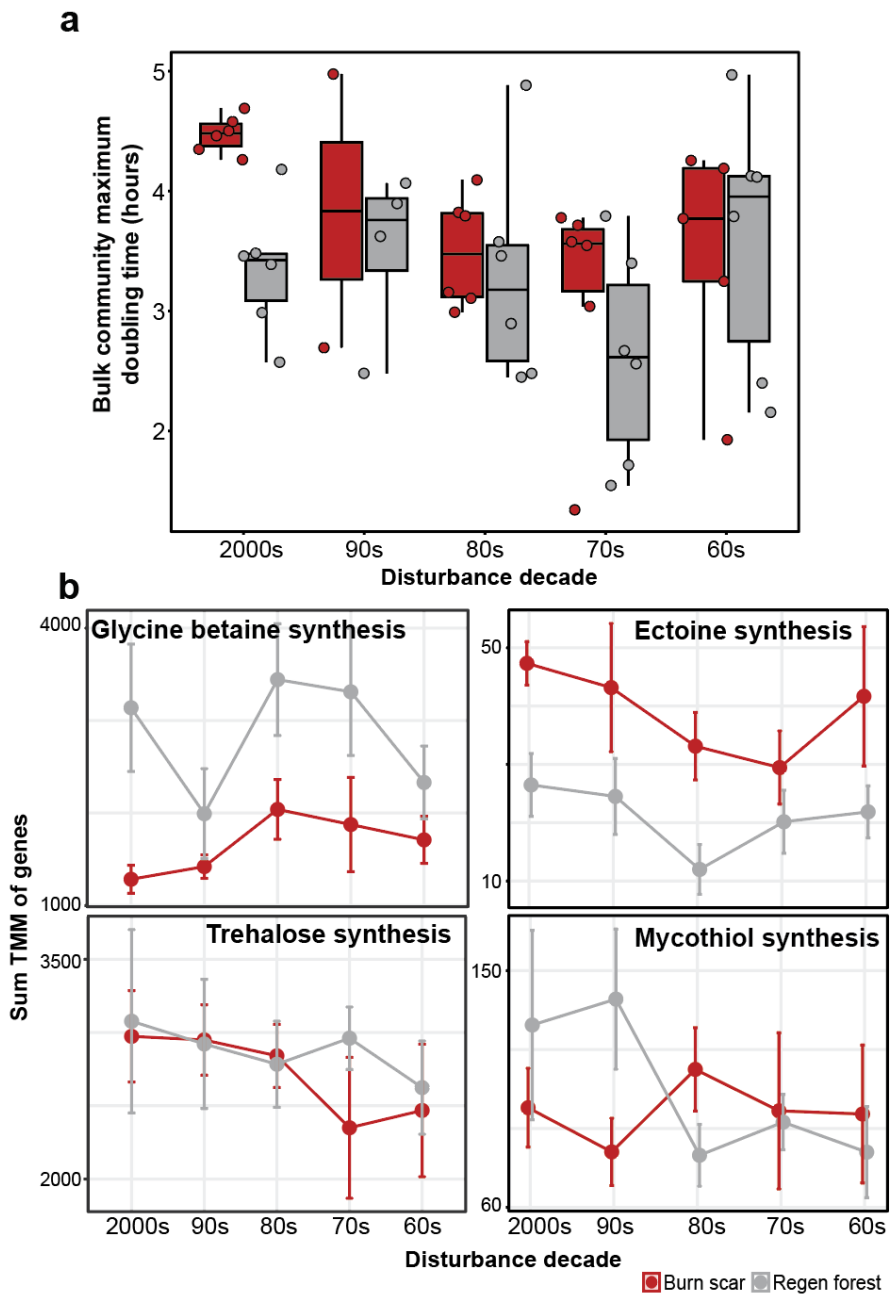

Figure 4.8 (A) Bulk community maximum doubling time (via gRodon, metagenome mode) across samples. **(B)** Summed normalized abundance of genes for synthesis of different stress protectants.

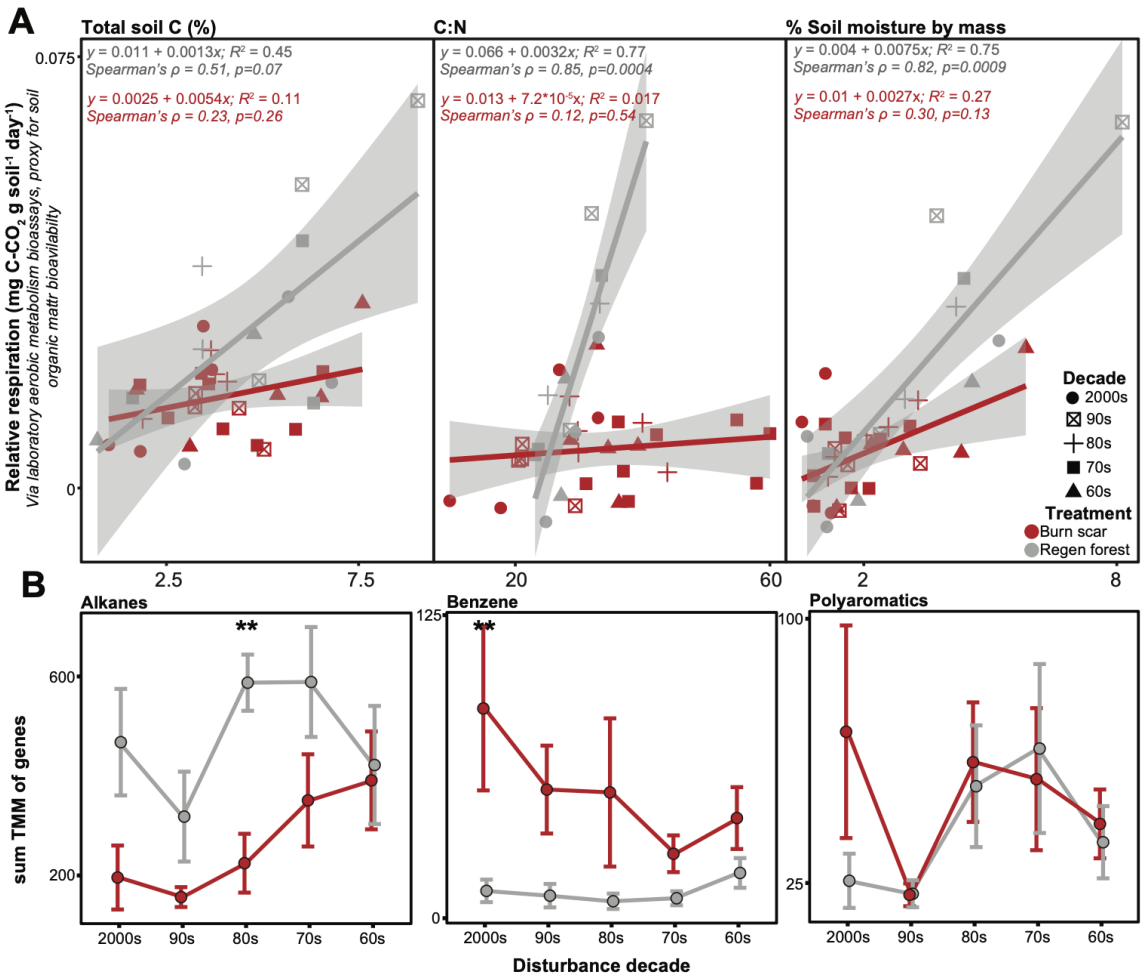

Figure 4.9 (A) Relative soil respiration calculated from laboratory bioassays relations with total soil C (%), C:N, and soil moisture, with linear regression and Spearman's correlation statistics. Shaded area shows 95% confidence interval of linear model. Soil respiration, and inferred organic matter bioavailability, is significantly positively correlated to all three soil variables in regen forest soils, but not the burn scar soils. **(B)** Average summed trimmed mean of M-values (TMM) of genes associated with the bacterial degradation of alkanes, benzene, and PAHs from metagenomes derived from burn scar and regen forest soil samples. Significant differences between burn scar and regen forest samples indicated with asterisks as indicated by Wilcoxon rank-sum test. *p<0.05, **p<0.01.

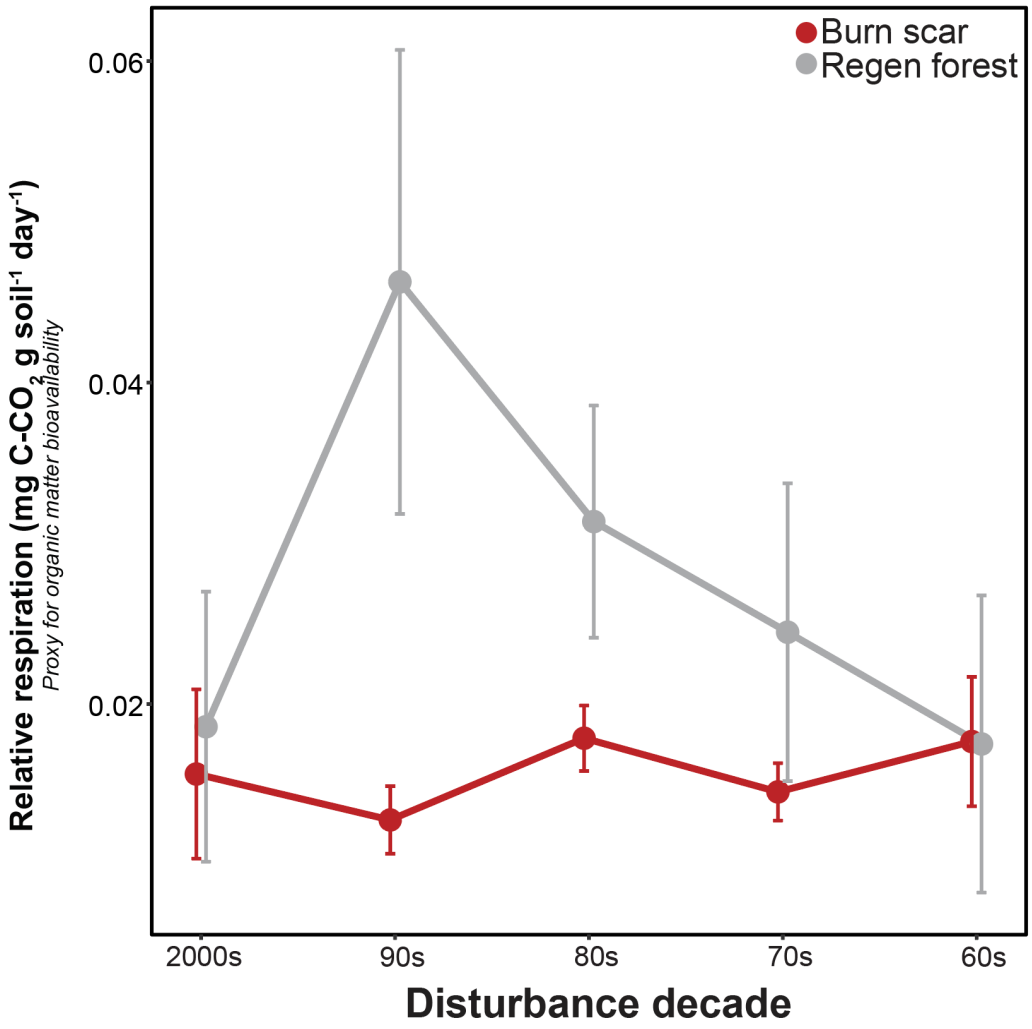

Figure 4.10 Average soil respiration, from laboratory incubations, of both burn scar and regen forest soils. Error bars represent the standard error of the mean.

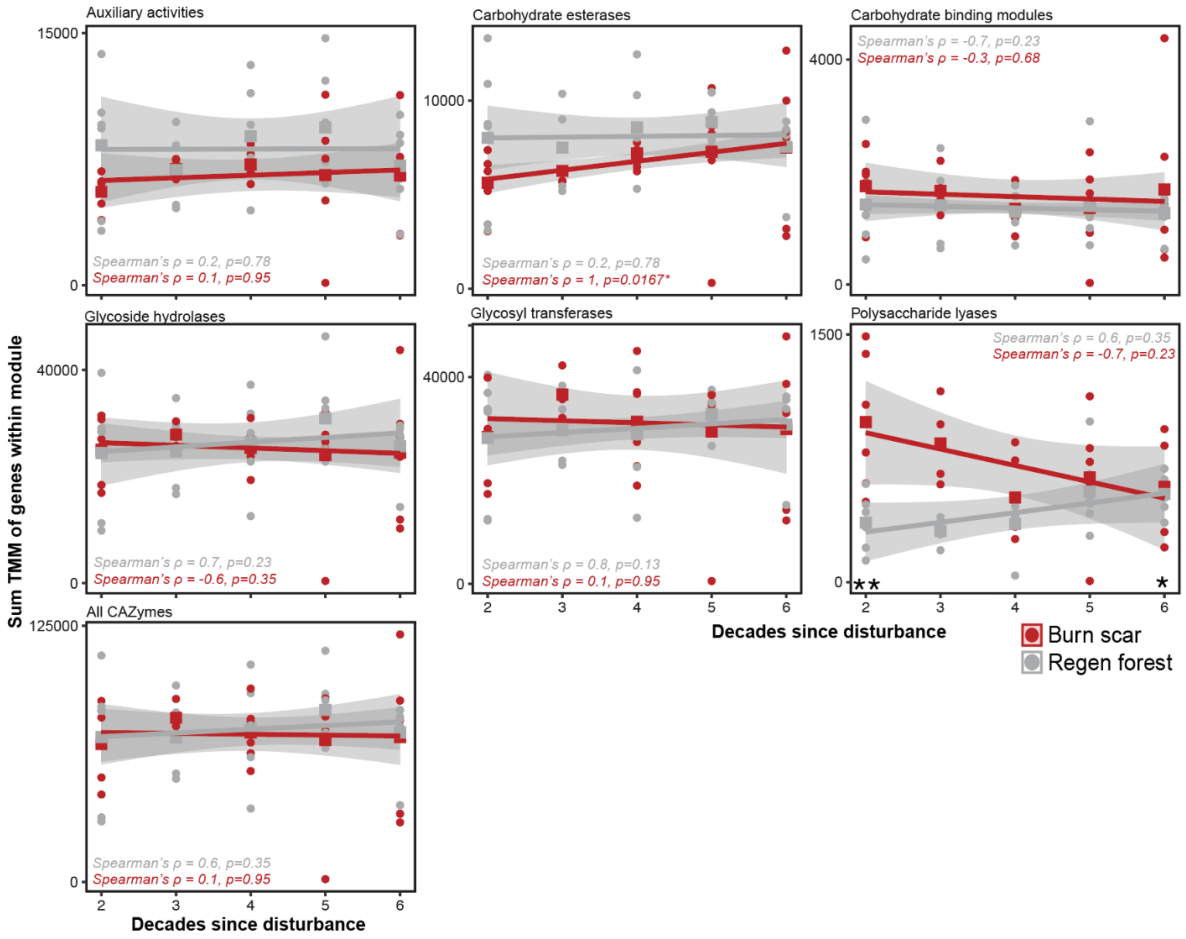

Figure 4.11 Sum TMM of CAZyme gene categories in different treatments. Circles show individual samples and squares show averages from these samples. Linear regression was run as a function of average sum TMM of genes within each treatment by decades since disturbance, and Spearman's rho values are reported. Shaded area shows 95% confidence interval of linear model. Significant differences between burn scar and regen forest samples within each decade are shown with asterisks as indicated by Wilcoxon rank-sum test. *p<0.05, **p<0.01.

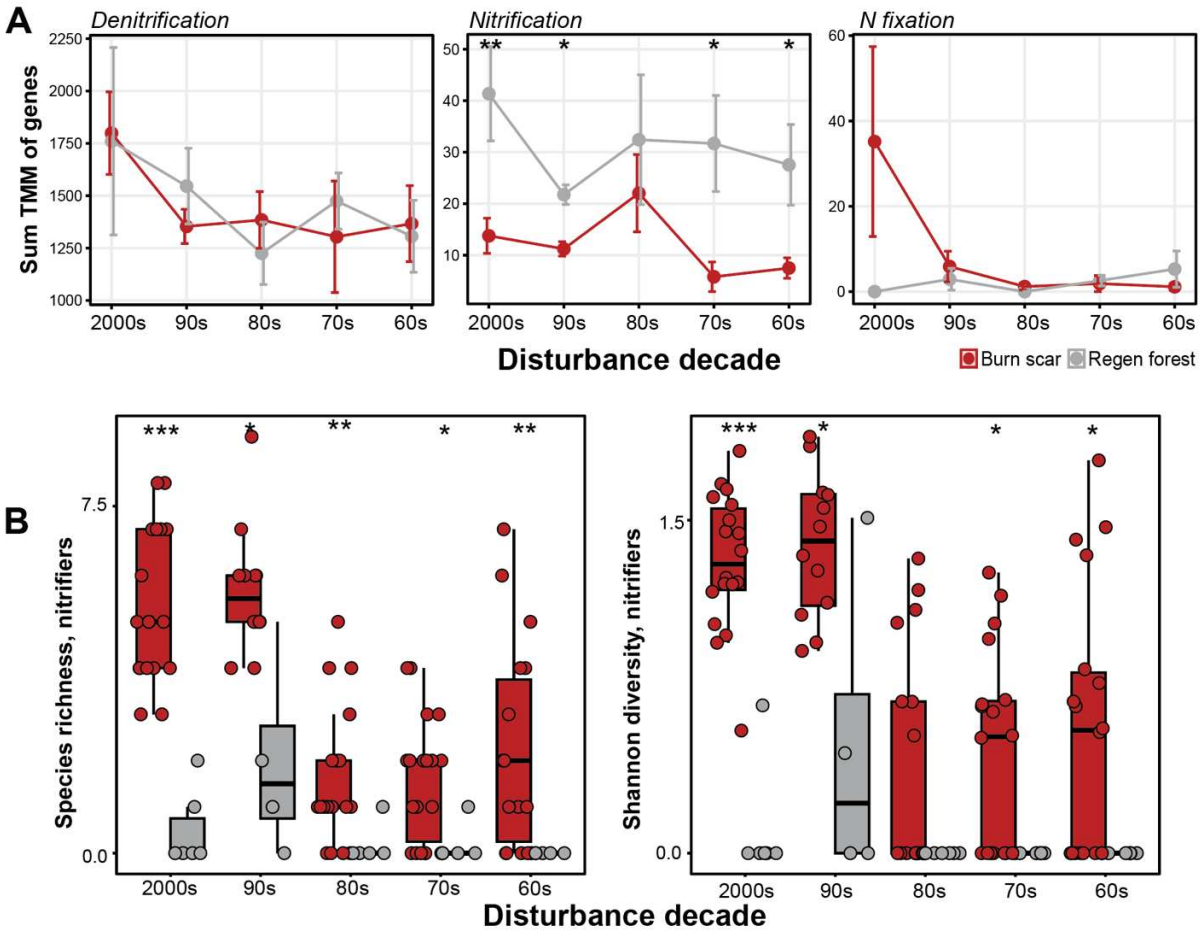

Figure 4.12 (**A**) Average sum TMM of genes for denitrification, nitrification, and N fixation over time. Error bars represent the standard error of the mean. (**B**) Diversity of putative nitrifiers from 16S rRNA gene sequencing data. Significant differences between burn scar and regen forest samples within each decade are shown with asterisks as indicated by Wilcoxon rank-sum test. *p<0.05, **p<0.01, ***p<0.001.

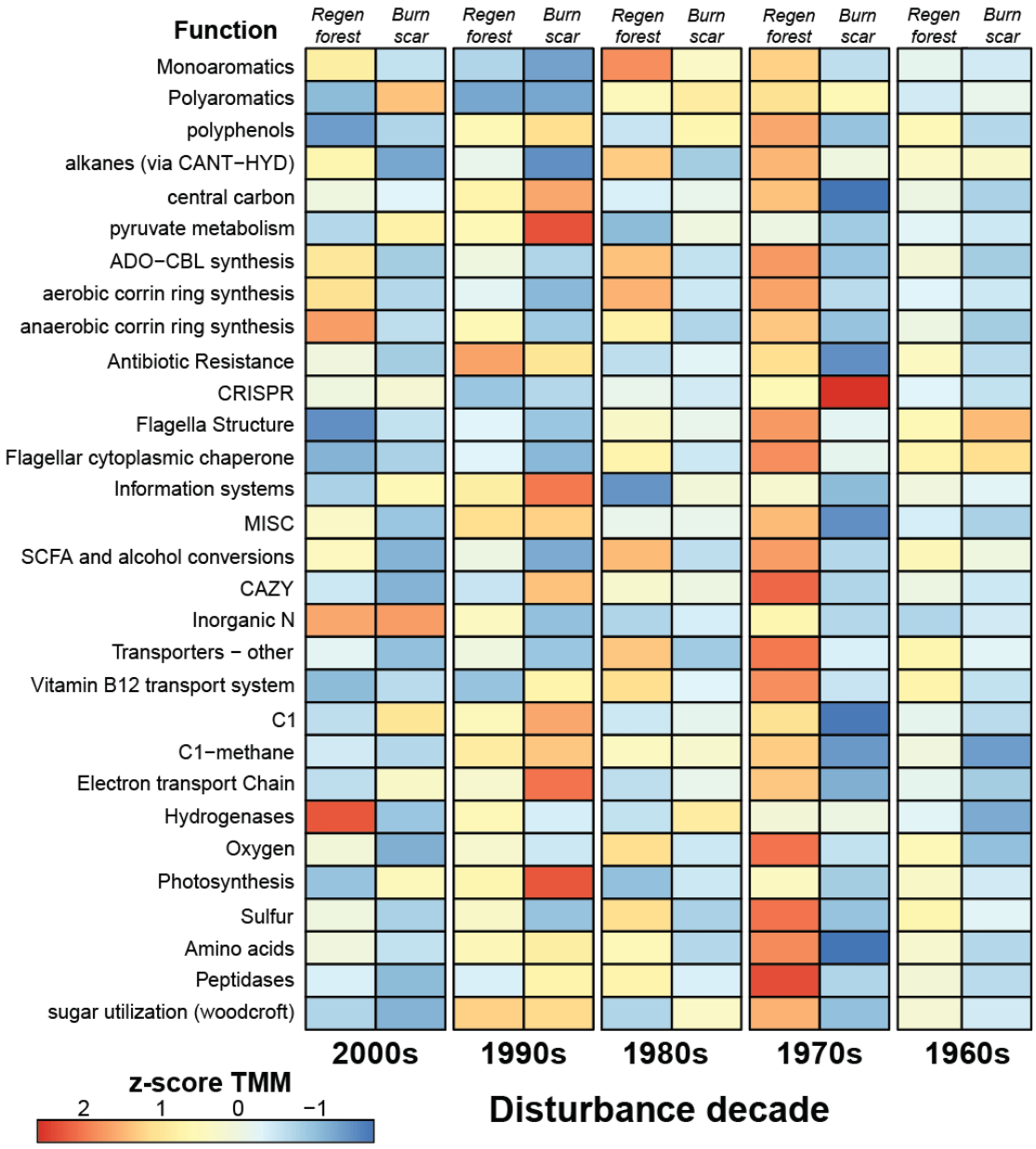

Figure 4.13 Z-score of the average TMM of genes within broad functional groups across treatments and disturbance decade. Genes grouped into broad functional groups by DRAM-assigned function 'header' and CANT-HYD annotation of genes for degrading alkanes, monoaromatics (added to genes annotated by DRAM), and polyaromatics (added to genes annotated by DRAM). Z-score was calculated within each individual function.

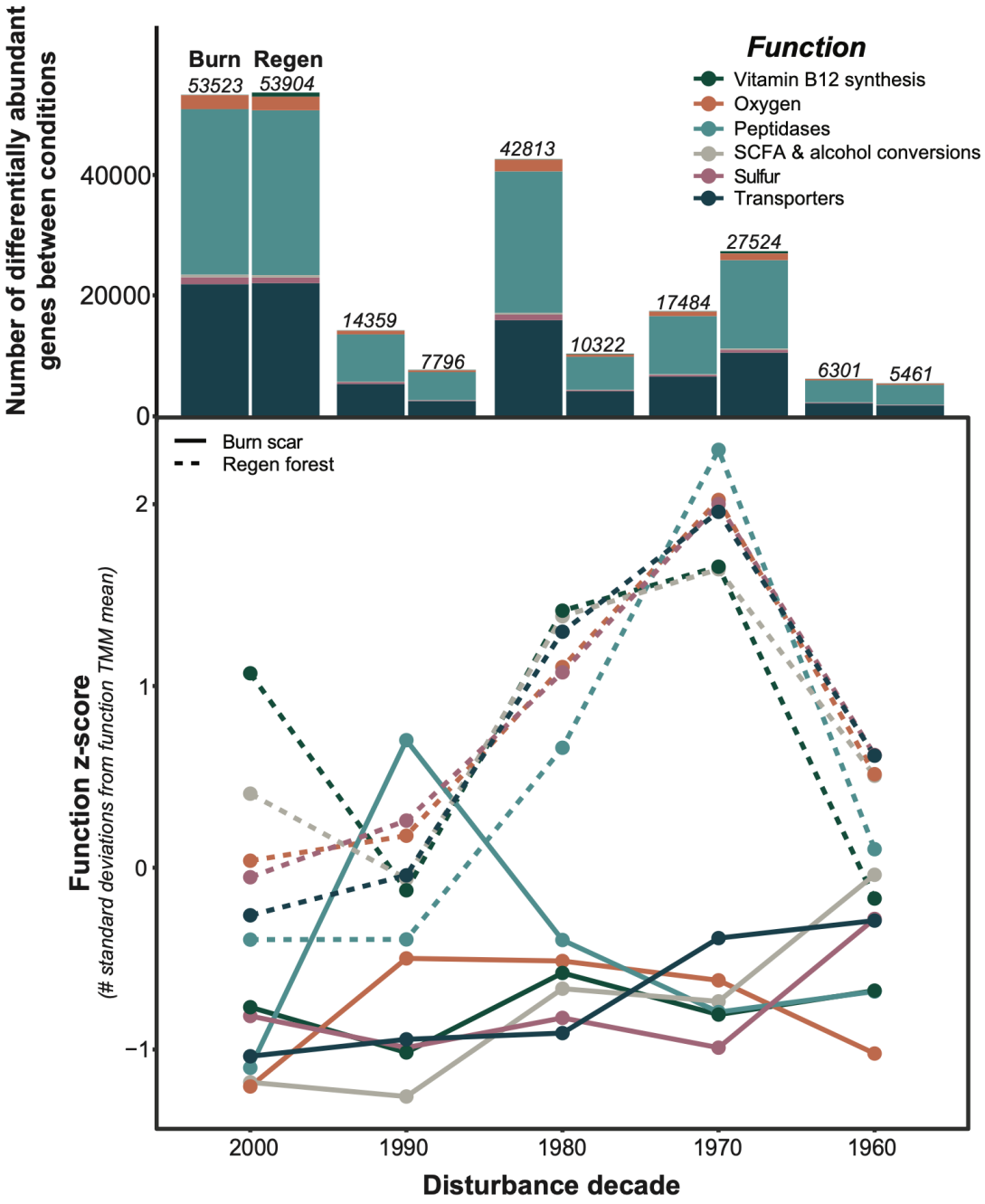

Figure 4.14 The function z-score (deviation from function mean across all time points and treatments; derived from function TMM) across time between regen forest (dashed line) and burn scar (solid line) soils, calculated within each function. Above, the number of differentially abundant genes within these functional categories between the two treatments over time.

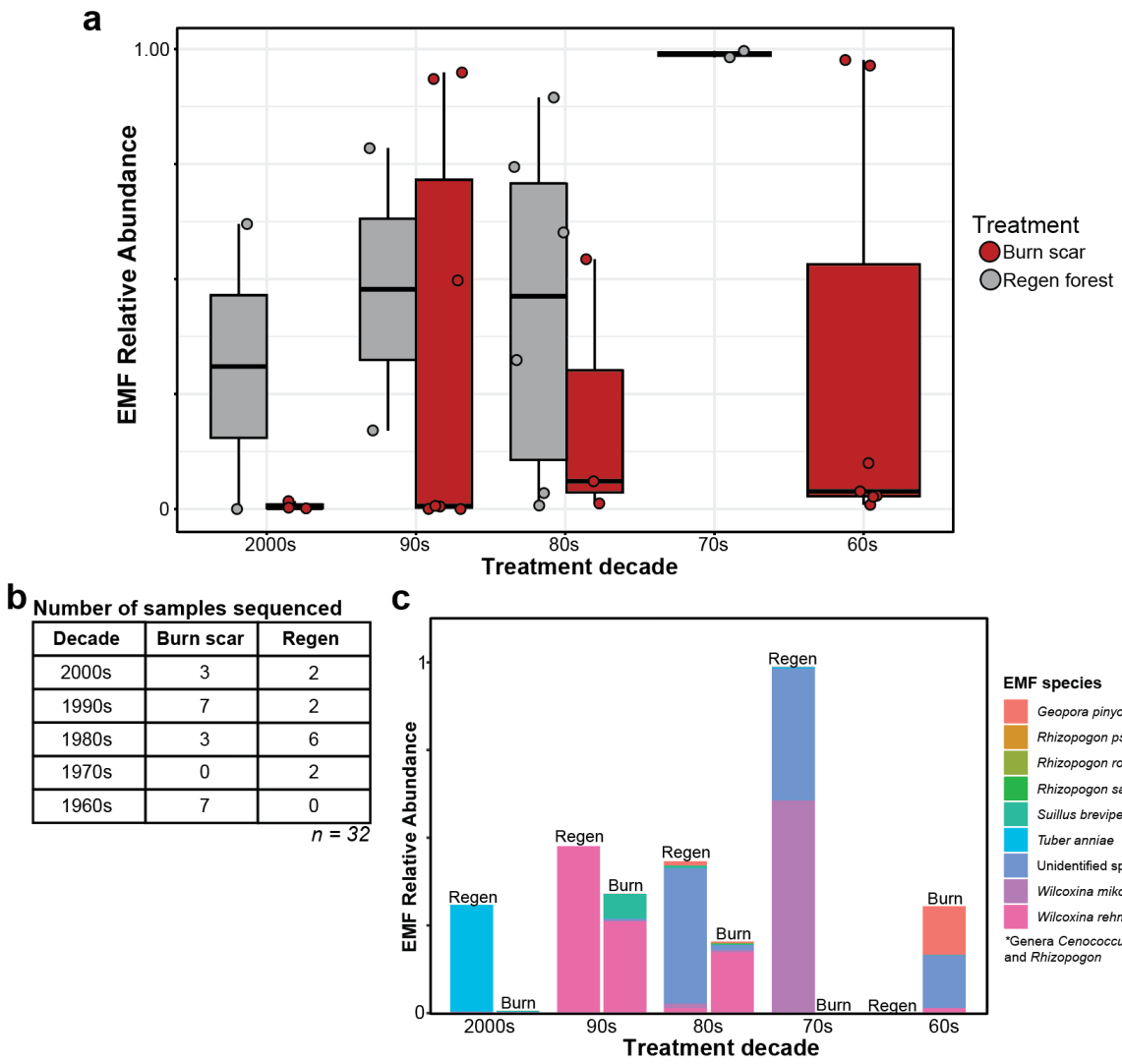

Figure 4.15 (a) EMF relative abundance from DNA extracted from root nodules of pine seedlings grown in soils collected from burn scars and regen forest sites across the chronosequence. (b) Total number of pine seedling root tips used for DNA sequencing. DNA was extracted from root nodules of pine seedlings that had EMF root colonization. (c) EMF relative abundance, colored by EMF species, of root nodules. See **Appendix C** for relevant data.

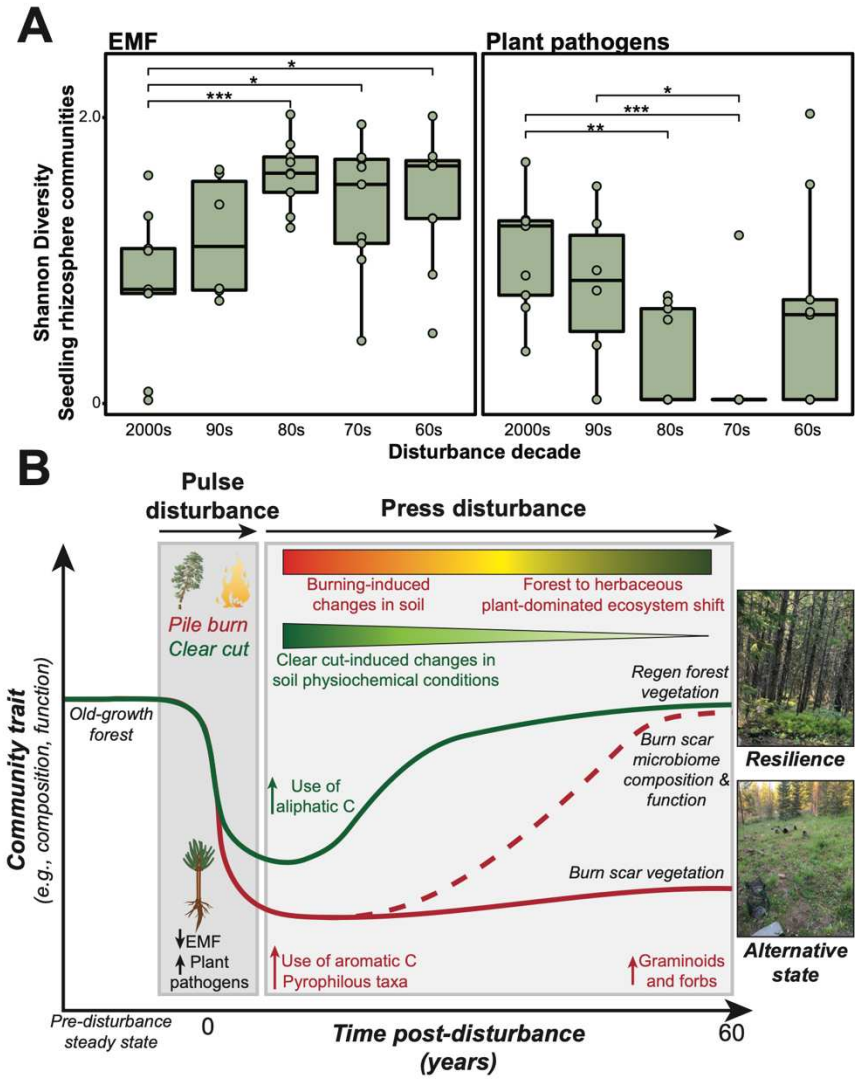

Figure 4.16 (A) Shannon Index of EMF (left) and plant pathogen (right) communities in rhizosphere of seedlings planted within burn scars. Significant differences between burn scar and regen forest samples indicated with asterisks as indicated by Wilcoxon rank-sum test. *p<0.05, **p<0.05, ***p<0.01, ***p<0.0001. **(b)** Conceptual diagram overviewing the ecosystem trajectory following disturbances in burn scar (i.e., pile burning) and regen forest (i.e., clear cut) soils. Both systems experience a pulse disturbance which causes a shift in vegetation and soil microbial communities, after which there is a long-term press disturbance. Within regen forest soils, the press disturbance is due to altered soil chemical conditions caused by clear cut, which lessens over time. In contrast, burn scar soils experience a press disturbance throughout the chronosequence, initially caused by fire-induced changes to soil physiochemical properties, which lessen over time and are replaced by a press disturbance caused by the ecosystem shift. During this ecosystem conversion, the aboveground community shifts from pine- to graminoid- and forb-dominated, but soil microbiome composition and function broadly begin to converge with regen forest soils.

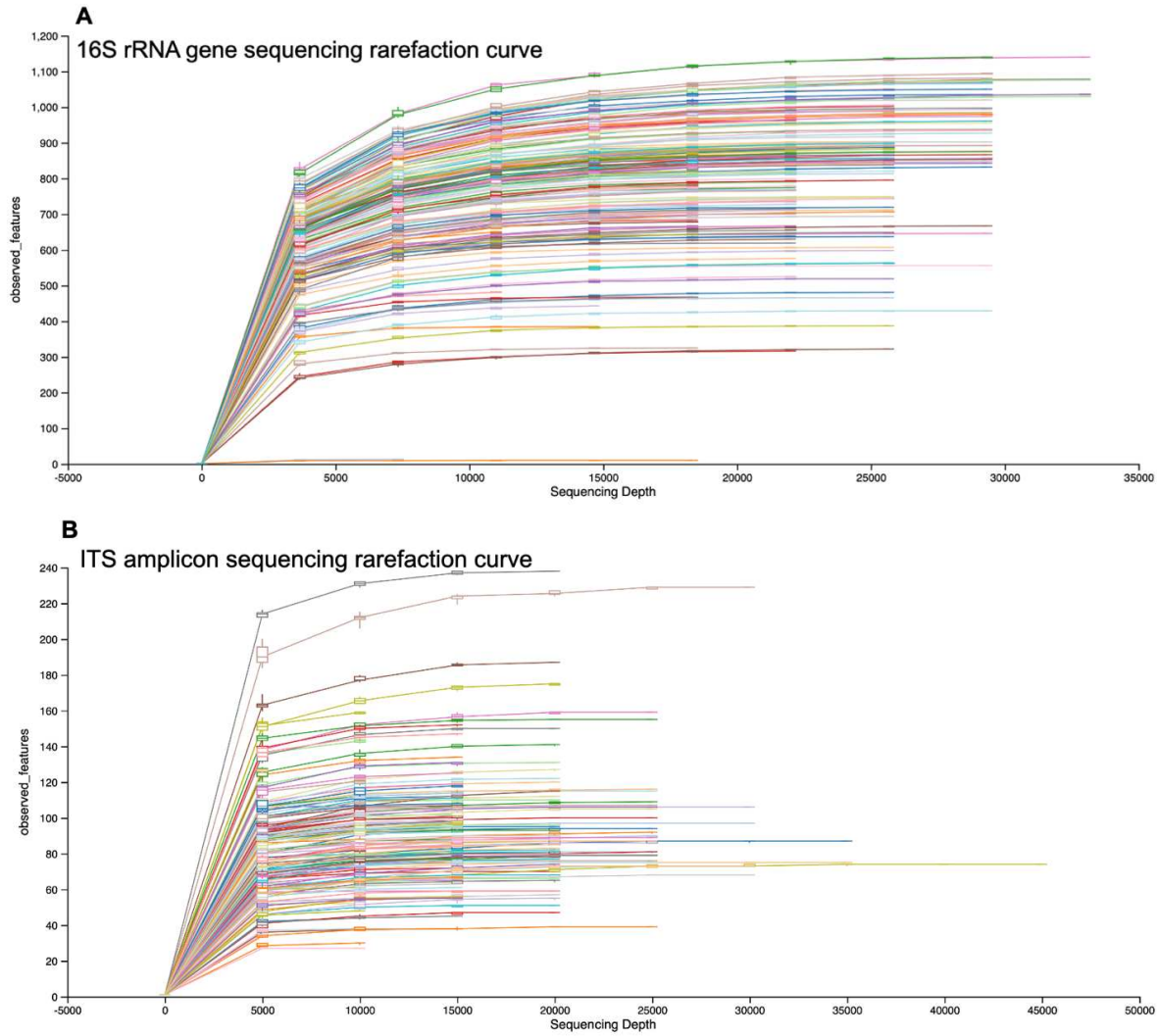

Figure 4.17 Rarefaction curves of 16S rRNA gene (A) and ITS amplicon sequencing data, generating using QIIME2 diversity plug-in *alpha-rarefaction* function to assess whether samples were sufficiently sequenced to compare alpha diversity. Each line represents an individual sample.

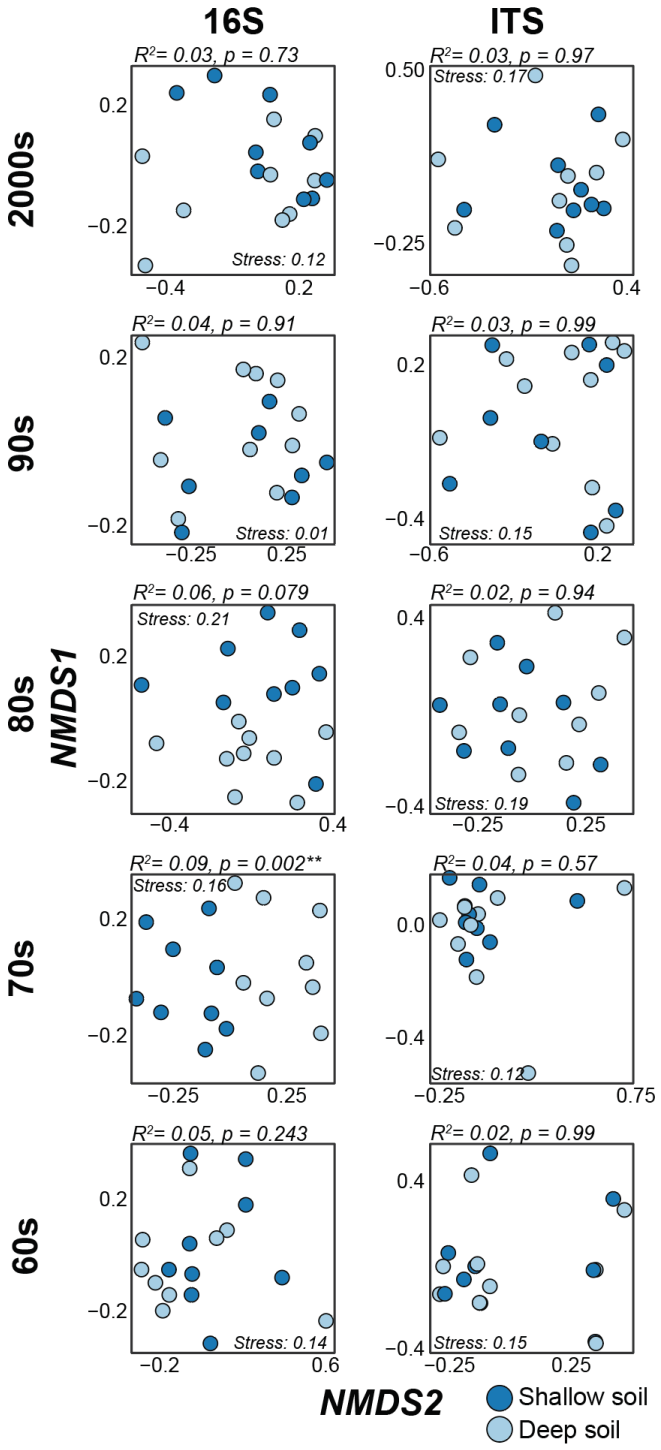

Figure 4.18 Non-metric multidimensional scaling (NMDS) ordinations of bacterial (left) and fungal (right) communities from burned shallow (dark blue) and deep (light blue) samples across all burn decades. The only communities that are significantly different (assessed using PERMANOVA, stats on each NMDS plot) between depths are the 70s bacterial communities. The similarity between depths is likely due to the deep penetration of heat into the soil column when burning the high fuel loads used on burn piles. Because of this, the shallow and deep soil samples are combined for all analyses presented here.

Table 4.1 Number of differentially abundant genes (calculated via DESeq2; p<0.01) within each treatment across decades. Calculated within-decade.

Decade	Treatment	# Differentially abundant genes	Total # in decade
2000s	Burn scar	218938	
	Regen forest	214588	433526
1990s	Burn scar	86997	
	Regen forest	57924	144921
1980s	Burn scar	194786	
	Regen forest	58192	252978
1970s	Burn scar	90073	
	Regen forest	116275	206348
1960s	Burn scar	39531	
	Regen forest	41410	80941

Table 4.2 Number of soil samples collected per treatment and number of samples utilized for metagenomics. 154 total soil samples collected.

Decade	Treatment	# Samples	# Samples utilized for metagenomic sequencing
2000s	Burn scar	18	6
	Regen forest	6	6
	Rhizosphere	9	N/A
1990s	Burn scar	12	4
	Regen forest	4	4
	Rhizosphere	6	N/A
1980s	Burn scar	18	6
	Regen forest	6	6
	Rhizosphere	9	N/A
1970s	Burn scar	18	6
	Regen forest	6	6
	Rhizosphere	9	N/A
1960s	Burn scar	18	6
	Regen forest	6	6
	Rhizosphere	9	N/A

Chapter 4 References

1. Sibold, J. S., Veblen, T. T. & González, M. E. Spatial and temporal variation in historic fire regimes in subalpine forests across the Colorado Front Range in Rocky Mountain National Park, Colorado, USA. *J. Biogeogr.* **33**, 631–647 (2006).

2. Hutto, R. L. *et al.* Toward a more ecologically informed view of severe forest fires. *Ecosphere* **7**, e01255 (2016).

3. Pausas, J. G. & Keeley, J. E. Wildfires as an ecosystem service. *Front. Ecol. Environ.* **17**, 289–295 (2019).

4. Parks, S. A. & Abatzoglou, J. T. Warmer and Drier Fire Seasons Contribute to Increases in Area Burned at High Severity in Western US Forests From 1985 to 2017. *Geophys. Res. Lett.* **47**, 1–10 (2020).

5. Higuera, P. E. & Abatzoglou, J. T. Record-setting climate enabled the extraordinary 2020 fire season in the western United States. *Glob. Change Biol.* gcb.15388 (2020) doi:10.1111/gcb.15388.

6. Fornwalt, P. J. *et al.* Did the 2002 Hayman Fire, Colorado, USA, Burn with Uncharacteristic Severity? *Fire Ecol.* **12**, 117–132 (2016).

7. Rodman, K. C. *et al.* A changing climate is snuffing out post-fire recovery in montane forests. *Glob. Ecol. Biogeogr.* 1–13 (2020) doi:10.1111/geb.13174.

8. Kleinman, J. S., Goode, J. D., Fries, A. C. & Hart, J. L. Ecological consequences of compound disturbances in forest ecosystems: a systematic review. *Ecosphere* **10**, e02962 (2019).

9. Enright, N. J., Fontaine, J. B., Bowman, D. M., Bradstock, R. A. & Williams, R. J. Interval squeeze: altered fire regimes and demographic responses interact to threaten woody species persistence as climate changes. *Front. Ecol. Environ.* **13**, 265–272 (2015).

10. Seidl, R. & Turner, M. G. Post-disturbance reorganization of forest ecosystems in a changing world. *Proc. Natl. Acad. Sci.* **119**, e2202190119 (2022).

11. Stevens-Rumann, C. S., Kemp, K. B., Higuera, P. E. & Rother, M. T. Evidence for declining forest resilience to wildfires under climate change. *Ecol. Lett.* **21**, 243–252 (2018).

12. Parks, S. A., Dobrowski, S. Z., Shaw, J. D. & Miller, C. Living on the edge: trailing edge forests at risk of fire-facilitated conversion to non-forest. *Ecosphere* **10**, (2019).

13. Davis, K. T. *et al.* Wildfires and climate change push low-elevation forests across a critical climate threshold for tree regeneration. *Proc. Natl. Acad. Sci.* **116**, 6193–6198 (2019).

14. Rodman, K. C. *et al.* Limitations to recovery following wildfire in dry forests of southern Colorado and northern New Mexico, USA. *Ecol. Appl.* **30**, e02001 (2020).

15. Barrios, E. Soil biota, ecosystem services and land productivity. *Ecol. Econ.* 269–285 (2007) doi:10.1016/j.ecolecon.2007.03.004.

16. van der Heijden, M. G. A., Martin, F. M., Selosse, M.-A. & Sanders, I. R. Mycorrhizal ecology and evolution: the past, the present, and the future. *New Phytol.* **205**, 1406–1423 (2015).

17. Crowther, T. W. *et al.* The global soil community and its influence on biogeochemistry. *Science* **365**, eaav0550 (2019).

18. Clemmensen, K. E. *et al.* Roots and Associated Fungi Drive Long-Term Carbon Sequestration in Boreal Forest. *Science* **339**, 1615–1618 (2013).

19. van der Heijden, M. G. A., Bardgett, R. D. & van Straalen, N. M. The unseen majority: soil microbes as drivers of plant diversity and productivity in terrestrial ecosystems. *Ecol. Lett.* **11**, 296–310 (2008).

20. Nelson, A. R. *et al.* Wildfire-dependent changes in soil microbiome diversity and function. *Nat. Microbiol.* **7**, 1419–1430 (2022).

21. Allison, S. D. & Martiny, J. B. H. Resistance, resilience, and redundancy in microbial communities. *Proc. Natl. Acad. Sci.* **105**, 11512–11519 (2008).

22. Isaac, L. A. & Hopkins, H. G. The Forest Soil of the Douglas Fir Region, and Changes Wrought Upon it by Logging and Slash Burning. *Ecology* **18**, 264–279 (1937).

23. McCulloch, W. F. Slash burning. *For. Chron.* 111–118 (1944).

24. Jiménez Esquilín, A. E., Stromberger, M. E., Massman, W. J., Frank, J. M. & Shepperd, W. D. Microbial community structure and activity in a Colorado Rocky Mountain forest soil scarred by slash pile burning. *Soil Biol. Biochem.* **39**, 1111–1120 (2007).

25. Busse, M. D., Shestak, C. J. & Hubbert, K. R. Soil heating during burning of forest slash piles and wood piles. *Int. J. Wildland Fire* **22**, 786 (2013).

26. Rhoades, C. C., Fegel, T. S., Zaman, T., Fornwalt, P. J. & Miller, S. P. Are soil changes responsible for persistent slash pile burn scars in lodgepole pine forests? *For. Ecol. Manag.* **490**, (2021).

27. Rhoades, C. C. & Fornwalt, P. J. Pile burning creates a fifty-year legacy of openings in regenerating lodgepole pine forests in Colorado. *For. Ecol. Manag.* **336**, 203–209 (2015).

28. Xiang, X. *et al.* Rapid recovery of soil bacterial communities after wildfire in a Chinese boreal forest. *Sci. Rep.* **4**, 3829 (2015).

29. Dove, N. C., Taş, N. & Hart, S. C. Ecological and genomic responses of soil microbiomes to high-severity wildfire: linking community assembly to functional potential. *ISME J.* **16**, 1853–1863 (2022).

30. Whitman, T. *et al.* Soil bacterial and fungal response to wildfires in the Canadian boreal forest across a burn severity gradient. *Soil Biol. Biochem.* **138**, 107571 (2019).

31. Pulido-Chavez, M. F. *et al.* Rapid bacterial and fungal successional dynamics in first year after chaparral wildfire. *Mol. Ecol.* **32**, 1685–1707 (2023).

32. Enright, D. J., Frangioso, K. M., Isobe, K., Rizzo, D. M. & Glassman, S. I. Mega-fire in redwood tanoak forest reduces bacterial and fungal richness and selects for pyrophilous taxa that are phylogenetically conserved. *Mol. Ecol.* **31**, 2475–2493 (2022).

33. Caiafa, M. V. *et al.* Distinct fungal and bacterial responses to fire severity and soil depth across a ten-year wildfire chronosequence in beetle-killed lodgepole pine forests. *For. Ecol. Manag.* **544**, 121160 (2023).

34. Dove, N. C., Klingeman, D. M., Carrell, A. A., Cregger, M. A. & Schadt, C. W. Fire alters plant microbiome assembly patterns: integrating the plant and soil microbial response to disturbance. *New Phytol.* **230**, 2433–2446 (2021).

35. Crowther, T. W. *et al.* Predicting the responsiveness of soil biodiversity to deforestation: a cross-biome study. *Glob. Change Biol.* **20**, 2983–2994 (2014).

36. Bastida, F. *et al.* Deforestation fosters bacterial diversity and the cyanobacterial community responsible for carbon fixation processes under semiarid climate: a metaproteomics study. *Appl. Soil Ecol.* **93**, 65–67 (2015).

37. Dini-Andreote, F., Stegen, J. C., van Elsas, J. D. & Salles, J. F. Disentangling mechanisms that mediate the balance between stochastic and deterministic processes in microbial succession. *Proc. Natl. Acad. Sci.* **112**, E1326–E1332 (2015).

38. Whitman, T. *et al.* Soil bacterial and fungal response to wildfires in the Canadian boreal forest across a burn severity gradient. *Soil Biol. Biochem.* **138**, 107571 (2019).

39. Whitman, T., Woolet, J., Sikora, M., Johnson, D. B. & Whitman, Ellen. Resilience in soil bacterial communities of the boreal forest from one to five years after wildfire across a severity gradient | Elsevier Enhanced Reader. *Soil Biol. Biochem.* 108755 (2022) doi:10.1016/j.soilbio.2022.108755.

40. Weissman, J. L., Hou, S. & Fuhrman, J. A. Estimating maximal microbial growth rates from cultures, metagenomes, and single cells via codon usage patterns. *PNAS* **118**, 1–10 (2020).

41. Newton, G. L., Buchmeier, N. & Fahey, R. C. Biosynthesis and Functions of Mycothiol, the Unique Protective Thiol of Actinobacteria. *Microbiol. Mol. Biol. Rev.* **72**, 471–494 (2008).

42. Richter, A. A. *et al.* Biosynthesis of the Stress-Protectant and Chemical Chaperon Ectoine: Biochemistry of the Transaminase EctB. *Front. Microbiol.* **10**, 1–20 (2019).

43. Rhoades, C. C. & Fornwalt, P. J. Pile burning creates a fifty-year legacy of openings in regenerating lodgepole pine forests in Colorado. *For. Ecol. Manag.* **336**, 203–209 (2015).

44. Faria, S. R. *et al.* Wildfire-induced alterations of topsoil organic matter and their recovery in Mediterranean eucalypt stands detected with biogeochemical markers. *Eur. J. Soil Sci.* **66**, 699–713 (2015).

45. Grayston, S. J., Vaughan, D. & Jones, D. Rhizosphere carbon flow in trees, in comparison with annual plants: the importance of root exudation and its impact on microbial activity and nutrient availability. *Appl. Soil Ecol.* **5**, 29–56 (1997).

46. Torres-Rojas, D. *et al.* Nitrogen speciation and transformations in fire-derived organic matter. *Geochim. Cosmochim. Acta* **276**, 170–185 (2020).

47. Dove, N. C., Safford, H. D., Bohlman, G. N., Estes, B. L. & Hart, S. C. High-severity wildfire leads to multi-decadal impacts on soil biogeochemistry in mixed-conifer forests. *Ecol. Appl.* **30**, eap.2072 (2020).

48. Nelson, M. B., Martiny, A. C. & Martiny, J. B. H. Global biogeography of microbial nitrogen-cycling traits in soil. *Proc. Natl. Acad. Sci.* **113**, 8033–8040 (2016).

49. Miao, L. *et al.* Abundant culturable diazotrophs within Actinomycetia rather than rare taxa are underlying inoculants for nitrogen promotion in desert soil. *Appl. Soil Ecol.* **184**, 104774 (2023).

50. Love, M. I., Huber, W. & Anders, S. Moderated estimation of fold change and dispersion for RNA-seq data with DESeq2. *Genome Biol.* **15**, 550 (2014).

51. Lu, X., Heal, K. R., Ingalls, A. E., Doxey, A. C. & Neufeld, J. D. Metagenomic and chemical characterization of soil cobalamin production. *ISME J.* **14**, 53–66 (2020).

52. Lochhead, A. G. & Burton, M. O. Soil as a Habitat of Vitamin-requiring Bacteria. *Nature* **178**, 144–145 (1956).

53. Palacios, O. A., Bashan, Y. & De-Bashan, L. E. Proven and potential involvement of vitamins in interactions of plants with plant growth-promoting bacteria—an overview. *Biol. Fertil. Soils* **50**, 415–432 (2014).

54. Schulten, H.-R. & Schnitzer, M. The chemistry of soil organic nitrogen: a review. *Biol. Fertil. Soils* **26**, 1–15 (1997).

55. Jan, M. T., Roberts, P., Tonheim, S. K. & Jones, D. L. Protein breakdown represents a major bottleneck in nitrogen cycling in grassland soils. *Soil Biol. Biochem.* **41**, 2272–2282 (2009).

56. Jones, D. L. *et al.* Soil organic nitrogen mineralization across a global latitudinal gradient. *Glob. Biogeochem. Cycles* **23**, (2009).

57. Malik, A. A. *et al.* Defining trait-based microbial strategies with consequences for soil carbon cycling under climate change. *ISME J.* **14**, 1–9 (2020).

58. Glassman, S. I., Levine, C. R., DiRocco, A. M., Battles, J. J. & Bruns, T. D. Ectomycorrhizal fungal spore bank recovery after a severe forest fire: some like it hot. *ISME J.* **10**, 1228–1239 (2016).

59. Peay, K. G., Garbelotto, M. & Bruns, T. D. Spore heat resistance plays an important role in disturbance-mediated assemblage shift of ectomycorrhizal fungi colonizing Pinus muricata seedlings. *J. Ecol.* **97**, 537–547 (2009).

60. Izzo, A., Canright, M. & Bruns, T. D. The effects of heat treatments on ectomycorrhizal resistant propagules and their ability to colonize bioassay seedlings. *Mycol. Res.* **110**, 196–202 (2006).

61. Glassman, S. I. *et al.* A continental view of pine-associated ectomycorrhizal fungal spore banks: a quiescent functional guild with a strong biogeographic pattern. *New Phytol.* **205**, 1619–1631 (2015).

62. McDowell, W. H. *et al.* A comparison of methods to determine the biodegradable dissolved organic carbon from different terrestrial sources. *Soil Biol. Biochem.* **38**, 1933–1942 (2006).

63. Thomas, G. W. Soil pH and soil acidity. *Methods Soil Anal. Part 3* 475–490 (1996).

64. Barnes, R. T., Smith, R. L. & Aiken, G. R. Linkages between denitrification and dissolved organic matter quality, Boulder Creek watershed, Colorado. *J. Geophys. Res. Biogeosciences* **117**, (2012).

65. Caporaso, J. G. *et al.* Ultra-high-throughput microbial community analysis on the Illumina HiSeq and MiSeq platforms. *ISME J.* **6**, 1621–1624 (2012).

66. Toju, H., Tanabe, A. S., Yamamoto, S. & Sato, H. High-Coverage ITS Primers for the DNA-Based Identification of Ascomycetes and Basidiomycetes in Environmental Samples. *PLOS ONE* **7**, e40863 (2012).

67. Bolyen, E. *et al.* Reproducible, interactive, scalable and extensible microbiome data science using QIIME 2. *Nat. Biotechnol.* **37**, 852–857 (2019).

68. Callahan, B. J. *et al.* DADA2: High-resolution sample inference from Illumina amplicon data. *Nat. Methods* **13**, 581–583 (2016).

69. Quast, C. *et al.* The SILVA ribosomal RNA gene database project: improved data processing and web-based tools. *Nucleic Acids Res.* **41**, D590–D596 (2012).

70. Kõljalg, U. *et al.* UNITE: a database providing web-based methods for the molecular identification of ectomycorrhizal fungi. *New Phytol.* **166**, 1063–1068 (2005).

71. Nguyen, N. H. *et al.* FUNGuild: An open annotation tool for parsing fungal community datasets by ecological guild. *Fungal Ecol.* **20**, 241–248 (2016).

72. Team, R. C. R: A language and environment for statistical computing. *R Found. Stat. Comput. Vienna Austria* (2021).

73. Oksanen, J. *et al.* Package 'vegan'. in (Springer Netherlands, Dordrecht, 2013). doi:10.1007/978-94-024-1179-9_301576.

74. McMurdie, P. J. & Holmes, S. phyloseq: An R Package for Reproducible Interactive Analysis and Graphics of Microbiome Census Data. *PLoS ONE* **8**, e61217 (2013).

75. Segata, N. *et al.* Metagenomic biomarker discovery and explanation. *Genome Biol.* **12**, R60 (2011).

76. Jiménez Esquilín, A. E., Stromberger, M. E., Massman, W. J., Frank, J. M. & Shepperd, W. D. Microbial community structure and activity in a Colorado Rocky Mountain forest soil scarred by slash pile burning. *Soil Biol. Biochem.* **39**, 1111–1120 (2007).

77. Busse, M. D., Shestak, C. J. & Hubbert, K. R. Soil heating during burning of forest slash piles and wood piles. *Int. J. Wildland Fire* **22**, 786 (2013).

78. Brady, M. K. *et al.* Soil Heating in Fire (<scp>SheFire</scp>): A model and measurement method for estimating soil heating and effects during wildland fires. *Ecol. Appl.* **32**, (2022).

79. Rusca, T. A., Kennedy, P. G. & Bruns, T. D. The effect of different pine hosts on the sampling of Rhizopogon spore banks in five Eastern Sierra Nevada forests. *New Phytol.* **170**, 551–560 (2006).

80. Bolyen, E. *et al.* Reproducible, interactive, scalable and extensible microbiome data science using QIIME 2. *Nat. Biotechnol.* **37**, 852–857 (2019).

81. Nguyen, N. H. *et al.* FUNGuild: An open annotation tool for parsing fungal community datasets by ecological guild. *Fungal Ecol.* **20**, 241–248 (2016).

82. Stegen, J. C., Lin, X., Konopka, A. E. & Fredrickson, J. K. Stochastic and deterministic assembly processes in subsurface microbial communities. **6**, 1653–1664 (2012).

83. Stegen, J. C., Lin, X., Fredrickson, J. K. & Konopka, A. E. Estimating and mapping ecological processes influencing microbial community assembly. *Front. Microbiol.* **6**, (2015).

84. Zhou, J. & Ning, D. Stochastic Community Assembly: Does It Matter in Microbial Ecology? *Microbiol. Mol. Biol. Rev.* **81**, e00002-17 (2017).

85. Stegen, J. C. *et al.* Quantifying community assembly processes and identifying features that impose them. *ISME J.* **7**, 2069–2079 (2013).

86. Kembel, S. W. *et al.* Picante: R tools for integrating phylogenies and ecology. *Bioinformatics* **26**, 1463–1464 (2010).

87. Danczak, R. E. *et al.* Ecological Assembly Processes Are Coordinated between Bacterial and Viral Communities in Fractured Shale Ecosystems. *mSystems* **5**, e00098-20 (2020).

88. Joshi, N. & Fass, J. Sickle: A sliding-window, adaptive, quality-based trimming tool for FastQ files. Preprint at (2011).

89. Li, D., Liu, C.-M., Luo, R., Sadakane, K. & Lam, T.-W. MEGAHIT: an ultra-fast single-node solution for large and complex metagenomics assembly via succinct de Bruijn graph. *Bioinformatics* **31**, 1674–1676 (2015).

90. Hyatt, D. *et al.* Prodigal: prokaryotic gene recognition and translation initiation site identification. *BMC Bioinformatics* **11**, 119 (2010).

91. Steinegger, M. & Söding, J. MMseqs2 enables sensitive protein sequence searching for the analysis of massive data sets. *Nat. Biotechnol.* **35**, 1026–1028 (2017).

92. Langmead, B. & Salzberg, S. L. Fast gapped-read alignment with Bowtie 2. *Nat. Methods* **9**, 357–359 (2012).

93. Shaffer, M. *et al.* DRAM for distilling microbial metabolism to automate the curation of microbiome function. *Nucleic Acids Res.* **48**, 8883–8900 (2020).

94. Eddy, S. R. Accelerated profile HMM searches. *PLoS Comput. Biol.* **7**, (2011).

95. Aramaki, T. *et al.* KofamKOALA: KEGG Ortholog assignment based on profile HMM and adaptive score threshold. *Bioinformatics* **36**, 2251–2252 (2020).

96. Khot, V. *et al.* CANT-HYD: A Curated Database of Phylogeny-Derived Hidden Markov Models for Annotation of Marker Genes Involved in Hydrocarbon Degradation. *Front. Microbiol.* **12**, 1–15 (2022).

97. Khot, V. *et al.* CANT-HYD: A Curated Database of Phylogeny-Derived Hidden Markov Models for Annotation of Marker Genes Involved in Hydrocarbon Degradation. *Front. Microbiol.* **12**, 1–15 (2022).

98. Weissman, J. L., Peras, M., Barnum, T. P. & Fuhrman, J. A. Benchmarking Community-Wide Estimates of Growth Potential from Metagenomes Using Codon Usage Statistics. *mSystems* **7**, e00745-22 (2022).

99. Kang, D. D. *et al.* MetaBAT 2: an adaptive binning algorithm for robust and efficient genome reconstruction from metagenome assemblies. *PeerJ* **7**, e7359 (2019).

100. Parks, D. H., Imelfort, M., Skennerton, C. T., Hugenholtz, P. & Tyson, G. W. CheckM: assessing the quality of microbial genomes recovered from isolates, single cells, and metagenomes. *Genome Res.* **25**, 1043–1055 (2015).

101. Chaumeil, P.-A., Mussig, A. J., Hugenholtz, P. & Parks, D. H. GTDB-Tk: a toolkit to classify genomes with the Genome Taxonomy Database. *Bioinformatics* **36**, 1925–1927 (2019).

102. Olm, M. R., Brown, C. T., Brooks, B. & Banfield, J. F. dRep: a tool for fast and accurate genomic comparisons that enables improved genome recovery from metagenomes through de-replication. *ISME J.* **11**, 2864–2868 (2017).

103. Bowers, R. M. *et al.* Minimum information about a single amplified genome (MISAG) and a metagenome-assembled genome (MIMAG) of bacteria and archaea. *Nat. Biotechnol.* **35**, 725–731 (2017).

Chapter 5: Conclusion

5.1 Research summary

The overarching objective of this doctoral research was to examine the effects of severe wildfire on the soil microbiome in forest ecosystems, with particular emphasis on identifying traits that facilitate the persistence of key pyrophilous microbial taxa and assessing the resulting impacts to soil carbon (C). Specifically, I aimed to investigate how varying burn severities influenced the post-wildfire soil microbiome and the duration of these effects. This was achieved by utilizing soil samples representing one to sixty years following burning (**Figure 1.1**).

My first research chapter (**Chapter 2**) began to answer this overarching research objective by providing a thorough analysis of the soil microbiome one year post-fire and across wildfire burn severity (low, moderate, and high severity)[1]. I used a suite of tools to characterize both the post-wildfire soil chemistry (FTICR-MS), microbiome composition (16S rRNA gene & ITS amplicon sequencing) and function (metagenomics and metatranscriptomics), and was able to characterize the entire soil microbiome, including viruses, fungi, and bacteria. With this extensive dataset, I found evidence of the role of fungi in degradation of pyrogenic C (PyC), revealed viral predation of active microbial taxa inhabiting post-wildfire soils (**Figure 2.17**), and identified potential traits that enabled Actinobacteria dominance in severely burned soils (e.g., ability to degrade aromatic C, **Figure 2.13**; stress resistance genes; fast growth, **Figure 2.8**) – some of which were also observed in the research presented in **Chapter 3**.

Chapter 3 extends the one year post-fire analyses performed in **Chapter 2** to over a decade post-fire by using genome-resolved metagenomic approaches on a set of soil samples collected from a chronosequence of wildfire scars representing 1, 3, 5, and 11 years post-fire along with low and high severity burned soils. This sequencing effort resulted in a metagenome-assembled genome (MAG) catalog consisting of 825 MAGs that was used to identify whether microbial genomic trait profiles drive soil microbiome succession following such a disturbance. I found evidence of the long-term importance of pyrophilous traits identified in **Chapter 2** – for example, fast growers were enriched in severely burned soils up to 11 years following wildfire (**Figure 3.17**). Further, I applied other trait-based classifications of microorganisms to the dataset (i.e., Y-A-S framework[2]) and discovered that taxa who preferentially invest in cellular resource acquisition machinery (e.g., carbohydrate-active enzymes, specialized transporters; **Figure 3.11**) were selected in severely burned soils over the entire chronosequence. The selection of these traits by wildfire likely has implications for soil C cycling, as both fast growing microbial taxa and those that investment into resource acquisition are hypothesized to grow less efficiently (lower carbon use efficiency; detailed in *Section 3.3.6*).

Finally, in **Chapter 4**, I utilized soil samples collected from a multidecadal chronosequence of burn pile scars that served as proxies for high severity burning to identify whether the soil microbiome is resilient during a burning-induced aboveground vegetation shift. The burn pile scars represented a burned coniferous forest, lacked reestablishment of pine, and became dominated by herbaceous plants (e.g., graminoids and forbs) over the chronosequence, presenting a unique opportunity to study the multidecadal belowground soil microbiome dynamics that underly a burning-induced

aboveground ecosystem shift. While I observed short-term impacts on soil microbiome composition and function linked to burning (e.g., enriched genes for degrading aromatic C, **Figure 4.9**; loss of heat-sensitive taxa, **Figure 4.5**), my findings suggest that, overall, the soil microbiome displayed resilience to the aboveground vegetation shift across the multidecadal chronosequence. Furthermore, I found evidence from *in situ* (**Figure 4.16**) and greenhouse (**Figure 4.15**) pine seedling assays that the initial burning-induced depletion of soil ectomycorrhizal fungi (EMF) might have initially hindered reestablishment of pine within the burn scars, resulting in the establishment and long-term persistence of grasses and shrubs.

Collectively, this comprehensive body of research conducted over the past five years significantly advances our understanding of the effects of severe wildfires on the soil microbiome in globally significant forest ecosystems.

5.2 Research implications for ecosystem restoration following wildfire

EMF, essential symbiotic partners of conifer tree species in western US forests, play a crucial role in facilitating plant access to vital nutrients and water in exchange for photosynthetically derived carbohydrates[3]. In **Chapter 2**, I observed a near-complete decimation of EMF (99% decrease in EMF relative abundance) one year following high severity wildfire. Additionally, **Chapter 4** presented evidence from *in situ* pine seedling and greenhouse bioassays that this burning-induced loss of EMF can persist for up to a decade. Notably, the loss of EMF in **Chapter 4** was associated with a subsequent increase in the relative abundances of plant pathogenic fungi (**Figure 4.16**). These findings suggest potential long-term regeneration obstacles within the subalpine pine

forests of the western US following severe wildfire. This challenge may be exacerbated by the fact that these forests were previously affected by severe mountain pine beetle outbreak in the early 21st century, with some sites experiencing approximately ~75% average overstory tree mortality[4]. Importantly, forest die-off caused by mountain pine beetle decreases belowground EMF diversity[5,6]. As climate change progresses and regions of the western US experience more severe and/or frequent wildfires, the loss of EMF could impede post-disturbance forest regeneration Inoculating burned sites with unburned control soils might counteract the depletion of soil microbial diversity and help restore the necessary EMF populations for successful pine reestablishment.

5.3 Significance in considering post-wildfire terrestrial carbon budgets

Wildfires drive significant ecosystem C loss by burning vegetation and surface soil C, which immediately reduces net primary productivity, and transforms other surface soil C to PyC, which is typically considered recalcitrant with long residence times. This addition of stable PyC is thought to help offset the loss of ecosystem C caused by combustion during wildfire. However, in **Chapter 2**, I presented evidence of PyC utilization by bacteria and fungi through expression of genes for degrading aromatics in high severity wildfire-impacted soils. This suggests that the high concentrations of soil PyC following severe wildfire selects for microorganisms capable of utilizing this substrate, potentially leading to further C losses. Additionally, **Chapter 4** demonstrated the long-term enrichment of fast growing taxa and taxa that invest in resource acquisition strategies – both of which both of which are hypothesized to increase soil C losses through less efficient growth or enhanced decomposition[2,7]. As we gain a deeper

understanding of the post-wildfire soil microbiome, we must consider how microbes interact with soil C and influence larger-scale ecosystem C cycling to predict how climate change is going to influence the C budgets of wildfire-prone systems.

5.4 Future research directions

5.4.1 Long-term implications of severe wildfire on ecosystem biogeochemistry

The field studies presented in **Chapter 2** and **Chapter 3** provide insights into the post-wildfire soil microbiome one to eleven years following wildfire. Though **Chapter 4** is a multidecadal field study, it focuses on smaller scale burn pile scars surrounded by unburned forest which might have facilitated soil microbiome recovery. Consequentially, future work is needed to assess the long-term ramifications of severe wildfire on the soil microbiome and subsequent ecosystem biogeochemistry. Dove et al (2020)[8] underscores the need for longer term wildfire studies by revealing four-decade impacts of severe wildfire to ecosystem biogeochemistry in the Sierra Nevada (e.g., decreased soil C and microbial respiration). Extended field studies are essentially for fully understanding the lasting impacts of severe wildfire on ecosystem biogeochemistry and C budgets in the carbon-rich forest ecosystems of the western United States. While ecosystem models offer valuable insights into long-term impacts, their accuracy relies on informed calibration and validation with field data. Additionally, refining these models to accurately represent post-fire soil microbiome dynamics is crucial, as highlighted in *Section 5.4.3*.

5.4.2 Testing metagenomic hypotheses in the laboratory

One of the overarching findings of this doctoral research was that wildfire selects for soil microbial taxa that possess specific traits that either facilitate their survival during

fire or promote their success in the post-fire environment. These conclusions were primarily drawn from multi-omics data generated from field samples, indicating the need for further validation, potentially through laboratory experiments. One hypothesis was that copiotrophs are favored in the post-wildfire soil environment, inferred from codon usage bias signatures in abundant MAGs within severely burned soils. While this hypothesis has also been suggested in other post-wildfire studies[9,10], it has not yet been experimentally confirmed in the laboratory for the putative pyrophilous taxa observed across various studies and post-fire ecosystems. Future research could involve isolating specific pyrophilous taxa (e.g., *Arthrobacter* and *Blastococcus*) in the laboratory and empirically testing their growth rates under controlled conditions and with different media (e.g., PyC). Another trait observed to be favored in post-wildfire soils was the genomic capability of taxa to degrade aromatic C, which constitutes a major component of PyC. Previous studies have documented several *Arthrobacter* species that can degrade a diverse range of aromatic compounds[11,12]. Additionally, *Blastococcus* taxa were observed to be among the most dominant and active in soils one year post-fire, expressing genes associated with the degradation of aromatic compounds (**Chapter 2**). Combined, this suggests that these genera play a significant role in degrading aromatics in soils following wildfire but these ideas have not been tested in a controlled laboratory setting. A laboratory study employing soil and PyC microcosms could be conducted, utilizing PyC generated from the combustion of isotopically labeled *P. contorta* seedlings grown in a continuous-labeling $^{13}CO_2$ chamber. Stable-isotope probing coupled with sequencing tools could then be employed to trace the incorporation of labeled C from PyC into microbial communities. Additionally, corresponding high-resolution soil chemistry analyses such as gas

chromatography-mass spectrometry (GC-MS) and nuclear magnetic resonance (NMR) spectroscopy could be utilized to provide further insights into the mechanisms underlying the degradation of PyC by these taxa in post-wildfire soils.

5.4.3 Incorporating relevant pyrophilous traits into ecosystem models

The addition of pertinent pyrophilous traits into mechanistic models presents an opportunity to scale up fine-scale findings and enhance our understanding of post-wildfire ecosystem dynamics at broader spatial and temporal scales. By incorporating traits such as the ability to degrade PyC, these models can better simulate how microbial communities respond to wildfires and influence biogeochemical processes over larger landscapes and longer timeframes. This integration could improve predictions of post-fire vegetation recovery, nutrient cycling, and ecosystem C sequestration potential, aiding in the development of more effective management strategies for fire-affected ecosystems. One such ecosystem model, EcoSIM (previously known as *ecosys*), is a comprehensive mechanistic model that stimulates the interdependent physical, hydrological, and biological processes that govern the ecosystem response to disturbance. EcoSIM has been broadly used to estimate methane fluxes from wetlands[13], estimate the C budget and crop yield of agroecosystems[14], quantify forest dynamics under drought[15], and has been more recently used to predict post-wildfire vegetation[16] and soil microbiome[17] dynamics in a boreal forest. Consistent with the findings presented here, the model revealed the post-fire proliferation of fast-growing bacterial heterotrophs in soil but unfortunately lacks resolution of specific bacterial metabolisms that we believe are prevalent in post-fire soils. For instance, a recent update to the source code (not yet published) endeavors to better simulate fire disturbances by incorporating elevated soil

temperatures, biomass combustion, and the formation of a "charcoal" soil C pool. Presently, the model depicts charcoal as predominantly inert to microbial decomposition, thereby constituting a significant addition of C to the ecosystem. Future research must focus on conducting laboratory experiments to refine rates of microbial soil PyC degradation to inform a more accurate model representation of this metabolism, which has been observed in both laboratory settings[18] and hypothesized in field studies presented here. This effort would help more accurately predict C fluxes in post-fire terrestrial ecosystems.

5.4.4 Eukaryotic metagenomic pipeline development

Fungi play a crucial role in terrestrial ecosystems, acting as key decomposers of recalcitrant soil organic matter (e.g., lignin, cellulose) and symbionts for aboveground vegetation. Soil fungal biomass also contributes significantly to the global soil C pool, making up approximately 12 Pg of soil C in global topsoil[19]. Fungi are crucial members of the soil microbiome in the pine forests studied here as the dominant tree species, *Pinus contorta*, forms a symbiotic mutually beneficial relationship with EMF.

In this doctoral research, I profiled shifts in soil fungal community compositional across all 3 research chapters using ITS amplicon sequencing (Chapter 3 ITS amplicon sequencing discussed in complementary manuscript[20]). Further, **Chapter 2** presented two fungal MAGs (*Section 2.3.7*) representing Ascomycota *Coniochaeta* and *Leotiomycetes* that encoded and expressed genes for degrading aromatic compounds, suggesting that pyrophilous fungi play a role in PyC degradation following wildfire. However, it's worth noting a significant disparity in the datasets accompanying this research: while I reconstructed and discussed 1651 bacterial MAGs throughout this

dissertation, only two fungal MAGs were obtained. This discrepancy underscores a prevalent bias towards prokaryotes in environmental metagenomic studies, despite the irrefutable importance of fungi in these ecosystems. This bias is not unique to my doctoral research but is a common trend observed across various soil metagenomic studies[21–23].

Using genome-resolved metagenomic approaches to profile eukaryotic community composition is notoriously more challenging than for prokaryotes with lesser developed bioinformatic pipelines. Eukaryotic genomes are more complex than bacterial genomes, with more repeated genetic elements like transposons or multiploidy that can render assembly and binning difficult[24] compared to bacteria. Bioinformatic tools have been developed to identify eukaryotic reads in shotgun metagenomic sequencing data (e.g., EukDetect[25], HumanMycobiomeScan[26], Tiara[27]), reconstruct (EukRep[28]) and annotate (FunGAP[29]) fungal genomes, and assess their completeness and quality (BUSCO[30]). However, despite the recent advancement of bioinformatic tools specialized for recovering eukaryotic genomes from metagenomic sequence data, the pipelines are still not as well-constrained, efficient, or successful as those for bacterial MAGs. For example, a recent study[31] used the EukRep pipeline to attempt to recover eukaryotic MAGs from 6000 terrestrial metagenomes available on JGI and found that only 215 of them yielded eukaryotic MAGs, only 447 total eukaryotic MAGs were generated, and only 197 of these could be taxonomically classified at the phyla level. Therefore, work is needed to further develop bioinformatic pipelines for the reconstruction, annotation, and analysis of fungal genomes generated from shotgun metagenomic sequencing datasets to better understand how environmental change impacts soil fungal communities.

Chapter 5 References

1. Nelson, A. R. *et al.* Wildfire-dependent changes in soil microbiome diversity and function. *Nat. Microbiol.* **7**, 1419–1430 (2022).

2. Malik, A. A. *et al.* Defining trait-based microbial strategies with consequences for soil carbon cycling under climate change. *ISME J.* **14**, 1–9 (2020).

3. Smith, S. E. & Read, D. Mycorrhizal Symbiosis. *Soil Sci.* **137**, 204 (1984).

4. Kayes, L. J. & Tinker, D. B. Forest structure and regeneration following a mountain pine beetle epidemic in southeastern Wyoming. *For. Ecol. Manag.* **263**, 57–66 (2012).

5. Pec, G. J. *et al.* Change in soil fungal community structure driven by a decline in ectomycorrhizal fungi following a mountain pine beetle (Dendroctonus ponderosae) outbreak. *New Phytol.* **213**, 864–873 (2017).

6. Treu, R. *et al.* Decline of ectomycorrhizal fungi following a mountain pine beetle epidemic. *Ecology* **95**, 1096–1103 (2014).

7. Roller, B. R. K. & Schmidt, T. M. The physiology and ecological implications of efficient growth. *ISME J.* **9**, 1481–1487 (2015).

8. Dove, N. C., Safford, H. D., Bohlman, G. N., Estes, B. L. & Hart, S. C. High-severity wildfire leads to multi-decadal impacts on soil biogeochemistry in mixed-conifer forests. *Ecol. Appl.* **30**, eap.2072 (2020).

9. Adkins, J., Docherty, K. M. & Miesel, J. R. Copiotrophic Bacterial Traits Increase With Burn Severity One Year After a Wildfire. *Front. For. Glob. Change* **5**, (2022).

10. Johnson, D. B., Woolet, J., Yedinak, K. M. & Whitman, T. Experimentally determined traits shape bacterial community composition one and five years following wildfire. *Nat. Ecol. Evol.* **7**, 1419–1431 (2023).

11. Arora, P. K. & Sharma, A. New metabolic pathway for degradation of 2-nitrobenzoate by Arthrobacter sp. SPG. *Front. Microbiol.* **06**, 1–6 (2015).

12. Ren, L. *et al.* Insight Into Metabolic Versatility of an Aromatic Compounds-Degrading Arthrobacter sp. YC-RL1. *Front. Microbiol.* **9**, 1–15 (2018).

13. Grant, R. F. & Roulet, N. T. Methane efflux from boreal wetlands: Theory and testing of the ecosystem model Ecosys with chamber and tower flux measurements. *Glob. Biogeochem. Cycles* **16**, 2-1-2–16 (2002).

14. Zhou, W. *et al.* Quantifying carbon budget, crop yields and their responses to environmental variability using the *ecosys* model for U.S. Midwestern agroecosystems. *Agric. For. Meteorol.* **307**, 108521 (2021).

15. Grant, R. F. *et al.* Net ecosystem productivity of boreal aspen forests under drought and climate change: Mathematical modelling with *Ecosys*. *Agric. For. Meteorol.* **140**, 152–170 (2006).

16. Mekonnen, Z. A., Riley, W. J., Randerson, J. T., Grant, R. F. & Rogers, B. M. Expansion of high-latitude deciduous forests driven by interactions between climate warming and fire. *Nat. Plants* **5**, 952–958 (2019).

17. Bouskill, N. J., Mekonnen, Z., Zhu, Q., Grant, R. & Riley, W. Microbial contribution to post-fire tundra ecosystem recovery over the 21st century. *Res. Sq.* 0–32 (2021) doi:10.21203/rs.3.rs-734815/v1.

18. Fischer, M. S. *et al.* Pyrolyzed Substrates Induce Aromatic Compound Metabolism in the Post-fire Fungus, Pyronema domesticum. *Front. Microbiol.* **12**, (2021).

19. He, L. *et al.* Global biogeography of fungal and bacterial biomass carbon in topsoil. *Soil Biol. Biochem.* **151**, 108024 (2020).

20. Caiafa, M. V. *et al.* Distinct fungal and bacterial responses to fire severity and soil depth across a ten-year wildfire chronosequence in beetle-killed lodgepole pine forests. *For. Ecol. Manag.* **544**, 121160 (2023).

21. Wu, X. *et al.* Genome-Resolved Metagenomics Reveals Distinct Phosphorus Acquisition Strategies between Soil Microbiomes. *mSystems* **7**, e01107-21 (2022).

22. Tas, N. *et al.* Impact of fire on active layer and permafrost microbial communities and metagenomes in an upland Alaskan boreal forest. *ISME J.* 1904–1919 (2014) doi:10.1038/ismej.2014.36.

23. Dove, N. C., Taş, N. & Hart, S. C. Ecological and genomic responses of soil microbiomes to high-severity wildfire: linking community assembly to functional potential. *ISME J.* **16**, 1853–1863 (2022).

24. Richard, G.-F., Kerrest, A. & Dujon, B. Comparative Genomics and Molecular Dynamics of DNA Repeats in Eukaryotes. *Microbiol. Mol. Biol. Rev.* **72**, 686–727 (2008).

25. Lind, A. L. & Pollard, K. S. Accurate and sensitive detection of microbial eukaryotes from metagenomic shotgun sequencing data. *bioRxiv* (2020) doi:2020.07.22.216580.

26. Soverini, M. *et al.* HumanMycobiomeScan: a new bioinformatics tool for the characterization of the fungal fraction in metagenomic samples. *BMC Genomics* **20**, 496 (2019).

27. Karlicki, M., Antonowicz, S. & Karnkowska, A. Tiara: deep learning-based classification system for eukaryotic sequences. *Bioinformatics* **38**, 344–350 (2022).

28. West, P. T., Probst, A. J., Grigoriev, I. V., Thomas, B. C. & Banfield, J. F. Genome-reconstruction for eukaryotes from complex natural microbial communities. *Genome Res.* **28**, 569–580 (2018).

29. Min, B., Grigoriev, I. V. & Choi, I.-G. FunGAP: Fungal Genome Annotation Pipeline using evidence-based gene model evaluation. *Bioinformatics* **33**, 2936–2937 (2017).

30. Manni, M., Berkeley, M. R., Seppey, M., Simão, F. A. & Zdobnov, E. M. BUSCO Update: Novel and Streamlined Workflows along with Broader and Deeper Phylogenetic Coverage for Scoring of Eukaryotic, Prokaryotic, and Viral Genomes. *Mol. Biol. Evol.* **38**, 4647–4654 (2021).

31. Saraiva, J. P., Bartholomäus, A., Toscan, R. B., Baldrian, P. & Nunes da Rocha, U. Recovery of 197 eukaryotic bins reveals major challenges for eukaryote genome reconstruction from terrestrial metagenomes. *Mol. Ecol. Resour.* **23**, 1066–1076 (2023).

Appendices

Appendix A: Chapter 2 Supplementary Files

See supplemental file AppendixA.zip

Supplementary Data 1. All sample metadata and associated chemistry data for subsets of samples.

Supplementary Data 2. All metatranscriptomics and metagenomics mapping information including sequencing depth, % reads assembled or binned, and number of MAGs used from each metagenome. This data file also includes all MAG information (completeness, contamination, taxonomy, etc.), their relative abundance across samples, and the selected MAGs of interest for High S and High D.

Supplementary Data 3. Kofamscan HMMs IDs for gene identification used in addition to DRAM and annotation results.

Supplementary Data 4. Metatranscriptomics data including MAG-level geTMM across samples, DRAM-annotated transcript-level geTMM across samples, all differential expression analyses output, and transcript-level geTMM across samples of transcripts from assemblies annotated as inorganic N cycling in DRAM.

Supplementary Data 5. Viral MAG (vMAG) MIUViG information including ID, assembly software, gene count, etc., annotation information of viral AMGs from DRAM, and the output from VirHostMatcher showing each putative MAG-viral linkage with the d2star value.

Supplementary Data 6. Linear discriminant analysis (LDA) output from 16S rRNA gene and ITS amplicon sequencing data, showing fungal and bacterial ASVs that are discriminant for burned or unburned soils.

Appendix B: Chapter 3 Supplementary Data

See supplemental file AppendixB.zip

Supplementary_Data_Ch3. Includes all information about data presented in Chapter 3, including sample metadata and chemistry data (Sheet A), information about metagenomic assemblies and processing (Sheet B), details about all 825 medium- and high-quality MAGs (Sheet C), MAG relative abundance across samples (Sheet D), MicroTrait trait profiles across MAGs (Sheet E), and list of dominant MAGs for all conditions and putative pyrophilous taxa MAGs (Sheet F).

Appendix C: Chapter 4 Supplementary Files

See supplemental file AppendixC.zip

Supplementary Data 1. All sample metadata, associated chemistry, and greenhouse bioassay experiment data.

Supplementary Data 2. Ecological modeling (i.e., β-nearest taxon index, βNTI, and Raup-Crick, RC_{BC}) analyses.

Supplementary Data 3. All metagenomics mapping information including sequencing depth, % reads assembled or binned, and number of MAGs used from each metagenome. This data file also includes all MAG information (completeness, contamination, taxonomy, etc.) for MAGs generated from this set of metagenomes.

Supplementary Data 4. All additional supplemental annotations used along with DRAM and gene annotations and associated coverage data associated with C and inorganic N cycling and functions presented in Fig. 4. This data file also includes the summed average geTMM of all broad functional categories across treatments.